

Exploring the Role of V δ 1⁺ $\gamma\delta$ T Cells in Immune Stress Surveillance

Stephen Paul Joyce

A thesis submitted to the
University of Birmingham
for the degree of
DOCTOR OF PHILOSOPHY

School of Cancer Sciences
College of Medical and Dental Sciences
University of Birmingham
January 2015

UNIVERSITY OF
BIRMINGHAM

University of Birmingham Research Archive

e-theses repository

This unpublished thesis/dissertation is copyright of the author and/or third parties. The intellectual property rights of the author or third parties in respect of this work are as defined by The Copyright Designs and Patents Act 1988 or as modified by any successor legislation.

Any use made of information contained in this thesis/dissertation must be in accordance with that legislation and must be properly acknowledged. Further distribution or reproduction in any format is prohibited without the permission of the copyright holder.

Abstract

$\gamma\delta$ T cells play a central role in the detection of epithelial stress as a component of the lymphoid stress surveillance response. Despite their implication in a range of conditions, including several cancers, little is known about how they interact with their antigenic targets, particularly the interaction of $\gamma\delta$ TCRs with their ligands. In this thesis I used molecular and structural modelling techniques to characterise recognition of an epithelial stress ligand, EphA2, by a $V\delta 1^+$ $\gamma\delta$ T cell, MAU. This resulted in a tripartite model of recognition, involving coordinated interaction of EphA2 with both the TCR and its cognate A-ephrin ligands on the T cell, and the identification of a surface patch on the ligand binding domain of EphA2 that potentially represents a TCR binding site. I also performed sequence-level TCR repertoire analysis to assess $\gamma\delta$ T cell populations in human colon and liver, and explored, the effect of chronic cytomegalovirus infection on the $V\delta 1^+$ $\gamma\delta$ T cell repertoire, the first such analysis of its kind. These studies suggested the $V\delta 2^{\text{negative}}$ repertoire in humans is diverse and largely private, but also highlighted a $V\gamma 5V\delta 1$ population that was selectively detected in cytomegalovirus-seropositive individuals, and may be involved in cytomegalovirus immunity.

Dedication

This thesis is dedicated to the memory of my Grandad

“What did you learn today?”

“... Nuffink?”

Acknowledgements

I would firstly like to thank my supervisors Professor Ben Willcox and Dr Carrie Willcox for their support and guidance throughout all stages this project. Aspects of this work were by funded by Cancer Research UK, the Wellcome Trust and the Medical Research Council. This work would not have been possible without contributions from our collaborators, Dr Julie Déchanet-Merville and colleagues from the University of Bordeaux, and Professor David Price and his group at the University of Cardiff.

I am grateful to all members of the Willcox group, past and present, for their roles over the past few years in shaping both this project, and myself as a scientist. I am very grateful to Dr Fiyaz Mohammed for his expert guidance on all things structural, as well as his meticulous attention to detail in proofing parts of this thesis. I would also like to thank Dr Mab Salim for his continued support in the lab, but most importantly, for always having my back.

I would also like to thank my family and loved ones, without whom all of the above would be meaningless. Emily, I can imagine that putting up with me doing this PhD was more stressful than it was for me actually doing it, but you still managed to keep me going throughout. This would not have been possible without you.

Finally, I am especially indebted to my parents, Bill and Denise Joyce. Your unrelenting support over the years has been one of my largest source of inspiration. Thank you for everything.

Table of Contents

1	Introduction	1
1.1	Background	2
1.2	Lymphoid stress surveillance is mediated by unconventional lymphocyte subsets	3
1.2.1	$\gamma\delta$ T cells survey host tissues for signs of stress.....	5
1.3	Different tissues are enriched with $\gamma\delta$ T cells exhibiting distinct V region usages. 7	
1.3.1	Murine epidermis is enriched with invariant V γ 5V δ 1 ⁺ $\gamma\delta$ T cells.....	7
1.3.2	Most human peripheral blood $\gamma\delta$ T cells express a V δ 2 ⁺ TCR.....	9
1.3.3	Human V δ 2 ^{negative} $\gamma\delta$ T cells represent a potentially diverse subset of $\gamma\delta$ T cells	11
1.4	The molecular basis of $\gamma\delta$ TCR ligand recognition	14
1.4.1	Human V γ 9V δ 2 ⁺ $\gamma\delta$ T cells recognise pAgs via BTN3A1	16
1.4.2	Structural analyses of $\gamma\delta$ TCR/ligand complexes.....	18
1.5	The expansion of dually reactive V δ 2 ^{negative} $\gamma\delta$ T cells following renal transplant 21	
1.5.1	The identification of TCR ligands for dually reactive V δ 2 ^{negative} $\gamma\delta$ T cells	22
1.5.2	EphA2: A target for epithelial stress surveillance $\gamma\delta$ T cells?	23
1.6	Clinical applications of $\gamma\delta$ T cells.....	27
1.7	Summary and thesis aims	29
1.8	Figures.....	31
2	Materials and Methods	33
2.1	Molecular cloning and construct design.....	34
2.1.1	Construct design and protein modelling.....	34
2.1.2	Expression and shuttle plasmids	34
2.1.3	PCR amplification and primers	35
2.1.4	Restriction enzyme digestion	36
2.1.5	DNA agarose gel electrophoresis and gel purification	36
2.1.6	DNA ligation.....	36
2.1.7	Site directed mutagenesis	37
2.1.8	Gibson assembly cloning	38
2.1.9	Lysogeny broth media and pouring LB agar plates	38
2.1.10	Transformation of competent bacteria.....	38
2.1.11	DNA purification	39
2.1.12	Di-deoxy terminator sequencing.....	39

2.2	Eukaryotic protein production.....	39
2.2.1	Transfection of S2 <i>Drosophila</i> cells	39
2.2.2	Expression in S2 <i>Drosophila</i> cells.....	40
2.2.3	Transient expression in mammalian HEK293T cells	41
2.2.4	SDS-PAGE	41
2.2.5	Western blot.....	42
2.2.6	Ni-NTA chromatography.....	43
2.3	Detection of protein binding	43
2.3.1	Biotinylation of proteins.....	43
2.3.2	Surface plasmon resonance overview.....	44
2.3.3	Immobilisation of biotinylated proteins.....	44
2.3.4	Immobilisation of Fc-tagged proteins	45
2.3.5	Binding studies	45
2.3.6	AlphaScreen.....	45
2.4	Cellular assays.....	46
2.4.1	Flow cytometry.....	46
2.4.2	The activation assay	47
2.5	$\gamma\delta$ T cell isolation from human Tissues.....	47
2.5.1	Colon.....	47
2.5.2	Liver	49
2.5.3	Peripheral blood	50
2.5.4	FACS and phenotyping of PBMCs	51
2.5.5	CMV IgG ELISA	51
2.6	$\gamma\delta$ T cell repertoire analysis	51
2.6.1	DNA-based repertoire analysis (immunoSEQ)	51
2.6.2	RNA-based repertoire analysis (Anchored 5'-RACE)	52
2.7	Tables.....	53
2.8	Figures.....	56
3	Establishing the Molecular Requirements for the Recognition of EphA2 by MAU T cells.....	62
3.1	Introduction	63
3.2	Results.....	65
3.2.1	Plate bound EphA2-Fc is sufficient to activate JRT MAU	65
3.2.2	Production of recombinant EphA2-Fc using 293T cells.....	66
3.2.3	No binding detected between MAU TCR and EphA2 using BIAcore.....	72
3.2.4	Interaction of ephrins with EphA2 is essential for the activation of MAU ...	75

3.2.5	TCR and ephrin interactions need to occur on the same EphA2 molecule ..	78
3.3	Discussion.....	79
3.4	Figures.....	85
4	Characterising the Interaction of the MAU TCR with EphA2	105
4.1	Introduction	106
4.2	Results.....	108
4.2.1	AlphaScreen suggests binding between EphA2 and MAU TCR.....	108
4.2.2	Modelling the interaction between EphA2 and MAU TCR.....	111
4.2.3	Mutation of the MAU CDR loops.....	115
4.2.4	Generation of the EphA2 ^{ALBD} mutant	117
4.2.5	AlphaScreen irregularities	118
4.2.6	The EphA2 LBD is sufficient for activation of JRT MAU.....	120
4.2.7	Determining the MAU TCR binding site of EphA2.....	122
4.3	Discussion.....	125
4.4	Tables	131
4.5	Figures.....	132
5	Analysing the TCR γ Chain Repertoire of $\gamma\delta$ T Cells in the Liver and Colon.....	157
5.1	Introduction	158
5.2	Results.....	161
5.2.1	Sample preparation	161
5.2.2	Contamination and the presence of PB-associated γ chains	164
5.2.3	Clonality and shared sequences	165
5.2.4	V region usage	167
5.2.5	Identification of clones of interest	168
5.3	Discussion.....	169
5.4	Tables	173
5.5	Figures.....	175
6	Investigating the Effect of Chronic CMV Infection on the V δ 1 ⁺ $\gamma\delta$ T Cell Repertoire in the Peripheral Blood of Healthy Donors	184
6.1	Introduction	185
6.2	Results.....	187
6.2.1	Study design and development.....	187
6.2.2	Analysis of sequencing data	190
6.2.3	MAU and other clones of interest were not represented in these samples.....	191
6.2.4	V δ 1 ⁺ TCR repertoires are highly private	192

6.2.5	V δ 1 ⁺ populations are polyclonal.....	193
6.2.6	V region usage of γ chain sequences.....	195
6.3	Discussion.....	197
6.4	Figures.....	204
7	Overall Discussion.....	211
7.1	Introduction	212
7.2	Ligand recognition by $\gamma\delta$ T cells	212
7.2.1	Ligand recognition by V δ 2 ^{negative} $\gamma\delta$ T cells	213
7.2.2	The role of the $\gamma\delta$ TCR and additional molecules in ligand recognition.....	216
7.2.3	The significance of the $\gamma\delta$ TCR CDR loops	217
7.2.4	Classification of V δ 2 ^{negative} $\gamma\delta$ T cell subpopulations	218
7.3	Using TCR repertoire analysis to analyse $\gamma\delta$ T cell populations	219
7.3.1	Combining repertoire and ligand identification studies	221
7.3.2	Expanding $\gamma\delta$ TCR repertoire studies	222
8	Appendices.....	223
9	References.....	236

List of Figures

Figure 1.1: Overview of the $\gamma\delta$ T cell subsets in mice and humans	31
Figure 1.2: Schematic of the MAU and LES $\gamma\delta$ T cell clones and key surface molecules	32
Figure 2.1: Maps of vectors used in transfection and cloning experiments	56
Figure 2.2: Maps of the pHL-FcHis and pHL-Avitag3 expression vectors.....	57
Figure 2.3: Primers used for the generation of ephrin receptor constructs.....	58
Figure 2.4: Cloning of the EphA2 ^{R103E} mutant	59
Figure 2.5: Overview of the immunoSEQ TCR sequencing methodology	60
Figure 2.6: Schematic representation of the Anchored RACE PCR	61
Figure 3.1: EphA2-Fc specifically activates JRT MAU	85
Figure 3.2: Structure of the EphA2 ectodomain.....	86
Figure 3.3: Expression and purification of EphA2-Fc using the 293T expression system ...	87
Figure 3.4: Amine coupling of the R10Z8E9 mAb to a CM5 BIAcore chip.....	88
Figure 3.5 : Verification of the intact conformation of EphA2 using anti-EphA2 pAb	89
Figure 3.6 : Cell surface staining of JRT MAU and LES by EphA2-Fc.....	90
Figure 3.7 : 293T EphA2-Fc activates JRT MAU equivalently to R&D EphA2-Fc	91
Figure 3.8 : MAU $\gamma\delta$ TCR construct.....	92
Figure 3.9 : Production of MAU TCR using the <i>Drosophila</i> S2 expression system	93
Figure 3.10 : Immobilisation of MAU TCR on a CM5 BIAcore chip.....	94
Figure 3.11 : Verification of MAU-Bt folding using BIAcore	95
Figure 3.12: Analysis of the MAU-Bt/EphA2-Fc interaction using BIAcore.....	96
Figure 3.13 : Binding of EphA2 to ephrins is required for the activation of JRT MAU	97
Figure 3.14 : Ribbon representation of the interaction between EphA2 and ephrinA1.....	98
Figure 3.15: Sequence alignment of the G-H loop region of the A-ephrin family	99
Figure 3.16: SDS-PAGE analysis of 293T-derived EphA2 ^{R103E} -Fc.....	100
Figure 3.17: Validation of the EphA2 ^{R103E} -Fc construct.....	101
Figure 3.18: Characterisation of the EphA2 ^{R103E} -Fc construct.....	102
Figure 3.19 : The TCR and ephrin signal from EphA2 have to occur on the same EphA2 molecule	103
Figure 3.20: Schematic of the proposed tri-partite EphA2 recognition complex	104
Figure 4.1: Structural diversity of $\gamma\delta$ TCR ligands.....	132
Figure 4.2: Validation of the AlphaScreen methodology	133
Figure 4.3 : Analysis of the EphA2-Fc/MAU-Bt interaction using AlphaScreen	134
Figure 4.4: Generation of the MAU TCR structural model.....	135
Figure 4.5: Stabilisation of the IgV domain of the Phyre-derived MAU δ chain model....	136

Figure 4.6 : Structural features of the MAU TCR model.....	137
Figure 4.7: Molecular surface electrostatic analysis of EphA2 and MAU TCR	138
Figure 4.8: Comparison of the size and structure of EphA2 and MAU TCR	139
Figure 4.9 : Flexibility between the FN1 and FN2 domains of EphA2	140
Figure 4.10: The use of CDR loops in $\gamma\delta$ ligand recognition	141
Figure 4.11 : Production of <i>Drosophila</i> S2-derived MAU V δ 1 CDR2 mutant (MAU 12)....	142
Figure 4.12 : Verification of MAU 12 folding	143
Figure 4.13 : Design of the EphA2 ^{ΔLBD} construct.....	144
Figure 4.14 : Production of 293T-derived EphA2 ^{ΔLBD} -Fc.....	145
Figure 4.15: Verification and characterisation of EphA2 ^{ΔLBD} -Fc.....	146
Figure 4.16: Characterising the role of the EphA2 LBD using AlphaScreen	147
Figure 4.17: Production of EphA2 and EphA4 LBD domain-swap mutants using the 293T expression system	148
Figure 4.18: Analysis of EphA2 LBD domain-swap mutants binding to ephrins	149
Figure 4.19: JRT MAU activation potential of the EphA2 LBD domain-swap mutants	150
Figure 4.20: Sequence alignments of the EphA2 and EphA4 LBDs	151
Figure 4.21: Structural comparison of the EphA2 and EphA4 LBDs	152
Figure 4.22: Molecular surface representation of the EphA2/ephrinA5 complex.....	153
Figure 4.23: Purification of 293T-derived EphA2 patch mutants.....	154
Figure 4.24: Characterisation of EphA2 surface patch mutants	155
Figure 4.25: Characterisation of the EphA2 ^{PATCH5} mutant.....	156
Figure 5.1: Overview of colon histology	175
Figure 5.2: Validation of chemical and enzymatic disruption of colon samples.....	176
Figure 5.3: Imaging of the colon sample digestion process	177
Figure 5.4: Depletion of $\alpha\beta$ T cells from single cell suspensions.....	178
Figure 5.5: Contamination of samples by MAU and the presence of PB-associated γ chains	179
Figure 5.6: Diversity and overlap of γ chain sequences	180
Figure 5.7: Overlap of top ranking sequences.....	181
Figure 5.8: γ chain V region usage and clonality	182
Figure 5.9: Identifying clones of interest in sequencing data	183
Figure 6.1: Development of $\gamma\delta$ T cell sorting strategy	204
Figure 6.2: Representative phenotyping of $\gamma\delta$ T cells	205
Figure 6.3: The effect of CMV infection on $\gamma\delta$ T cell populations	206
Figure 6.4: V γ 9V δ 2-associated γ chain sequences	207
Figure 6.5: Clonality of the top 30 γ and δ chains	208
Figure 6.6: Usage of γ chain gene segments by CMV-serostatus.....	209
Figure 6.7: Clonality of specific γ chains.....	210

List of Tables

Table 2.1: Primers used for the amplification of ephrin receptor constructs.....	53
Table 2.2: Primers for site directed mutagenesis of the MAU TCR CDR loops	54
Table 2.3: Antibodies used to stain and phenotype PBMCs	55
Table 4.1: MAU CDR mutation strategy	131
Table 5.1: Overview of the samples used in the immunoSEQ analysis.....	173
Table 5.2: $\gamma\delta$ clones of interest	174

Abbreviations

ATP	Adenosine triphosphate
β₂M	β2-microglobulin
C	Constant
CAR	Chimeric antigen receptor
CD	Cluster of differentiation
CDR	Complementarity determining region
CMV	Cytomegalovirus
CRD	Cysteine rich domain
D	Diversity
DAMP	Damage-associated molecular patterns
DC	Dendritic cells
DETC	Dendritic epidermal T cells
DNA	deoxyribonucleic acid
DSS	4,4-dimethyl-4-silapentane-1-sulfonic acid
DTT	Dithiothreitol
EBV	Epstein-barr virus
EDC	N-ethyl-N5 (3-diethylaminopropyl)-carbodiimide
EDTA	Ethylenediaminetetraacetic acid
EGF	Epithelial growth factor
ELISA	Enzyme-linked immunosorbent assay
EMT	Epithelial to mesenchymal transition
Fab	Fragment antigen binding
Fc	Fragment crystallisable
FN	Fibronectin
FPPS	Farnesyl pyrophosphate synthase
GBM	Glioblastoma
gl	Glycoprotein-I
GPI	Glycophosphatidylinositol
GVHD	Graft-versus-host disease
HBS	Hepes buffered saline
HMBPP	(E)-4-Hydroxy-3-methyl-but-2-enyl pyrophosphate
HRP	Horseradish peroxidase
IEL	Intraepithelial lymphocyte
Ig	Immunoglobulin
IHC	Immunohistochemistry
IL	Interleukin
IP	Immunoprecipitation
IPP	Isopentenyl pyrophosphate
J	Joining
JRT	Jurkat

K_d	Dissociation constant
LB	Lysogeny broth
LBD	Ligand binding domain
LN	Lymph node
LP	Lamina propria
LPL	Lamina propria lymphocytes
LPS	Lipopolysaccharide
mAb	Monoclonal antibody
MEP	2-C-methyl-D-erythritol 4-phosphate/1-deoxy-D-xylulose 5-phosphate pathway
MHC	Major histocompatibility complex
MICA	MHC class I polypeptide related sequence A
MO	Monocyte
MT	Metallothionien
MΦ	Macrophage
Ni-NTA	Nickel-nitrilotriacetic acid
NK	Natural killer
NMR	Nuclear magnetic resonance
pAb	polyclonal antibody
pAg	phosphoantigen
PAMP	Pathogen associated molecular patterns
pAPC	Professional antigen presenting cell
PB	Peripheral blood
PBMCs	Peripheral blood mononuclear cells
PBS	Phosphate buffered saline
PCR	Polymerase chain reaction
PDVF	Polyvinylidene difluoride
PEI	Polyethylenimine
PMSF	Phenylmethylsulfonyl fluoride
PRR	Pattern recognition receptors
qRT-PCR	Real-time RT-PCR
RACE	Rapid amplification of cDNA ends
RMSD	Root-mean-square deviation
RT-PCR	Real-time reverse transcription polymerase chain reaction
RTK	Receptor tyrosine kinase
RU	Resonance units
SCID	Severe combined immunodeficiency
SDM	Site directed mutagenesis
SDS-PAGE	Sodium dodecyl sulphate polyacrylamide gel electrophoresis
SEC	Size exclusion chromatography
siRNA	Small interfering ribonucleic acid
SPR	Surface plasmon resonance
TBS	Tris buffered saline
TCA	Trichloroacetic acid

TCR	T cell receptor
TdT	Terminal deoxynucleotidyl transferase
TEMED	Tetramethylethylenediamine
TGF-β	Transforming growth factor β
T_h2	T helper 2
TLR	Toll-like receptor
TM	Transmembrane
V	Variable
WT	Wild type
αGalCer	α -galactosylceramide

1

Introduction

1.1 Background

The cellular adaptive immune response is largely coordinated by $\alpha\beta$ T cells. In the periphery, mature $\alpha\beta$ T cells express a heterodimeric T cell receptor (TCR) at the cell surface, which, in conjunction with the co-receptors CD4 or CD8, recognise non-self peptidic antigen presented in the context of major histocompatibility complex (MHC) molecules on host cells¹. In contrast, $\gamma\delta$ T cells represent an unconventional subset of T cells, which express a heterodimeric TCR consisting of one γ and one δ chain, and unlike $\alpha\beta$ T cells, recognise ligands in a non-MHC dependent manner².

The genes encoding for all four of the TCR chains (α , β , γ and δ) were discovered contemporaneously in the 1980s³, and yet specific, in depth knowledge of the function and activity of $\gamma\delta$ T cells is still severely lacking compared to their $\alpha\beta$ counterparts. Both $\alpha\beta$ and $\gamma\delta$ T cells emerged at the same evolutionary time point 400-500 million years ago⁴, and are present in all vertebrates, suggesting that they may have evolved similarly complex, and perhaps complementary, roles in the vertebrate immune system. Indeed, $\gamma\delta$ T cells have been shown to play key roles in immunoprotection, immunoregulation, tumour recognition and recognition of cellular stress⁵.

Compared to their $\alpha\beta$ counterparts, there has been comparatively little progress in $\gamma\delta$ T cell biology in recent years, especially in the elucidation of physiologically relevant human $\gamma\delta$ T cell ligands, and the molecular nature of their interactions with TCR. This may largely be because many of the principles established from $\alpha\beta$ T cell biology, such as the conserved recognition of MHC-presented antigen, do not seem to apply to $\gamma\delta$ T cells, and an understanding of $\gamma\delta$ T cell biology may require novel paradigms of immune recognition to be established.

Key developments in the understanding of the immunobiology of $\gamma\delta$ T cells may unlock a powerful compartment of the immune system for clinical manipulation, offering significant advances in the treatment of conditions such as cancer, complementing a well-established body of existing immunotherapeutic strategies⁶.

1.2 Lymphoid stress surveillance is mediated by unconventional lymphocyte subsets

Immune surveillance is proposed to play a key role in the early detection and control of various insults to tissues, such as infection and transformation⁷. This process is thought to involve the constant monitoring of host tissue by the immune system, allowing for the rapid detection of these processes at an early stage. Unconventional T cell subsets, specifically $\gamma\delta$ T cells, have been shown to contribute towards the immune surveillance of host tissues⁸.

Conventional immune surveillance involves the surveying of host tissue for signs of infectious agents by cells of the myeloid lineage, such as dendritic cells (DC), macrophages (M Φ), and monocytes (MO). These cells express invariant, non-clonal pattern recognition receptors (PRRs), which have been shown to recognise a wide range of pathogen-associated molecular patterns (PAMPs), originating from a broad spectrum of microbes and viruses¹. Typically, PAMPs are not specific to an individual bacterium or virus, but are usually ubiquitous components common to many pathogens, such as lipopolysaccharide (LPS), an integral component of the outer membrane of all Gram-negative bacteria, which is recognised by toll-like receptor 4 (TLR 4)⁹. This non-pathogen-specific recognition of PAMPs results in the myeloid cells initiating local effector functions, such as cytolysis and phagocytosis, as well as undergoing a process of differentiation in order to migrate to local lymphoid tissue, wherein they present antigen, in the context of MHC, to cognate naïve T

cells. Upon activation, these T cells undergo a process of clonal expansion and differentiation, before being trafficked to the affected tissue via the blood¹. These pathogen-specific T cells are then capable of eliciting specific adaptive immune responses towards their targets, as well as performing pleiotropic immunoregulatory functions.

The surveillance of non-microbial stresses however, is less well elucidated. Damage-associated molecular patterns (DAMPs) are autologous antigens which are either expressed, upregulated or exposed in response to various stresses, such as transformation. While some stress signals, such as ureate and ATP, which are released from dying cells¹⁰, can be recognised by myeloid cells, the majority cannot¹¹. One such DAMP is the MHC class I like molecule MICA, the expression of which is upregulated by cellular dysregulation¹². In principle, lymphoid cells able to recognise such stress signals are able to rapidly initiate strong, local effector responses, without the need to migrate, or undergo clonal expansion. This interaction leads to a local inflammatory response which increases both the bactericidal and cytotoxic activity of lymphocytes⁸. Although the non-pathogen-specific lymphoid stress response is unlikely to completely eradicate a pathogen, it may play a role in the containment and maintenance of tissue integrity, while simultaneously shaping the downstream adaptive immune response⁸. Cells suited to such a task would not have to undergo the time-consuming processes of migration and differentiation, and might be focused during development on the recognition of a limited range of stress-linked antigens. Unconventional lymphoid subsets are able to make a key contribution to the immune surveillance of stressed tissue. Arguably, the prototypical unconventional T cell is the $\gamma\delta$ T cell, which exhibits key properties compatible with the fast acting lymphoid stress

surveillance model, and research has shown may play a key role in the detection of early stages of both infections and cancers.

1.2.1 $\gamma\delta$ T cells survey host tissues for signs of stress

In mice, certain $\gamma\delta$ T cell subsets are thought to exist as resident, pre-expanded populations, which display a constitutive 'active, yet resting' phenotype, which is likely acquired during development^{13,14}. Such properties have also been described for the peripheral blood (PB)-associated subset of $\gamma\delta$ T cells in humans². These characteristics make these cells ideally suited for the rapid detection of, and initiation of effector responses towards, stress, as they bypass the delay required for the clonal expansion and migration of conventional adaptive effector cells, thus facilitating a more immediate response. This has been demonstrated experimentally in murine xenograft models, in which immunodeficient mice injected with human $\gamma\delta$ T cells were exposed to bacterial infection, and a strong $\gamma\delta$ T cell mediated immuno-protective response was observed one day after the original infection, and all bacteria were cleared by day six, before cell division had taken place¹⁵. The intravenous addition of pamidronate, an agonist for these human $\gamma\delta$ T cells, markedly increased the antibacterial properties of these cells, demonstrating a $\gamma\delta$ T cell mediated antimicrobial response within one day following initial exposure.

Resting $\gamma\delta$ T cells, like naïve $\alpha\beta$ T cells, are not thought to recirculate between the blood and lymphatic system in humans. However, upon activation, the PB-associated $\gamma\delta$ T cells have been shown to switch to a lymph node (LN)-homing chemokine receptor profile, characterised by the upregulation of the LN-homing marker CCR7, and a decrease in peripheral tissue-association markers¹⁶. Furthermore, the authors also identified $\gamma\delta$ T cells in gastrointestinal lymphoid tissues, suggesting that this LN-homing phenotype is indeed

trafficking $\gamma\delta$ T cells to LNs. Interestingly, the presence of CCR7-expressing $\gamma\delta$ T cells in gastrointestinal lymphoid tissues was not found to increase upon acute infection, suggesting that these cells provide continual immune surveillance¹⁶.

Human PB-associated $\gamma\delta$ T cells have also been convincingly shown to act as professional antigen presenting cells (pAPCs). This was first described after the observation that, after short term co-culture with a PB-associated $\gamma\delta$ T cell agonist, these cells were able to uptake protein antigens and subsequently process and present them as peptides, in the context of MHC class II, to naïve CD4⁺ T cells¹⁷.

Subsequent studies have also demonstrated the ability of these cells to cross-present tumour-associated antigens to CD8⁺ $\alpha\beta$ T cells. Daudi lymphoma cells, opsonised with an anti-CD20 monoclonal antibody (mAb), were shown to be lysed by PB-associated $\gamma\delta$ T cells. Subsequently, tumour-associated antigens were internalised by these PB-associated $\gamma\delta$ T cells, processed and presented as peptide antigens to CD8⁺ $\alpha\beta$ T cells in the context of MHC class I. This process appears to be tightly controlled by the interaction of the Fc receptor CD16 on the surface of the $\gamma\delta$ T cells, with antibodies. This requirement is proposed to represent the 'licensing' of these $\gamma\delta$ T cells to perform their adaptive pAPC roles, as a result of their innate killing and internalisation of target cells¹⁸.

As a further example of how $\gamma\delta$ T cells may mediate systemic immune responses, a recent study has revealed a link between stress induced lymphocyte activation and IgE mediated atopy in mice¹⁹. Ligands encountered at the same time as cutaneous epithelial stress induced strong T helper 2 (T_H2)-associated atopic responses, and required NKG2D mediated signalling between the stressed epithelia and $\gamma\delta$ T cells. This process may serve as an

example of the role of lymphoid stress surveillance in shaping downstream immune responses.

Collectively, the studies demonstrate the ability of $\gamma\delta$ T cells, in the context of local stress surveillance responses, interact with the systemic immune compartment in order to polarise appropriate downstream adaptive immune responses, an area which, overall, is still poorly understood.

1.3 Different tissues are enriched with $\gamma\delta$ T cells exhibiting distinct V region usages

$\gamma\delta$ T cell subsets are enriched in discrete anatomical sites, depending on their particular variable (V) region usages, resulting in relatively homogeneous, but distinct, antigen receptor repertoires for each tissue². This is most apparent and well documented in the mouse, in which V region usage can reliably be mapped to distinct anatomical sites²⁰. Throughout this thesis, $\gamma\delta$ TCR chains will be identified using the nomenclature of Heilig and Tonegawa²¹ for murine $\gamma\delta$ T cells and Lefranc and Rabbitts²² for human $\gamma\delta$ T cells.

1.3.1 Murine epidermis is enriched with invariant V γ 5V δ 1⁺ $\gamma\delta$ T cells

Arguably the best characterised $\gamma\delta$ T cell subset in mice express the invariant V γ 5V δ 1 TCR, which account for more than 90% of mouse dendritic epidermal T cells (DETCs)²³. These cells are derived from the first wave of rearrangements of the V γ locus, and their selection is dependent on the presence of the butyrophilin-family protein Skint-1 in the embryonic thymus²⁴. This V γ 5V δ 1⁺ DETC subset has been shown to be important in the maintenance of tissue integrity²⁵, protection against chemically induced skin carcinoma²⁶, and have also been shown to suppress cutaneous graft versus host disease (GVHD)²⁷. Despite the amount

of evidence signifying the importance of $V\gamma 5V\delta 1^+$ DETCs in the control of body-barrier homeostasis in mice, any peripheral ligands which interact directly with the TCR have yet to be conclusively identified.

A recent study using intravital dynamics-immunosignal correlative microscopy has revealed that $V\gamma 5V\delta 1$ DETC TCRs are constitutively clustered, and functionally activated in the steady state *in vivo*²⁸. These TCR clusters were found to localise to anchored T cell projections at the tight junctions of squamous keratinocytes. In response to tissue stress, in the form of full-thickness wounding, the T cells redistribute their TCR towards the basal epidermis and tissue resident Langerhans cells. This suggests that the $V\gamma 5V\delta 1$ DETC TCR is likely to constitutively interact with self-ligands in the steady state, and the involvement of integrin-dependent tight junction projections, suggests that the TCR may be monitoring the spatial pattern of the putative ligand at cell-cell junctions.

In contrast to this, a study using $V\gamma 5V\delta 1$ DETC TCR tetramers to stain mouse tissue sections suggested that $V\gamma 5V\delta 1$ TCR ligands are not constitutively expressed in healthy tissue, yet are rapidly upregulated in response to wounding, in a tightly controlled fashion²⁹. Interestingly, blocking of the DETC TCR/ligand interaction with this tetramer following injury delays wound healing, supporting the role of DETCs in the early stages of response to cutaneous injury. It is unclear whether this methodology shows true upregulation of ligand, or re-localisation from tetramer inaccessible cell-cell junctions post-injury, consistent with the findings of Chodaczek *et al.*²⁸ These studies provide an insight into the potential nature of $V\gamma 5V\delta 1^+$ DETC TCR ligands, and provide a platform from which further studies may reveal the identity of the much sought-after ligands.

Other potential ligands for different murine $\gamma\delta$ T cell subsets are also being investigated. Binding assays using soluble-multimeric recombinant TCRs (smTCR) derived from murine invariant $V\gamma 6V\delta 1^+$ and $V\gamma 1V\delta 6.3^+$ T cell clones have been suggested to reveal a ligand, or ligands, which are constitutively expressed on resident peritoneal M Φ in healthy tissue, and is common to at least two distinct TCRs³⁰. Infection with the bacterium *Listeria monocytogenes* invoked the rapid upregulation of this ligand, consistent with a stress ligand which can activate cells of the lymphoid stress surveillance compartment. The ligand has not yet been identified, but it is known to be independent of β_2 microglobulin (β_2M), an essential subunit of some MHC-like molecules³¹.

1.3.2 Most human peripheral blood $\gamma\delta$ T cells express a $V\delta 2^+$ TCR

$\gamma\delta$ T cell subsets and their tissue localisation is less well understood in humans than in mice, markedly more so than the knowledge gap in the understanding of $\alpha\beta$ T cell populations between the two species³². This likely because there appears to be little overlap between the two species with regards to $\gamma\delta$ T cell subset TCR chain usages, properties and ligands they recognise³³.

The best characterised of the human $\gamma\delta$ T cell subsets is the $V\delta 2^+$ PB-associated subset, which constitute on average between 2% and 5% of $CD3^+$ cells in the PB of humans, although this is highly variable depending on the individual². The vast majority of PB-associated $\gamma\delta$ T cells (>70%³⁴) display the pairing of the $V\delta 2$ chain with the $V\gamma 9$ chain, and cells bearing this receptor are referred to interchangeably as either the $V\gamma 9V\delta 2^+$ or PB-associated $\gamma\delta$ T cell subset.

Despite the increasing appreciation for the diverse role $V\gamma 9V\delta 2^+$ $\gamma\delta$ T cells play in the immune system, detailed information on how these cells interact with their target cells is

still unclear. $V\gamma 9V\delta 2^+$ $\gamma\delta$ T cells have been shown to be activated, in a TCR-dependent manner, by low levels of low-molecular weight, non-peptidic phosphoantigens (pAgs)³⁵. One such molecule is isopentenyl pyrophosphate (IPP)³⁶, a host-derived metabolite of the mevalonate isoprenoid biosynthesis pathway, which is found in all host cells, and is essential for cell survival³⁷.

$V\gamma 9V\delta 2^+$ $\gamma\delta$ T cell reactivity is not limited to host-derived antigens however. One of the most potent activators of these cells is hydroxy-methyl-butenyl pyrophosphate (HMBPP), which has been demonstrated to be 30,000-fold more potent activator of $V\gamma 9V\delta 2^+$ cells than IPP³⁸. HMBPP is a metabolite in the bacterial-specific 2-C-methyl-D-erythritol 4-phosphate (MEP) isoprenoid biosynthesis pathway, which is distinct from the host mevalonate isoprenoid biosynthesis pathway from which IPP is derived. This striking difference in activation potential between microbial and self-derived pAgs likely allows for the detection of small amount of infecting pathogen, without reacting against healthy host tissue which expresses basal levels of the weakly stimulatory host-derived metabolites. Furthermore, following transformation, components of the mevalonate pathway are often disrupted, and this can increase the production of pAg metabolites to levels sufficient to activate $V\gamma 9V\delta 2^+$ T cells³⁶. This mechanism therefore potentially allows $V\gamma 9V\delta 2^+$ T cells to recognise both stress and infection of host cells via pAg metabolites.

In keeping with this observation, $V\gamma 9V\delta 2^+$ $\gamma\delta$ T cells are capable of recognising, and killing a range of myeloma and lymphoma cell lines *in vitro*, such as Daudi³⁹ and K562⁴⁰, in a TCR-dependent manner. The magnitude of responses to these cells was increased by the addition of amino bisphosphonates (such as zoledronate), which result in the accumulation

of IPP by the inhibition of the enzyme farnesyl pyrophosphate synthase (FPPS), which catalyses the metabolism of IPP derived metabolites in the mevalonate pathway³⁶.

In addition to pAg recognition, some data suggest that V γ 9V δ 2⁺ $\gamma\delta$ T cells can also recognise whole protein antigens via their TCR, although convincing molecular data for these interactions is largely lacking. Such whole protein antigens include the mitochondrial F1-ATPase, which is ectopically expressed on the cell surface in a range of cancers⁴¹, heat shock proteins⁴², as well as viral proteins such as the herpes virus glycoprotein-I (gI)⁴³. More recently, a study has highlighted human MutS homolog 2 (hMSH2), a nuclear protein and prominent cancer biomarker which plays a central role in DNA mismatch repair mechanisms, as a potential V γ 9V δ 2 TCR ligand⁴⁴. hMSH2 was found to be ectopically expressed on the surface of a panel of epithelial tumour cells, as well as Epstein–Barr virus (EBV) infected cells, and these cells elicited cytolytic effector functions of V γ 9V δ 2 $\gamma\delta$ T cells in a TCR and NKG2D dependent manner.

Collectively, these data suggest a role for V γ 9V δ 2⁺ $\gamma\delta$ T cells in the detection of, and protection against both cellular stress and infection through the recognition of pAgs and, potentially, other less well-characterised whole protein antigens.

1.3.3 Human V δ 2^{negative} $\gamma\delta$ T cells represent a potentially diverse subset of $\gamma\delta$ T cells

Non-PB-associated $\gamma\delta$ T cells are referred to as V δ 2^{negative} $\gamma\delta$ T cells, as the V δ 2 chain is almost exclusively used by V γ 9V δ 2⁺ $\gamma\delta$ T cells in adults. V δ 2^{negative} $\gamma\delta$ T cells form a substantial component of the intraepithelial lymphocyte (IEL) compartment, and in human colon can constitute up to 20% of epithelial CD3⁺ lymphocytes, 90% of which express V δ 1⁺ $\gamma\delta$ TCRs, although these numbers are highly variable between individuals.

The V δ 1⁺ classification is occasionally used synonymously with the V δ 2^{negative} classification, but this is incorrect as the V δ 2^{negative} $\gamma\delta$ T cell population also includes cells expressing V δ 3⁺ and V δ 5⁺ TCRs, and there is currently no evidence to suggest that these cells have identical properties to V δ 1⁺ $\gamma\delta$ T cells.

V δ 2^{negative} cells have been found to be enriched within several epithelial tumours, such as kidney and colon carcinomas⁴⁵, and also are involved in the immune response to cytomegalovirus (CMV) infection⁴⁶. Despite an increasing appreciation for the diverse role V δ 2^{negative} $\gamma\delta$ T cells play in the immune system, few physiologically significant ligands, and the precise molecular nature of their interaction with TCR, have been characterised

V δ 1⁺ $\gamma\delta$ T cells have repeatedly been associated with recognition of CD1 molecules, a family of MHC-like proteins which are typically associated with presenting self and bacterial lipids to natural killer T (NKT) and other unconventional T cells⁴⁷. This finding is particularly interesting as CD1 molecules are the only ligands to which both murine and human $\gamma\delta$ T cells display reactivity³³.

V δ 2^{negative} $\gamma\delta$ T cells demonstrating reactivity towards CD1c, which is upregulated during the process of inflammation-induced differentiation of MO into DC⁴⁸, were isolated by stimulating peripheral blood lymphocytes (PBLs) with autologous CD1c expressing DC and *Mycobacterium tuberculosis* extract⁴⁹. Subsequently, several independent studies have also isolated human V δ 1⁺ $\gamma\delta$ T cells which appear to detect specific lipid antigens, both host-derived and microbial, presented by CD1d^{50,51}. These cells were isolated by staining $\gamma\delta$ T cells with lipid-loaded CD1d tetramers, and the majority of these cells (>80% in some instances) expressed a V δ 1⁺ $\gamma\delta$ TCR.

Two of the TCRs isolated from these studies have been characterised in detail. The DP10.7 TCR (V γ 4V δ 1) was isolated from healthy PBMCs stained by CD1d tetramers loaded with the self-lipid, sulfatide. The 92C TCR (V γ 5V δ 1) was isolated from PBMCs stained by CD1d tetramers loaded with the microbial glycolipid α -galactosylceramide (α GalCer). These TCRs were subsequently used in molecular and structural studies to elucidate the $\gamma\delta$ TCR binding mode, and these studies provide further insight into the immunobiology of CD1d-reactive $\gamma\delta$ T cells, and this will be discussed in detail in section 1.4.1.

The apparent affinity for MHC-like molecules by V δ 2^{negative} $\gamma\delta$ T cells suggests that these cells may be restricted to recognition of these molecules. This is unlikely, as in these study only a small percentage (<1% in some instances) of V δ 1⁺ $\gamma\delta$ T cells could be stained by lipid-CD1d tetramers^{50,51}. Furthermore, the ability of V δ 1⁺ $\gamma\delta$ T cells to discriminate between lipids presented by CD1d is also unclear, as staining of V δ 1⁺ $\gamma\delta$ T cells with non-lipid-loaded CD1d tetramers was also observed in these studies.

Collectively, this suggest that attempts to identify new ligands for V δ 2^{negative} $\gamma\delta$ T cells should not be restricted to MHC-like molecules, and that non-MHC-like molecules are still viable candidates for recognition by V δ 2^{negative} $\gamma\delta$ T cells.

1.3.3.1 V δ 2^{negative} $\gamma\delta$ T cells are involved in the immune response to CMV

V δ 2^{negative} $\gamma\delta$ T cells have been convincingly argued to play a role in the immune response to CMV. CMV is a double stranded DNA β -herpes virus which is known to chronically infect between 50% and 90% of the population⁵². Following acute infection, CMV enters a non-symptomatic latent phase, characterised by a decrease in the production and expression of viral proteins⁵³. Initiation and maintenance of this latent cycle is thought to be largely influenced by chronic immune control of the CMV lytic processes⁵³. Therefore, CMV

reactivation often occurs in immunocompromised patients, and can result in severe clinical implications⁵⁴.

CMV infection has repeatedly been shown to cause the specific expansion of highly differentiated V δ 2^{negative} $\gamma\delta$ T cells in the PB, while V δ 2⁺ subsets remain largely unaffected. Furthermore, expansions of $\gamma\delta$ T cells in CMV reactivation in immunocompromised transplant patients is correlated with resolution of viraemia, suggesting a protective antiviral role for these cells⁵⁵.

Despite the potential importance of these populations, little is currently known regarding the TCR usage profile and ligand recognition by these cells. Spectratyping studies have characterised these expansions as oligoclonal^{46,56}, which suggests that the expansion is antigen-driven. However, such studies provide no information on the particular $\gamma\delta$ TCR chains present in these populations, nor their antigen-recognition profiles. Advances in this area are necessary to increase the understanding of how $\gamma\delta$ T cells interact with this important model virus.

1.4 The molecular basis of $\gamma\delta$ TCR ligand recognition

The $\gamma\delta$ TCR is a heterodimeric antigen receptor, consisting of one γ and one δ chain, expressed on the surface of $\gamma\delta$ T cells. The genes which encode these receptors are located within three loci, the TCR γ and TCR β loci are located separately on chromosome 7, whereas the TCR δ and TCR α genes share a single locus on chromosome 14⁵⁷. Somatic recombination between the variable V-J and V-D-J gene segments for γ and δ respectively provides diversity for the receptor, similarly to α and β chain recombination in $\alpha\beta$ T cell development. The human β locus spans ~0.6Mb and contains 62-65 V gene segments, of which around 40 have been shown to be functional². In contrast, the human γ locus spans

only 0.1Mb, and contains 6 functional V gene segments⁵⁷. The V gene segments contain the germline-encoded complementarity determining regions (CDR) CDR1 and CDR2. The CDR3 region constitutes the recombined V-J segments (for γ) or V-D-J (for δ), as well nucleotides inserted randomly by P- and N-nucleotide addition⁵⁷. Theoretically there are approximately 10^{16} possible TCRs which can be produced from these genetic components, however individual T cell subsets show biased use of TCR V gene segments, with some subsets expressing invariant/semi-invariant TCRs with identical/highly-similar junctional sequences²⁰.

Structurally, each TCR chain consists of two immunoglobulin (Ig) folds, one for each of the variable (V) and constant (C) regions, and each fold constitutes around 7 β strands arranged in two antiparallel β sheets and, and the CDR regions of the V region are exposed, flexible loops⁵⁸. V regions in the γ and δ chains are structurally similar to $\alpha\beta$ V regions, however the C regions are drastically different, owing to differences in the formation of disulphide bonds between the γ and δ chains. Also unique is the orientation of the C and V regions, which is due to an unusually small angle between the two domains⁵⁸. This is interesting because it implies that $\gamma\delta$ TCRs may be able to form different signalling complexes than $\alpha\beta$ TCRs, due to different structural constraints.

Several structures of $\gamma\delta$ TCRs have been completed, and they have aided our understanding of the potential molecular nature of their interactions. The first structure determined of a human V γ 9V δ 2⁺ pAg-reactive $\gamma\delta$ TCR was published in 2001, and described an antigen receptor with similarities to both $\alpha\beta$ TCRs, as well as antibodies⁵⁸.

Analysis of the structure suggested that all six CDR loops are potentially important for the binding of pAgs, which has subsequently been confirmed by mutational studies⁵⁹, and this

may explain the canonical usage of the V γ 9 and V δ 2 chains by pAg-reactive T cells. Such structures of receptors alone, however, cannot reveal the details molecular nature of the interaction between TCR and ligand. Indeed, over ten years since the publication of this structure, it is still not known precisely how V γ 9V δ 2 TCRs interact with pAg-sensitised targets, although this is starting to be uncovered, and is discussed in detail in section 1.4.1.

The role of the $\gamma\delta$ TCR as the sole facilitator of peripheral ligand recognition in $\gamma\delta$ T cells has recently been brought into question. A study identified a population of murine CD27⁺ $\gamma\delta$ T cells whose peripheral activation was not mediated by the TCR, but solely by cytokines, leading them to suggest that, for this subset, the $\gamma\delta$ TCR may predominantly be required for the selection, maturation and trafficking of the $\gamma\delta$ T cells⁶⁰. In contrast, CD161⁺ human $\gamma\delta$ T cells have been shown to be TCR-hyporesponsive unless given co-stimulation through CD161⁶¹, and so perhaps the costimulatory requirements of the CD27⁺ murine population have yet to be established. However, overall these studies indicate that gaining an improved understanding of $\gamma\delta$ immunobiology is likely to shed light on novel paradigms of immune regulation relative to conventional $\alpha\beta$ T cell subsets.

1.4.1 Human V γ 9V δ 2⁺ $\gamma\delta$ T cells recognise pAgs via BTN3A1

It has long been established that V γ V δ 2⁺ $\gamma\delta$ T cells are specifically activated by both host-associated and pathogen-associated pAgs, however the molecular nature of this interaction has only recently begun to be uncovered. Direct binding has not been observed between pAgs and V γ V δ 2 TCRs, and this therefore suggests that other molecules may be involved in the host cell in order to facilitate activation. This is supported by the observation that cell-cell contact is required between the V γ V δ 2⁺ T cell and the pAg-treated cell for

activation^{62,63}, and that murine cells are unable to activate V γ V δ 2 T cells in this way, suggesting that these critical molecule(s) are primate specific^{64,65}.

Butyrophilin-3A1 (BTN3A1) has since been identified as a molecule essential for V γ V δ 2⁺ γ δ T cell activation by pAgs. BTN3A1 knockdown studies in V γ 9V δ 2⁺ γ δ T cell-activating cell lines have been shown to prevent activation, and subsequent reintroduction can re-confer sensitivity⁶⁶. BTN3A1 is a member of the BT3 family, an Ig superfamily of transmembrane proteins implicated in many biological processes⁶⁷. All members contain IgV (N terminal) and IgC (C terminal) extracellular domains, and all but BTN3A2 contain an intracellular B30.2 domain. When cross-linked with an agonist antibody, all BTN3A family members can activate V γ V δ 2 T cells *in vivo*, however only BTN3A1 can activate when exposed to pAgs⁶⁶. This suggests that pAg-mediated stimulation may activate V γ 9V δ 2⁺ T cells via alterations in the rearrangement of the BTN3A1 ectodomain.

However, it is still unclear exactly how this molecule confers the signal to V γ 9V δ 2⁺ T cells, and which domains are involved. A study by Vavassori *et al.*⁶⁸ suggested BTN3A1 acts as an antigen presenting molecule, binding pAgs in its extracellular IgV domain for recognition by V γ 9V δ 2 TCRs, providing an X-ray crystal structure of pAgs IPP and HMBPP bound to the extracellular IgV domain of BTN3A1. However, since publication, the studies' crystallographic data has been called into question, particularly with regard to the modelling of the pAgs into the electron density⁶⁹.

A competing theory, published subsequently, indicates that it is the intracellular B30.2 domain of BTN3A1 which directly binds pAgs, and the authors provide more convincing X-ray crystal data to support this⁶⁹. Using these X-ray crystal complexes they identified a small, positively charged pocket which they propose binds the pAgs. Amino acid residue

differences in this region could explain why BTN3A3 fails to activate V γ 9V δ 2⁺ $\gamma\delta$ T cells, despite the presence of a B30.2 domain. The authors subsequently suggest that BTN3A1 potentially translates this as a signal to the TCR via a reduction in membrane mobility and clustering, which had been previously observed in cells exposed to intracellular pAgs⁶⁶. Unpublished data from the Willcox group provides further support for this second model, as nuclear magnetic resonance (NMR) has demonstrated interactions formed between IPP and the intracellular B30.2 domain of BTN3A1. However, despite this increased understanding of pAg sensing, definitive molecular mechanisms are unclear and conclusive TCR binding to BTN3A1 has not been shown.

1.4.2 Structural analyses of $\gamma\delta$ TCR/ligand complexes

The first complex structure to demonstrate a $\gamma\delta$ TCR bound to ligand was the murine G8 $\gamma\delta$ TCR in complex with the nonclassical MHC class I molecule, T22³¹, and structural analysis of this interaction suggests a convergence of innate and adaptive recognition strategies. Adams *et al.* reported that G8 utilises a combination of both genetically diverse and germline-encoded regions of its CDR3 δ loop to bind to the side of T22. The majority of the interacting residues originate from the germline-encoded D δ 2 segment, suggesting an innate-like pre-disposition for T22 binding. Shin *et al.* used T22 tetramers to identify and clone T22-reactive $\gamma\delta$ T cells, and have demonstrated that this full length D δ 2 segment is present in a substantial population of mouse $\gamma\delta$ T cells, and use the reading frame which encodes the sequence SEGYE⁷⁰.

The use of the recombination-derived diverse residues in the CDR3 δ chain may complement the innate-like ligand recognition by allowing rapid coevolution of the TCR along with its ligand, allowing for the adaptation to rapid changes within an individual,

while providing the framework for broader innate-like recognition among the whole species. These data suggest that $\gamma\delta$ TCRs that recognise ligand in this manner can recognise a limited range of antigens (perhaps one D δ segment for each), with affinity being fine-tuned by random recombination components.

It is important to consider how representative this mechanism may be when considering the other potential $\gamma\delta$ TCR/ligand interactions identified. G8 recognition of T22 requires the presence of $\beta 2M$, yet mice deficient in $\beta 2M$ do not display the immunodeficiency phenotypes of $\gamma\delta^{-/-}$ mice, indicating that there are other mechanisms available for the recognition of ligands by $\gamma\delta$ TCRs in mice². Furthermore, the small contribution of CDR1 and CDR2 towards T22 reactivity is not easy to reconcile with the importance of V regions in the distribution and tissue localisation of $\gamma\delta$ T cell subsets.

1.4.2.1 Structural analyses of $V\delta 1^+$ $\gamma\delta$ TCRs interacting with CD1d

As discussed in section 1.3.3, structural complexes have recently been determined for the interaction of two $V\delta 1^+$ $\gamma\delta$ TCRs, 92C⁵¹ and DP10.7⁵⁰, with lipid-bound CD1d. Despite some similarities, these complexes surprisingly demonstrate remarkable differences in both the binding modes of the two TCRs with CD1d and well as lipid discrimination strategies. In both structures, contacts between the TCR and CD1d are largely facilitated by interactions between the CDR1 loop of the $V\delta 1$ chain and the $\alpha 2$ helix of the CD1d lipid binding platform. This is supported by van der Waals interactions between the $V\delta 1$ CDR3 loop, and to an extent the $V\delta 1$ CDR2, and the $\alpha 1$ helix of the CD1d lipid binding platform. In both structures, lipid specificity is conferred by interactions between CDR3 junctional residues of either the γ (92C) or δ (DP10.7) chain and the lipid head groups.

Strikingly, the two structures reveal different requirements for the V γ chains of the TCRs for binding to CD1d. The 92C TCR uses 3 residues of the γ chain CDR3 loop to facilitate antigen specificity by forming polar-contacts the α GalCer head group, whereas the γ chain of the DP10.7 TCR does not form interactions with either CD1d or sulfatide. This apparent minimal contribution from the γ chain may explain the lack of conservation of γ chains of CD1d interacting TCRs identified in both studies, as well as a further, independent, study⁷¹. These differences in CDR involvement result in different TCR footprints on the CD1d lipid binding platform, and although in both instances the V δ 1 CDR1 loop forms contacts with the α 1 helix of the binding platform, the region of the helix they interact with differs between the complexes.

The disparity of binding mode between the two structures calls into question the conclusions from both studies that these V δ 1⁺ $\gamma\delta$ T cells have a physiological role in specifically recognising lipids presented by CD1d. Although seemingly similar to the mode of recognition of MHC-presented peptides by $\alpha\beta$ T cells (where in broad terms the germline-encoded CDR1 and CDR2 loops of the α and β chains form contacts with the peptide binding platform whereas the variable CDR3 loops confer antigen specificity⁷²), there are several key differences. Primarily the non-conserved TCR footprint appears to defeat the evolutionary purpose of a conserved presentation molecule, which one would expect to enable invariant interactions with the presenting molecule, allowing the recombined elements of the immune receptor to differentiate between a diverse range of presented antigens. However, the binding mode observed not only differs between each receptor considerably, but in each case is perhaps more reminiscent of antibody binding of three-dimensional epitopes, which happen to be similar on both the sulfatide- and α GalCer-bound CD1d lipid-binding platform regions.

Collectively, these studies provide great insight into the molecular nature of interactions of $\gamma\delta$ TCRs with their ligands, although work is still needed to fully characterise the role of individual TCR elements, such as the CDR loops, particularly in antigen recognition by $V\delta 2^{\text{negative}}$ $\gamma\delta$ T cells.

1.5 The expansion of dually reactive $V\delta 2^{\text{negative}}$ $\gamma\delta$ T cells following renal transplant

In 2005, Halary *et al.* reported the expansion of $V\delta 2^{\text{negative}}$ $\gamma\delta$ T cells in the blood of immunocompromised renal transplant patients following acute infection with CMV⁷³. In these patients, the circulating $\gamma\delta$ T cell repertoire comprised up to 50% of total PB T cells.

Clones were generated from the $V\delta 2^{\text{negative}}$ $\gamma\delta$ T cells which demonstrated strong reactivity towards CMV-infected fibroblasts *in vitro*, in an MHC- and NKG2D-independent manner. Individual $V\delta 2^{\text{negative}}$ clones also showed strong reactivity to various cancer cell lines, such as HT29 and 293T⁷³, and subsequent unpublished data from the laboratories of Julie Déchanet-Merville and David Vermijlen have shown that there seems to be considerable diversity in the pattern of cancer cell lines these $V\delta 2^{\text{negative}}$ clones recognise. These interactions were shown to be TCR-dependent, as determined by the use of antibodies to block CD3 and $\gamma\delta$ TCRs (C δ domain). Furthermore, the TCR was found to become downregulated following activation, as is typically observed in TCR-mediated responses⁷⁴. Finally, transduction of the TCR genes from the dually-reactive clones into Jurkat (JRT)-T3.5 cells, conferred reactivity towards the same set of cell lines.

These findings led to the hypothesis that these $\gamma\delta$ T cell clones were recognising stress ligands induced by both viral infection and transformation, via their $\gamma\delta$ TCRs. In order to fully understand these interactions, identification of these ligands was required.

1.5.1 The identification of TCR ligands for dually reactive $V\delta 2^{\text{negative}}$ $\gamma\delta$ T cells

Two of the clones isolated from these expanded populations of $V\delta 2^{\text{negative}}$ $\gamma\delta$ T cells were selected for further study, designated MAU ($V\gamma 9V\delta 1$) and LES ($V\gamma 4V\delta 5$). To determine the ligands for these two clones, an antibody blocking screen was conducted by immunising BALB/c mice with the activating HT29 cell line, and CMV infected fibroblasts. Two of the antibodies generated in this screen displayed immunofluorescence staining profiles of recognised target cells for these clones. The 6G8 antibody was able to block reactivity to such cell lines by the MAU clone, but did not affect reactivity of the LES clone. Conversely, the 2E9 antibody blocked reactivity by the LES clone, but not the MAU clone. Based on this observation, it was therefore assumed that the ligands for the blocking antibodies 2E9 and 6G8 were the ligands for LES and MAU respectively.

In the Willcox laboratory, the 2E9 and 6G8 blocking antibodies were then used in co-immunoprecipitation (co-IP) experiments to isolate their respective ligands. The molecules co-immunoprecipitated from activating cell lysates were analysed by mass spectrometry, and were identified as endothelial protein C receptor (EPCR) and ephrin receptor A2 (EphA2) for LES and MAU respectively. It was therefore proposed that these molecules are the ligands for the LES and MAU $\gamma\delta$ TCRs.

The most striking feature of these two ligands is that they are not only expressed on cells infected by CMV *in vivo*, but also up regulated on transformed epithelial cells⁷³. This raises

the possibility that these molecules act as major targets for $\gamma\delta$ T cell stress surveillance, or are prototypic of the type of ligand recognised in this context.

Subsequent studies from our group have confirmed the status of EPCR as a ligand for the LES TCR by virtue of surface plasmon resonance (SPR) binding analyses, and the interaction has partly been characterised through mutagenesis studies. Confirmation of an interaction between the MAU TCR and EphA2 however, has yet to be established, and the molecular mechanisms underpinning the potential interaction remain elusive.

1.5.2 EphA2: A target for epithelial stress surveillance $\gamma\delta$ T cells?

EphA2 has been implicated in the progression and maintenance of several cancers, and is a major target for current immunotherapeutic approaches⁷⁵. The understanding of its role as a stress surveillance ligand for $V\delta 2^{\text{negative}}$ $\gamma\delta$ T cells may reveal additional methods for the clinical manipulation of this molecule.

EphA2 belongs to the largest subfamily of tyrosine kinase receptors (RTKs), the ephrin receptors. The 16 identified ephrin receptors have a distinct and diverse range of physiological roles, including in embryonic development, nervous system development and angiogenesis⁷⁵. The ephrin receptors were first identified in 1987, in a series of screens designed to identify RTKs involved in various cancers⁷⁶. Initially classed as orphan receptors, it was not until 7 years later that the first ligands of the ephrin receptors were identified by soluble receptor affinity methods (reviewed in⁷⁷).

The cognate ligands of ephrin receptors are the ephrins which are classified as either A- or B-ephrins, and like the ephrin receptors, have been shown to be involved with many developmental processes⁷⁵. B-ephrins are transmembrane proteins, with small cytosolic regions. A-ephrins are small proteins, of around 200 amino acids, which are tethered to the

cell surface via glycosylphosphatidylinositol (GPI) anchors, and so possess neither transmembrane nor cytosolic regions⁷⁸. GPI anchors are a post translational modification added to the C terminal end of a diverse group of proteins during production and processing, and act as a crucial determinant of signalling activity and localisation⁷⁸. EphA2 promiscuously binds all A-ephrins, but does not interact with the TM B-ephrins. EphA4 however, a structurally similar ephrin receptor family member, binds all A-type ephrins, and also all transmembrane B-ephrins⁷⁹.

All ephrins share a conserved core region, including 4 invariant cysteine residues near the C terminus, which may represent a semi-conserved receptor binding motif. Unusually for RTK ligands, the ephrins also have high sequence homology, with approximately 30-70% identity⁷⁷. Ephrin receptors bind their ligands with high affinity, with many interactions having a dissociation constant in the nM range⁷⁷. Furthermore, there is much evidence for the clustering of ephrin receptors and ligands during the formation of signalling complexes⁸⁰.

The structure of EphA2 and the molecular nature of its interactions with ligands is well understood⁸⁰. EphA2 is a 130kDa transmembrane protein, with 5 extracellular domains. The N terminal domain is the ligand binding domain (LBD), a 173 residue domain responsible for binding A-ephrins. The ectodomain also possess a cysteine rich domain (CRD) consisting of a Sushi and epidermal growth factor (EGF) like domain, as well as two fibronectin (FN) repeats proximal to the membrane. Intracellularly, EphA2 contains a kinase and sterile α motif (SAM) domain, which mediate the proteins signalling functions. LBDs for the different ephrin receptors seem to bind their respective subset of ligands in distinct ways, which explains the unique ephrin ligand repertoire for each ephrin receptor^{79,81,82}.

1.5.2.1 The role of EphA2 in tumour formation and progression

EphA2 has been linked to the formation and progression of several cancers^{75,78}. Despite this, its role in the development and maintenance of transformation is complex, and only just beginning to be understood. Unlike other members of the ephrin receptor family, which are largely limited to expression during development, EphA2 is primarily located on dividing epithelial cells in the lung, skin and small intestine^{83,84}, where it is suspected to play roles in the regulation of cell growth, survival, migration, and angiogenesis (reviewed in⁸⁵).

EphA2 is tightly confined to areas of cell-cell contact, and is heavily dependent on E-cadherins for correct localisation and ligand interactions⁸⁶. Immunofluorescence microscopy experiments revealed that the decreased expression of E-cadherins resulted in EphA2 being redistributed away from areas of cell-cell contacts. Furthermore, this resulted in the exposure of EphA2 epitopes previously inaccessible by antibodies⁸⁶. The exposure of previously hidden epitopes in response to the inhibition of E-cadherins, which is a key process in epithelial-mesenchymal transition (EMT) in cancers⁸⁷, suggests that the immune system may have evolved to recognise these epitopes via $\gamma\delta$ T cells, as their exposure indicates the breakdown of cell-cell junctions.

The complex role of EphA2 in the progression and maintenance of malignancies seems to depend heavily on cell type and micro-environment⁸⁸. EphA2 is located in chromosomal region 1p36, for which loss of heterozygosity is observed in many cancers⁸⁹. Furthermore, EphA2 expression has also been shown to be controlled by mRNA stability⁹⁰ and p53 mediated transcription⁹¹.

Immunohistochemistry (IHC) analysis shows that EphA2 is strongly overexpressed in 61% of glioblastoma (GBM) patient tumours⁹², 76% of ovarian cancers⁹³ and 85% of prostate

adenocarcinomas⁹⁴. Furthermore, the increased expression of EphA2 has been linked with increased malignancy and poor clinical prognosis⁷⁸. In some cases however, such as in HeLa cervical cancer cell lines and U373MH glioma cells, EphA2 levels are decreased compared to healthy cells⁹⁰. Interestingly, gene profiling analyses show that EphA2 message levels are decreased in a range of cancers compared to benign tissue, several of which show increased levels by immunohistochemistry approaches⁸³, suggesting a complex role for EphA2 in cancer governed by mechanisms at both the message and protein level.

It is suggested that in healthy tissue EphA2 provides a tumour suppressive function, whereby it negatively regulates tumour growth upon binding with its ligands, which results in receptor phosphorylation⁷⁸. Upon transformation, EphA2 displays dramatic alterations in subcellular localisation and is located in sites of membrane ruffling in aggressive tumour cells⁹⁵. Similarly, loss of E-cadherin results in re-localisation of EphA2 away from areas of cell-cell contact. These unstable cell contacts are thought to prevent effective ligand/receptor interactions, and therefore promote the growth of the tumour as a result⁹⁵. This is supported by the observation that EphA2 overexpressed on tumours is usually found in an un-phosphorylated form, suggesting limited interactions with ligand⁹⁶. Furthermore, the expression profile of ephrinA1 in many cancers suggests that ephrinA1 is downregulated from the cell surface, again, preventing sufficient EphA2/ligand interactions, and hence suppressing its tumour suppressive functions⁹⁷.

1.5.2.2 EphA2 as a target for immunotherapy

Due to its overexpression in a wide range of cancers, and strong association with clinical progression, EphA2 has become a major target for cancer immunotherapy, and a large body of research is dedicated to delivering such strategies (reviewed in⁷⁵). There are

currently two categories of approaches being investigated for the clinical targeting of EphA2. The first is the use of EphA2 as a target for delivery of exogenous anticancer compounds and novel chimeric antigen receptors (CARs). For example, use of bacterial toxins bound to ephrinA1 have shown promising results, enabling them to be targeted to EphA2 bearing tumours⁹⁸. A second approach is to directly manipulate and inhibit the transforming properties of EphA2 to treat cancers, such as the use of specific monoclonal antibodies which are able to bind EphA2 and induce receptor phosphorylation and downregulation, restoring tumour suppressive functions⁹⁹.

Clearly the close association of EphA2 expression to the establishment and progression of tumours, and association with poor prognosis, increased metastasis and decreased survival has established it as a key cancer therapeutic target. It is therefore interesting to speculate that $\gamma\delta$ T cells may have evolved to target EphA2 for precisely the same reasons, as part of their role in surveillance of epithelial stress in the context of the 'lymphoid stress response' hypothesis. In order to explore this possibility further, it is important to consider the potential molecular mechanisms of such an interaction, and build on the structural and functional knowledge base of EphA2 and its ligands to identify key components required for the formation of an active $\gamma\delta$ T cell recognition complex.

1.6 Clinical applications of $\gamma\delta$ T cells

There is a growing body of evidence supporting the potential significance of $\gamma\delta$ T cells in the treatment of various cancers^{34,100}. $\gamma\delta$ T cell based therapies are particularly attractive as they circumvent the requirement for MHC-restriction demanded by conventional $\alpha\beta$ T cell based approaches³⁴, and also avoids immune evasion following MHC downregulation, as is observed on many tumours¹⁰¹. Furthermore, these cells often exhibit high levels of

cytotoxicity and high potential for cytokine release, likely due to their existence as pre-expanded populations in some contexts³⁴. Promising results from phase I and II clinical trials have fuelled a growing interest in the development of $\gamma\delta$ T cell-based cancer immunotherapies¹⁰²⁻¹⁰⁴.

Studies in mice have heavily implicated $\gamma\delta$ T cells in the protection from carcinogenesis, particularly DETCs, which are involved in body-barrier surveillance²⁸. $\gamma\delta$ T cell deficient (TCR $\delta^{-/-}$) mice are more susceptible to chemically induced skin carcinoma²⁶ and colorectal carcinoma¹⁰⁵ than control mice. More recently, IL-17 producing circulating $\gamma\delta$ T cells ($\gamma\delta$ T17) have been shown to play a pivotal role in the efficacy of chemotherapy induced anticancer immune responses¹⁰⁶.

Research is not limited to murine models however, as human V γ 9V δ 2⁺ $\gamma\delta$ T cells show strong MHC-unrestricted cytotoxic activity against tumours and prostate cancer cell lines *in vitro*^{107,108}. V γ 9V δ 2⁺ cells expanded *ex vivo* and then adoptively transferred into severe combined immunodeficiency (SCID) mice, demonstrated responses towards B cell lymphoma and melanoma, as well renal, pancreatic, and nasopharyngeal carcinomas³⁴. Furthermore, there are currently three phase I clinical trials in place involving the *ex vivo* manipulation of the human V γ 9V δ 2⁺ $\gamma\delta$ T cell subset, each showing signs of promising results, and in each case improved clinical outcomes correlate with the expansion of $\gamma\delta$ T cells¹⁰²⁻¹⁰⁴. Several of the studies include the administration of aminobisphosphonates, such as zoledronate, which sensitise the tumour cells to V γ 9V δ 2⁺ $\gamma\delta$ T cells³⁶.

The knowledge of V γ 9V δ 2 TCR ligands, and the availability of established pharmaceuticals to augment their anticancer functions, has resulted in substantial attention being devoted towards them. Recently however, there has been increasing interest in V δ 2^{negative} subsets,

due to the striking observation that certain V δ 2^{negative} $\gamma\delta$ T cell subsets display dual reactivity towards both CMV-infected cells and various tumours^{73,109}. This subset may also play a role in immunosurveillance of cancer development, as immunocompromised kidney transplant patients who have expansions of V δ 2^{negative} $\gamma\delta$ T cells have a decreased risk of post-transplant malignancies in the 6 years following surgery¹¹⁰.

These trials and investigations suggest that there is considerable potential to exploit the tumour surveillance and anti-tumour properties of $\gamma\delta$ T cells clinically. Ultimately, however, the molecular basis of target cell recognition by $\gamma\delta$ TCRs is unclear, and advances in this area are essential if we are to understand the mechanism behind their involvement in anti-tumour effects, and potentially manipulate these mechanisms to develop novel cancer treatments.

1.7 Summary and thesis aims

$\gamma\delta$ T cells have been shown to play a pivotal role in the detection and maintenance of cellular stress, and form a key component of the lymphoid stress surveillance compartment. The emerging potential of $\gamma\delta$ T cells in the therapeutic treatment of cancers suggests that $\gamma\delta$ T cell biology is a key area to develop, potentially allowing the manipulation of a powerful immune compartment, to complement a successful body of $\alpha\beta$ -based therapeutic strategies³⁴.

Although several $\gamma\delta$ TCR ligands have been characterised, the structural features and recognition modalities of the majority of $\gamma\delta$ TCR ligands remain largely undetermined. In humans, despite recent progress in the understanding of V γ 9V δ 2⁺ $\gamma\delta$ T cell recognition of antigens, our understanding of the V δ 2^{negative} recognition strategies is less clear. Despite documented recognition of MHC-like molecules, such as CD1d, by some V δ 2^{negative} $\gamma\delta$ T

cells, the diverse recognition modes involved suggest that ligand identification studies should not be confined to such molecules, as there likely exist several distinct modalities of ligand interactions with $\gamma\delta$ TCRs.

The further characterisation of $V\delta 2^{\text{negative}}$ TCR mediated reactions will hopefully provide a molecular framework for the detection of further ligands, allowing for the accelerated detection of more epithelial stress-related molecules. The regulation and expression patterns of these molecules, as well information regarding how they interact with the immune system, may reveal more about how damaged tissues communicate with local immune cells, as well as revealing previously unknown characteristics of molecules which are used as stress signals, thus unveiling potentially clinically exploitable mechanisms.

In summary, several key questions remain unanswered regarding $V\delta 2^{\text{negative}}$ $\gamma\delta$ T cells, in regard to the nature of relevant TCR ligands, how they are recognised. In this thesis I aim to characterise the molecular nature of the interaction between the $V\delta 1^+$ $\gamma\delta$ TCR MAU and an epithelial stress ligand EphA2, to establish whether this interaction aligns with the general principles of $\gamma\delta$ TCR recognition discussed so far, or represents a novel recognition strategy.

I also aim to explore the potential of using various sequence-level TCR repertoire analysis techniques to analyse $\gamma\delta$ T cell populations in human tissue and blood samples, and this will include an analysis of the effect of chronic CMV infection on the receptor usage of $V\delta 1^+$ $\gamma\delta$ T cells in PB.

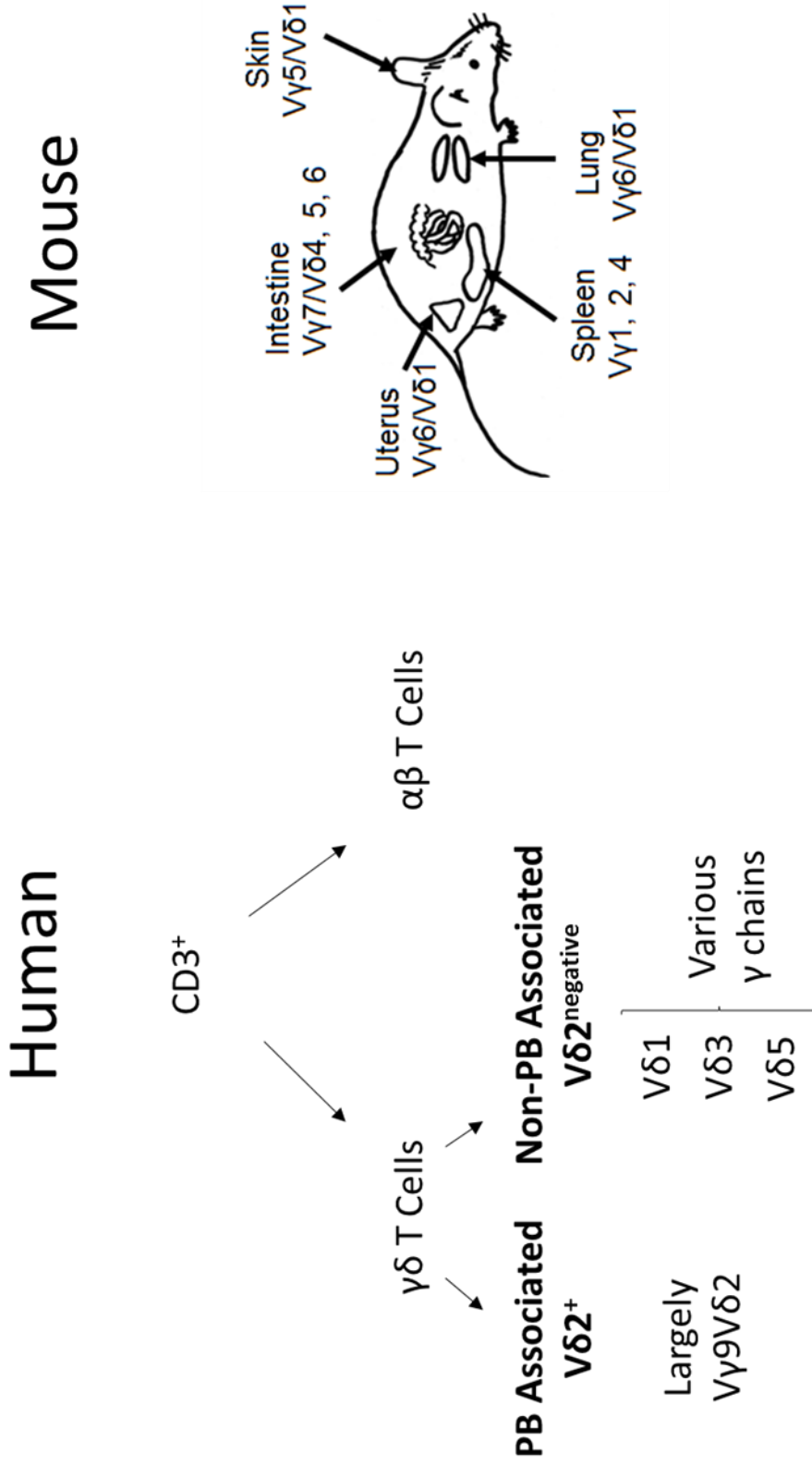


Figure 1.1: Overview of the γδ T cell subsets in mice and humans

γδ T cell subsets are well characterised in the mouse, where γδ TCRs displaying particular V region usages can reliably be mapped to distinct anatomical sites. In humans, the best-characterised subset is the peripheral blood associated Vδ2⁺ subset, which is largely populated by γδ T Cells bearing a Vγ9Vδ2 TCR. Vδ2^{negative} γδ T cells are typically associated with epithelial surfaces, and consist of Vδ1, Vδ3 and Vδ5 chains paired with various γ chains.

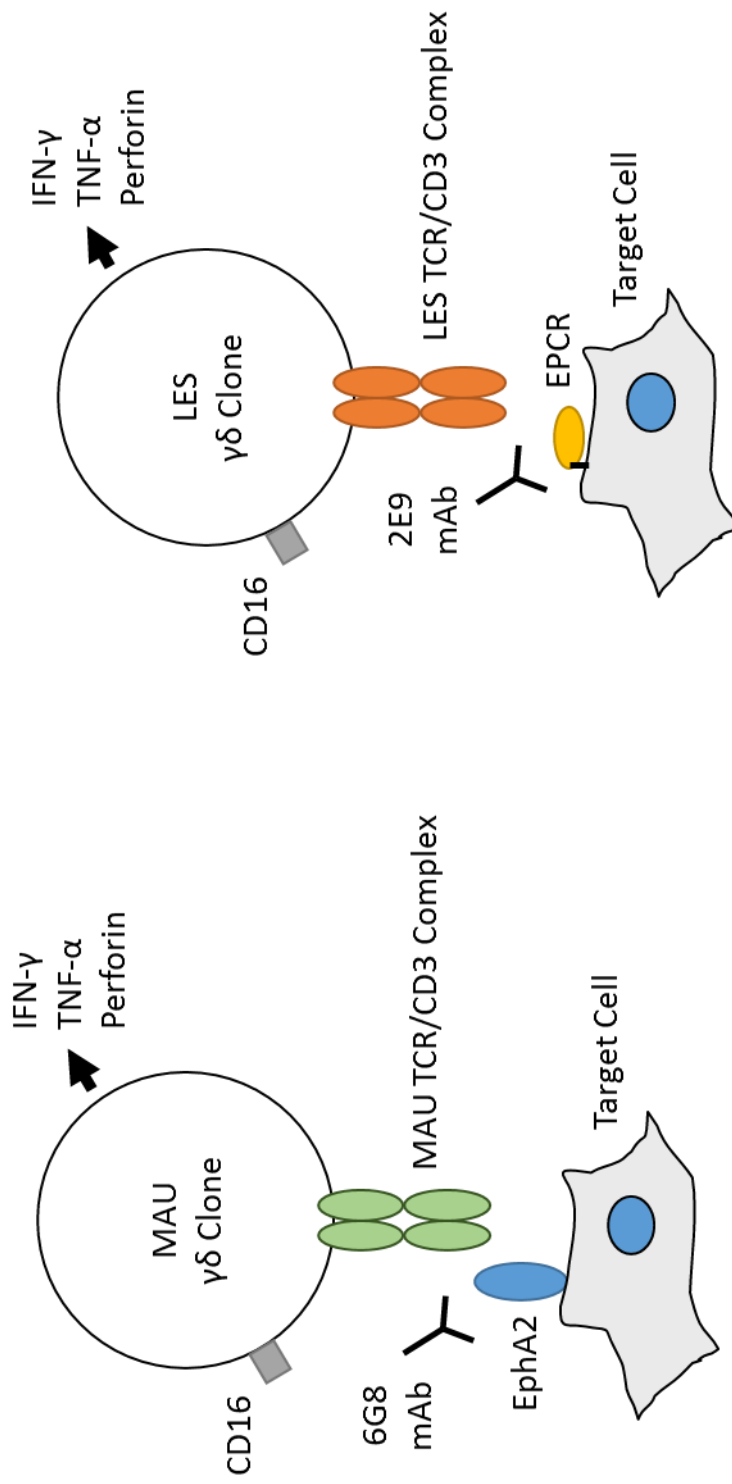


Figure 1.2: Schematic of the MAU and LES $\gamma\delta$ T cell clones and key surface molecules

Two $\gamma\delta$ T cell clones, MAU and LES, were isolated from immunocompromised renal transplant patients suffering acute CMV infection. These cells were dually reactive to both CMV infected fibroblasts and various cancer cell lines, as determined by IFN- γ , TNF- α and perforin production. Activation of MAU and LES by HT29 cells could be blocked by the addition of the mAbs 6G8 and 2E9 respectively. The proteins to which the 6G8 and 2E9 antibodies bound were determined by mass spectrometry as EphA2 and EPCR respectively, and were established as the ligands for these $\gamma\delta$ TCRs

Materials and Methods

2.1 Molecular cloning and construct design

2.1.1 Construct design and protein modelling

Where applicable, information useful for the design of recombinant proteins (such as domain boundaries) was obtained from published studies and the protein data bank (PDB). If available, protein structures were analysed using WinCoot V0.8¹¹¹ to determine the suitability of potential constructs by assessing at the surrounding amino acid environment and structural constraints.

If protein structures were not available, predictive models were generated by inputting the protein's amino acid sequence into Phyre¹¹², which predicts protein structures by comparing their primary sequence to structures with high sequence identify.

Predictive models of protein-protein interactions were generated using WinCoot¹¹¹ and PyMol V1.7 (Schrödinger). Surface electrostatics models were generated using DelPhi¹¹³. Sequence alignments diagrams were generated using PRALINE¹¹⁴.

2.1.2 Expression and shuttle plasmids

The pMT/Bip/V5-His (Invitrogen) plasmid was used for stable transfection of $\gamma\delta$ TCR genes into *D. melanogaster* S2 cells. pMT/Bip/V5-His contains a metallothionein (MT) promoter for CuSO₄ inducible expression of the gene of interest, a poly-histidine (6xHis) tag for detection and purification of the protein, and an ampicillin resistance gene (Figure 2.1A). pMT/Bip/V5-His was co-transfected with the selection plasmid pCoHygro (Life technologies), containing the bacterial hygromycin B phosphotransferase gene, under control of the constitutive *D. melanogaster* Copia 5'-LTR promoter.

pHL-Avitag3 and pHL-FcHis¹¹⁵ plasmids were used to transiently express biotin and human-Fc-tagged recombinant proteins in HEK293T cells respectively. Target genes were expressed under the chick β -actin promoter and were flanked 3' by a 6xHis tag and either a biotin ligase (BirA) recognition site sequence or a human IgG γ 1 hinge and Fc sequence. pHL plasmids also contain an ampicillin resistance gene (Figure 2.2).

pCR-Blunt (Life Technologies) was used as a blunt-ended product shuttle vector to more easily manipulate blunt ended PCR products, and contains a kanamycin resistance gene (Figure 2.1B).

2.1.3 PCR amplification and primers

Custom primers were designed for each construct and ordered desalted to 50nmol scale (Life Technologies). Primers were reconstituted in 10mM Tris pH8/1mM EDTA and stored at -20°C. Primer sequences are listed in Tables 2.1 and 2.2. The construct designs are detailed in Figures 2.3 and 2.4. Template DNA was acquired as fully sequenced cDNA clones (Thermo Scientific) and amplified by transfection into competent DH5 α *Escherichia coli* cells (Bioline). Amplified sequences were isolated using the ISOLATE II Plasmid Mini Kit (Bioline).

Polymerase chain reaction (PCR) was facilitated by either of the two proofreading enzymes Q5 (New England Biolabs) or Pfu Turbo (Agilent). PCR mixtures typically contained 200nM dNTPs (Life Technologies), 20pmols of each forward and reverse primers, 1X polymerase buffer, 2.5U of enzyme, 200ng DNA template and finally made up to 50 μ l with molecular grade water (Sigma). Thermocycling was performed using a 2720 thermal cycler (Applied Biosystems), with cycling conditions used as per manufacturer's instructions.

2.1.4 Restriction enzyme digestion

Restriction enzyme digestion of DNA was achieved with various restriction endonucleases (Figures 2.1 and 2.2, New England Biolabs) using the manufacturer recommended buffers and incubation times. Where compatible buffers and conditions unavailable for two or more enzymes for a double digest, single digests were performed sequentially. DNA was purified at each stage using the QIAquick Gel Extraction Kit (Qiagen).

2.1.5 DNA agarose gel electrophoresis and gel purification

DNA samples were diluted in 1X loading dye (40% sucrose, 0.5% bromophenol blue) and loaded into an agarose gel (1% agarose (Sigma)) in TBE Buffer (89mM Tris base, 89mM Boric acid and 2mM EDTA) with the addition of ethidium bromide for visualization by ultraviolet (UV) light. Samples were separated by size by the application of 80V across the gel until the desired separation was achieved. The 1kb plus ladder (Life technologies) was used for fragment size determination. DNA bands were extracted from the agarose gel using the QIAquick Gel Extraction Kit (Qiagen). Digital images of separations were captured using the Gene Snap platform (Syngene).

2.1.6 DNA ligation

DNA was digested by restriction endonucleases as previously described. Digested vectors were treated with alkaline phosphatase (Roche) for 30 minutes at 37°C to prevent self-ligation. Inserts and vectors with complementary cohesive ends were incubated at a ratio of 5:1 using T4 DNA ligase (Roche), in a total volume of 10µl in ligase buffer. Samples were incubated at 16°C overnight.

Blunt-ended ligation of PCR products into the pCR-Blunt vector was achieved using the Zero Blunt PCR Cloning Kit (Life Technologies) and the ExpressLink T4 DNA Ligase, as per the manufacturer's instructions. To achieve optimal efficiency, inserts were ligated overnight.

2.1.7 Site directed mutagenesis

For mutation of the MAU TCR, overlapping primers of ~42 nucleotides covering the desired mutation site were designed, with complementary base changes (1-3bp per primer set, Table 2.2). 15 pmoles of each primer was used in a PCR reaction, along with the wild type (WT) TCR template sequence, as previously described.

Amplification was achieved using the Q5 polymerase (NEB), resulting in nicked circular strands. Dpn1 (New England Biolabs) was used to digest methylated template DNA, leaving the mutated PCR product undigested. These constructs were then transformed into competent DH5 α cells (Bioline), where repair of the nicks in the mutated plasmid occurs.

To generate the EphA2^{R103E} mutant, an alternative split PCR methodology was used (Figure 2.4). To achieve this, mutant site directed mutagenesis (SDM) primers were combined with their corresponding forward or reverse primer for the WT construct and amplified, resulting in two PCR amplification products which cover the gene of interest and possessed the R103E mutation. These two amplification products were then used as the template in a further PCR, in which the forward and reverse WT primers were used to create a full length PCR product containing the mutations. This amplification product was then restricted digested and cloned as previously described.

2.1.8 Gibson assembly cloning

EphA2 domain-swap mutants were generated using the Gibson Assembly Master Mix Kit (Figure 2.3C and D, New England Biolabs). The EphA2 and EphA4 ligand binding domains (LBD) were amplified as previously described, with primers containing 20bp vector-specific overlaps for the desired vector insertion sites. pHL-Fc vectors containing either EphA2 or EphA4 sequences lacking the LBD (Δ LBD) were linearized using AgeI (New England Biolabs, Figure 2.2) and the LBD sequences were inserted as per the manufacturers instructions. Briefly, 50ng of linearized vector was combined with a 3-5 fold excess of insert DNA, 10 μ l of 2X Master Mix and dH₂O up to a total volume of 20 μ l. Samples were heated at 50°C for 15 minutes and transformed into competent DH5 α cells (Bioline) as previously described.

2.1.9 Lysogeny broth media and pouring LB agar plates

LB-EZ Mix power (Sigma) was used to make Lysogeny broth (LB) (10g in 500ml dH₂O, and autoclaved). To create LB agar plates, 7.5g of agar (Sigma) was added to the LB-EZ Mix powder prior autoclaving. For resistance selection, media was allowed to cool to 55°C and the desired antibiotic was added (Ampicillin (Sigma) 100 μ g/ml or Kanamycin (Sigma) 50 μ g/ml). The warm LB agar was then poured into petri dishes, allowed to cool to room temperature and stored at 4°C.

2.1.10 Transformation of competent bacteria

DH5 α chemically competent *E. coli* (Bioline) were thawed on ice. 10-50ng of purified DNA was added to 20 μ l of cells and incubated for 30 minutes on ice. Cells were then heat shocked for 90 seconds in a waterbath at 42°C to allow internalisation of the DNA. Immediately, 250 μ l of SOC medium (Bioline) was added, and then incubated at 37°C for 1 hour at 200 rpm to allow for expression of the antibiotic resistance genes. 100 μ l of this

suspension was then spread onto a pre-warmed agar selection plate, and incubated overnight at 37°C.

2.1.11 DNA purification

Single colonies were picked from LB-agar plates and grown in 5mls of antibiotic-containing LB overnight (37°C/200rpm). Bacterial pellets were harvested by centrifugation and the ISOLATE II Mini Kit (Bioline) was used to isolate plasmid DNA. To purify large amounts of DNA, 500ml of culture was grown overnight and, and plasmid DNA was isolated using the Plasmid Mega Kit (Qiagen). Yield and purity of the DNA was analysed by measuring $A_{260/280}$ using a spectrophotometer and agarose gel electrophoresis, as previously described. After successful cloning, constructs were validated by test digestions with restriction endonucleases to determine whether the restriction fragments match those predicted.

2.1.12 Di-deoxy terminator sequencing

DNA sequencing of clones was carried out by the Functional Genomics Facility at the University of Birmingham using the Bigdye Terminator Sequencing platform (Applied Biosystems). Sequencing histograms were analysed using the Sequencher V5.3 program (Agilent Technologies)

2.2 Eukaryotic protein production

2.2.1 Transfection of S2 *Drosophila* cells

Drosophila Schneider 2 (S2) cells were transfected with DNA constructs using the Calcium Phosphate Transfection Kit (Invitrogen). Parental (non-transfected) S2 cells were seeded at a density of 1×10^6 cells/ml in complete growth media (CGM, Schneider's *Drosophila* Medium, Modified, with L-glutamine (Lonza), supplemented with 10% FCS (Sigma)) in a 6

well tissue culture plate. Cells were incubated at 27°C until they reach a density of $2-4 \times 10^6$ cells/ml, which was typically reached after 36 hours.

Due to excessive cell death at the recommended concentrations, half the amount of DNA and reagents suggested by the manufacturer were used for transfection. 9.5µg of construct DNA was mixed with 2M CaCl₂, sterile water and the pCoHygro (Invitrogen) selection plasmid. This solution was then slowly added drop wise to HBS solution (Invitrogen), using a slow vortex, resulting in a fine precipitate forming after 40 minutes. This solution was then added drop wise to the parental S2 cells, which were then incubated for 24h at 27°C.

The following day, media was removed from the cells which were subsequently washed twice with fresh CGM. Cells were then pelleted by centrifuged at 100g for 10 minutes and replaced in the same well with fresh CGM. Two days later, cells were washed as before and replaced with CGM containing 300µg/ml of the selection agent hygromycin B (Selection media, Invitrogen). The selection media was replaced approximately every 4-5 days until cells were seen to be dividing (typically after 3-4 weeks). At this stage, cells were transferred to a 25ml tissue culture flask in 6ml of selection media.

2.2.2 Expression in S2 *Drosophila* cells

To induce protein expression, transfected cell cultured were scaled up to 500ml shaking cultures in 1L vented flasks. Cells were seeded at a density of 1×10^6 cells/ml and to prevent cell clumping 0.05% Pluronic F-68 surfactant (Life Technologies) was added. Flasks were incubated at 80rpm at 27°C. Cells were induced during their logarithmic growth phase (as determined by cell density, typically $4-10 \times 10^6$ cells/ml) by the addition of 500µM CuSO₄. Cell supernatants were then harvested after 5 days, and clarified by centrifugation, firstly at 100g for 10 minutes to pellet the S2 cells and finally at 5000g for 10minutes to pellet any

other non-soluble media components. If not being used immediately, clarified supernatant was stored at 4°C after addition of 0.02% sodium azide.

2.2.3 Transient expression in mammalian HEK293T cells

HEK293T cells were grown in DMEM + 8% FCS (Sigma) on a 10cm tissue culture dish until they reached ~90% coverage. For small-scale test expressions, cells were grown in a 6 well tissue culture plate and the recombinant construct was transfected using polyethylenimine (PEI). Prior to transfection, media was removed from the cells and replaced with Optimem (Life Technologies). 2µg of DNA and 15µg of PEI were mixed vigorously for 10 minutes in 150µl of Optimem. The transfection solution was then added drop wise to the HEK293T cells. After 5 days, the supernatant was tested for the presence of specific protein by a western blot, using an anti-C terminal poly histidine specific antibody.

For large-scale expression, cells were transferred to a 2L roller bottle in 250ml of DMEM + 8% FCS until confluence was reached. Media was then removed and replaced with 250ml DMEM + 2% FCS. The transfection solution was prepared in a similar fashion to test expressions, containing 435µg DNA, 2.7mls PEI in 27 ml of Optimem. On day 5, the supernatant was harvested and centrifuged at 5000g to remove debris. Unless being used immediately, supernatant was stored with 0.02% sodium azide at 4°C.

2.2.4 SDS-PAGE

SDS-PAGE 12.5% resolving gels (5.74ml 12.5% gel mix (0.765M Tris pH8.8, 0.2% SDS in dH₂O), 4.16ml 30% acrylamide (Geneflow), 100µl 0.1% ammonium persulphate (APS) and 4µl TEMED (Sigma)) were injected into 1mm Biorad glass cassettes. 1ml 100% isopropanol was added to level the mixture and remove any air bubbles. Once dried, the stacking gel

(3.2ml stacking gel mix (150mM Tris pH6.8 + 0.12% SDS), 40µl 0.1% APS, 4µl TEMED) was added along with a 1.0mm 10 well comb (Biorad).

Protein samples were prepared by mixing 1-10µl of protein suspension with 5X loading buffer (125mM Tris pH8, 8M urea, 10% glycerol and 6% SDS, bromophenol blue) up to a final volume of 20µl with dH₂O. 200mM DTT was also added to reducing samples. Samples were then vortexed, boiled at 95°C for 5 minutes, briefly centrifuged and then loaded onto the SDS-PAGE gel, which was inserted into an SDS-PAGE tank containing SDS-PAGE running buffer (0.1% SDS, 90g Tris and 183g Glycine). Samples were passed through the stacking gel with the application of 100V across the gel, and subsequently through the resolving gel at 180V. Proteins were visualised with Instant Blue stain (Expedion) and de-stained after 10 minutes with dH₂O.

2.2.5 Western blot

Protein samples were separated by SDS-PAGE as previously described. Proteins were transferred from the acrylamide gel to PVDF membrane (GE Healthcare) for one hour (300v/400mA) in transfer buffer (10% Ethanol, 190mM Glycine and 25mM Tris). The membrane was incubated for 1 hour at room temperature with either 5% milk or 2.5% bovine serum albumin (BSA, Sigma) to minimise non-specific antibody binding. The membrane was then washed 3 times with TBS-T (20mM Tris pH 7.5, 150mM NaCl and 0.1% Tween-20 (Sigma)). The membrane was then incubated with the primary antibody (mouse anti-C terminal poly-HIS (Invitrogen), 1:5000 dilution in 1xTBS, 0.1% Tween and 3% BSA) for 40 minutes at room temperature, before being washed a further three times with TBS-T. The secondary antibody (HRP-conjugated goat anti-mouse mAb (Sigma)) was added to the membrane in 5% milk + TBS-T (1:1000) for a further 40 minutes at room temperature.

HRP was detected using the EZ-ECL chemiluminescence kit (Biological Industries) and exposing the blot to light sensitive film (Amersham) in a dark room, which was subsequently developed.

2.2.6 Ni-NTA chromatography

Supernatants containing specific protein were placed into dialysis tubing (10kDa, Sigma) and dialysed in PBS overnight at 4°C to remove excess amino acids, which may compete for binding to the nickel beads. 1ml of nickel beads (Ni-NTA, Qiagen) was added to an Econo column (BIO-RAD) and washed with 10ml PBS + 10mM Imidazole. Dialysed supernatant was passed over the beads by gravity flow at 4°C at a rate of 1ml/minute. Afterwards the column was washed with 500ml PBS + 10mM imidazole to remove non-specific proteins, and this was determined by measuring A_{280} at various time points. Specific protein was then removed from the beads by 10ml PBS + 250mM Imidazole applied by gravity flow. Protein concentration was quantified by measuring A_{280} . To separate the protein from Imidazole, the protein solution was passed through a desalting column (GE Healthcare) and eluted into PBS.

2.3 Detection of protein binding

2.3.1 Biotinylation of proteins

Ni-NTA purified proteins expressed with a BirA recognition site were exchanged into 3ml of biotinylation buffer (100mM Tris pH7.5, 20mM NaCl, 5mM $MgCl_2$) using PD10 desalting columns (GE Healthcare). Biotinylation was achieved using 0.56mM biotin (Sigma), 1mM ATP (Sigma), 1X protease inhibitors (Roche) and BirA enzyme (non-commercial) for four

hours at room temperature. Finally, the proteins were buffer exchanged back into PBS using PD10 columns to remove excess biotinylation reagents.

2.3.2 Surface plasmon resonance overview

Surface plasmon resonance (SPR) assays were conducted using a BIAcore 3000 (GE Healthcare). All reactions were carried out at 25°C in HBS-EP buffer (10mM HEPES pH 7.4, 150mM NaCl, 3.4mM EDTA, 0.005% surfactant P20) unless otherwise stated. Data was collected at 10Hz and analysed using the BIAevaluation software (GE Healthcare).

2.3.3 Immobilisation of biotinylated proteins

Biotinylated proteins were immobilized onto a CM5 sensor chips. Briefly, the chip was normalised by the addition of 500µl BIAnormalising solution to all flow cells at a rate of 10µl/min. Streptavidin was then amine coupled to the chip at pH 5.0. 50µl of both 0.2M N-ethyl-N5 (3-diethylaminopropyl)-carbodiimide (EDC) and 0.5M N-hydroxysuccinimide (NHS) were combined and injected at 10µl/min over all flow cells. Next, 60µl of streptavidin (0.5mg/ml in 10mM sodium acetate pH 5.5) was injected, followed by an injection of 70µl of 1M ethanolamine pH 8.5 to block excess carboxy-esters on the chip surface. Finally, the chip surface was washed with 800µl of glycine-HCL pH2.5 to remove any uncoupled streptavidin. Biotinylated proteins were diluted in HBS-EP and injected over individual flow cells at a rate of 5µl/min to bind to the streptavidin. Comparable levels of proteins were immobilized onto each flow cell as measured by resonance units (RU). Reference cells were left without bound protein.

2.3.4 Immobilisation of Fc-tagged proteins

Fc-tagged proteins were immobilised using the R10Z8E9 anti human Fc monoclonal antibody. The antibody was amine coupled to a CM5 chip in an identical fashion to streptavidin, at 25 µg/ml in 10mM Na Acetate, at pH 4.5.

2.3.5 Binding studies

Analytes were stored on ice and centrifuged at 13k RPM immediately prior to use to pellet any aggregates. Depending on the experiment, analytes were either injected at one concentration or serially diluted prior to injection. Typically, analytes were injected at 10µl/min until equilibrium was reached. For antibody binding experiments, the antibody analyte was removed from the immobilised protein using Gentle Ag/Ab Binding Buffer (Pierce).

2.3.6 AlphaScreen

To detect protein-protein interactions the AlphaScreen assay was also used. The AlphaScreen IgG (Protein A) detection kit (PerkinElmer) was used, which contains Protein A coated acceptor beads and streptavidin coated donor beads. Samples were diluted in alpha buffer (12mM Tris pH 7.4, 10mM NaCl, 5mM MgCl₂, 0.1% BSA, 0.05% Tween). All readings were taken using the PHERAstar FS plate reader (BMG Labtech) with the default AlphaScreen assay settings. Samples were prepared and read in a half-area 96 well white microplate (PerkinElmer). For each experiment, proteins were either titrated within the experiment or used at concentrations identified in previous titration experiments.

Reagents were added in 10µl increments to a total volume of 40µl/well. dH₂O was used in place of samples as controls. Firstly, the Fc-tagged proteins were added to each well,

immediately followed by the biotin conjugated molecules. Plates were left to incubate at room temperature for 20 minutes, gently shaking. Donor and Acceptor beads were vortexed, pulse centrifuged at 13k rpm before being diluted into alpha buffer to a final concentration of 100µg/ml. 10µl of each bead suspension was then added to each well, resulting in a final well volume of 40µl. To ensure samples were mixed effectively, plates were centrifuged at 2000 rpm for 5 minutes, and incubated for 2 hours at room temperature under gentle agitation before being analysed

The raw emission output for each sample was then divided by the highest value of either of the single proteins on their own (with the beads), to give a signal:background ratio which accounts for inherent stickiness of the reagents.

2.4 Cellular assays

2.4.1 Flow cytometry

Flow cytometry was performed using either an LSR II (BD Bioscience) or Accuri (BD Biosciences) depending on the number of fluorophores needing to be used. Cells were stained and stored in chilled MACS buffer (Miltenyi Biotech), except for the pacific blue viability stain (Invitrogen), which was performed in PBS. Samples were also stored for up to 3 days in 1% PFA at 4°C. Unless otherwise stated, cells were stained for 20-30 minutes at 4°C and washed twice with excess, chilled MACS buffer.

Single colour controls were obtained by using anti-mouse Ig, κ/Negative control compensation particles set (Invitrogen).

Samples were collected using either FACsDiva (BD Biosciences) or the C6 Acquisition program (BD Biosciences) depending on whether the LSR II or Accuri C6 was used

respectively. All further analysis was performed on exported FCS files using FlowJo V7 (Tree Star Inc).

2.4.2 The activation assay

Flat-bottomed 96 well tissue culture plates were incubated overnight with Fc-tagged proteins at 50µg/ml in 100µl PBS (except for EphA4-Fc and OKT3 at 10µg/ml) at 4°C. The following day, wells were washed three times with PBS. JRT3.5 T cells retro-virally transduced with $\gamma\delta$ TCR genes (Described in⁷³) were added to the wells in 100µl RPMI +8% FCS at a concentration of 0.5×10^6 cells/ml and, incubated for 4 hours at 37°C + CO₂. Afterwards, cells were removed to a 96 well V-bottomed plate. Wells were washed vigorously with PBS to remove any cells adhered to the plate surface. Cells were washed 3 times with MACS buffer (Miltenyi Biotec) and stained with 5µl of anti CD69-PE (BD Biosystems) in 195µl MACS buffer for 20 minutes. Cells were then washed a further three times with MACS buffer before being transferred into sample tubes in either MACS buffer or 1% PFA if they were to be stored for up to 3 days at 4°C. Samples were then read on the flow cytometer as previously described.

2.5 $\gamma\delta$ T cell isolation from human Tissues

2.5.1 Colon

Colorectal resection patients were recruited from the Queen Elizabeth II hospital, Birmingham, UK. Informed written consent was obtained from all patients and local ethical permission (South Birmingham Local Regional Ethics Committee) was obtained prior to the study. Samples were classified as normal colon, and were resected tissue distal from the tumour site.

Samples were washed three times in RPMI media (Sigma) and vigorously shaken to remove any remaining mucous and faecal matter. Samples were then cut into $\sim 3\text{mm}^3$ pieces using scalpels. The diced samples were then incubated in 20ml CRM (RPMI, 10% FCS + streptomycin (Sigma)) with 0.1mM EDTA and 0.1mM DTT at 37°C for 20 minutes under agitation. To ensure maximum dissociation, samples were vortexed intermittently throughout the incubation. Media was then removed from the sample and stored at 4°C, and this process was repeated 5 times. The pooled media was then passed through an RPMI moistened nylon mesh (65 μm , John Stanniar) to obtain a single cell suspension. This suspension was then centrifuged at 1500 rpm and re-suspended in 10ml RPMI + 10% FCS.

The remaining tissue was washed twice with serum-free RPMI and then incubated in a similar fashion in serum-free RPMI (SF-RPMI) containing 0.5mg/ml collagenase A (Roche), for 30 minute incubations. After 4 washes, media was pooled, filtered and centrifuged as previously described.

Lymphocytes were enriched from each of the single cell suspensions by discontinuous gradient centrifugation using Percoll (Sigma). Percoll SIP was prepared by mixing 9 parts Percoll with 1 part 2.5M NaCl. Percoll SIP was then diluted to both 30% and 70% solutions using 0.25M NaCl. In a 50ml tube, 15ml of 30% SIP was gently layered over 15ml 70% SIP whilst taking care not to mix the solutions. Each of the 10ml cell suspensions was then gently layered over the Percoll gradient, and the tubes were centrifuged at 1,500 RPM for 25 minutes with the brake off, enriching lymphocytes at the 70:30 Percoll interface. The white lymphocyte cloud was then removed using a Pasteur pipette into a 50ml tube, topped up with 50ml MACS buffer and washed three times by centrifugation to remove the Percoll.

Cells were then stained with antibodies for magnetic sorting and flow cytometry analysis. Following the three MACS washes, cells were re-suspended in residual volume and stained with 10µl CD3-APC , 10µl αβ-PE (Miltenyi Biotec) and 3µl γδ FITC antibodies for twenty minutes at 4°C in the dark. Cells were then washed with an excess of MACS buffer and again re-suspended in residual volume, before addition of 20µl anti-PE microbeads (Miltenyi) and incubation for 20 minutes at 4°C in the dark. Finally the cells were washed with excess MACS buffer. 5% of pre-sorted cells were removed for flow cytometry analysis.

Magnetic separation of cells was achieved using a MidiMACS magnet (Miltenyi Biotec), with LD magnetic depletion columns (Miltenyi Biotec) as per the manufacturer's instructions. Briefly, columns were attached to the magnet and washed twice with 1ml of MACS buffer. The labelled cells were resuspended in 500µl of MACS buffer and added to the columns, and the elutant was collected. The eluted fraction was then washed in MACS buffer, with 5% of cells being kept for flow cytometry analysis. Remaining cells were then pelleted by centrifugation at 13,000 rpm with a microfuge. Supernatant was removed and the pellets were stored at -80°C. For samples to be analysed by DNA-based sequencing, genomic DNA was isolated using the QIAamp DNA mini kit as per the manufacturer's instructions. DNA samples were also stored at -80°C.

2.5.2 Liver

Liver samples were obtained from patients suffering from various non-viral liver diseases at the Queen Elizabeth II Hospital, Birmingham, UK. Written, informed consent was obtained for all patients. Samples were washed thoroughly and vigorously in RPMI (Sigma) several times to remove any mucous, contaminants and non-tissue-associated lymphocytes. Samples were then diced using scalpels into 3mm³ sections before being

washed again in RPMI, and then in 200ml of PBS. The Stomacher (Seward) apparatus was then used to dissociate the tissue fully. Briefly, RPMI was added to the liver in a 2:1 ratio (~250ml) in a Stomacher bag. The air was removed from the bag and sealed by heat using an impulse sealer. The bag was then placed in the Stomacher machine and homogenised at 230 rpm for 5 minutes (260rpm for particularly fibrous tissue).

The tissue was then filtered using an RPMI dampened nylon mesh (63 μ M, John Stanniar), and washed with PBS several times to ensure all media has passed through, resulting in a single cell suspension. This suspension was then transferred into 50ml tubes and centrifuged at 2000rpm for 5 minutes. This was repeated until the supernatant became clear. Lymphocytes were then enriched from this suspension using Lympholyte (Cedarlane Labs). 25ml of these samples was layered over 25ml of Lympholyte in a 50ml tube before being centrifuged at 800g for 20 minutes with the brake off. White blood cells were enriched at the lymphocyte interface, and were removed into PBS using a Pasteur pipette. Samples were then stained and sorted using magnetic beads as previously discussed for the colon samples.

2.5.3 Peripheral blood

Healthy lab donors, under the age of 30, were recruited from the School of Cancer Sciences, University of Birmingham, UK. Informed, written consent was obtained from all donors and ethical permission was obtained prior to the study. Peripheral blood (PB) samples (60ml) were obtained from donors, and mononuclear cells were obtained by density gradient centrifugation using Lymphoprep (Nycomed). Briefly whole blood was diluted to double volume with SF-RPMI (Sigma) and layered using Lymphoprep, before being centrifuged at 1500 rpm for 25 minutes (with minimal acceleration and no brake). To obtain plasma, the

top layer was removed, further centrifuged (1500 rpm, 10 minutes) and stored in 1ml aliquots in cryovials at -80°C.

Mononuclear cells were removed from the intermediate layer and washed 3x with RPMI + 8% FCS. Cells were counted and stored in freezing media (90% FCS, 10% DMSO, 0.45µm filtered) in ~10x10⁶ cells/1ml aliquots. Samples were stored for short term at -80°C and for longer periods in liquid nitrogen.

2.5.4 FACS and phenotyping of PBMCs

PBMCs were analysed by flow cytometry as previously described, using the antibody panels detailed in Table 2.3. FACS to isolate γδ T cell populations was conducted by Professor David Price and colleagues from the University of Cardiff.

2.5.5 CMV IgG ELISA

To determine the CMV-serostatus of donors, a CMV IgG ELISA kit was used (Biocheck) as per the manufacturer's instructions. Wells coated with lysed CMV infected cells were exposed to the plasma obtained previously to check for the presence of CMV antigen specific antibodies. After the assay, A₄₅₀ was measured using the Pherastar Fs (BMG Labtech). Donors with a CMV index of 1.0 or higher were deemed to be CMV-seropositive.

2.6 γδ T cell repertoire analysis

2.6.1 DNA-based repertoire analysis (immunoSEQ)

Recombined δ chain sequences of γδ T cells isolated from liver and colon samples were sequenced by immunoSEQ¹¹⁶ (Adaptive Biosystems). This technologies utilises a proprietary mixture of primers specific for the different variable (V) and joining (J) γ chain

recombination elements to amplify the diverse γ CDR3 regions of genomic DNA (Figure 2.5). Results were analysed using the immunoSEQ analysis software (Adaptive Biosystems), R (R Foundation for Statistical Computing) and Excel (Microsoft).

2.6.2 RNA-based repertoire analysis (Anchored 5'-RACE)

Sequencing of γ and δ chain CDR3 regions from the mRNA of $\gamma\delta$ T cells derived from the PB of healthy lab donors was conducted by Professor David Price and colleagues from Cardiff University¹¹⁷. This approach utilises template-switch anchored reverse transcription polymerase chain reaction (RT-PCR) to amplify rearranged $\gamma\delta$ TCR transcripts. Briefly, cDNA is generated from extracted mRNA using an oligo(dT) primer. The reverse transcriptase (RT) adds a short deoxycytidine (dC) sequence to the 3' end of the antisense cDNA strand, to which a SMART II oligonucleotide primer binds. The RT then transcribes the 5' section of the SMART II oligonucleotide onto the 3' end of the cDNA molecule, which acts as an anchor for specific amplification (Figure 2.6).

Touchdown PCR is then performed on the single cDNA strand using a combination of $\gamma\delta$ C region specific and anchor-complementary primers. These amplification products are then sub-cloned into cloning vectors and transformed into competent *E. coli*. Finally, plasmids from individual colonies are then sequenced.¹¹⁷ Results were analysed using R (R Foundation for Statistical Computing) and Excel (Microsoft).

2.7 Tables

Primer Identifier	Sequence (5' -> 3')
572	CCGG ACC GGT GAA GTG GTA CTG CTG GAC TTT GCT GC
573	CGG GGT ACC GTT GCC AGA TCC CTC CGG G
615	CCGG ACC GGT AAG AAG TGC CCC GAG CTG CTG
617	CCGG ACC GGT GTC ACA GGT TCC AGG GTA TAC
618	GTAC CGT ACG TGT GGA GTT AGC CCC ATC TCC
677	CCGG ACC GGT TGT CCA CTC ACA GTC CGC AAT C
684	GGG TTG CGT AGC TGA AAC CGG TGA AGT GGT ACT GCT GGA CTT TGC
688	GGG TTG CGT AGC TGA AAC CGG TGT CAC AGG TTC CAG GGT ATA CC
689	GCA GCT CGG GGC ACT TCT TAC CGG TTT TAT AGA ACA CAC GGA CTG ATA CC
692	GCG GAC TGT GAG TGG ACA CTT ACC GGT CTT GTA GTA GAC ACG GAC GGA G

Table 2.1: Primers used for the amplification of ephrin receptor constructs

Primer identifier corresponds to the primers in the overview of the constructs (Figures 2.3 and 2.4). Blue = Restriction endonuclease overhangs. Red = AgeI or KpnI restriction sites.

Chain	CDR	Round	F/R	Primer I.D	Sequence	
V γ 9	CDR1	1	Forward	619	5' GTGGTGTCTGGAATAACACGTTCTGCAACATCTGTATATTGG 3'	
			Reverse	620	5' CCAATATACAGATGTTGCAGAACGTGTTATTCCAGACACCAC 3'	
		2	Forward	621	5' GGTGTCTGGAATAACACGTTATGAAACATCTGTATATTGGTATCG 3'	
			Reverse	622	5' CGATACCAATATACAGATGTTTCATAACGTGTTATTCCAGACACC 3'	
		3	Forward	623	5' GGTGTCTGGAATAACACGTTATGAAAAATCTGTATATTGGTATCG 3'	
			Reverse	624	5' CGATACCAATATACAGATTTTTTCATAACGTGTTATTCCAGACACC 3'	
	CDR2	1	Forward	625	5' CAGTTCCTAGTGTCCATTCTATCTGACGGCACTGTCAGAAAAGG 3'	
			Reverse	626	5' CCTTCTGACAGTGCCGTCAGATAGAATGGACACTAGGAACTG 3'	
		2	Forward	627	5' CTAGTGCCATTCTATCTAACGGCCTTGTCAGAAAAGGAATCCGG 3'	
			Reverse	628	5' CCGATTCTTTCTGACAAGGCCGTTAGATAGAATGGACACTAG 3'	
	CDR3	1	Forward	629	5' CTGTGCCTGTGGGAGGTGTGGCGTGTGAGAACTCTTTGGCAG 3'	
			Reverse	630	5' CTGCCAAAGAGTTTCTCAACACGCCACACCTCCACAAGGCACAG 3'	
		2	Forward	631	5' CTGTGCCTGTGGGAGGAGTGGCGTGATGAGAACTCTTTGGCAG 3'	
			Reverse	632	5' CTGCCAAAGAGTTTCTCATCACGCCACTCTCCACAAGGCACAG 3'	
	V δ 1	CDR1	1	Forward	633	5' GAACTGCCTGTATGAAACACGTTGGCGGTCATATTATATTTTTTG 3'
				Reverse	634	5' CAAAAAATATAATATGACCGCAACGTGTTTCATACAGGCAGTTC 3'
			2	Forward	635	5' GAACTGCCTGTATGAATCACGTTTCGCGGTCATATTATATTTTTTG 3'
				Reverse	636	5' CAAAAAATATAATATGACCGCGAACGTGATTCATACAGGCAGTTC 3'
3			Forward	637	5' GAACTGCCTGTATGAATTACGTTTCGCGGTCATATTATATTTTTTG 3'	
			Reverse	638	5' CAAAAAATATAATATGACCGCGAACGTAATTCATACAGGCAGTTC 3'	
CDR2		1	Forward	639	5' GATTTTCCTTATTCGCCGGGTTCTCGTGAACAGAATGCAAAAAG 3'	
			Reverse	640	5' CTTTTTGCACTTCTGTTACAGAGAACCCCGCGAATAAGGAAAATC 3'	
		2	Forward	641	5' GATTTTCCTTATTCGCTGGGGTTATCGTGAACAGAATGCAAAAAG 3'	
			Reverse	642	5' CTTTTTGCACTTCTGTTACAGATAACCCAGCGAATAAGGAAAATC 3'	
		3	Forward	643	5' GATTTTCCTTATTCGCTGGGGTTATCGTAAAACAGAATGCAAAAAG 3'	
			Reverse	644	5' CTTTTTGCACTTCTGTTACGATAACCCAGCGAATAAGGAAAATC 3'	
CDR3		1	Forward	645	5' GGGGACCTTACCGGCGTACCTATCCTCAACAACTCATCTTTGG 3'	
			Reverse	646	5' CCAAAGATGAGTTTGTGAGGATAGGTACGCCGTAAGGTCCCC 3'	
		2	Forward	647	5' GGGGACCTTACCGGCGAACCTAAGCTCAACAACTCATCTTTGG 3'	
			Reverse	648	5' CCAAAGATGAGTTTGTGAGCTTAGGTTCCGCCGTAAGGTCCC 3'	

Table 2.2: Primers for site directed mutagenesis of the MAU TCR CDR loops

Each forward and reverse (F/R) primer pair was used in combination for each round of SDM, which were performed sequentially. Each mutant contained one mutated CDR.

	Antibody	Source	Dilution	$\mu\text{l}/10^6$ Cells
$\gamma\delta/\alpha\beta$	$\alpha\beta$ -FITC	BD Biosciences		10
	$\gamma\delta$ -PE	Beckman Coulter		7
	CD3E-APC	Invitrogen	1:10	2
	Viability-Pacific Blue	Invitrogen		1
FACS	V δ 2-FITC	Biolegend	1:10	3
	$\gamma\delta$ -PE	Beckman Coulter		7
	CD3E-APC	Invitrogen	1:10	2
	Viability-Pacific Blue	Invitrogen		1
Phenotyping	V δ 1-FITC	Thermo Fisher		3
	V δ 2-PE	Biolegend	1:10	1
	V γ 9-PE-Cy5	Beckman Coulter	1:10	1
	CD3E-APC	Invitrogen	1:10	2
	Viability-Pacific Blue	Invitrogen		1
	CD45RA AF700	Biolegend	1:10	1
	CD27-APC-Cy7	eBioscience		2
	CD16 PE-Cy7	Biolegend	1:10	3

Table 2.3: Antibodies used to stain and phenotype PBMCs

PBMCs were stained with one of three panels, ' $\gamma\delta/\alpha\beta$ ', 'FACS' or 'Phenotyping'. Volume of reagent used to stain 1×10^6 cells is listed in the right-most column. If stock solutions were diluted with MACS buffer prior to use, the dilution ratio is shown in the 'Dilution' column.

2.8 Figures

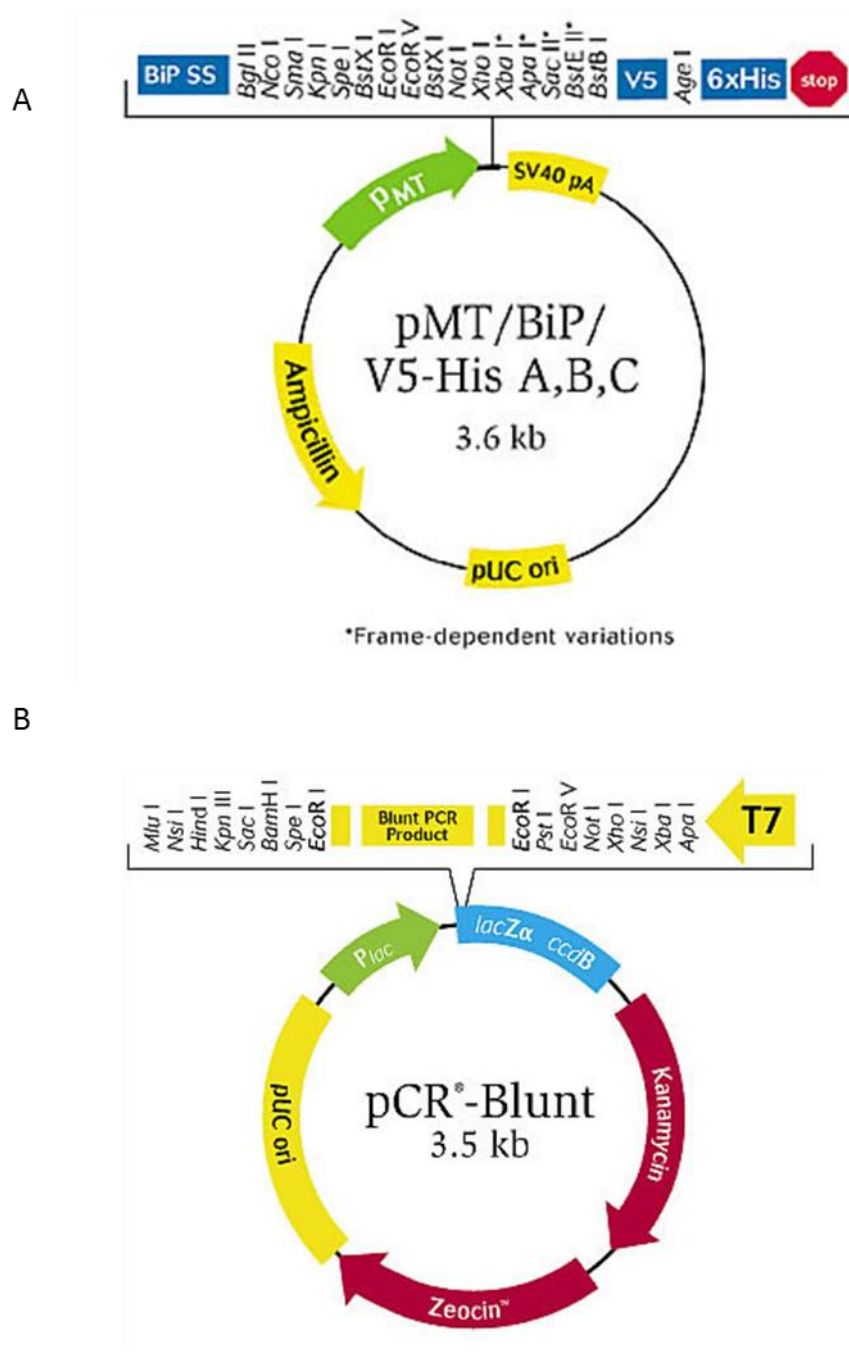


Figure 2.1: Maps of vectors used in transfection and cloning experiments

(A) The pMT/Bip/V5-His (Invitrogen) vector was used to transfect *Drosophila melanogaster* S2 cells with recombinant $\gamma\delta$ TCR constructs for protein expression. (B) pCR-Blunt was used as a shuttle vector for the cloning of recombinant constructs.

Images provided by¹¹⁸.

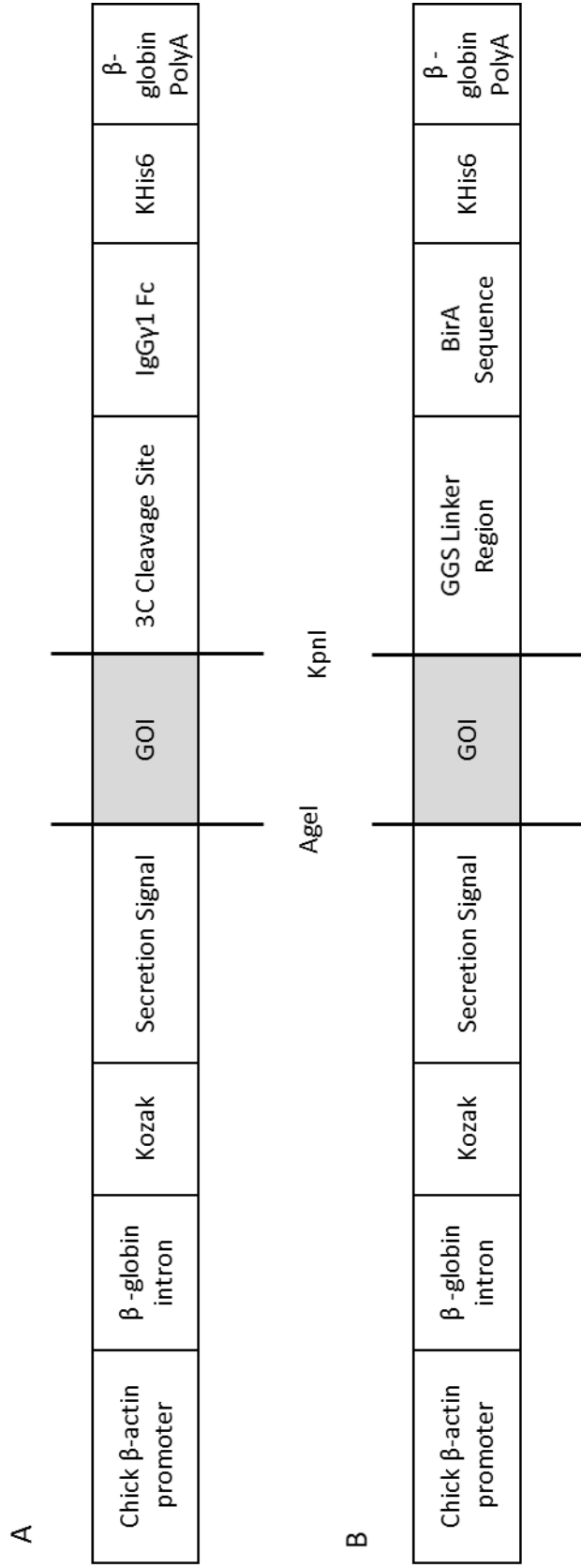


Figure 2.2: Maps of the pHL-FcHis and pHL-Avitag3 expression vectors

Vector maps for the pHL-FcHis (A) and pHL-Avitag3 (B) vectors used for the transfection of HEK293T cells with recombinant ephrin receptor constructs. Constructs (GOI) were cloned into the vectors using the AgeI and KpnI restriction sites.

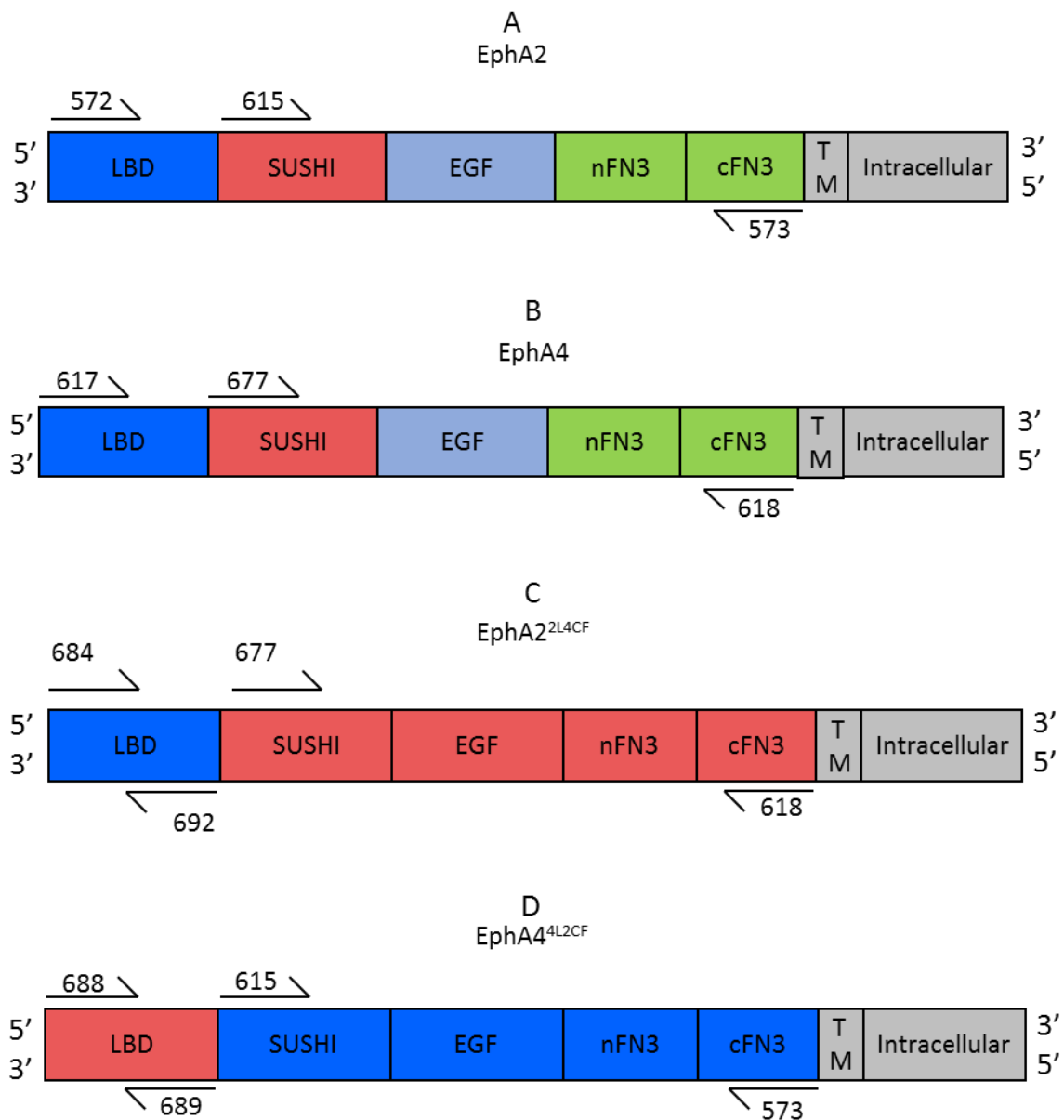


Figure 2.3: Primers used for the generation of ephrin receptor constructs

The three digit primer reference refers to primers used for PCR amplification of ephrin receptor constructs, as shown in Table 2.1. (A) EphA2^{WT} (572) and EphA2^{ΔLBD} (615) forward primers were paired with the 573 reverse primer. (B) EphA4^{WT} (617) and EphA4^{ΔLBD} (677) forward primers were paired with the 618 reverse primer. (C+D) EphA2 LBD swap mutants were generated by combining LBD sequences with ΔLBD sequences using the Gibson assembly methodology. Blue domains are derived from EphA2, and Red domains are derived from EphA4.

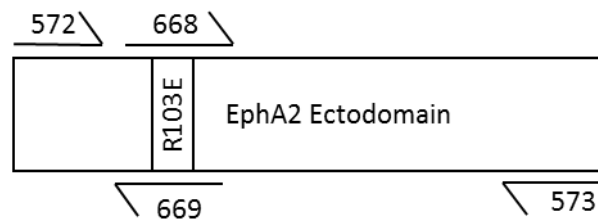


Figure 2.4: Cloning of the EphA2^{R103E} mutant

The EphA2R103E mutant was generated using a split PCR methodology. Primers containing the desired R103E mutation (668 and 669, Table 2.1) were paired with the corresponding forward and reverse EphA2WT construct primers to generate two PCR products. These products were then combined and used as a template in another PCR using the EphA2 WT forward and reverse primers, yielding a full length amplification product containing the R103E mutation.

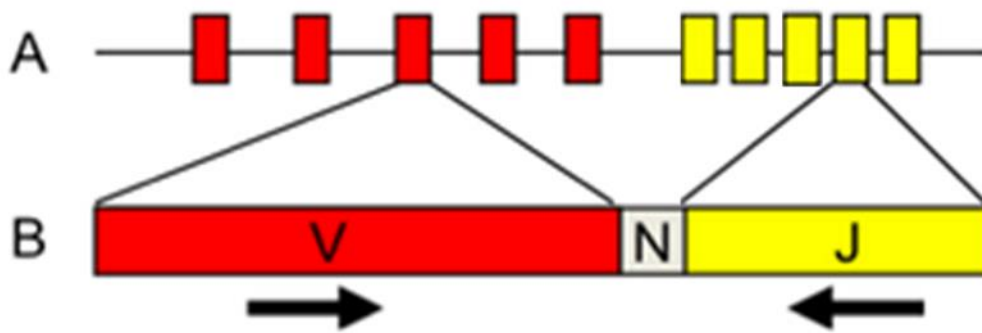


Figure 2.5: Overview of the immunoseq TCR sequencing methodology

(A) Multiple V_γ and J_γ gene segments exist in the germline γ TCR locus. (B) These gene segments recombine during development to produce a single V-J combination. Additional, non-template diversity is introduced at the junctions by insertion of random nucleotides (N). immunoseq utilise a combination of primers specific for different V and J gene segments to selectively amplify the V-J junction, which is then sequenced. Figure provided by immunoseq.

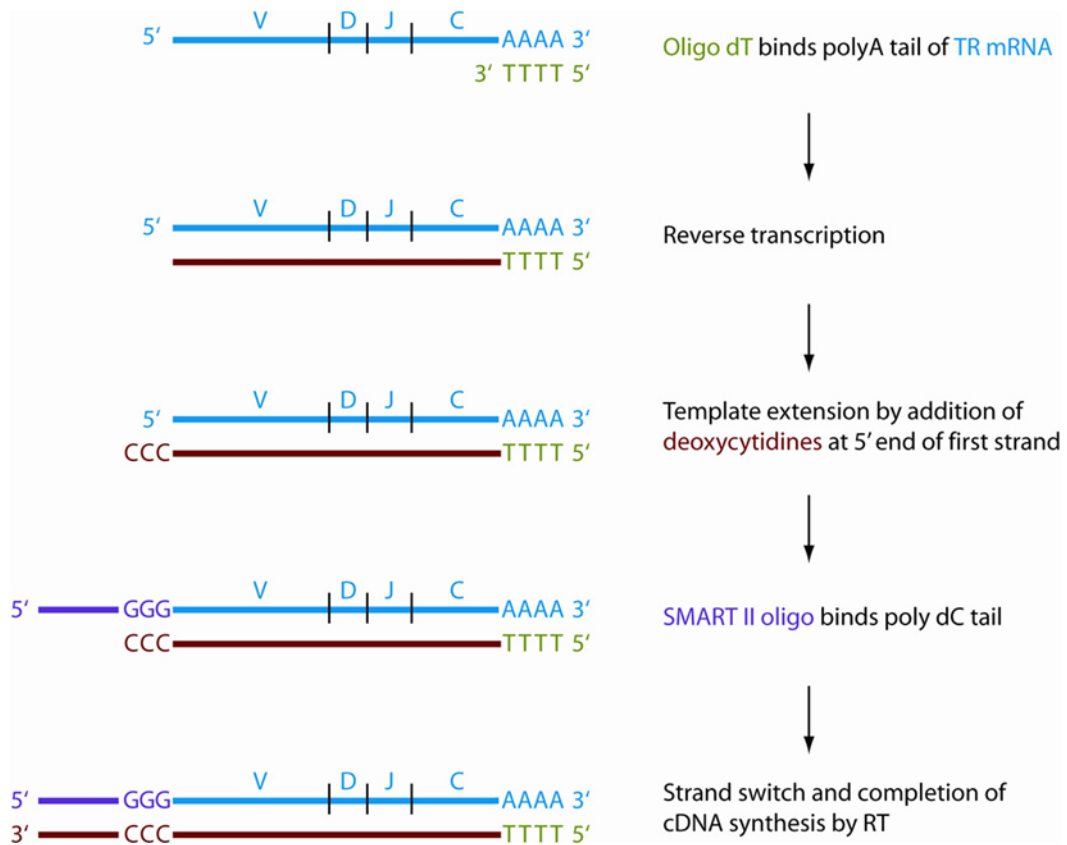


Figure 2.6: Schematic representation of the Anchored RACE PCR

An Oligo dT primer is used to initiate the reverse transcription of mRNA transcripts. The terminal transferase activity of the reverse transcriptase (RT) results in the addition of a short deoxycytidine (dC) sequence to the 3' end of the antisense cDNA chain. The SMART II oligo primer binds to this sequence, and the RT transcribes the 5' section of the SMART II oligo to the 3' end of the antisense cDNA strand. C γ and C δ specific primers are used in conjunction with an anchor-complementary primer (i.e. the 3' region) to amplify the TCR chains.

Image adapted from¹¹⁷

3

Establishing the Molecular Requirements for the Recognition of EphA2 by MAU T cells

3.1 Introduction

$\gamma\delta$ T cells contribute towards immunoprotection and the maintenance of epithelial integrity as part of the lymphoid stress surveillance compartment⁸. Despite their implications in a range of immunological responses, including cancer immunosurveillance²⁰, there is limited molecular data with respect to how $\gamma\delta$ T cells interact with target cells.

Typically, T cells interact with target cells using a combination of surface molecules which collectively provide multiple signals, both antigen specific and non-specific, which contribute towards initiating a signalling cascade, resulting in relevant effector functions¹¹⁹. Specificity is usually conferred by the TCR, an antigen-specific receptor which is produced by somatic recombination events, although alternative TCR independent mechanisms have been described for $\gamma\delta$ T cells⁶⁰.

In $\alpha\beta$ T cells, which constitute the majority of the adaptive arm of the immune system, the primary signal is initiated by the binding of TCR to peptide-MHC complexes. This primary signal is enhanced by secondary signals provided by non-antigen-specific co-receptors, which simultaneously bind the MHC molecule. The role of co-receptors has not been well defined in $\gamma\delta$ T cells¹²⁰, and their relevance to the activation of $\gamma\delta$ T cells as a whole is unclear.

This comprehensive knowledge of both the molecular nature of the interaction of $\alpha\beta$ T cells with their targets and the signalling apparatus involved has led to the development of a wide array of biomolecular and cellular techniques which have rapidly accelerated the understanding of $\alpha\beta$ T cell biology. For example, the use of MHC tetramers¹²¹ has only been possible due to an in depth molecular understanding of the $\alpha\beta$ TCR recognition events.

If similar paradigms were established for $\gamma\delta$ T cells, it could facilitate comparable advances in the understanding of $\gamma\delta$ T cell immunobiology, potentially bridging the knowledge gap between the two fields. This could lead to new immunotherapeutic strategies utilising $\gamma\delta$ T cells which, unlike $\alpha\beta$ T cells, are not restricted to specific MHC-haplotypes, and so could be used more broadly.

Previous studies from our group and collaborators have identified EphA2 as a potential ligand for a V δ 2^{negative} $\gamma\delta$ T cell clone called MAU. MAU (also known as clone 5-4) was derived from a CMV-seropositive renal transplant patient, following polyclonal stimulation and cloning by limiting dilution⁷³. The MAU clone responded to CMV-infected fibroblast and various cell lines. EphA2 was identified as a potential ligand by using blocking antibodies to immunoprecipitate the ligand from activating cell lysates.

EphA2, a member of the ephrin receptor family of receptor tyrosine kinases (RTK), has been implicated in a range of biological processes, including the initiation and progression of several cancers⁷⁵. This suggests that EphA2 is a highly plausible candidate as a stress ligand for recognition by the immune system. Indeed, EphA2 has been targeted in a range of immunotherapeutic strategies, such as targeting glioblastoma with EphA2-specific chimeric antigen receptors (CARs) in pre-clinical models, with promising results¹²². Understanding how the immune system interacts with such biologically important molecules is therefore important, especially as no interaction has previously been characterised between an immune receptor and ephrin receptors, and so this may represent a completely novel interaction modality.

The aim of this chapter is to establish the broad criteria for the recognition of EphA2 by MAU, and define the molecules involved. Improved understanding of the surface molecules

involved is vital in order to fully comprehend the nature of this potentially important recognition of an epithelial stress ligand by a V δ 2^{negative} $\gamma\delta$ T cell.

3.2 Results

3.2.1 Plate bound EphA2-Fc is sufficient to activate JRT MAU

Both $\alpha\beta$ and $\gamma\delta$ T cells are typically activated via their TCR, and so it was important to determine whether MAU is activated by EphA2 in this way. To achieve this, JRT3-T3.5 (JRT3) cells were established by our collaborators which had been transduced with various TCR genes using a lentiviral transduction system¹²³. JRT3 cells are a derivative of the Jurkat $\alpha\beta$ T cell leukaemia cell line, which contain a mutation in the β chain locus, and therefore do not natively express a TCR complex at the cell surface¹²⁴. Once these cells become activated via their TCR, they signal through the CD3 complex and express CD69, an early T cell activation marker⁶². Since JRT3 cells are less dependent on other activatory and costimulatory receptors than primary T cell clones, any observable activation should be largely dependent on the TCR.

To determine whether the interaction of EphA2 with MAU is TCR dependent, the MAU TCR was isolated in the JRT3 cell line, and exposed to EphA2. Recombinant EphA2 protein expressed with a human Fc-tag (EphA2-Fc, R&D Systems) was immobilised on a 96 well plate, and the JRT3 cells transduced with either the MAU or control TCR (LES, a V γ 4V δ 5 TCR) were incubated in the plate for 4 hours. JRT3 activation was then measured by detecting surface expression of CD69 by flow cytometry. This technique is referred to throughout this thesis as the “activation assay”. OKT3, an anti-CD3 ϵ monoclonal antibody which activates TCR transduced JRT3 cells was used as the positive control in these

experiments. Plate bound EphA2-Fc was sufficient for activation of JRT MAU (Figure 3.1). In contrast, JRT3 cells transduced with either the LES (Figure 3.1) or a range of other $\gamma\delta$ TCR genes (data not shown) failed to be activated by EphA2-Fc. This showed that the recognition of EphA2 by MAU is TCR mediated, as recognition could be specifically conferred to JRT3 cells by transducing MAU TCR genes. These experiments also demonstrated that the costimulatory ligands or adhesion molecules on the surface of the stressed cell are not necessarily required for EphA2 mediated activation of JRT MAU. EphA4, a fellow ephrin receptor family member which is structurally homologous to EphA2 (77% sequence similarity¹²⁵) failed to activate JRT MAU (Figure 3.1), highlighting that this interaction is not applicable to all ephrin receptors.

3.2.2 Production of recombinant EphA2-Fc using 293T cells

It is important when using recombinant proteins to ensure reproducibility between various protein sources. For example, protein misfolding and contamination can occur during protein production, which may impact downstream experiments¹²⁶. Furthermore, verification that EphA2 constructs could be reliably produced in our laboratory was essential in order to plan EphA2 mutagenesis approaches later in this study. For this reason, the activation assay was repeated with both commercially available EphA2-Fc from R&D Systems used in the preceding section (R&D EphA2-Fc), which was produced from an NS0-derived mouse myeloma cell line, and EphA2-Fc produced in the Willcox laboratory by transient transfection of human HEK 293T cells (293T EphA2-Fc).

The 293T expression system provides a protein production and folding pathway very similar to that undertaken by proteins *in vivo* in humans, rendering it more physiologically relevant than non-mammalian production systems¹¹⁵. For example, bacterial expression systems

lack glycosylation machinery, and insect cells generate only simple glycosylation compared to mammalian cells, and so the glycosylation signature of recombinant proteins produced in these systems would not necessarily represent what is present physiologically¹²⁷. To ensure a representative comparison, the negative control protein EphA4-Fc was also obtained from both sources.

The EphA2 ectodomain is 507 residues long and comprised of 5 globular domains. The ligand binding domain (LBD) is a 172 residue domain at the N terminus of EphA2 which is responsible for binding the A-ephrin ligands of EphA2. To the C terminus of the LBD is a Sushi domain followed by an EGF domain, which collectively form a cysteine rich domain (CRD). Finally, two membrane proximal fibronectin domains (FN1 and FN2) are located at the C terminus (Figure 3.2A+B)⁸⁰. The cytoplasmic region of EphA2 contains several signalling domains, including a kinase domain. EphA2 and EphA4 ectodomain constructs were designed using a combination of domain prediction features of the UniProt tool¹²⁸ and existing construct information which has been used to clone these constructs successfully in the literature⁸⁰. Based on this data, the N-terminal residues G25 and N26 of the R&D EphA2-Fc construct were omitted from the 293T EphA2-Fc construct (E27-N534) (Figure 3.2C). The 293T EphA4-Fc construct incorporated residues V20 to N529 (Figure 3.2C). Inserts were cloned into the pHL-Fc vector (which contains 6His- and a human IgG Fc-tags)¹¹⁵ and used to transfect HEK 293T cells. His tagged EphA2-Fc was then purified using Ni-NTA chelate chromatography.

3.2.2.1 Verification of EphA2-Fc folding

In order to verify that the 293T-derived EphA2 was folded in its native state, several approaches were used. Establishment of reliable techniques to measure 293T EphA2

folding was crucial in order to confidently appraise folding of EphA2 mutants produced later in the study.

Superficially, early indicators of successful folding can be determined during the protein purification process. For example, a well expressed protein hints at correct folding, since protein accumulating in the cytoplasm is an indicator of misfolding as the protein enters the cellular recycling machinery. Using HEK 293T cells, high levels of EphA2-Fc expression were observed at day 5 post transfection (Figure 3.3A). Other approaches, such as a comparison between reduced and non-reduced samples on SDS PAGE gels, ensure proteins are migrating correctly for their predicted sizes, and dimerising in the correct fashion. For example, reduced EphA2-Fc samples derived from Ni-NTA purification migrated at approximately 100kDa, higher than its predicted monomer size of 83kDa (53kDa EphA2 + 30kDa Human IgG γ 1) (Figure 3.3B). This difference between observed migration and that predicted from the primary sequence suggests that EphA2 is glycosylated in some capacity. Interestingly, this was also observed with the NS0-derived R&D EphA2-Fc (Figure 3.3B) and is highlighted on the product specification. In contrast, the non-reduced EphA2-Fc sample migrated at approximately twice the size of the reduced sample, consistent with an EphA2-Fc dimer facilitated by the Fc-tag. Purity of EphA2-Fc produced in this system was high, with no discrete contaminant bands visible by SDS PAGE (Figure 3.3B). Typical yields of EphA2-Fc eluted from the Ni-NTA column were 1.5mg from 250ml of supernatant (Figure 3.3B). The non-reducing sample of R&D EphA2-Fc contained several contaminant bands, likely protein degradation products resulting from long term storage. These bands were not present in the 293T EphA2 sample. 293T EphA4-Fc purification was equivalent to 293T EphA2-Fc (data not shown).

A more robust method to determine correct protein folding was to analyse 293T EphA2-Fc with quantifiable approaches. Firstly, binding of an anti-EphA2 goat IgG polyclonal antibody (pAb, R&D Systems) to EphA2-Fc was measured by surface plasmon resonance (SPR) using the BIAcore platform. SPR measures changes in protein concentration via alterations in refractive index adjacent to a sensor surface, with measurements given in resonance units (RU). Typically, antibodies specifically recognise tertiary structure epitopes on proteins, and therefore their binding would indicate correct folding, at least in the domain containing the specific epitope. pAbs are less suited for this approach however, as they can also contain antibodies specific for short secondary structure sequences, which do not require native folding for binding. However, as a comparison between identical proteins this approach can still provide useful information on folding.

To test the binding of the anti-EphA2 pAb to 293T EphA2-Fc, a CM5 BIAcore chip was coated with R10Z8E9 (a mouse monoclonal antibody (mAb) specific for the human Fc fragment¹²⁹) by amine coupling (Figure 3.4). 293T EphA2-Fc and control proteins were then immobilised on the R10Z8E9 coated chip in individual flow cells (Figure 3.5A). The anti-EphA2 pAb was subsequently injected over the chip as the analyte. These experiments showed that the anti-EphA2 pAb bound to both 293T and R&D-derived EphA2-Fc constructs (Figure 3.5B), suggesting that 293T EphA2-Fc is correctly folded. Interestingly, the 293T EphA2-Fc bound approximately 150 RU more anti-EphA2 pAb than the R&D construct. This observation could be due to the different mammalian expression systems used to produce the two constructs, or that the R&D protein was purchased over a year previously, and so may have degraded whilst in storage. Indeed, evidence for the latter can be observed in Figure 3.3B, which shows nonspecific bands in the non-reducing sample of R&D EphA2-Fc, which may represent protein degradation products.

The second quantitative analysis of correct protein folding was to determine whether the 293T EphA2-Fc was able to bind its natural ligands, A-ephrins. EphA2 binds A-ephrins with nM affinity⁷⁷, and requires the presence of a hydrophobic binding pocket in the LBD⁸², therefore it can be assumed that if 293T EphA2-Fc successfully binds ephrins, it is correctly folded. Initially, BIAcore was attempted in order to demonstrate successful binding of 293T EphA2 to ephrinA1. In these experiments, ephrinA1-Fc was injected over the immobilised ephrin receptors. However, since it has proven difficult to produce non-Fc-tagged ephrinA1 in the 293T system (data not shown), the analyte also bound the R10Z8E9 antibody. In order to circumvent this, two approaches were employed. Firstly, the R10Z8E9 coated CM5 chip was saturated with receptor protein. Despite these efforts, binding of ephrins to the negative control cells were observed, suggesting ephrinA1-Fc bound to R10Z8E9. Secondly, irrelevant ephrinB1-Fc (which does not bind EphA2) was used to saturate the chip prior to ephrinA1-Fc injection. This approach also yielded an increase in RU on the control flow cell, demonstrating that ephrinA1-Fc was still binding the R10Z8E9 coated on the chip (data not shown).

As an alternative to BIAcore, ephrin binding by 293T EphA2-Fc was determined by surface staining of JRT3 cells, which are known to express ephrins A1 and A4 (J Déchanet-Merville, unpublished). 293T and R&D-derived EphA2-Fc were used to stain the surface of JRT MAU and the Fc-tag was bound by an AF488 conjugated goat anti-human Fc secondary antibody (eBioscience), which was detected by flow cytometry. 293T EphA2-Fc was able to stain the surface of JRT MAU at equivalent levels to R&D EphA2-Fc (Figure 3.6). The secondary antibody alone was used as an isotope control. Similarly, 293T EphA4-Fc stained JRT LES cells at equivalent levels to the commercial R&D counterpart (data not shown).

To verify that this staining was not as a result of the EphA2/MAU TCR interaction, 293T EphA2-Fc was used to assess whether it could stain JRT LES, a clone that is not activated by EphA2. These results highlighted that 293T EphA2-Fc stained JRT LES at equivalent levels to JRT MAU and thus demonstrating that staining is not TCR specific (Figure 3.6B). Furthermore, 293T EphA4-Fc, which does not activate either JRT MAU or LES, stains both cell types equivalently (Figure 3.6B). Finally, previous experiments in our laboratory using PI-PLC to cleave GPI-linked A-ephrins from JRT MAU and LES completely abrogated staining by both EphA2-Fc and EphA4-Fc, confirming that staining is not mediated by the TCR, and demonstrating that 293T EphA2 successfully binds surface ephrins. Collectively, the BIAcore and surface staining experiments showed that 293T EphA2-Fc is correctly folded; as it was bound by an EphA2 pAb and recognised its cognate ligands equivalently to commercial R&D EphA2-Fc.

Finally, further verification was achieved with the activation assay as 293T EphA2-Fc activates JRT MAU to the same extent as R&D EphA2-Fc (Figure 3.7). Non-Fc-tagged EphA2 (EphA2-Avi, cloned into the pHL-AviTag vector), which was also produced in the 293T expression system, activated JRT MAU equivalently to the Fc-tagged constructs, demonstrating that activation is not dependent on Fc-tag mediated EphA2 dimerization (Figure 3.7). Collectively, these data revealed that activation is not an artefact of a specific protein production batch or methodology, and is reproducible with a range of verified protein sources. Furthermore, 293T production of EphA2 mutants is a viable approach for future experiments. For all subsequent experiments, 293T EphA2-Fc and EphA4-Fc were used, and will be referred to as EphA2-Fc and EphA4-Fc respectively.

3.2.3 No binding detected between MAU TCR and EphA2 using BIAcore.

Since EphA2-Fc is sufficient for activating JRT MAU in a TCR dependent manner, this strongly implied that the MAU $\gamma\delta$ TCR specifically recognises EphA2. In order to unequivocally demonstrate that the MAU TCR forms direct contacts with EphA2, the subsequent step was to show direct binding between these two molecules.

BIAcore has previously been used to successfully demonstrate binding between $\gamma\delta$ TCRs and their ligands^{51,123}, and is a useful tool for quantifying molecular interactions, including those of low affinity. To test for binding, recombinant MAU TCR protein was produced using the *Drosophila* S2 expression system¹³⁰. Soluble TCRs are historically difficult to produce, and mammalian expression systems like 293T have largely been ineffective¹³¹. Despite not being as physiologically comparable as the 293T expression system, TCRs can be produced in relatively large amounts using this *Drosophila* system. The γ and δ chain of MAU were separately cloned into pMT/Bip/V5-His vectors, which contain either acidic or basic leucine zipper motifs to facilitate heterodimeric chain pairing¹³² (Figure 3.8). These constructs were then transfected into S2 *Drosophila* cells, and the supernatant was harvested after 5 days. The protein was then purified using Ni-NTA chelate chromatography, which binds the His tag on each chain. Yields were typically around 1.5mg from 1L of S2 supernatant (Figure 3.9A). SDS-PAGE analysis of fractions eluted from the Ni-NTA column revealed two discrete bands at approximately 45kDa each. These bands migrated higher than would be predicted from their primary sequence (33.6 kDa and 34.4 kDa for the γ and δ chains respectively), which suggested the TCR is glycosylated. Purity of TCR obtained varied between protein batches, with a mixture of high and low molecular weight contaminants. Under non-reducing conditions, the MAU γ and δ chains revealed a single band which migrated at

approximately 90kDa, suggesting the formation of a $\gamma\delta$ dimer. At this stage however, it was not possible to establish if this was a heterodimeric TCR, as the molecular weight of the γ and δ chains are similar, and the 90kDa band in the non-reducing sample may represent a homodimer (Figure 3.9A).

The purified MAU TCR was biotinylated using the BirA enzyme in the presence of biotin and ATP, which acts on the BirA signal sequence engineered onto the C terminus of the δ chain¹³³. Biotinylation was confirmed by western blot, using HRP-conjugated streptavidin (Figure 3.9B).

To confirm that the TCR chains were folded correctly, and dimerising to form a $\gamma\delta$ TCR heterodimer, BIAcore was used to measure binding of V γ 9, V δ 1 (both Beckman Coulter) and pan- $\gamma\delta$ (BD Biosystems) specific mAbs to the purified recombinant protein. A CM5 BIAcore chip was coated with streptavidin by amine coupling (Figure 3.10A), and biotinylated MAU-TCR (MAU-Bt) and control proteins were immobilised to individual flow cells. Protein levels were standardised to around 2000 RU for consistent analysis across samples (Figure 3.10B). Each antibody was then flowed over the cell individually and binding was detected by the increase in RU of the flow cell containing the immobilised TCR. Antibodies were stripped after each injection using Gentle Ag/Ab Elution Buffer (Pierce), which indiscriminately removed bound antibodies without altering the pH, and so should have minimal impact on the folding of the bound receptors. Both MAU-Bt and the control LES-Bt bound the pan- $\gamma\delta$ antibody equivalently, suggesting correct conformation for the MAU $\gamma\delta$ heterodimer (Figure 3.11A). Secondly, MAU-Bt specifically bound the anti V γ 9 and V δ 1 mAbs, whereas LES-Bt (V γ 4V δ 5) did not (Figure 3.11B+C). Collectively, these results

suggested that both the γ and δ chains of MAU-Bt were independently folded correctly, and they combined to form a complete $\gamma\delta$ TCR heterodimer.

The binding of EphA2-Fc to MAU-Bt was analysed using BIAcore, with a previous TCR immobilisation strategy as described for the antibody confirmation experiments. With MAU-Bt immobilised to the sensor chip, binding with EphA2-Fc could not be detected when injected over the cell at concentrations up to $6\mu\text{M}$ (Figure 3.12). This technique has successfully been previously used to detect interactions between $\gamma\delta$ TCRs and ligands¹²³, but lack of detectable binding does not necessarily suggest there is no interaction between the proteins, as some recognition events are difficult to detect using this system. For example, the interaction between CD4 and MHC class II is undoubtedly physiologically relevant, but is undetectable by SPR as it has a low dissociation constant (K_D) ($150\text{--}200\mu\text{M}$)¹³⁴. Also, due to the immobile nature of proteins bound to the chip, the interactions detected by BIAcore often cannot account for clustering or multimeric interactions.

This binding study was also conducted in the reverse orientation, with EphA2-Fc immobilised to an R10Z8E9 coated CM5 chip and monomeric MAU-Bt injected over the immobilised EphA2 at concentrations over $100\mu\text{M}$. In addition, this experiment was repeated by injecting dextramer-multimerised MAU TCR (>20 TCRs/molecule) (C. Willcox, unpublished). Neither experiment demonstrated specific binding between EphA2-Fc and MAU-Bt (data not shown). This suggests either a very weak affinity interaction, or that conformational constraints of the BIAcore system are preventing the detection of binding.

This lack of detectable BIAcore binding suggests that, if there is an interaction between EphA2 and MAU TCR, it may be facilitated by clustering, or other cell surface components may be involved. Since the activation assays showed that plate bound EphA2-Fc alone is

sufficient to induce activation of JRT MAU (Figure 3.1), if other factors are required they are likely to be located on the JRT3 cell surface. Likely candidates for such a molecule are the ephrins, the cognate ligands for the ephrin receptors, which bind with high affinity, with many interactions having a dissociation constant in the nM range⁷⁷. Also, such a strong interaction may allow EphA2 to induce TCR triggering in spite of the low affinity of the MAU TCR/EphA2 interaction.

3.2.4 Interaction of ephrins with EphA2 is essential for the activation of MAU

The presence of ephrinA1 and ephrinA4, both ligands of EphA2, on the surface of JRT3 cells has been demonstrated using polyclonal antibodies (J Déchanet-Merville, unpublished). Furthermore, EphA2-Fc and EphA4-Fc demonstrated TCR-independent binding of surface ephrins on JRT3 cells previously in this chapter (Figure 3.6), a finding which is also reported by another group¹³⁵. This group also proposed that A-ephrins are present on CD4⁺ T cells, which were stained with EphA2-Fc *ex vivo* following culturing for five days, demonstrating that expression is not limited to the JRT3 cell lines, and may be expressed by T cells *in vivo*. Collectively, these results strongly suggest that ephrins are present on the surface of JRT MAU, and therefore could potentially be involved in the interaction between EphA2 and MAU.

To investigate the potential role of ephrins in the interaction between EphA2 and MAU, a number of strategies were employed to disrupt the well-characterised interaction between EphA2 and its A-ephrin ligands. In a previous study from our group, preliminary experiments indicated the importance of ephrins for this interaction. Briefly, these included the use of PI-PLC to cleave GPI-linked surface proteins (such as the A-ephrins) from the surface of JRT3 cells and pre-blocking EphA2-Fc with soluble ephrinA1-Fc in the activation

assay. These experiments are summarised in Figure 3.13. These initial experiments, although useful for indicating the potential importance of A-ephrins, were not specific enough to directly implicate them in the interaction between EphA2 and MAU. For example, the PI-PLC cleavage indiscriminately cleaves all GPI-linked proteins, some of which may be required for activation, independently of ephrins. Also, the Fc-tag on the ephrinA1 used in the experiment may have blocked other sites distinct from the ephrin binding site preventing TCR binding to EphA2, implying that ephrin binding could not specifically be implicated. In order to build on these results, a mutant EphA2-Fc molecule was produced in 293T cells which specifically lacked the ability to bind A-ephrins.

Himanen and colleagues used X-ray crystallography to extensively characterise the EphA2 ephrin binding pocket of the ligand binding domain (LBD) by studying complexes with the ligand ephrinA1⁸². The EphA2-ephrinA1 interface exhibits a buried surface area of 2350Å² and is dominated by a several polar and non-polar interactions. This study identified 4 residues within the EphA2 ephrin binding pocket which are critical for binding ephrinA1. The EphA2 binding pocket is predominantly hydrophobic, and the surface-exposed hydrophobic residues T101, A190 and L192 mediate non-polar interactions with the aliphatic groups of Q109, P113, F114 and T115 of the G-H loop of ephrinA1, which provides the majority of the binding energy (Figure 3.14). The biological significance of these residues was assessed in another study, in which EphA2 binding pocket residues T101, A190 and L192 were mutated, and cells transduced with these mutants failed to exhibit EphA2 clustering when exposed to ephrin stimulus⁸⁰. In addition to these hydrophobic interactions, EphA2 binding pocket residue R103 forms a salt bridge with E119 of the G-H loop of ephrinA1, which the authors describe as a 'latch' to stabilise the binding facilitated by the hydrophobic interactions (Figure 3.14). Interestingly, ephrinA1 residue E119 is

conserved in all A-ephrins (Figure 3.15). Furthermore, residues at positions 109, 113, 114 and 115 of ephrinA1 which provide the majority of the hydrophobic interactions with the EphA2 LBD are also highly conserved within the A-ephrin family, and so this mechanism of binding and stabilisation is likely applicable to binding of all A-ephrin ligands of EphA2, not just ephrinA1¹³⁵ (Figure 3.15). This suggested that disruption of these interactions should ablate binding of all A-ephrin ligands to EphA2. With this in mind, an EphA2-Fc mutant incorporating charge reversal of R103 to glutamic acid (EphA2^{R103E}) was generated by altering the WT codon GAG to CGT. It was envisaged that the introduction of E103 may prevent binding to ephrins due to electrostatic repulsion effects (Figure 3.14). This construct was cloned into the pHL-Fc vector, expressed in 293T cells and purified as previously described for the WT EphA2-Fc construct. Expression levels, yield, SDS PAGE migration and purity for EphA2^{R103E}-Fc were equivalent to the WT construct (Figure 3.16).

Further BIAcore experiments were performed in order to confirm that the R103E mutation had not compromised the natural conformation of EphA2. These results established that EphA2^{R103E}-Fc bound the anti-EphA2 pAb equivalently to the WT protein when analysed by BIAcore, implying correct folding (Figure 3.17A). This suggested that molecules which interact with other regions of EphA2 are likely to remain unaffected by this mutation. Next, the surface of JRT MAU and JRT LES were stained with the mutant to test the ability of EphA2^{R103E}-Fc to bind ephrins. In contrast to WT protein, EphA2^{R103E}-Fc failed to stain the surface of the JRT3 cells (Figure 3.17B), suggesting that ephrin binding had been completely ablated. The charge reversal mutation seemed to provide enough repulsive energy to negate the other hydrophobic interacting residues in the pocket, and thus significantly reduce binding to ligand.

Finally, EphA2^{R103E}-Fc failed to activate JRT MAU when used in the previously described activation assay (Figure 3.18A). This strongly implicates ephrins as being vital to the interaction of EphA2 with MAU, as a single specific amino acid substitution deep in the ephrin binding pocket can completely knock out activation of JRT MAU by EphA2-Fc. Moreover, this finding also enforces that the ephrin receptor staining of JRT3 cells (Figure 3.6) is due solely to ephrin binding, as staining is completely abrogated by the R103E mutation, thus further supporting the observation that ephrins are present on the JRT3 cell surface.

3.2.5 TCR and ephrin interactions need to occur on the same EphA2 molecule

At this stage it was established that activation of JRT MAU by EphA2-Fc requires the interaction of at least two cell surface molecules with EphA2, the MAU TCR and ephrins. To further characterise this interaction, it was important to determine whether these interactions take place on the same EphA2 molecule, or if they could be provided separately. This is an important distinction as it has implications for not only the spatial restrictions involved in the formation of such a complex, but also for the intracellular signalling pathway used by activation.

In order to determine this, the two required signals (ephrin and TCR) were divided between two molecules in an activation assay, with both EphA4-Fc and EphA2^{R103E}-Fc placed in the same well on a 96 well plate. In this experiment, EphA4-Fc would bind ephrins on the cell surface (as EphA4 binds the same ephrins as EphA2⁸⁸) providing the 'ephrin signal' and EphA2^{R103E}-Fc would provide the 'TCR signal'. EphA2^{R103E} is identical to the WT EphA2 with the exception that it incorporates a single amino acid substitution which abrogates ephrin binding and prevents activation of JRT MAU. This approach assumes that the MAU TCR

does not bind within the ephrin binding pocket in a way that is dependent on R103. Indeed, the R103E substitution is buried deep within the binding pocket and therefore is unlikely to be able to contact the TCR. Despite using various ratios and concentrations of both reagents activation of JRT MAU was not observed in this experiment, suggesting that both ephrin and TCR interactions are required to take place on the same EphA2 molecule for the initiation of signalling (Figure 3.18B). These models are shown as a schematic in Figure 3.19.

3.3 Discussion

Unlike for $\alpha\beta$ T cells, there is currently no widely accepted paradigm for the molecular nature of the interactions between $\gamma\delta$ TCRs and their ligands, and so it is still unclear whether there is a conserved recognition modality, shared between various receptors, or different modalities are used depending on the TCR, ligand and physiological context. Therefore it is important to gain an in-depth understanding of a wide range of $\gamma\delta$ TCRs and how they interact with their ligands in order to identify common features which may be shared by multiple receptors.

$\gamma\delta$ T cells likely play a key role in the detection of stress as part of the lymphoid stress surveillance compartment⁸, and an improved understanding of how they interact with their target molecules on a molecular level will allow for rapid advances in this field, equivalent to what has been achieved with $\alpha\beta$ T cells.

The results detailed in this chapter have outlined the broad molecular requirements for the interaction of a $V\delta 2^{\text{negative}}$ $\gamma\delta$ T cell MAU with EphA2, an epithelial stress ligand. Recognition of EphA2 by MAU is TCR specific, and successful interaction with ephrins on the $\gamma\delta$ cell surface by EphA2 is also required. Finally, these interactions need to take place on a single EphA2 molecule, suggesting the formation of a tri-partite recognition complex.

The MAU TCR was shown to be essential for the activation of JRT3 cells by EphA2, as JRT3 cells transduced with other $\gamma\delta$ TCR genes failed to be activated. It was important to determine whether the MAU TCR is involved in MAU interactions with target cells, as although there is a consensus that the TCR mediates the interaction between $\gamma\delta$ T cells and their targets, this is not always the case. For example, most $\gamma\delta$ T cells express NKG2D, an activatory receptor typically found on natural killer (NK) cells which recognises stress ligands such as MICA and the ULBP family, which have been shown to activate $\gamma\delta$ T cells independently of their TCR¹². More recently, it has been suggested that in mice, certain subsets of $\gamma\delta$ T cells predominantly use their TCR during T cell development in the thymus, and peripheral effector functions, including killing, are mediated solely by cytokines⁶⁰.

Interaction of ephrins with EphA2 was shown to be essential for the activation of JRT MAU by EphA2-Fc, because mutation of R103, a residue deep in the ephrin binding pocket of EphA2, completely ablates activation. It was also demonstrated that the ephrins and MAU TCR had to interact with the same molecule of EphA2-Fc, as activation of JRT MAU by EphA2^{R103E}-Fc could not be rescued by the addition of EphA4-Fc. Beyond providing a potential framework for $V\delta 2^{\text{negative}}$ $\gamma\delta$ T cell interactions with their ligands, this specific interaction with the epithelial stress ligand EphA2 may represent a key component of the lymphoid stress surveillance response. The formation of this tri-partite complex represents a novel approach to ligand recognition by using a combination of $\gamma\delta$ TCR and ephrin ligand to detect the presence of a stress ligand.

EphA2 and its ligands are implicated in many biological pathways, and have a complex role in the initiation and development of several cancers⁸⁵. Broadly, the literature suggests that in healthy epithelium, EphA2 is bound to ephrins in a trans manner, and restricted to cell-

cell contacts⁸⁶. Several studies suggest that this results in a formation of a complex signalling cluster⁸⁰. When bound in its native state, EphA2 has been shown to possess tumour suppressor properties⁷⁸, and when unbound from ephrin, oncogenic characteristics have been demonstrated⁹⁷. A key process of epithelial cancer progression is epithelial to mesenchymal transition (EMT), whereby cells lose their epithelial properties, such as E-cadherin expression. E-cadherin has been shown to modulate EphA2 localisation and function⁹⁵, and during EMT EphA2 becomes separated from its ligands and is dispersed evenly around the cell surface, whereas it is usually restricted to cell contacts. Furthermore, it has been demonstrated that distinct EphA2 epitopes are available for antibody binding on normal and malignant cells⁸⁶, supporting that this molecule could be recognised by the immune system only in its non-clustered state. Therefore the role of EphA2 as a stress ligand may be to signal these conditions by being exposed in an unbound form and available for both TCR and ephrin binding.

It is conceivable that MAU T cells specifically recognise unbound EphA2 by virtue of the ephrins on their cell surface. This chapter clearly shows that the MAU $\gamma\delta$ TCR is key to this interaction, and it may be that it specifically recognises ephrinA1-bound EphA2, although this was not detected by BIAcore (C. Willcox, unpublished). This would bring TCR signalling components towards the cell's existing contact with a stress ligand, with the potential to initiate effector functions. It has also been demonstrated that A-ephrins can associate with the Src family kinases Lck and Fyn¹³⁶, which are key to the initiation of the TCR signalling cascade¹³⁷, typically a task associated with the co-receptors CD4 and CD8 in $\alpha\beta$ T cells¹³⁸. However CD4 and CD8 are not commonly expressed on $\gamma\delta$ T cells, and it can therefore be envisaged that the establishment of this tri-partite signalling complex can bring these Src family kinases to the TCR-EphA2 complex. Previous studies from our group have shown

phosphorylation of key signalling components such as ZAP70 when MAU is activated by EphA2, demonstrating that the TCR signalling cascade is indeed initiated by this interaction.

Because the GPI-linked A-ephrins do not possess a cytoplasmic region, their association with intracellular signalling machinery is likely due to their association with transmembrane proteins, such as the p75 neurotrophin receptor¹³⁹, although the adapter proteins on T cells have not yet been identified¹³⁵. This therefore adds the possibility that a fourth molecule may be involved in this interaction, as an intermediary between GPI-linked A-ephrins and cytoplasmic kinases. A schematic of this model is shown in Figure 3.20.

This model could represent a novel recognition modality utilised by the lymphoid stress surveillance system. Unlike $\alpha\beta$ T cells which specifically recognise MHC-bound peptide by their TCR, MAU may recognise a stress signal by a non-immune receptor molecule, which then recruits the TCR as a method of initiating T cell signalling for effector functions. Such an approach could conceivably be used by a range of receptors, relying on specific TCR for development, trafficking and almost as co-receptor for initiating signalling.

To advance these findings, it is important to further characterise the role of ephrins in this interaction. Although these results indicate that ephrins are required for activation, it is still not apparent which ephrins are capable of facilitating this interaction. EphA2 can bind all of the GPI-linked A-ephrins, which have a diverse biological and signalling profile, which may have implications for their involvement in this interaction⁷⁷. Furthermore, although this study clearly demonstrated the presence of A-ephrins on the surface of JRT3 cells, there is little evidence on the presence of A-ephrins on $\gamma\delta$ T cells *in vivo*. Characterising their expression on such cells is an obvious extension to this study. One study demonstrated the presence of A-ephrins on *ex vivo* CD4⁺ T cells by staining with soluble

EphA2-Fc, however expression was only apparent after culturing in human serum for 5 days¹³⁵. If this expression pattern extends to $\gamma\delta$ T cells, perhaps surface expression of A-ephrins can be altered, adding a layer of control to the recognition strategy.

The lack of detectable binding between EphA2-Fc and MAU-Bt provides some key insights into this interaction, and ultimately led to the finding that ephrins are central to activation by EphA2. BIAcore is a reliable application for detecting binding between proteins, but does have limitations for certain types of interactions. Therefore, although binding cannot be detected, it does not necessarily mean that there is no physiologically relevant interaction between EphA2 and MAU TCR. For example, the interaction of CD4 with MHC class II molecules cannot be detected by BIAcore, yet CD4 is a well-established and characterised co-receptor in CD4⁺ T cells, and its ectodomain has even been crystallised in complex with class II MHC¹⁴⁰. It is important to consider the wider physiological context in these situations, and immobilised proteins on a BIAcore chip are not very representative of this, and factors such as clustering, which is a key component of EphA2/ligand interactions, cannot be accounted for. It could also be that intracellular signalling components are required for binding, as demonstrated by the importance of Lck association for the co-receptor function of CD4 and CD8¹³⁸.

It would be useful to expand these findings beyond the MAU JRT3 transductant, which serves as a model for TCR based activation. Jurkat cells cannot be used for in depth analysis of effector functions, such as cytokine production profiles, which would provide information on how MAU may interact with target cells and other immune cells after activation. Unfortunately, the MAU clone is no longer available, which provides a limit on how physiologically relevant these models can be. Isolation of further EphA2-reactive

clones would enable these experiments to be undertaken. Interestingly, the V γ 9V δ 1 chain pairing has frequently been observed in the peripheral blood of both healthy donors (see Chapter 6) and chronic myeloid leukaemia (CML) patients (D. Lewis, unpublished). This suggests that if this chain pairing is required for EphA2 reactivity, this recognition modality may be common within the population, allowing for the isolation of further reactive clones.

These broad requirements identified for the recognition of EphA2 by MAU TCR provided key insights into the molecular nature of this interaction, and has led to the development of a model for the recognition of an epithelial stress ligand by a V δ 2^{negative} $\gamma\delta$ T cell, which may be applicable to other $\gamma\delta$ T cells.

3.4 Figures

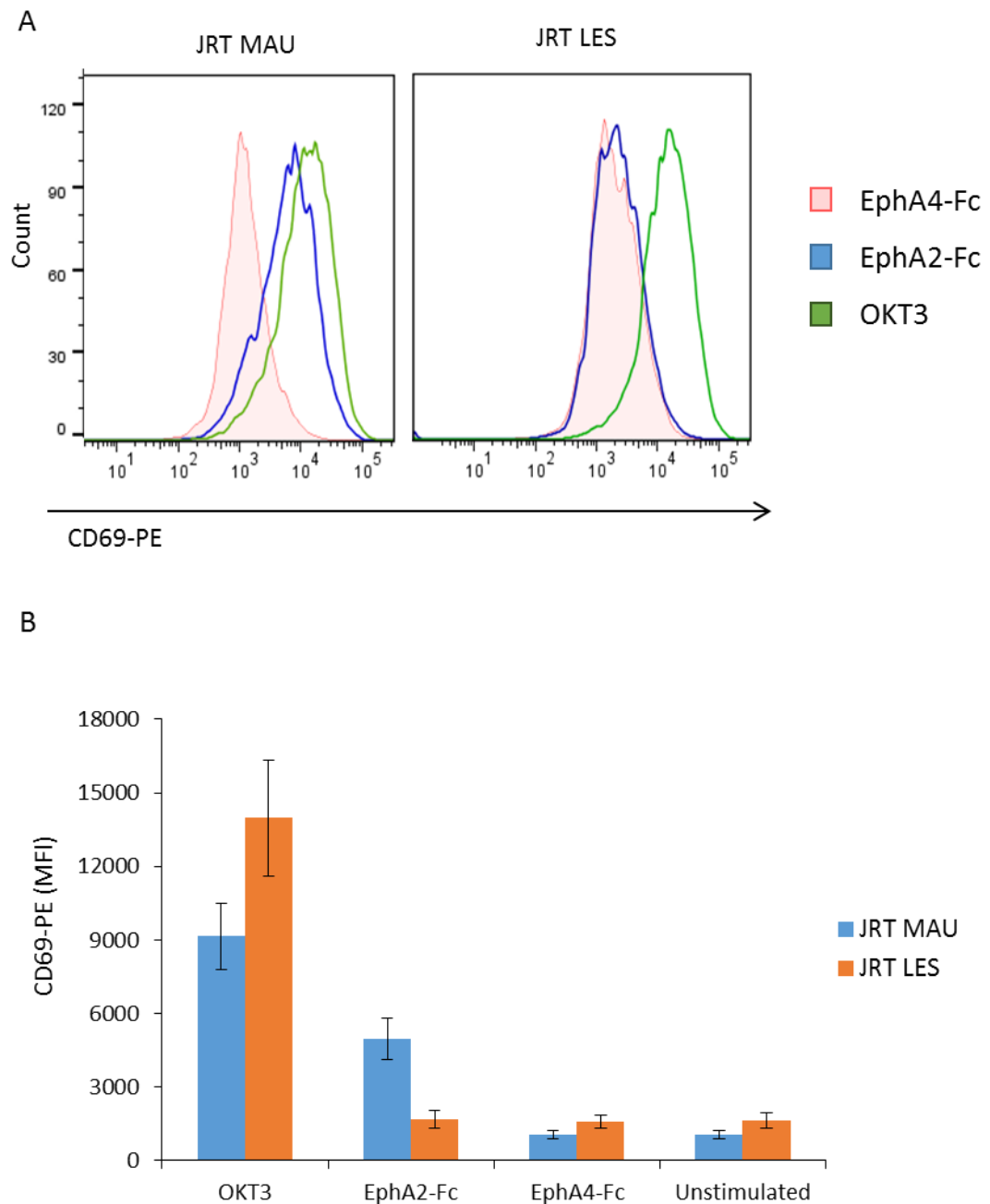


Figure 3.1: EphA2-Fc specifically activates JRT MAU

EphA2-Fc, EphA4-Fc and OKT3 were immobilised on a 96-well plate and incubated with 5×10^5 of either JRT MAU or JRT LES for 4 hours. Activation was then measured by CD69 upregulation using flow cytometry. (A) Representative histograms showing the shift in peaks when JRT3 cells were exposed to different stimulants. (B) Quantification of experiments. ($n=3$, error bars =SD).

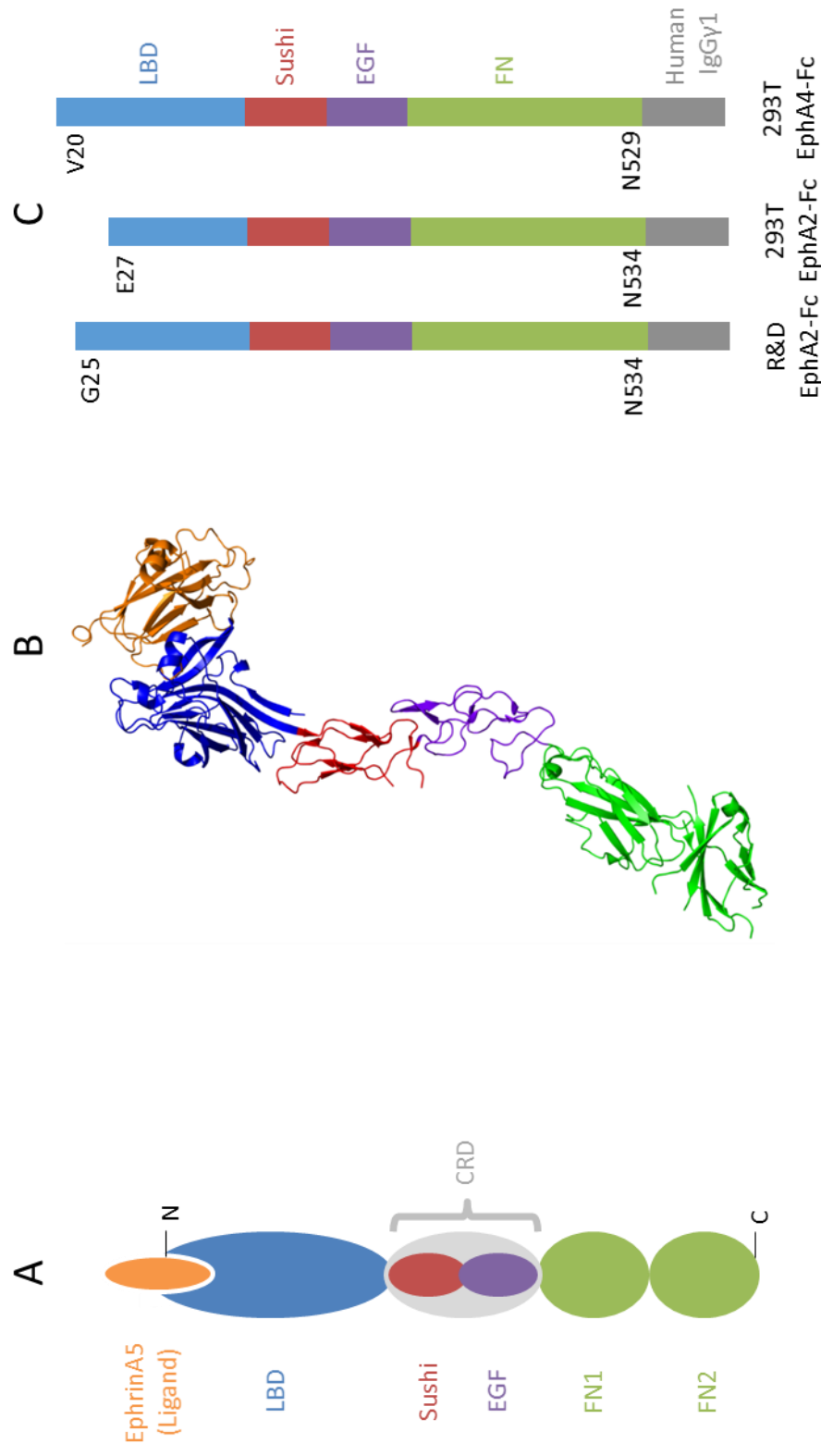


Figure 3.2: Structure of the EphA2 ectodomain

(A) Schematic representation of EphA2 ectodomain bound to ephrinA5 ligand. The ligand binding domain (LBD) is responsible for binding ephrin ligands. The Sushi and EGF domains collectively comprise the cysteine rich domain (CRD). Finally, there are two fibronectin domains (FN) at the C terminus (B) Ribbon representation of EphA2 bound to ephrinA5 (Structure obtained from the Protein Dank Bank, PDB: 2X11) (C) Schematic representation of R&D EphA2-Fc, 293T EphA2-Fc and 293T EphA4-Fc constructs.

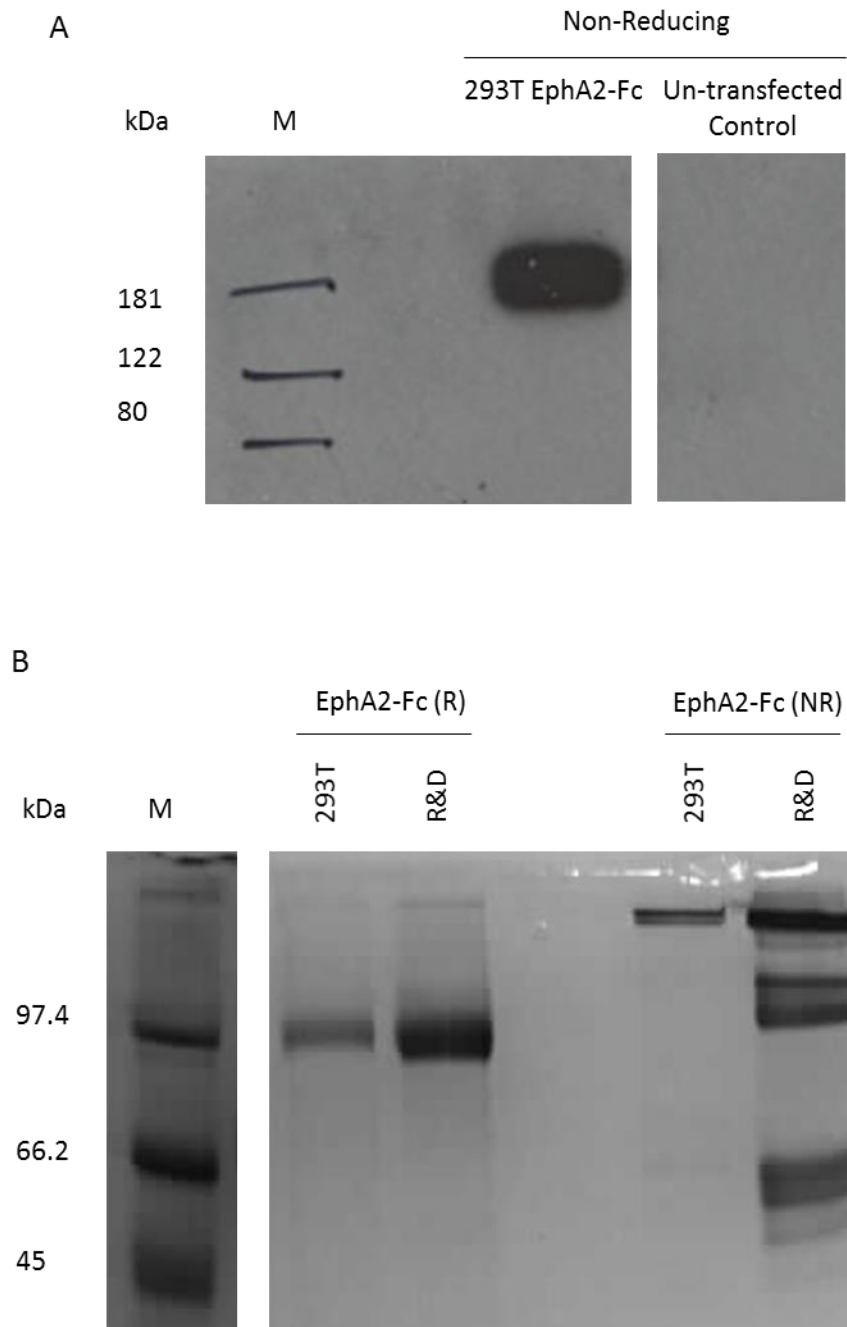


Figure 3.3: Expression and purification of EphA2-Fc using the 293T expression system

(A) Western blot showing the expression levels of EphA2-Fc at day 5 post transfection, probed using an HRP conjugated anti-His antibody. (B) SDS PAGE gel (Instant Blue) showing reduced (R) and non-reduced (NR) Ni-NTA purified EphA2-Fc. The non-reducing R&D EphA2-Fc sample shows several lower molecular weight bands, potentially representing degradation products. Yields were typically 1.5mg from 250ml of 293T supernatant.

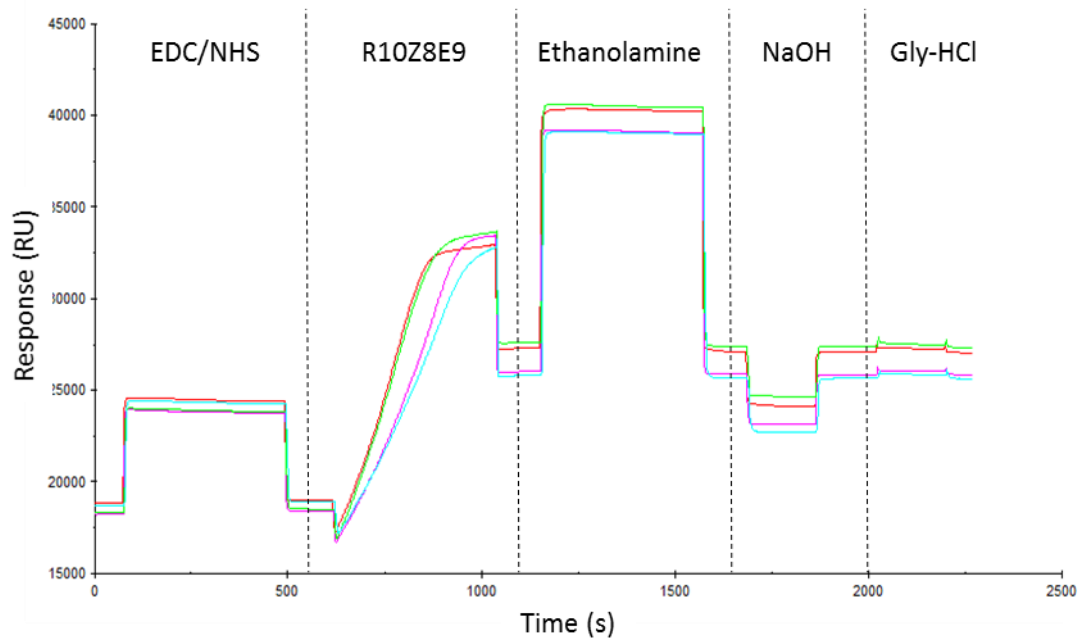


Figure 3.4: Amine coupling of the R10Z8E9 mAb to a CM5 BIAcore chip

The chip surface was first activated using EDC/NHS to generate surface esters. The R10Z8E9 anti-Fc mAb was then immobilised onto the chip surface by binding of primary amines to the surface esters. Ethanolamine was then used to saturate any remaining surface esters. Finally, NaOH and Gly-HCl were used to remove any non-covalently bound molecules and adjust the pH of the flow cell for the experiment.

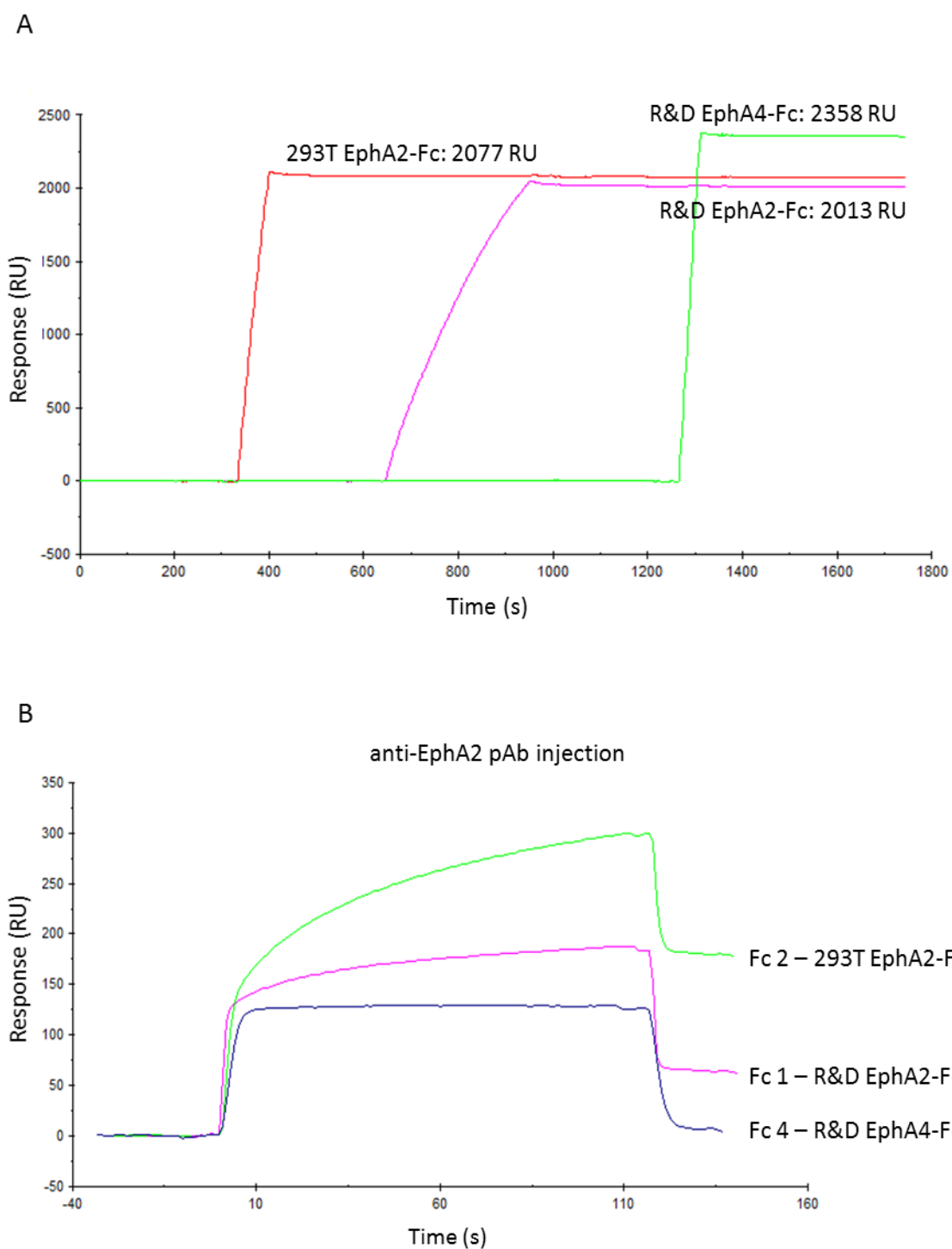


Figure 3.5 : Verification of the intact conformation of EphA2 using anti-EphA2 pAb

(A) Immobilisation of Fc-tagged ephrin receptors to the R10Z8E9 coated CM5 chip. Protein levels were normalised to approximately 2000 RU. (B) Binding of the anti-EphA2 pAb to the immobilised ephrin receptors. The anti-EphA2 pAb bound R&D EphA2-Fc and 293T EphA2-Fc, and failed to bind the EphA4-Fc control.

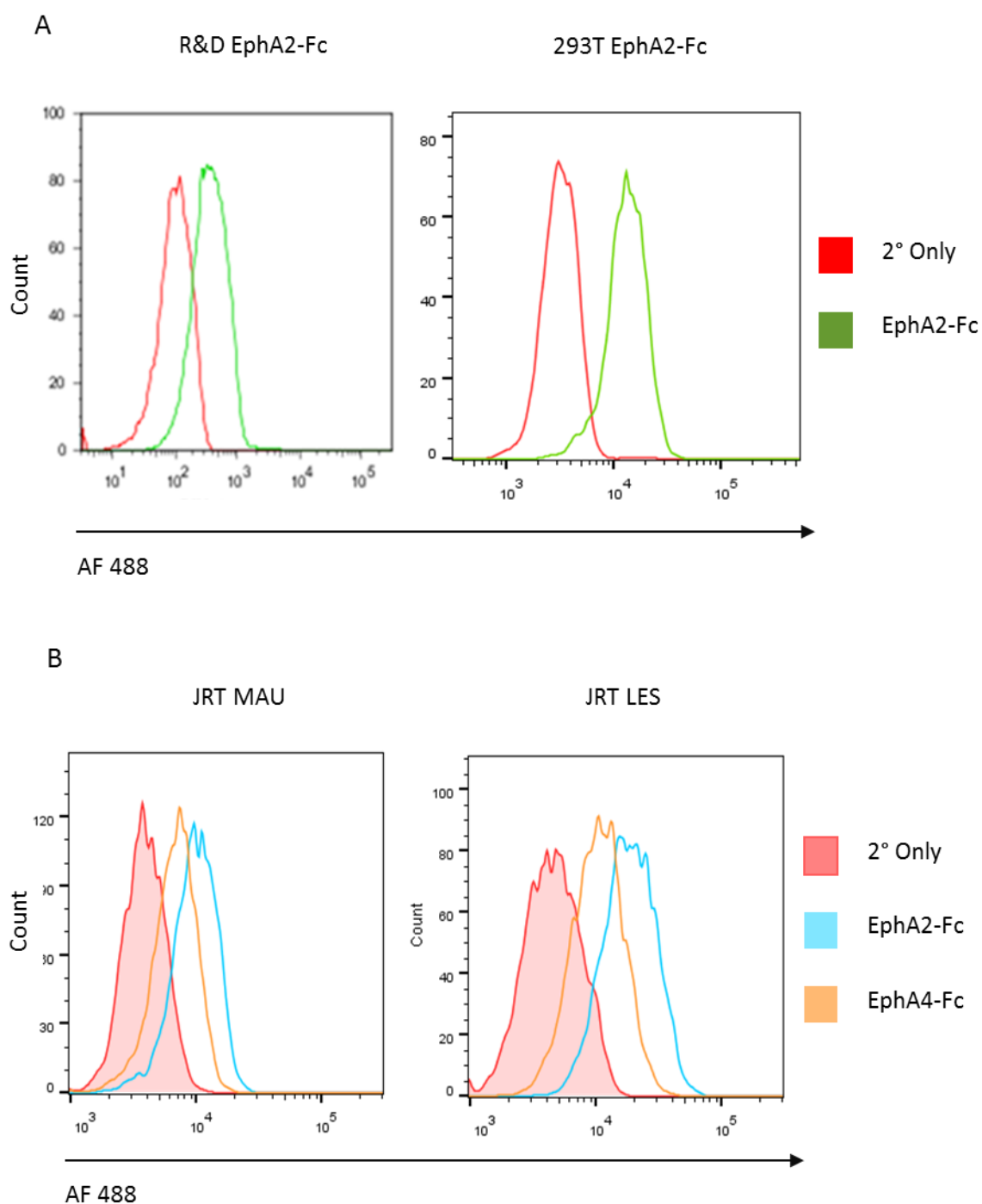


Figure 3.6 : Cell surface staining of JRT MAU and LES by EphA2-Fc

(A) 293T EphA2-Fc and R&D EphA2-Fc were used to stain the surface of JRT MAU cells, which were detected using an AF488 conjugated goat anti-human Fc secondary antibody. The two constructs stained the surface equivalently. (B) JRT MAU and JRT LES were stained equivalently by EphA2-Fc and EphA4-Fc. (Representative, $n=3$).

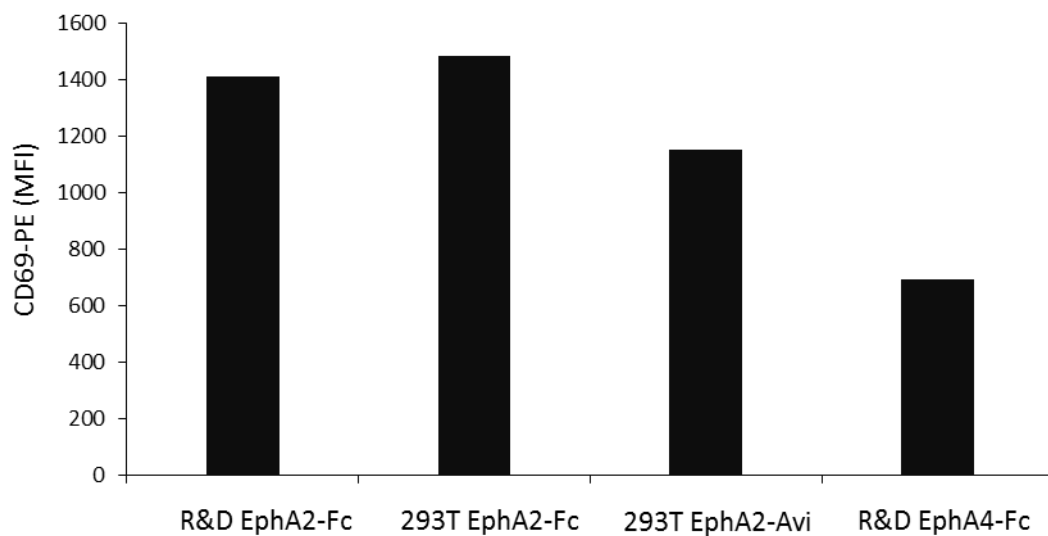


Figure 3.7 : 293T EphA2-Fc activates JRT MAU equivalently to R&D EphA2-Fc

Fc-tagged ephrin receptors were immobilised on a 96-well plate and incubated with JRT MAU cells for 4 hours. Activation was then measured by CD69 upregulation. 293T-derived EphA2-Fc activated JRT MAU equivalently to R&D EphA2-Fc. EphA2 engineered to a biotinylation AviTag instead of a dimerising Fc-tag (EphA2-Avi), also activated JRT MAU. (Representative, $n=3$).

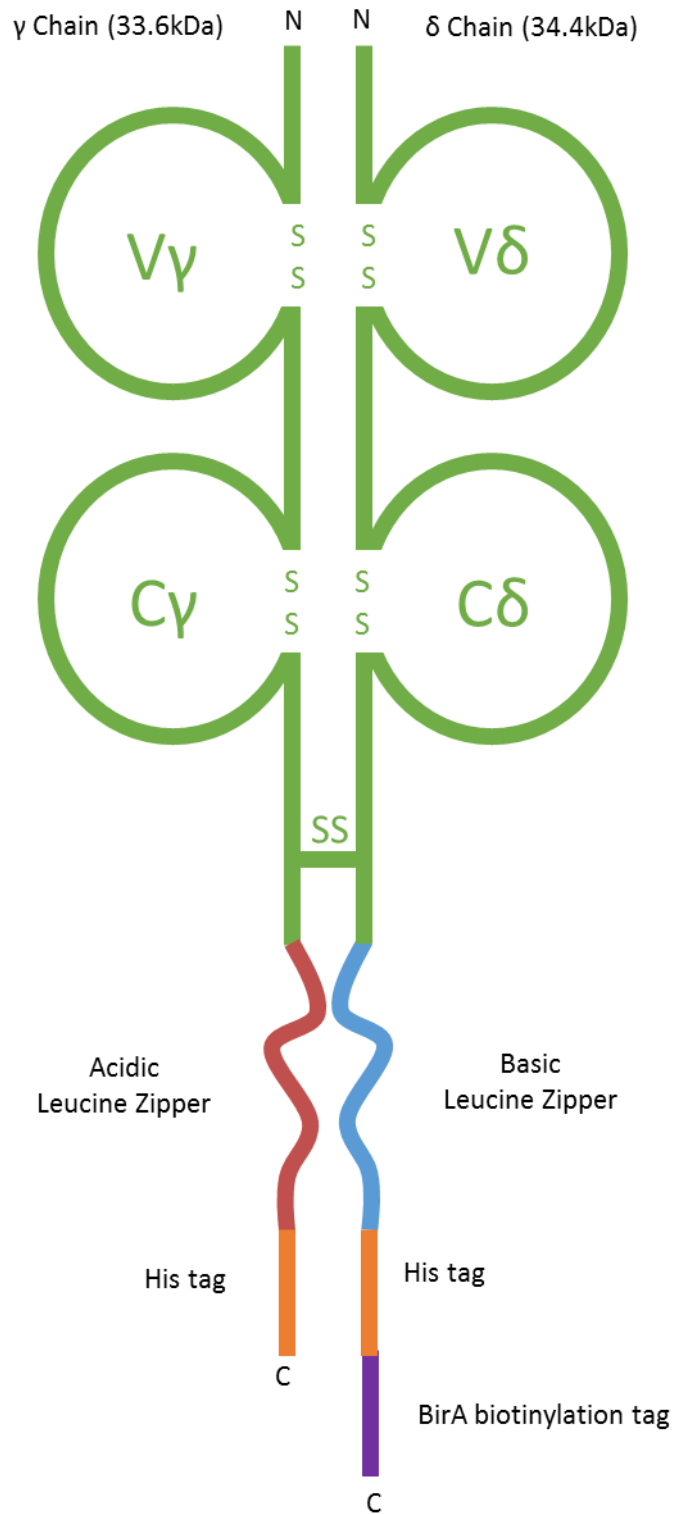


Figure 3.8 : MAU $\gamma\delta$ TCR construct

Schematic of recombinant MAU $\gamma\delta$ TCR construct expressed in S2 *Drosophila* cells. The open circles represent the Ig domains of either the constant (C) or variable (V) domains. SS denotes a disulphide bond. The basic and acidic leucine zipper motifs ensure heterodimeric TCR formation.

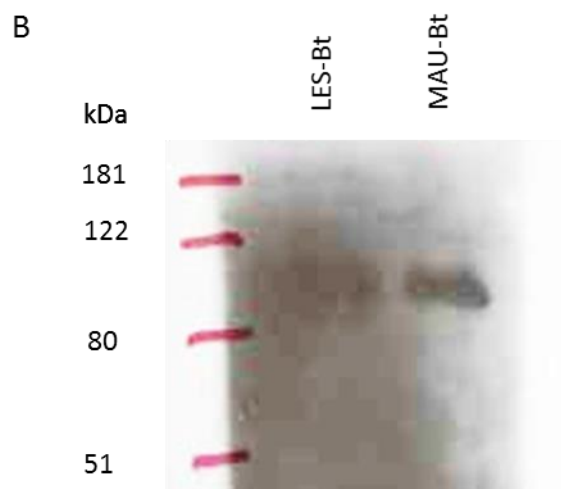
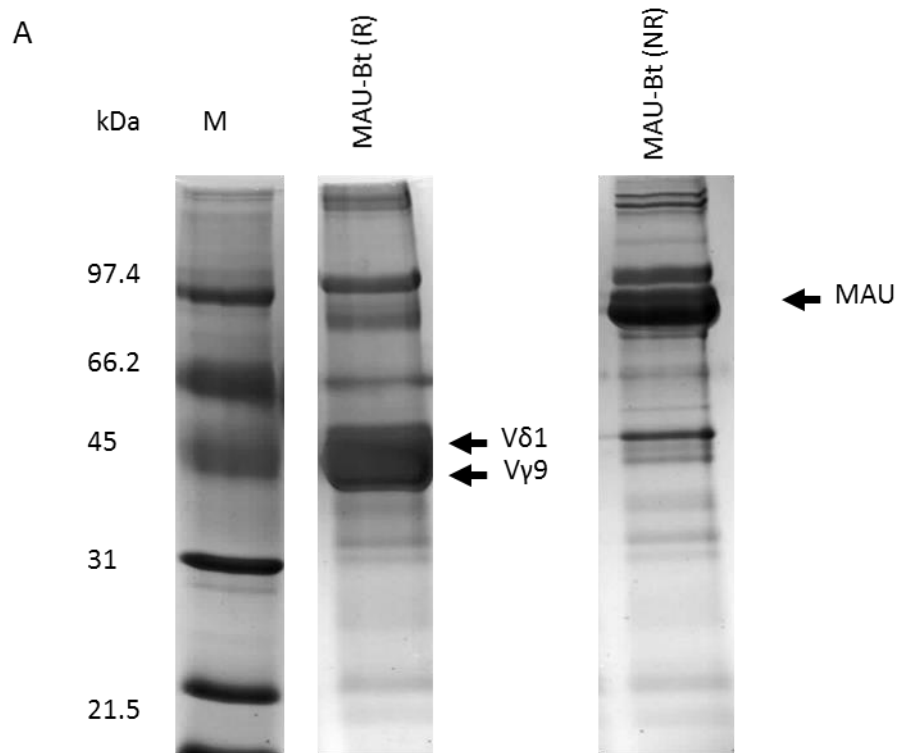


Figure 3.9 : Production of MAU TCR using the *Drosophila* S2 expression system

(A) Reducing (R) and non-reducing (NR) SDS PAGE analysis (instant blue) of Ni-NTA purified MAU TCR. The γ and δ chains are visible as discrete bands in the non-reducing sample, migrating at approximately 45kDa. The dimeric construct migrates at approximately 90kDa in the non-reduced sample. Yield was typically 1.5mg from 1L of S2 supernatant. (B) Western blot of MAU-Bt to show successful biotinylation of MAU TCR, probed using a HRP-conjugated streptavidin construct.

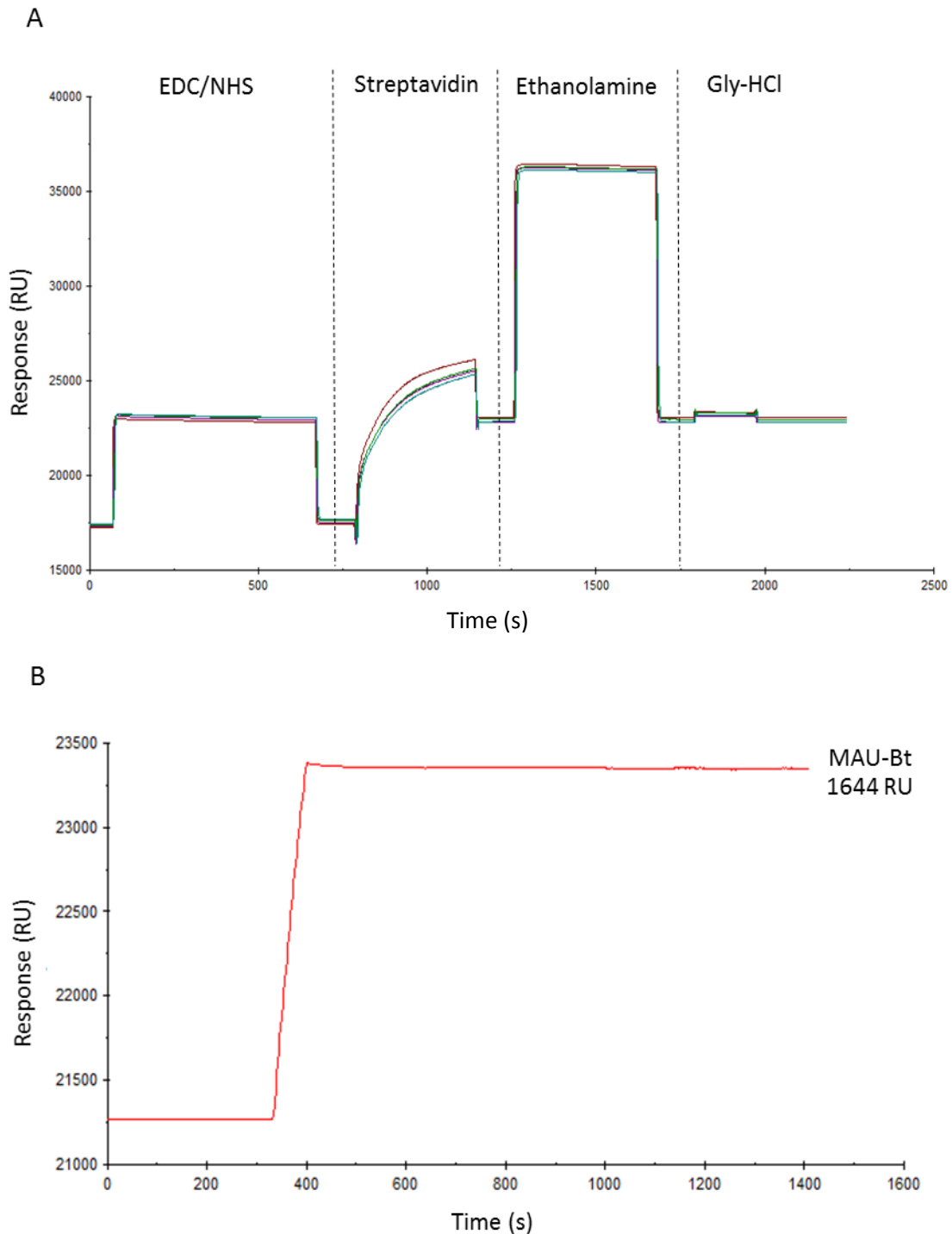


Figure 3.10 : Immobilisation of MAU TCR on a CM5 BIAcore chip

(A) Amine coupling of streptavidin to the CM5 chip, highlighting the reagents used for each injection. First the surface was activated using EDC/NHS to generate surface esters. Streptavidin was then immobilised onto the chip surface by the binding of primary amines to the surface esters. Ethanolamine was then used to saturate any remaining surface esters. Finally, Gly-HCl was used to remove any non-covalently bound molecules and adjust the pH of the flow cell. (B) Immobilisation of biotinylated MAU TCR to the streptavidin coated CM5 chip.

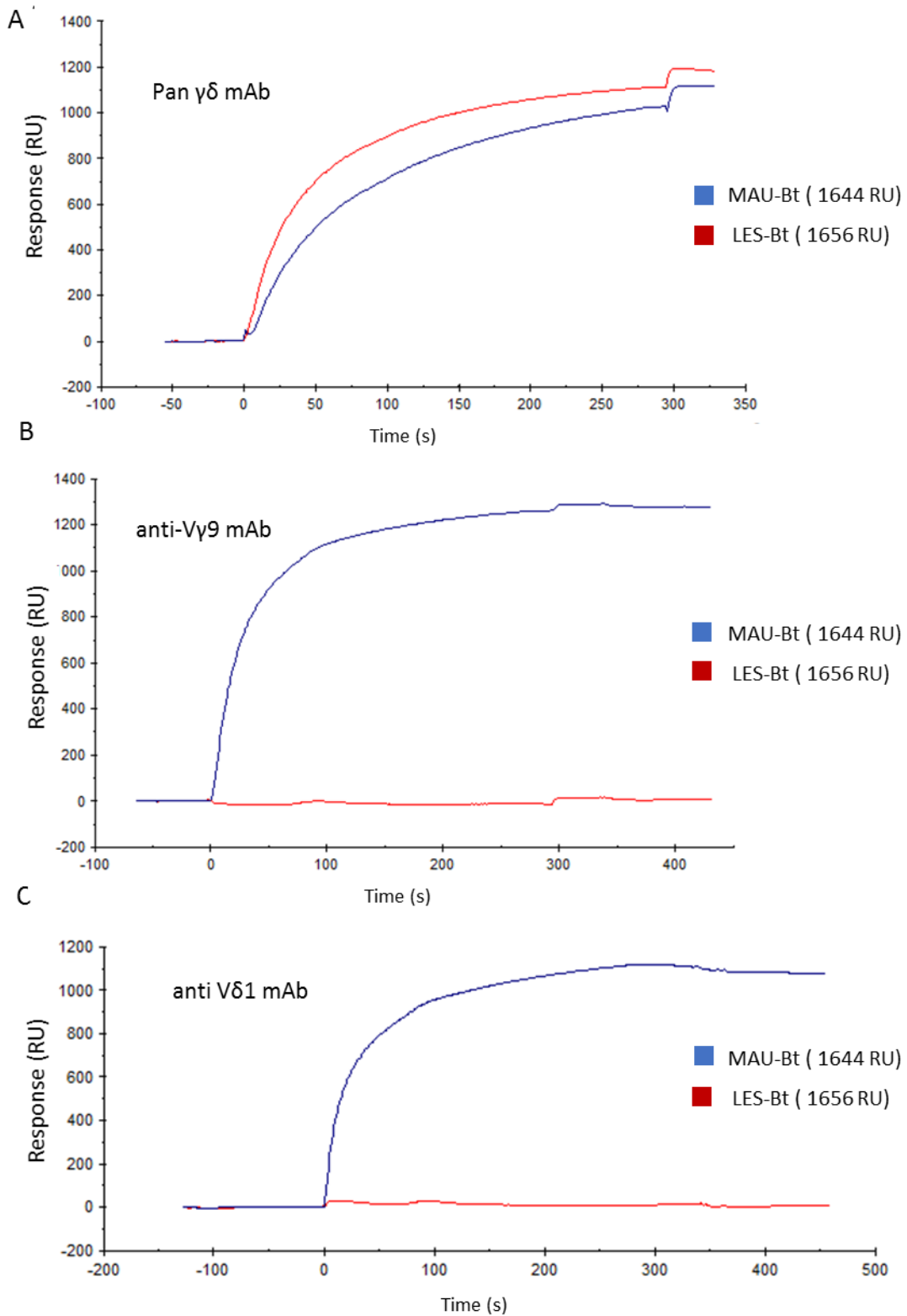


Figure 3.11 : Verification of MAU-Bt folding using BIAcore

Biotinylated TCRs were immobilised to a streptavidin coated CM5 chip and $\gamma\delta$ TCR specific mAbs were injected over the flow cells. (A) The pan- $\gamma\delta$ mAb binds both MAU-Bt and LES-Bt. Anti-V γ 9 (B) and anti-V δ 1 (C) mAbs specifically bind the V γ 9V δ 1 MAU TCR, but not the V γ 4V δ 5 LES TCR. Number in brackets represents amount of TCR immobilised on the chip.

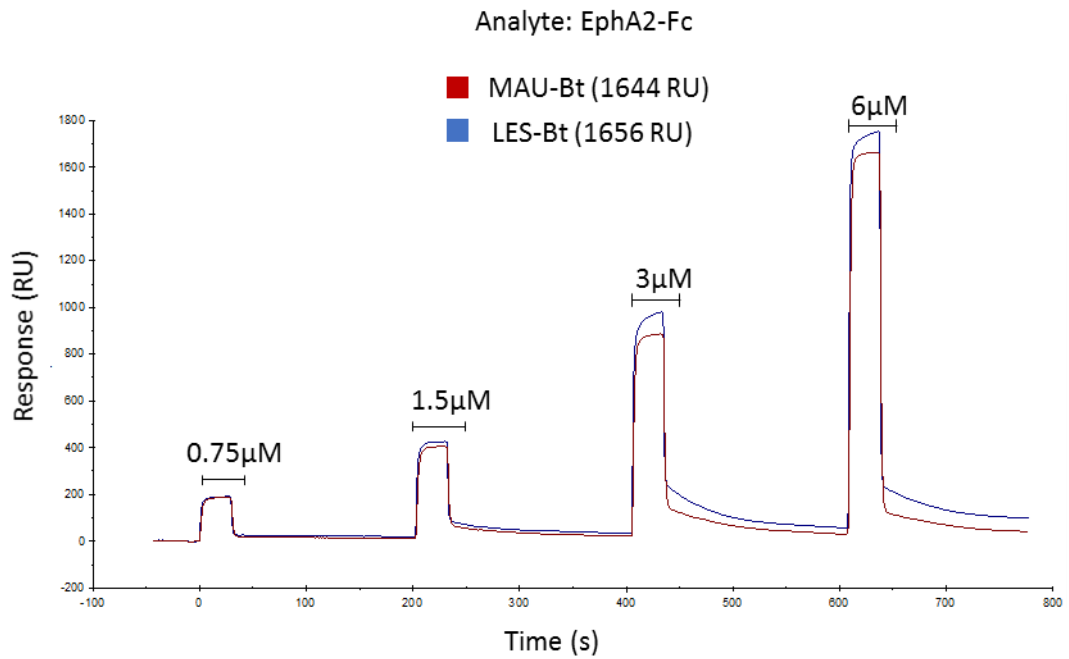


Figure 3.12: Analysis of the MAU-Bt/EphA2-Fc interaction using BIAcore

LES-Bt and MAU-Bt were immobilised onto a streptavidin coated CM5 chip, and EphA2-Fc was injected over the chip with a peak concentration of 6μM. EphA2-Fc demonstrated no specific binding to MAU-Bt when compared to the control LES-Bt. Number in brackets represents RU of TCR immobilised on CM5 chip.

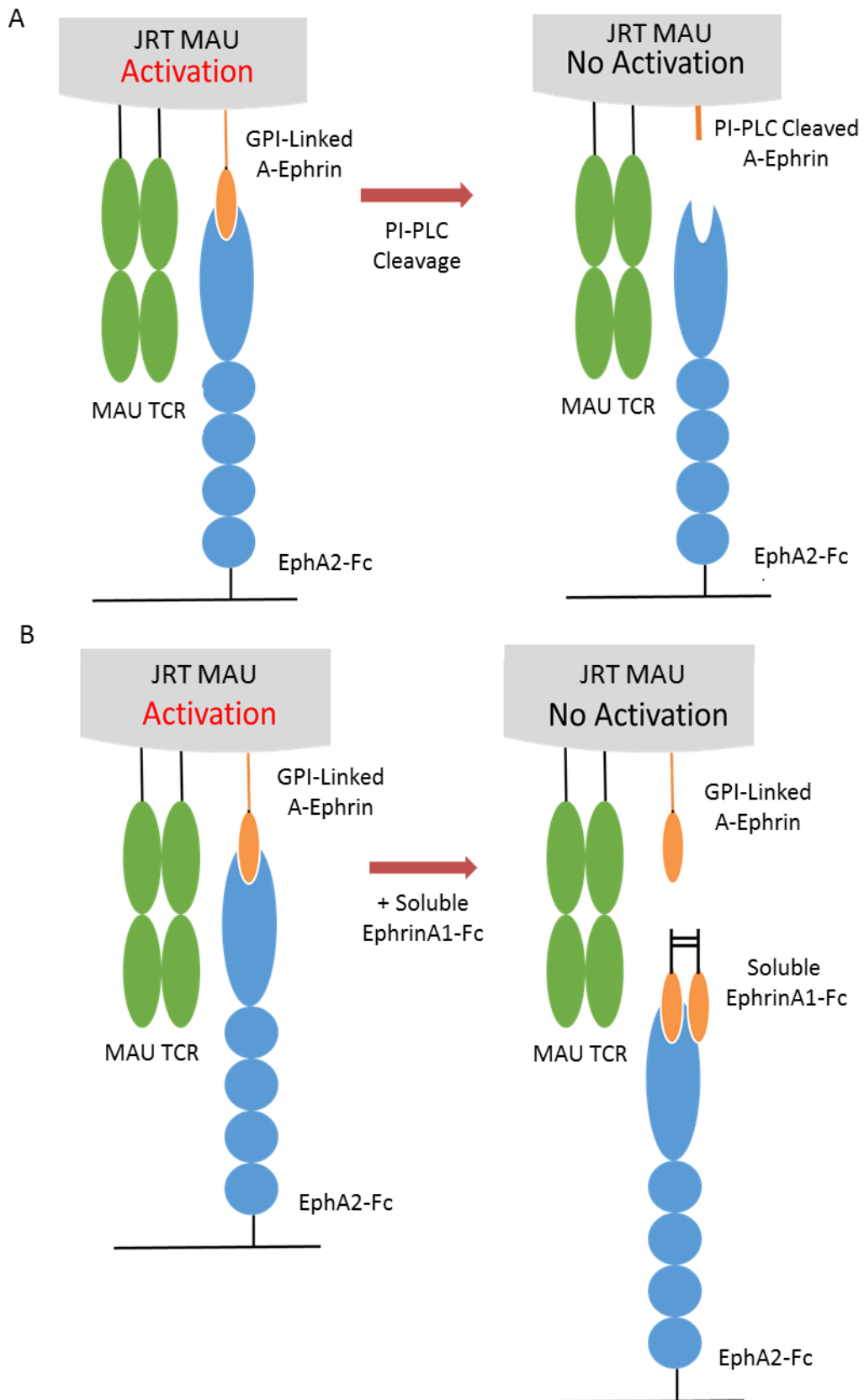


Figure 3.13 : Binding of EphA2 to ephrins is required for the activation of JRT MAU

Schematic summary of previous experiments. PI-PLC cleavage of GPI-linked A-ephrins from the surface of JRT MAU (A) and blocking of the EphA2 ephrin binding pocket with soluble ephrinA1-Fc (B) prevents activation of JRT MAU.

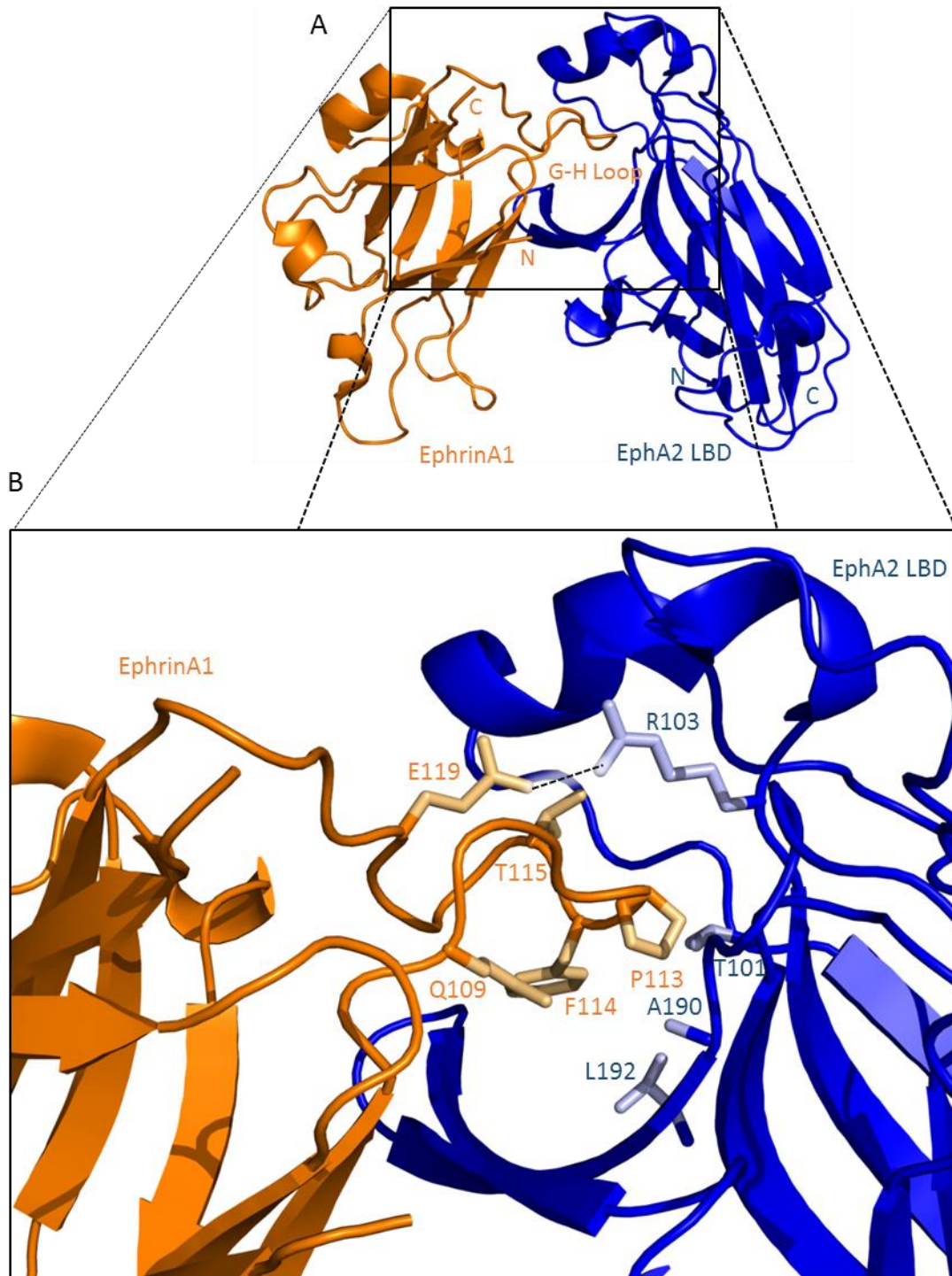


Figure 3.14 : Ribbon representation of the interaction between EphA2 and ephrinA1

(A) Binding is largely facilitated by hydrophobic interactions between the hydrophobic pocket of EphA2 LBD and the G-H loop of ephrinA1. (B) Close-up view of the binding pocket. Binding is secured by the salt bridge formed between R103 in the EphA2 binding pocket and E119 of the G-H loop of ephrinA1 (black dotted line). T101, A190 and L192 of the EphA2 binding pocket provide the majority of the hydrophobic interactions with residues T115, P113, F114 and Q109 of the G-H loop of ephrinA1 (Structure obtained from the Protein Dand Bank, PDB: 3HEI).

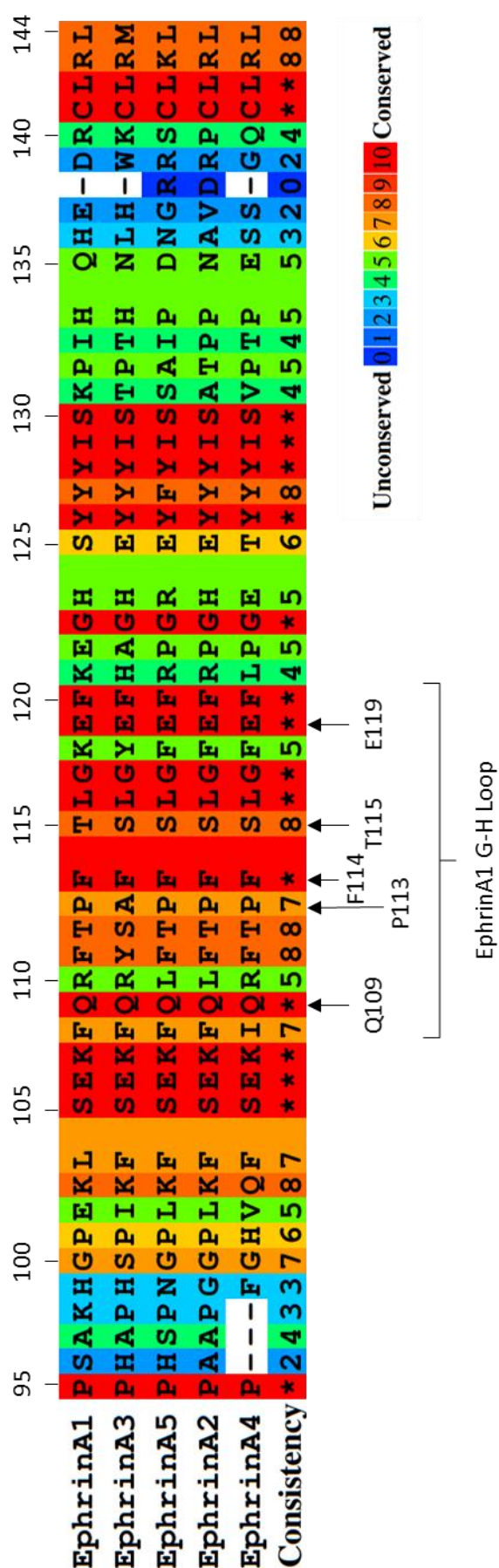


Figure 3.15: Sequence alignment of the G-H loop region of the A-ephrin family

The sequences of the A-ephrin family were aligned using PRALINE. The G-H binding loop is homologous amongst A-ephrins, including the key EphA2 binding residues at positions 109, 113, 114, 115 and 119. The colour scheme of the alignment represents amino acid conservation, 0 = unconserved and 10 = conserved. All residue numbers correspond to EphrinA1. UniProt entries for ephrinA1 – A5 = P20827, O43921, P52797, P52797 and P52803 respectively.

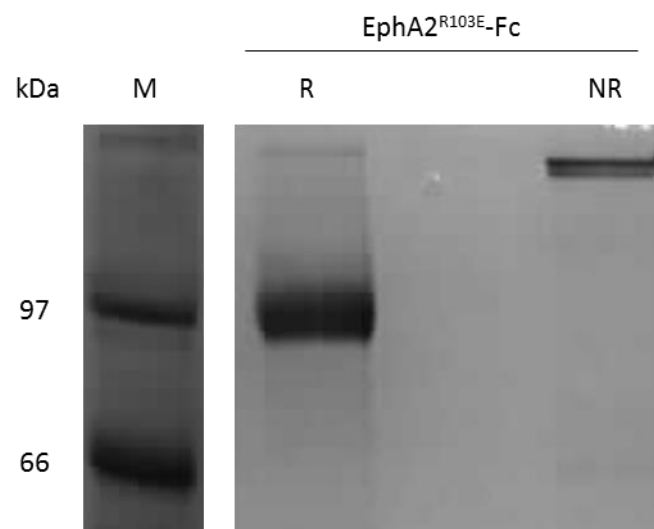


Figure 3.16: SDS-PAGE analysis of 293T-derived EphA2^{R103E}-Fc

EphA2^{R103E}-Fc was purified using Ni-NTA chromatography. Reduced (R) sample migrates at approximately 100kDa, equivalent to the WT EphA2-Fc construct. The non-reduced (NR) samples migrates at approximately twice this size. Proteins visualised with Instant Blue.

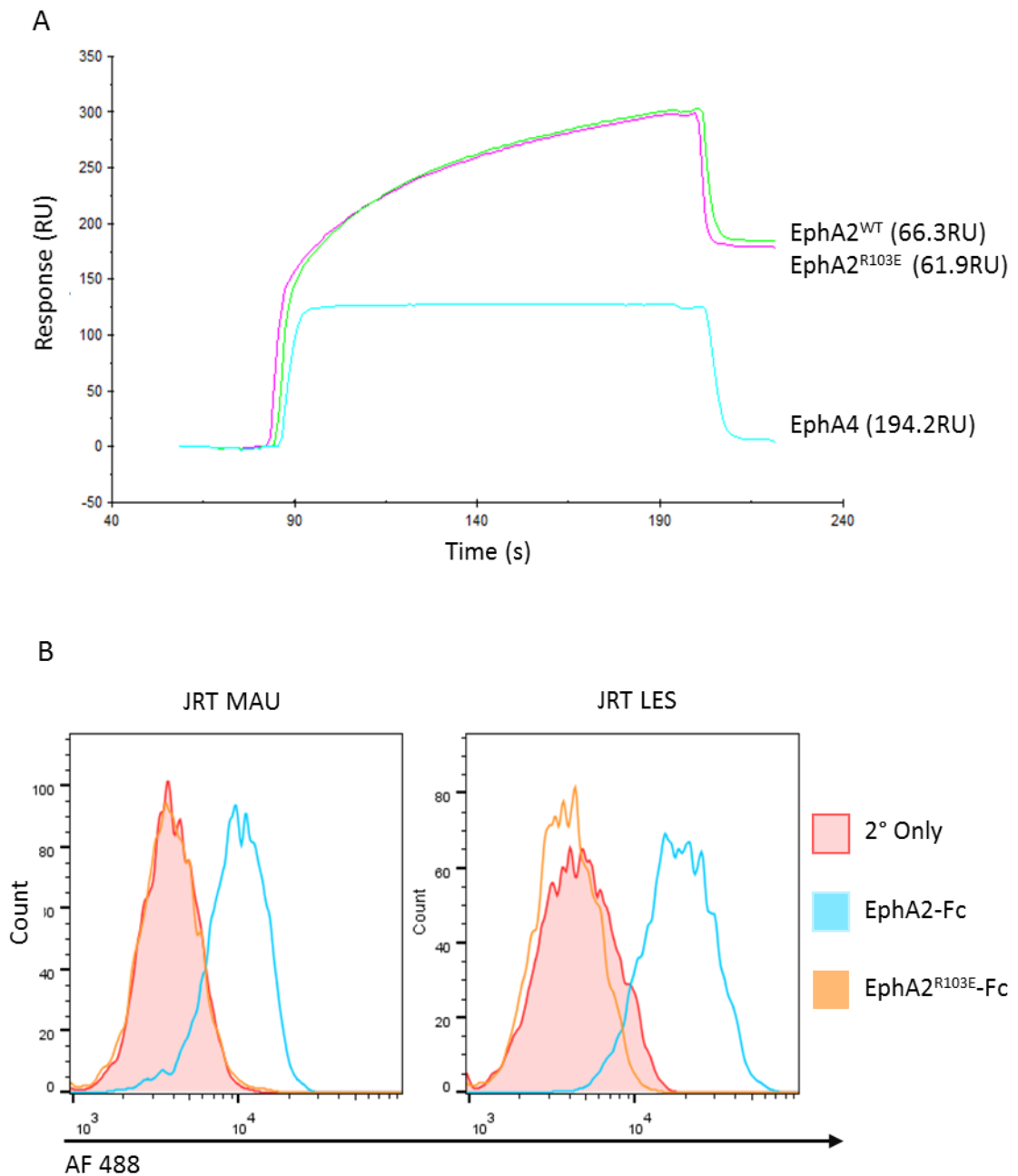


Figure 3.17: Validation of the EphA2^{R103E}-Fc construct

(A) Fc-tagged ephrin receptors were immobilised on a R10Z8E9 coated CM5 BIAcore chip. Anti-EphA2 pAb was then injected over the chip. Equivalent binding to the WT EphA2-Fc was observed. Figure in brackets represents RU of receptor immobilised on the chip. (B) Fc-tagged ephrin receptors were used to stain either JRT MAU or JRT LES cells, and were detected using an AF488 conjugated goat anti-human Fc secondary antibody. EphA2^{R103E}-Fc failed to bind the surface of either cell type. (Representative, $n=3$).

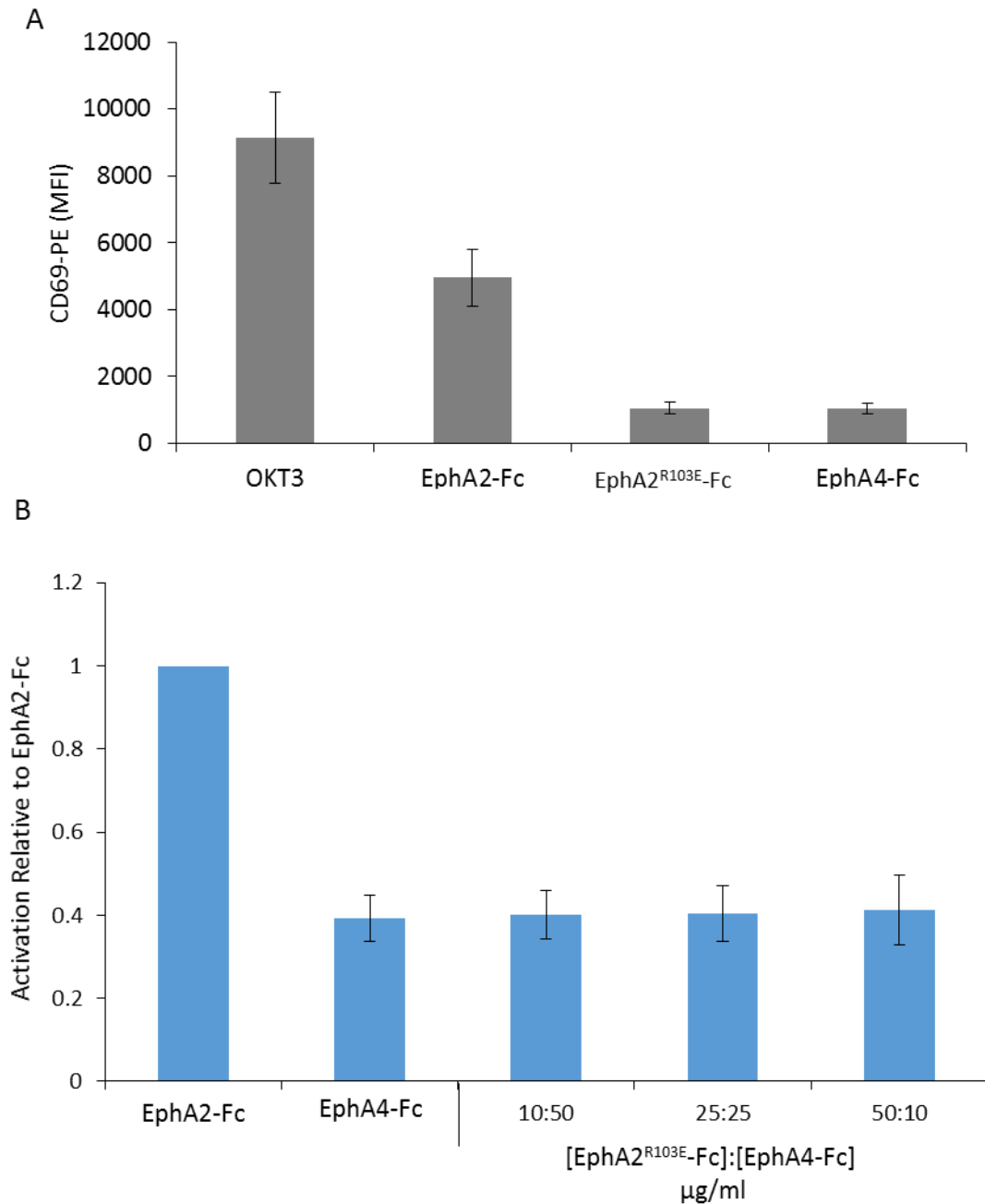


Figure 3.18: Characterisation of the EphA2^{R103E}-Fc construct

(A) Fc-tagged ephrin receptors were immobilised on a 96-well plate and incubated with JRT MAU cells for 4 hours. Activation was measured by CD69 upregulation. (B) EphA2^{R103E}-Fc and EphA4-Fc were coated onto a 96 well plate at various concentrations and incubated with JRT MAU cells for 4 hours. Activation was measured by CD69 upregulation. EphA2^{R103E}-Fc was unable to rescue activation of JRT MAU by EphA2-Fc. ($n=3$, error bars =SD).

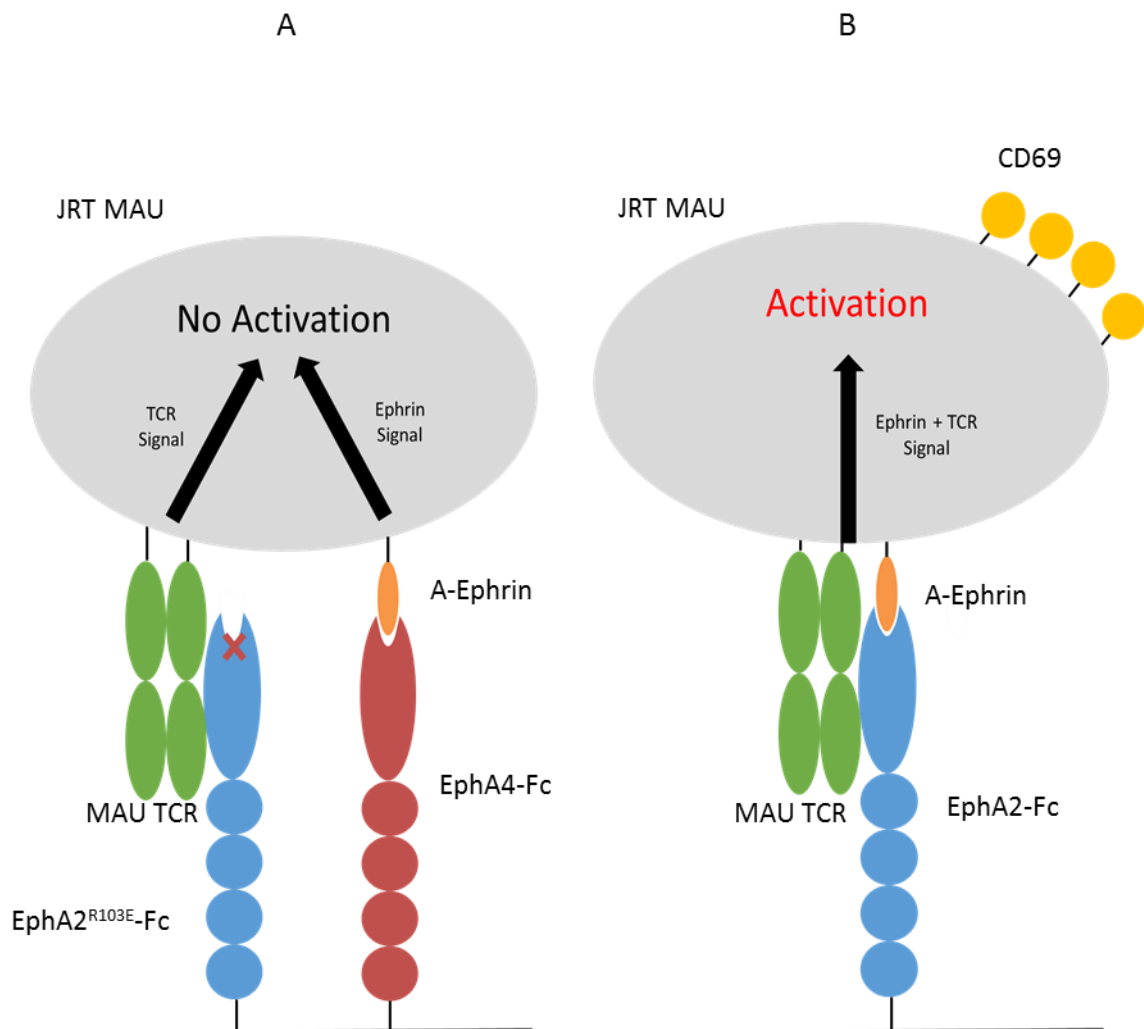


Figure 3.19 : The TCR and ephrin signal from EphA2 have to occur on the same EphA2 molecule

(A) EphA2^{R103E}-Fc (E103 designated by red cross) fails to activate JRT MAU in the presence of EphA4-Fc. MAU TCR is able to bind EphA2^{R103E}-Fc and EphA4-Fc is able to bind surface ephrins. (B) JRT MAU can only be activated when the TCR and ephrin signal originate from the same EphA2-Fc molecule.

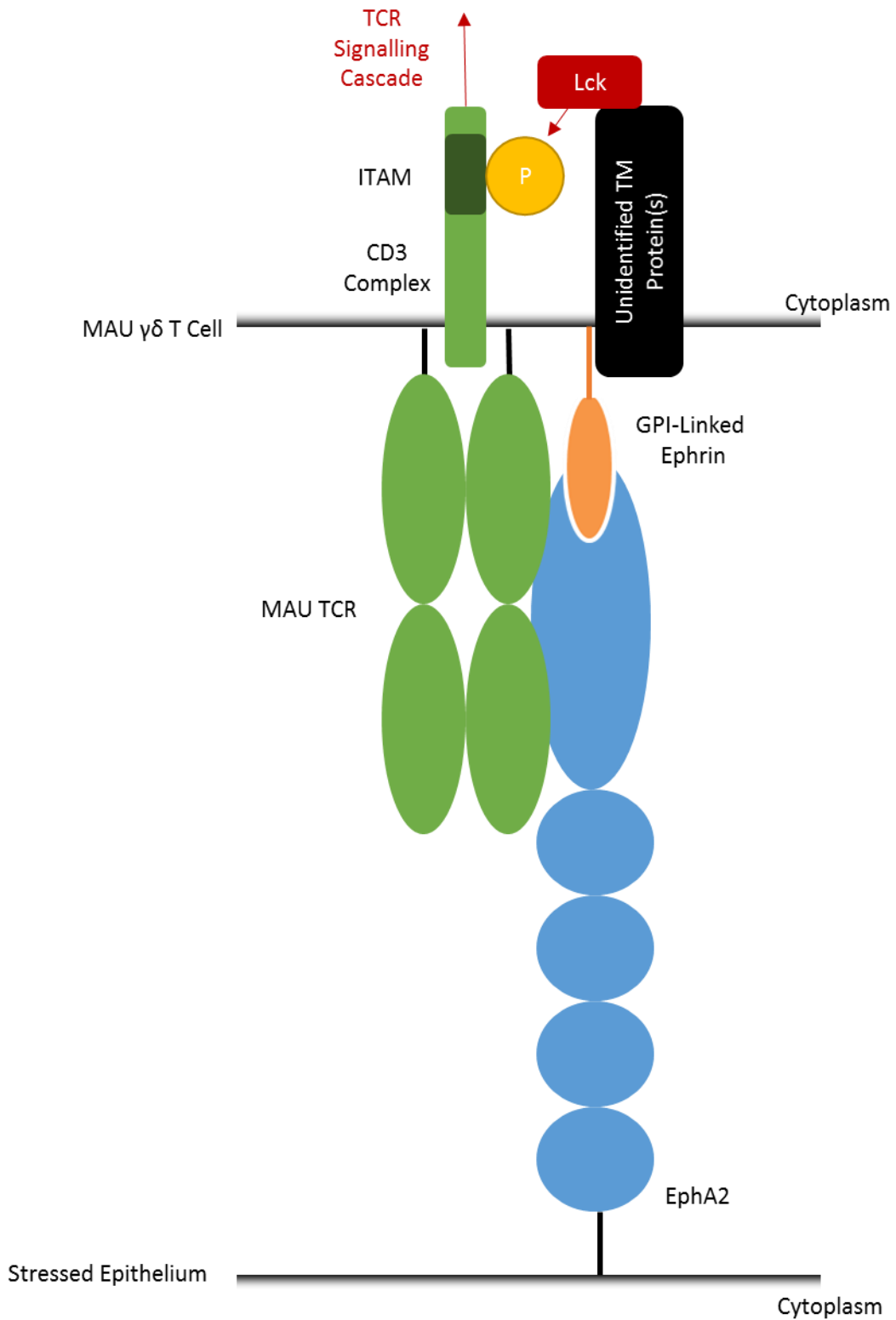


Figure 3.20: Schematic of the proposed tri-partite EphA2 recognition complex

Schematic of model demonstrating the tri-partite recognition complex formed by EphA2, MAU and ephrins. In this model, GPI linked ephrins associate with TM proteins which can recruit intracellular Src family kinases such as Lck. These kinases then phosphorylate the ITAMs of the CD3 complex, initiating a TCR signalling cascade.

Characterising the Interaction of the MAU TCR

with EphA2

4.1 Introduction

In the previous chapter, the broad requirements for recognition of an epithelial stress ligand by a $V\delta 2^{\text{negative}}$ $\gamma\delta$ T cell were established. EphA2 recognition requires the MAU $\gamma\delta$ TCR and successful binding of ephrins, on the same molecule. This is unlike any previously characterised immune receptor interaction, and the unusual nature of this recognition modality warrants further investigation. The aim of this chapter is to expand upon these findings, and define the role of the TCR in this interaction, by identifying the TCR binding site and which regions of the MAU TCR are involved.

There have been limited studies on the structure of $\gamma\delta$ TCRs, with 5 structures reported to date^{31,50,51,58,141}. All of these structures strongly suggest that one or more of the CDR loops projecting out from the receptor are likely to mediate contacts with their ligands. Of these 5 $\gamma\delta$ TCR structures, three are complex structures of $\gamma\delta$ TCRs bound to ligand, one describing the interaction of murine G8 $\gamma\delta$ TCR with the stress inducible T22 MHC-like molecule³¹, and two describing $V\delta 1^+$ $\gamma\delta$ TCRs interacting with lipid-loaded CD1d^{50,51}. The complex structures invariably implicate the $\gamma\delta$ TCR CDR loops as direct mediators of recognition, specifically the CDR3 δ loops. The exact role of these CDR loops is not conserved between these interactions however, with the two structures of $\gamma\delta$ TCRs complexed with lipid-loaded CD1d proposing different recognition modalities and involvement of the γ chains.

How representative these studies are for the $\gamma\delta$ TCR repertoire is unclear. For example, typically less than 1% of the $V\delta 1^+$ population can be stained by lipid-loaded CD1d tetramers⁷¹. Potential $\gamma\delta$ TCR ligands identified to date have demonstrated considerable structural diversity and can be broadly categorised into one of two groups, MHC-like and

non-MHC-like (Figure 4.1). It is easy to envisage how these recognition modalities may apply to the MHC-like ligands, but their extension to the non-MHC-like ligands, such as EphA2, is less well defined.

However, even within the MHC-like $\gamma\delta$ TCR ligands, recognition seems to be considerably diverse. For example, EPCR, a lipid presenting MHC-like molecule is specifically recognised by a $\gamma\delta$ TCR in a lipid-independent manner, on the underside of lipid binding platform¹²³. This is in contrast to T22 and CD1d, which interact with their respective $\gamma\delta$ TCR via the lipid binding groove, and CD1d presents lipids to $\gamma\delta$ T cells^{31,50,51}.

Increased understanding of the molecular basis for the recognition of EphA2 by MAU is potentially important for outlining paradigms for the structural basis of the $\gamma\delta$ TCR interaction with non MHC-like molecules, which could be used to fully characterise the interaction of $\gamma\delta$ TCRs with currently known ligands. This improved knowledge could also expedite ligand identification by identifying structural characteristics within ligands associated with $\gamma\delta$ T cell recognition. For example, other members of the ephrin receptor family may be recognised by $\gamma\delta$ T cells, and this data may allow for a more directed approach at detecting such interactions. Furthermore, there is also potential to exploit such findings to develop approaches with an aim to mimic or enhance such an interaction clinically. Indeed, EphA2 is a significant cancer target, and the subject of a number of therapeutic approaches¹⁴², and therefore understanding how the immune system interacts with this molecule could prove a significant development.

4.2 Results

4.2.1 AlphaScreen suggests binding between EphA2 and MAU TCR

Direct binding data between recombinant versions of proteins is a powerful indication that two molecules interact. Early attempts at BIAcore SPR experiments to detect binding between EphA2 and MAU TCR in our laboratory have proven unsuccessful, as discussed in the previous chapter. In order to overcome the limitations of BIAcore, AlphaScreen technology was subsequently explored. AlphaScreen is a microplate-based bead assay in which recombinantly tagged proteins are bound to either a donor or an acceptor bead. If the two recombinant proteins bind, the donor and acceptor beads are brought into close proximity. The donor bead is then excited with light at 680nm, causing it to emit a singlet of oxygen ($^1\text{O}_2$). If the acceptor bead is close enough to the donor bead, this $^1\text{O}_2$ causes the acceptor to emit light at a wavelength of between 580nm and 620nm, which is detected by the plate reader (Figure 4.2A). For this study, biotinylated MAU TCR (MAU-Bt) was bound to streptavidin-coated donor beads and EphA2-Fc was bound to protein A-coated acceptor beads. Production of these recombinant proteins was discussed in detail in Chapter 3.

Since the use of AlphaScreen to detect protein-protein interactions was a new technology adopted by the group, several steps were undertaken to validate this approach. Firstly, the AlphaScreen beads were supplied with a biotinylated rabbit IgG fragment (IgG-Bt), which binds both the streptavidin donor and protein A acceptor beads simultaneously. This control produced large emissions when incubated with the AlphaScreen beads across a range of concentrations, in line with the product documentation (Figure 4.2A). Secondly, to examine the system with recombinant proteins produced in our laboratory, binding of the anti-V γ 9 antibody to MAU-Bt was assessed. This experiment showed strong evidence

of specific binding between these two reagents (Figure 4.2B). Collectively, these experiments demonstrated that the AlphaScreen methodology could be successfully utilised with our recombinantly expressed proteins.

Initial screens for interaction between EphA2-Fc and MAU-Bt were performed as a titration of both proteins, which allows for the assessment of binding behaviour over a range of protein concentrations, as well as for the determination of the correct concentration of reagents to use for future experiments. This process is particularly important for the AlphaScreen assay, due to the 'hooking effect'. Because AlphaScreen beads are not washed after binding to the tagged proteins, any residual protein following saturation remains free in solution. These unbound proteins are then available to bind their bead-bound partners, and thus prevent a bead bound protein from binding. This results in a decrease in signal as the concentration of protein increases, as fewer beads are brought into close proximity to facilitate $^1\text{O}_2$ transfer. A similar effect was also observed in the control experiment performed with biotinylated rabbit IgG at antibody concentrations over 1.5nM (Figure 4.2A), caused by an excess of IgG fragments.

Controls in these experiments were designed to account for non-specific stickiness of the proteins with the beads. Therefore, the results for this technique are represented as a ratio of emission to background (emission:background). With this approach, background is defined as the highest emission of either of the two protein partners individually, at the same concentration, with both donor and acceptor beads.

These titration experiments demonstrated a clear dose-dependent binding pattern between EphA2-Fc and MAU-Bt (Figure 4.3A), with the hooking effect apparent at EphA2-Fc concentrations above 0.15 μM . MAU-Bt does not appear to reach sufficiently high

concentrations to achieve the hooking effect. This is consistent with a low affinity monomeric MAU-Bt, in contrast to the dimeric EphA2-Fc. EphA4-Fc, which failed to activate JRT MAU in the previous chapter, was used as a control and produced much lower emission:background ratios when used with MAU-Bt over identical concentration ranges (data not shown). As confirmation of this approach for detection of binding between $\gamma\delta$ TCRs and ligands, binding of the LES $\gamma\delta$ TCR with its ligand EPCR, which has been demonstrated by BIAcore, shows a similar pattern (J Déchanet-Merville, unpublished). The ideal concentration of EphA2-Fc and MAU-Bt was then determined by selecting two concentrations which produce a considerable emission:background ratio, whilst not using excessive amounts of protein. For the following experiments, concentrations of 0.7 μ M of MAU-Bt and 0.15 μ M of ephrin receptor were selected.

To expand these initial titrations, AlphaScreen experiments were conducted with TCR and ephrin receptor controls. These experiments typically showed strong specific binding between EphA2-Fc and MAU-Bt, with emission:background ratios of greater than 35 (Figure 4.3B). In contrast, EphA2-Fc showed no binding to either LES-Bt (a V γ 4V δ 5 TCR) or LDN5-Bt (an $\alpha\beta$ TCR), highlighting that this binding was TCR specific. Finally, EphA4-Fc failed to bind MAU-Bt.

These results strongly indicated that AlphaScreen is a viable approach to detect $\gamma\delta$ TCR/ligand interactions, and that MAU-Bt directly binds EphA2-Fc, supporting previous data described in Chapter 3. This is strengthened by the observation that EphA4-Fc, which does not activate JRT MAU, failed to bind MAU-Bt.

The establishment of a direct binding assay for this interaction also allowed for the development of mutagenesis approaches to dissect the nature of the binding between EphA2 and MAU TCR.

4.2.2 Modelling the interaction between EphA2 and MAU TCR

4.2.2.1 Modelling of the MAU TCR

To further characterise the interaction between EphA2 and the MAU TCR, molecular modelling was performed to generate hypotheses about their binding mode which would be used to inform future mutagenesis experiments.

Currently, there is no structure available for the MAU TCR, and so a model was generated using Phyre¹¹². This program predicts the three dimensional structure of a protein by comparing its amino acid sequence with previously determined protein structures. To model the MAU TCR, the MAU V γ 9 chain was modelled on the V γ 9 chain of the G115 human V γ 9V δ 2 TCR structure (PDB: 1HXM)⁵⁸, and the MAU V δ 1 chain was modelled on the δ chain of the murine G8 TCR (PDB: 1YPZ)³¹. These templates were selected by the Phyre software due to their high sequence identity to the MAU γ and δ chains (94% and 54% respectively). During this analysis, the crystal structure of the V δ 1⁺ 9C2 TCR was unavailable⁵¹. The δ chain of this TCR possesses 98% sequence identity with the MAU δ chain, considerably higher than that for the G8 TCR δ chain used in this study. Despite this, the G8 based model used in this study was modelled with a 99.97% confidence, which the authors of the program suggest is sufficient to generate a model between 2-4Å root-mean-square deviation RMSD from the true structure¹¹². Indeed, when aligned with the 9C2-derived δ chain model, the models are very similar (including the flexible CDR loops) and have an RMSD of 1.7Å,

suggesting that despite the lower sequence identity, the G8 based δ chain model is largely comparable to the 9C2 based model (data not shown).

A complete model for the MAU $\gamma\delta$ TCR heterodimer was formed by overlaying each chain onto the human G115 V γ 9V δ 2 structure (PDB: 1HXM⁵⁸) using WinCoot¹¹¹ (Figure 4.4).

The resulting MAU $\gamma\delta$ TCR model was then analysed and compared to previously determined $\gamma\delta$ TCR structures to ensure that the model maintained core structural characteristics associated with these structures. The $\gamma\delta$ TCR structures generated to date describe four characteristic Ig folds, two in each chain forming the variable (V) and constant (C) regions. In each chain of the MAU model, the V and C domains are clearly defined Ig folds, consisting of characteristic antiparallel β -sheets closely packed together and stabilised by a disulphide bond. The Ig core region is further stabilised by an invariant tryptophan residue (W36) , and various non-polar interactions mediated by hydrophobic residues¹⁴³. The MAU V δ 1 variable domain is shown in Figure 4.5 as a representative example.

The CDR1, 2 and 3 regions of MAU were defined by the IMGT V-QUEST tool¹⁴⁴, and when mapped onto the MAU TCR model, they are represented as solvent exposed flexible loops (Figure 4.6), similar to previously determined $\gamma\delta$ TCRs, suggesting that they may be involved in binding to ligands, as demonstrated for the T22/G8³¹ and CD1d/9C2⁵¹ interactions. MAU CDR loops were labelled using a two digit system, whereby the first digit represents the TCR chain (V γ 9 or V δ 1) and the second digit signifies the CDR. For example, the V γ 9 CDR3 loop is referred to as 93.

This analysis, combined with the high sequence identity between MAU and the template structures, suggested that the Phyre-derived MAU model is a plausible representation of the MAU $\gamma\delta$ TCR structure.

4.2.2.2 Exploring models of EphA2 and MAU TCR

Exploring potential models of the interaction between EphA2 and MAU TCR would help to shape future mutagenesis work by defining constraints for the interaction and to predict potential binding sites. Although computational models are available for the prediction of binding sites, these approaches are only reliable once the number of potential sites has been reduced, and potential residues involved have been experimentally verified.

Firstly, surface electrostatics analysis of EphA2 using DelPhi (PDB:2X10⁸⁰) was used to detect potential binding sites between EphA2 and MAU TCR, with the aim to identify specific electrostatic signatures which are often associated with protein-protein interactions, such as distinct complementary electropositive/electronegative patches on either molecule. The analysis revealed no such signatures (Figure 4.7). Therefore, given the large surface area of EphA2, more constraints were needed in order to restrict the number of potential MAU binding sites.

To gain a better understanding of the relative size and shape of EphA2 and MAU TCR, attempts were made to manually model the tripartite complex formed between EphA2, ephrins and the MAU TCR. This model would assist in shaping further mutagenesis work by excluding any regions of EphA2 or MAU TCR which are unlikely to interact with each other, either through steric restrictions or size constraints. The complex structure of EphA2 and ephrinA5 (PDB 2X11⁸⁰), as well as the Phyre-derived MAU TCR model, were manually modelled with WinCoot¹¹¹ (Figure 4.8).

In order to reduce the number of potential binding sites, the size of the two molecules and their relative orientation of domains were carefully scrutinised, to determine if any domains of EphA2 and MAU TCR could be excluded from participating in this interaction, either through steric hindrance or inability to reach them from the surface of the T cell (Figure 4.8). Unfortunately, the protein structures and models do not provide any information on how the proteins are displayed on the cell surface, as the regions which connect the membrane proximal domain with the transmembrane region are likely to be flexible, and so it is not possible to determine either how the protein is situated relative to the membrane, but also how long the linker regions are spatially given the large number of conformations they can adopt. With these considerations in mind, the modelling suggested that the MAU TCR could theoretically contact all domains of EphA2, with no sites either out of reach, or sterically excluded by other domains. This was unexpected, given that EphA2 is approximately twice the length of the MAU TCR (160Å to 80Å respectively). This is likely due to the observation that EphA2 is unlikely to extrude perpendicularly from the plasma membrane¹⁴⁵, thereby reducing the distance it extends laterally from the cell surface.

Comparison of multiple EphA2 structures revealed considerable flexibility in the membrane proximal region, with a relative rotation of approximately 71° between the two FN domains of EphA2^{80,145}, suggesting a hinge-like nature of the FN1-FN2 linker (Figure 4.9). These studies also noted points of flexion between the LBD-Sushi domains and within the EGF domain, but relative positions of these domains was largely stable^{80,145}. Analysis of the crystal structure of EphA4 revealed considerably less flexibility between the FN1 and FN2 domains of this protein compared to EphA2, resulting in the FN2 domain packing tightly to the FN1 domain, with little variation between crystals¹⁴⁶. The functional consequences of this difference in flexibility between EphA2 and EphA4 is unclear, but may impact on

receptor-membrane interactions and orientation relative to the cell surface, implying that EphA2 can adopt a wider array of orientations on the cell surface, which further complicates the modelling process.

In summary, this modelling revealed that the TCR could potentially bind to all domains of EphA2, and so if computational methods were to be used to generate a viable model of the trimeric complex, additional constraints through domain deletion mutagenesis would be required.

4.2.3 Mutation of the MAU CDR loops

Although it had been determined that the MAU TCR interacts with EphA2, which regions of the TCR are involved in the interaction was still unclear. The MAU TCR model revealed that the CDR loops are solvent exposed, flexible loops. This suggested that they were promising candidates to be involved in ligand binding, similar to the previously characterised $\gamma\delta$ TCR ligand interactions^{31,51} (Figure 4.10A, B).

In order to test this hypothesis, several CDR loop mutants of MAU-Bt were designed. Using the MAU Phyre model, residues encompassing the exposed CDR loops were selected for mutation. The prominent and flexible nature of the CDR loops indicated that they are unlikely to play an important role in maintaining the V-domain fold. Hence, these CDR loops could be subjected to relatively major changes to disrupt potential binding with EphA2, without compromising the overall fold of the V domain. For each CDR, four residues were selected for mutation, and substituted for residues of different size, hydrophobicity or charge. In addition, codon changes were also considered when selecting substitution residues in order to minimise changes to the WT sequence, which simplified PCR steps (Table 4.1). As an example, the MAU V γ 9 CDR3 loop contains the residues 102VQSV105 at

the tip of the loop (Figure 4.10C, left). The MAU Phyre model suggested that these residues were not involved in mediating contacts with the δ chain or the framework regions of the V γ 9 domain (Figure 4.6). It was therefore decided to mutate these residues to 102EWRD105 (Figure 4.10C, right).

To clone these mutants, site directed mutagenesis (SDM) was used to modify the WT MAU V γ 9 and V δ 1 constructs. With this approach, there is a maximum number of bases which can be changed per mutagenic primer pair, to ensure the primer can still bind the template. Therefore, the final mutants were formed through several rounds of SDM amplifications, using the previous mutant as the template for the subsequent SDM amplification. The base changes for each of the 6 MAU CDR loops are listed shown in Appendix 4.1. MAU mutants were classified using a two digit system, whereby the first digit represents the TCR chain (V γ 9 or V δ 1) and the second digit signifies the CDR. For example, the V γ 9 CDR3 loop mutant is referred to as MAU 93.

Sequence-verified mutated constructs were expressed in the *Drosophila* S2 expression system, and purified using Ni-NTA chelate chromatography and biotinylated as previously described in Chapter 3. TCR yields were typically 1.5mg of specific protein per 1L of S2 supernatant, equivalent to the yield of WT MAU TCR (Figure 4.11). To ensure correct folding of the mutant MAU chains, and formation of heterodimeric TCR, BIAcore was used to detect binding of pan $\gamma\delta$, V γ 9-specific and V δ 1-specific mAbs as previously described. In these experiments, biotinylated mutant MAU constructs were immobilised to a streptavidin coated CM5 chip, and TCR-specific monoclonal antibodies were injected over the immobilised TCRs (Figure 4.12). All mutant MAU TCRs successfully bound the mAbs,

suggesting that they were folded correctly, despite incorporating drastic mutations within their CDR loops.

4.2.4 Generation of the EphA2^{ΔLBD} mutant

Concurrently with the production of the MAU TCR CDR loop mutations, an EphA2 mutant was produced which lacked the ligand binding domain (EphA2^{ΔLBD}, Figure 4.13B), with the aim of using the AlphaScreen assay to determine whether this domain was critical for MAU TCR binding.

While designing the EphA2^{ΔLBD} mutant, the domain boundaries were carefully defined. Domains are independently folded regions of a protein, usually connected by short, flexible sections of amino acids. Therefore, if the protein is truncated at these short sections, the remaining domains should fold correctly. EphA2 domain boundaries were first identified using the UniProt database¹²⁸, which predicts domains based on published studies and conserved amino acid motifs. These boundaries were then verified by examining the crystal structure of the EphA2 ectodomain (PDB: 2X10⁸⁰). One of the important factors to consider was the amino acid environment proximal to the domain boundaries. For example, there is a disulphide bond formed between cysteine residues 201 and 205 of the Sushi domain near the boundary of the LBD (Figure 4.13A). Disulphide bonds are key components of tertiary structure, and disrupting them could potentially result in protein misfolding, so it was important to incorporate C201 into the Sushi domain in order to maintain this disulphide bond. The EphA2^{ΔLBD} construct encompassed residues K119 to N534 (Figure 4.13B).

With the domain boundaries defined, the EphA2^{ΔLBD} mutant was then cloned using domain-specific PCR primers into the pHL-Fc vector. This construct was then expressed in the 293T

expression system and purified by Ni-NTA chelate chromatography as previously described. Yields of EphA2^{ΔLBD}-Fc were consistent with WT EphA2-Fc, around 1.5mg of specific protein from 250ml of S2 supernatant. SDS-PAGE analysis of fractions eluted from the Ni-NTA column revealed that EphA2^{ΔLBD}-Fc migrates at its predicted size of 63kDa under reducing conditions (Figure 4.14).

To confirm correct folding of the EphA2^{ΔLBD}-Fc construct, BIAcore was used to detect the binding of an anti-EphA2 pAb. This experiment revealed that despite lacking the LBD, EphA2^{ΔLBD}-Fc successfully bound the anti-EphA2 pAb, suggesting that the remaining domains were correctly folded (Figure 4.15A). Consistent with the premise that ephrin binding is essential for activation of JRT MAU by EphA2, EphA2^{ΔLBD}-Fc failed to activate JRT MAU (Figure 4.15B).

4.2.5 AlphaScreen irregularities

The EphA2^{ΔLBD} and MAU CDR loop mutants were used in the AlphaScreen assay in order to determine whether the TCR bound the EphA2 LBD, and if binding was CDR-dependent. These initial AlphaScreen experiments suggested that the EphA2^{ΔLBD}-Fc construct bound specifically to MAU-Bt, usually with a higher emission:background ratio than WT EphA2-Fc (Figure 4.16). These results suggested that the LBD of EphA2 was not critical for binding MAU TCR.

However, as more data were collected, several anomalies were observed particularly with the controls, thereby raising doubt as to the reliability of the AlphaScreen assay. For example, on several occasions WT EphA2-Fc protein showed no binding with WT MAU-Bt, despite previous results demonstrating robust binding. Furthermore, in some experiments binding between the negative control EphA4-Fc and MAU-Bt was noted (data not shown).

Hence, it was deemed necessary to re-examine the reagents and controls used in these experiments with the aim of obtaining more consistent results before the AlphaScreen assay could be used to determine regions of EphA2 and MAU TCR that were critical for binding.

Revisiting the titration assay to gain an improved understanding of the effect of varying concentrations of reagents in the experiment yielded further inconsistent results, ranging from unequivocal binding between EphA2-Fc and MAU-Bt to highlighting no binding between these molecules (data not shown). To further complicate matters, binding was occasionally observed between EphA4-Fc and MAU-Bt. In order to determine the underlying cause of these varying results, several steps were undertaken to control most variables in the assay.

Firstly, preliminary experiments had shown that the buffer used in the AlphaScreen assay has a large effect on the binding observed. To account for this, significant care was taken to ensure buffer batches were as consistent as possible, and due to the addition of BSA, buffer was filter sterilised and stored at 4°C to inhibit bacterial growth. It was also noticeable that different batches of MAU-Bt from the same production system yielded variable binding results.

In order to control for TCR purity and background contaminants, the TCR was further purified using size exclusion chromatography (SEC). Briefly, a batch of MAU TCR (MAU VII) was purified using Ni-NTA chromatography and a PD10 desalting column as previously described. Half of the purified protein was further purified using SEC, producing a much purer sample (data not shown). Further experimental details are available in Chapter 2. Interestingly, when these two proteins were used in the AlphaScreen assay to detect

binding to EphA2-Fc, the SEC purified MAU-Bt failed to bind, whereas the Ni-NTA purified MAU-Bt demonstrated binding at two concentrations (data not shown). This result suggested that the ability to detect MAU-Bt/EphA2-Fc interaction may be dependent upon the level of impurities present in the recombinant protein samples.

Collectively these data suggested that the AlphaScreen assay is not a robust system in which to test this interaction between EphA2 and MAU. Although initial binding data appeared to be reproducible, which prompted the production of mutants to use in this assay, subsequent discrepancies and unpredictable controls raised doubts over the reliability of the data. Our collaborators also independently reported similar inconsistencies despite promising early results. For these reasons it was decided to abandon the AlphaScreen assay as means of detecting binding between EphA2 and MAU TCR. Potential reasons for this are discussed in section 4.3.

Although not entirely reproducible, the early results do provide an indication that EphA2 does indeed bind MAU TCR, enough to justify further characterisation of this interaction. The data also suggested that MAU TCR binds the EphA2^{ΔLBD} construct, suggesting the TCR binds EphA2 at a domain other than the LBD. Again it is important to note that these results were only used to inform further experiments, and are not conclusive.

4.2.6 The EphA2 LBD is sufficient for activation of JRT MAU

In lieu of a reliable direct binding assay, the more robust and reproducible activation assay was used to determine the domain of EphA2 to which the MAU TCR binds.

Firstly, to assess whether the MAU TCR interacted with the EphA2 LBD, an EphA2 LBD construct engineered to an Fc-tag was designed. This construct proved difficult to express in the 293T system, and several constructs were designed with different domain

boundaries to overcome potential protein folding errors. Ultimately, this domain could not be expressed as an Fc protein in the 293T expression system (data not shown). It was possible that the EphA2 Sushi domain is required for the correct folding of the LBD, as several interdomain interactions are formed between them¹⁴⁵.

In lieu of the EphA2 LBD-Fc construct, an alternative strategy was devised. Two constructs were generated in which the LBDs of EphA2 and EphA4 were swapped (Figure 4.17A). EphA2^{2L4CF} contains the LBD of EphA2 and the CRD and FN domains of EphA4 whereas the EphA2^{4L2CF} is comprised of LBD of EphA4 and the CRD and FN domains of EphA2. Domain-specific primers were used to amplify the LBDs of EphA2 and EphA4 from a cDNA template, and these were cloned into the EphA2 and EphA4 Δ LBD constructs previously generated using the Gibson assembly protocol. These constructs were then expressed in the 293T expression system and purified as discussed in Chapter 3. Yields and purity of both mutants were equivalent to EphA2 WT (1.5mg from 250ml supernatant) and migrated equivalently to their WT counterparts based on analysis by SDS-PAGE (Figure 4.17B).

Due to the chimeric nature of these constructs, binding of the EphA2 pAb to determine correct folding would not have been informative. Instead, binding to ephrins was used as an indicator of correct folding. This was measured by staining the surface of JRT MAU cells, as detailed in Chapter 3. Briefly, EphA2^{2L4CF}-Fc stained JRT MAU equivalently to WT EphA2-Fc, and EphA2^{4L2CF}-Fc stained JRT MAU equivalently to WT EphA4-Fc (Figure 4.18).

These domain-swap mutants were subsequently used in the activation assay with JRT MAU cells. This revealed that EphA2^{2L4CF}-Fc (the construct containing the EphA2 LBD) specifically activated JRT MAU at levels equivalent to WT EphA2-Fc. The inverse construct, EphA2^{4L2CF}-Fc failed to activate JRT MAU (Figure 4.19). These results demonstrated that the EphA2 LBD

is sufficient for activating JRT MAU. As the presence of the MAU TCR is essential for this interaction, this suggested that the MAU TCR binds EphA2 within the LBD. Since previously it has been established that ephrin and TCR binding occurs on the same EphA2 molecule, it can be concluded that the MAU TCR is binding the EphA2 LBD at a site distinct from the ephrin binding pocket.

This finding contradicts the preliminary AlphaScreen data presented in this chapter, which suggested that the TCR binds distal to the EphA2 LBD (Figure 4.16). If this scenario was correct, the EphA2^{4L2CF}-Fc construct would be expected to activate JRT MAU, with the EphA4 LBD providing the ephrin signal, while the TCR would bind the EphA2 portion of the construct. Considering the reliability issues associated with the AlphaScreen, further characterisation of EphA2-MAU TCR interaction was undertaken using the activation assay.

4.2.7 Determining the MAU TCR binding site of EphA2

The data presented so far suggested that the MAU TCR binds the EphA2 LBD, contrary to the AlphaScreen data. In order to identify the TCR binding site in this domain, several EphA2 constructs were designed with mutations at potential TCR binding sites. These 'patch mutants' were then used in the activation assay to assess their effect on activation of JRT MAU.

To identify potential binding sites, the amino acid sequences of the LBDs of JRT MAU activating EphA2 and the non-activating EphA4 were aligned using Clustal¹⁴⁷, in order to identify non-conserved residues between the two proteins (Figure 4.20). Since ephrin and TCR signals originate from the same EphA2 molecule (see Chapter 3), these interactions most likely occur at distinct sites. Therefore based on the crystal structure of the EphA2-ephrinA5 receptor-ligand pair (PDB: 2X10)⁸⁰ residues either involved in the binding of

ephrins, or those predicted to be inaccessible due to involvement in ephrin binding, were excluded (Appendix 4.2). In addition, EphA2 residues involved in the formation of multimeric signalling complexes were also omitted. These surfaces are important for the correct formation of EphA2-ligand clusters upon EphA2 binding ephrins^{80,145}. As ephrin binding is essential for the recognition of EphA2 by MAU, this would likely result in clustering of EphA2 on the stressed cell. With this in mind, it is conceivable that the TCR binding site is unlikely to be located within the EphA2 clustering interfaces, and therefore these were also excluded as potential TCR contact residues (Appendix 4.2).

In addition, the LBDs of EphA2 (PDB code 2X10⁸⁰) and EphA4 (PDB code 4BK4¹⁴⁶) were aligned (Figure 4.21), to investigate whether localised conformational changes existed between these ephrin receptor molecules which may account for differences in binding to MAU TCR. Again, ignoring areas of the LBD involved in clustering and ephrin binding, areas which differed structurally were noted. Moreover, comparisons between the liganded (PDB code 2X11⁸⁰) and unliganded (PDB 2X10⁸⁰) forms of EphA2 LBD were made to determine regions that differ in conformation upon binding ephrins, which may also suggest potential TCR binding sites. Finally, non-conservative residues that were likely to play a critical role in maintaining the overall LBD fold were excluded. For example, residues that are inward-facing are likely to be involved in stabilising the core domain rather than binding to ligands, which is usually facilitated by surface-exposed residues. Combining these different filtering processes led to the identification of 18 residues eligible for mutation which were grouped according to location into five distinct patches (Figures 4.21 and 4.22). For this study, patches 1, 2, 4 and 5 were selected for mutation. Despite meeting the preceding criteria, patch 3 was excluded due to its close proximity to the Sushi domain, implying that MAU

TCR is unlikely to interact with this region (Figure 4.22). This strategy yielded a final list of candidate residues for mutation (Appendix 4.3).

Unlike the TCR mutagenesis strategy, the EphA2 patch mutants incorporated more conservative substitutions, as several of the residues were close to key structural regions, and hence drastic substitutions may have impeded correct protein folding and ephrin binding activity. The strategy underlying the introduction of mutations was such that any change should hopefully be significant enough to affect TCR binding. With this in mind, alanine scanning mutagenesis was deemed inappropriate, as changes may not significantly impact TCR binding. Sequence alignments of the LBDs of the ephrin receptor family were used (Appendix 4.2) in order to assess which residues could be tolerated at each position with minimal impact on the overall fold of the LBD (descriptions of the substitutions are detailed in Appendix 4.3). Final sequences are shown in Appendix 4.4.

For cloning of the patch mutants, mutant LBD regions were synthesised using gBlock technology (Integrated DNA Technologies). These were then cloned into the WT EphA2^{ΔLBD}-Fc constructs using the Gibson assembly methodology. These mutant constructs were then transfected into 293T cells and purified by Ni-NTA chelate chromatography as previously described. Protein yields were slightly higher than for WT EphA2-Fc, averaging 2mg of protein per 250ml of S2 supernatant. SDS-PAGE analysis of Ni-NTA purified EphA2 patch mutants revealed that they migrated equivalently to WT EphA2-Fc and displayed similar levels of purity (Figure 4.23). Correct folding was again confirmed by surface staining of JRT MAU, and all 4 patch mutants stained the surface equivalently, slightly higher than the WT EphA2-Fc batch (Figure 4.24A). More importantly, this confirmed that none of the mutations had affected ephrin binding to EphA2-Fc.

The ability of these EphA2 patch mutants to activate JRT MAU was determined using the activation assay. Patch mutants 1, 2 and 4 activated JRT MAU equivalently to WT EphA2, whereas EphA2^{PATCH5}-Fc failed to do so, with activation levels comparable to EphA4-Fc (Figure 4.24B). These results suggested that the area of EphA2 covered by the patch 5 mutant is vital for the activation of JRT MAU by EphA2. The observation that EphA2^{PATCH5}-Fc successfully stained the surface of JRT MAU strongly suggested that this was not due to defective ephrin binding, and therefore represents a region that is essential for activation, but distinct from ephrin binding. Detailed analysis of patch 5 reveals the exposed nature of these mutated residues, and despite their proximity to the ephrin binding pocket, they are unlikely to affect the fold of the J-K loop of EphA2⁸², which forms the roof of the ephrin binding pocket (Figure 4.25). Furthermore, the side chains of these patch 5 residues do not protrude into the binding pocket, and so are unlikely to effect the hydrophobic interactions which are likely to energetically drive the ephrin binding interaction.

Therefore, this approach identified a potential MAU TCR binding site in the LBD of EphA2, which is not involved in the binding of ephrins, but critical for the activation of JRT MAU by EphA2-Fc.

4.3 Discussion

In Chapter 3, the broad requirements for the activation of MAU by EphA2 were established, highlighting that both ephrins and MAU TCR were required to interact with the same EphA2 molecule. This chapter aimed to further characterise the role of the MAU TCR in this interaction.

The results presented in the preceding sections of this chapter strongly suggest that the MAU TCR binds EphA2 within the LBD. A surface patch of $\sim 355\text{\AA}^2$ on the LBD of EphA2 was

also identified as being crucial for the activation of JRT MAU by EphA2-Fc. This region could constitute the MAU TCR binding site.

AlphaScreen was used as a potential methodology to detect direct binding between recombinant EphA2-Fc and MAU-Bt. Despite promising early results, the reliability of this approach was questioned, and the technique was ultimately not pursued further. During the troubleshooting process, it was determined that the AlphaScreen assay was extremely sensitive to several variables including buffer conditions and contaminants, which varied between protein batches. Such sensitivity renders this assay unsuitable for this study. Because of this, conclusive direct binding between EphA2 and MAU TCR has yet to be demonstrated, despite strong evidence for this interaction. Undoubtedly, the demonstration of direct binding would greatly strengthen the proposal that EphA2 is a ligand for the $\gamma\delta$ TCR MAU. Therefore it is necessary to expand this study, and explore new approaches for the detection of direct binding between these molecules, such as Isothermal titration calorimetry, which is used to determine the thermodynamic properties of interactions in solution.

Although the MAU CDR loop mutants were not used in this study due to AlphaScreen reliability issues, their design, production and conformational verification provides a strong foundation for further research to elucidate the role of the MAU CDR loops in this interaction. In lieu of a reliable binding assay to determine the EphA2 binding capability of the soluble versions of these mutants, these constructs could readily be cloned into lentiviral transduction vectors and expressed as functional, surface-bound TCRs in JRT3 cells. These transductants could then be used to screen for EphA2 reactivity. As the folding capacity of the soluble versions of these mutants has already been verified in this study

using BIAcore, it indicates that these TCRs are likely to express well in the JRT3 cells, similarly to the WT MAU TCR construct.

The EphA2/EphA4 LBD swap experiments demonstrated that the EphA2 LBD can confer TCR specificity, and is sufficient for activation of JRT MAU. This strongly suggests that the MAU TCR binds the LBD of EphA2. This finding directly contradicts the AlphaScreen data, which suggested binding between EphA2^{ΔLBD}-Fc and MAU-Bt. Although this observation carries less weight due to unreliable controls, it could nevertheless represent a legitimate result. Indeed, as the results of WT EphA2 binding to MAU-Bt were taken to suggest a strong possibility of binding, it is important to consider the EphA2^{ΔLBD} result in the same fashion, and therefore establish how these contradictory results align with each other.

Although the EphA2 4L2CF EphA4/EphA2 domain-swap mutant failed to activate JRT MAU, this does not exclude the possibility that the TCR may interact with both LBD and Sushi domains, and so the MAU TCR could still bind the EphA2 ΔLBD region in some capacity. It is possible that this interaction can be sufficiently detected by AlphaScreen, but is inadequate for activating JRT MAU. Conversely, the remaining TCR footprint on the EphA2 LBD region of the EphA2^{2L4CF}-Fc construct may provide sufficient binding affinity to successfully activate JRT MAU, without the need for the EphA2 Sushi domain. Another possibility, if the AlphaScreen result is valid, is that the EphA2 LBD specifically acts on the Sushi domains of both EphA2 and EphA4, conferring TCR binding to this domain.

To conclusively demonstrate the sole importance of the EphA2 LBD in activating JRT MAU, it would be ideal to recombinantly express the EphA2 LBD alone. Attempts to express this construct were unsuccessful, despite several constructs reported in the literature produced in both 293T⁸² and *Drosophila* SF9¹⁴⁵ expression systems. Perhaps the engineering of a

construct with irrelevant globular domains to promote folding will allow for successful expression, and this should be explored further.

The EphA2 surface patch mutagenesis identified a 355Å² region of the LBD as crucial for the activation of JRT MAU by EphA2-Fc. Despite this patch's proximity to the ephrin-binding pocket of EphA2, successful binding of EphA2^{PATCH5}-Fc to ephrins on the surface of JRT MAU demonstrated that ephrin binding was unaffected by this mutation. It may be that this patch represents either part of, or the entire TCR binding site. It is also possible however that this region is involved in activation of JRT MAU by EphA2-Fc, but does so without directly interacting with the MAU TCR.

By analysing the EphA2/ephrinA5/MAU complex modelling, it is difficult to envisage how the TCR could potentially interact with this region, given its proximity to the T cell surface. However, as discussed in the modelling section, the molecules involved in this interaction are likely to be highly flexible with regard to their position relative to the cell surface, and so this possibility cannot be excluded. For example, studies of EphA2 and EphA4 crystal structures demonstrate considerable changes in relative orientations upon clustering, which likely impact their orientation on the cell surface⁸¹. Furthermore, GPI-linked A ephrins have been shown to localise in caveolae microdomains, which form small invaginations in the plasma membrane¹⁴⁸. These are thought facilitate the formation of A ephrin signalling complexes¹⁴⁸, and it is conceivable that these changes in membrane structure may facilitate binding of the MAU TCR to EphA2.

It is tempting to use these results to computationally model a binding interaction between EphA2 and the MAU TCR. However, since the region of the TCR involved in binding has not yet been established, this would likely not yield reliable results, due to the large number

of possible binding sites. Therefore, developments in the understanding of which regions of the MAU TCR are involved with binding EphA2 are needed to facilitate such modelling. A model of the binding mode would provide greater insight into the residues involved, allowing for more specific and subtle mutagenesis studies, such as alanine scanning mutagenesis.

It cannot be excluded that the interaction of MAU with EphA2 is facilitated by the V region framework regions of the γ and/or δ chains, and not the CDR loops. Such regions would appear to be able to more readily interact with Patch 5, as judged by the modelling. Despite the proximity of the C domains of the MAU TCR to patch 5 in the model, they are unlikely to be involved in binding, as $\gamma\delta$ TCRs have only two distinct C γ regions and one C δ region¹⁴⁹. If these regions were providing specificity, many more $\gamma\delta$ T cells would demonstrate reactivity towards EphA2.

The ultimate analysis of the binding mode between two proteins could be achieved by obtaining a complex structure by X-ray crystallography. This would allow for detailed analysis of the residues involved in binding. Typically, receptor/ligand crystallographic studies are likely to be challenging for low affinity interactions, however based on the finding of the study that the MAU TCR likely binds the EphA2 LBD, crystal complex trials of MAU TCR and the EphA2 LBD could be attempted. If the two proteins bind, such an analysis would not only confirm this, but also provide unparalleled detail into the nature of the binding mode.

It is possible however that this patch 5 region of EphA2 is not involved with binding to the MAU TCR, and plays another critical role in the activation of MAU by EphA2, perhaps by interacting with another molecule on the surface of MAU T cells. The previous chapter

discussed the possible role of A-ephrins in this interaction as localising Lck to the MAU TCR. However, due to A-ephrins' lack of transmembrane (TM) or cytosolic domains, they likely associate with Lck through other TM proteins¹³⁵. Perhaps these A-ephrin-associated TM proteins also interact with EphA2-Fc to facilitate activation of MAU. This could also explain the difficulty in obtaining evidence of binding between EphA2 and MAU, as MAU may directly interact with these Lck/ephrin-associated molecules, forming a more complicated recognition complex.

In order to identify such molecules, immunoprecipitation experiments could be used to extract A-ephrin-associated molecules from activated JRT MAU lysates, and ultimately identified by mass spectrometry.

4.4 Tables

Chain/CDR	Position	WT Residue	Characteristic	Mutant Residue	Characteristic
91	30	I	medium, non-polar	R	large, positively charged
	31	S	small, polar	Y	large, polar, aromatic
	32	A	small, non-polar	E	large, negatively charged
	33	T	small, polar	K	large, positively charged
92	53	S	small polar	L	medium, non-polar
	54	Y	large, polar, aromatic	S	small, polar
	55	D	small, negatively charged	N	small, polar
	57	T	small, polar	L	medium, non-polar
93	102	V	small, non-polar	E	large, negatively charged
	103	Q	large, polar	W	large, non-polar, aromatic
	104	S	small, polar	R	large, positively charged
	105	V	small, non-polar	D	small, negatively charged
	27	T	small, polar	L	medium, non-polar
11	28	S	small, polar	R	large, positively charged
	29	W	large, non-polar, aromatic	S	small, polar
	30	W	large, non-polar, aromatic	R	large, positively charged
12	51	Q	large, polar	W	large, non-polar, aromatic
	53	S	small, polar	Y	large, polar, aromatic
	54	D	small, negatively charged	R	large, positively charged
	55	E	large, negatively charged	K	large, positively charged
13	99	V	small, non-polar	E	large, negatively charged
	101	I	medium, non-polar	K	large, positively charged
	102	T	small, polar	L	medium, non-polar
	103	D	small, negatively charged	N	small, polar

Table 4.1: MAU CDR mutation strategy

Mutational strategy for the MAU TCR CDR loop mutants. The chain and CDR loop are identified using the two digit identification system where the first digit signified the chain (9 or 1) and the second denotes the CDR loop (1, 2 or 3). WT and mutant residues are characterised by size and charge.

4.5 Figures

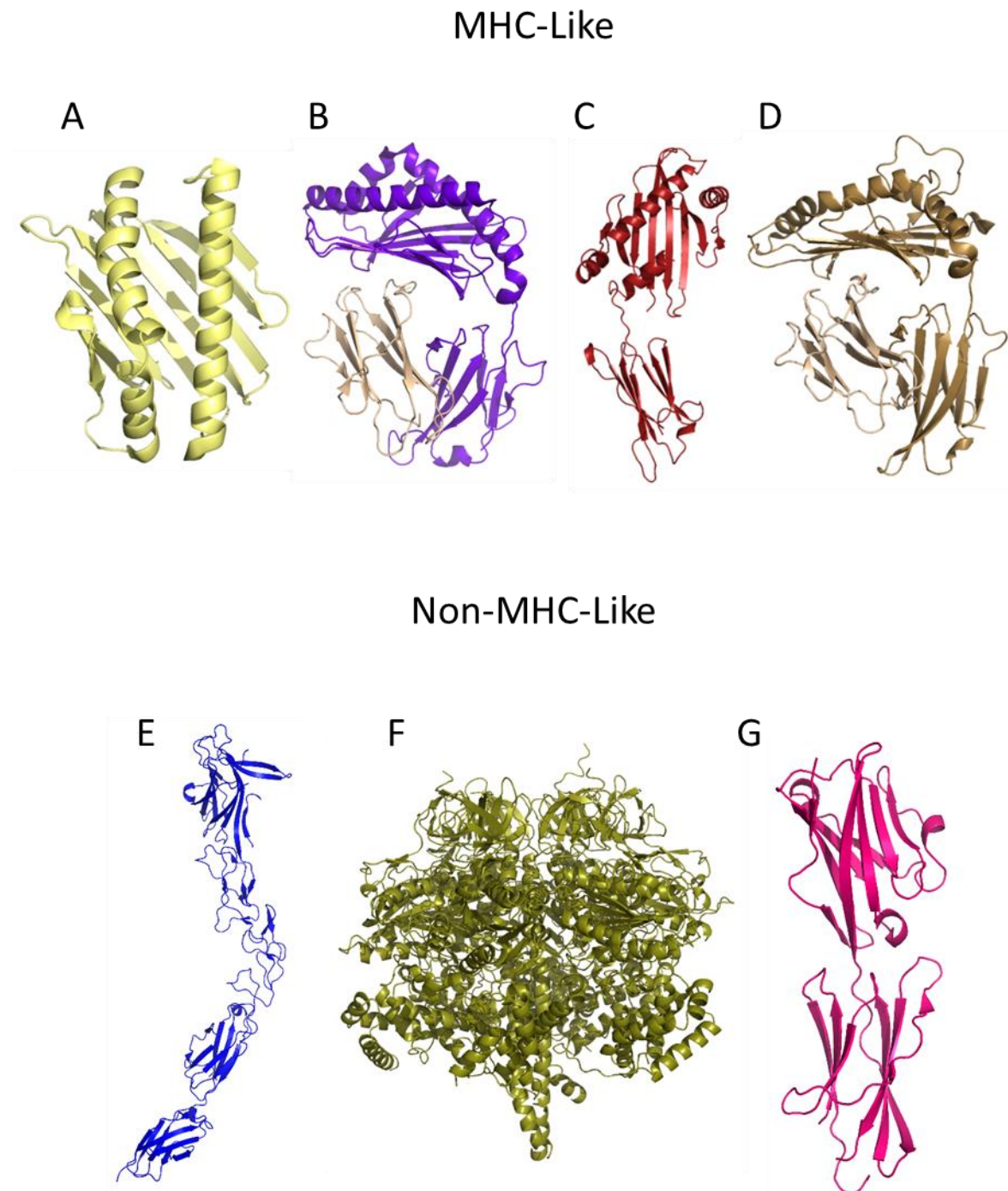


Figure 4.1: Structural diversity of $\gamma\delta$ TCR ligands

Structures of a selection of the proposed $\gamma\delta$ TCR ligands, grouped into MHC-like (A-D) and non-MHC-like (E-G). (A) EPCR (PDB: 1L8J) (B) CD1d (PDB: 4LHU) (C) MICA (PDB: 1B3J) (D) T22 (PDB: 1C16) (E) EphA2 (PDB: 2X10) (F) F1-ATPase (PDB: 1BMF) (G) BTN3A1 (PDB: 4F80). To date, the TCR binding mode has only been described in detail for CD1d (B) and T22 (D). Structures not to scale. Structures obtained from the Protein Dank Bank.

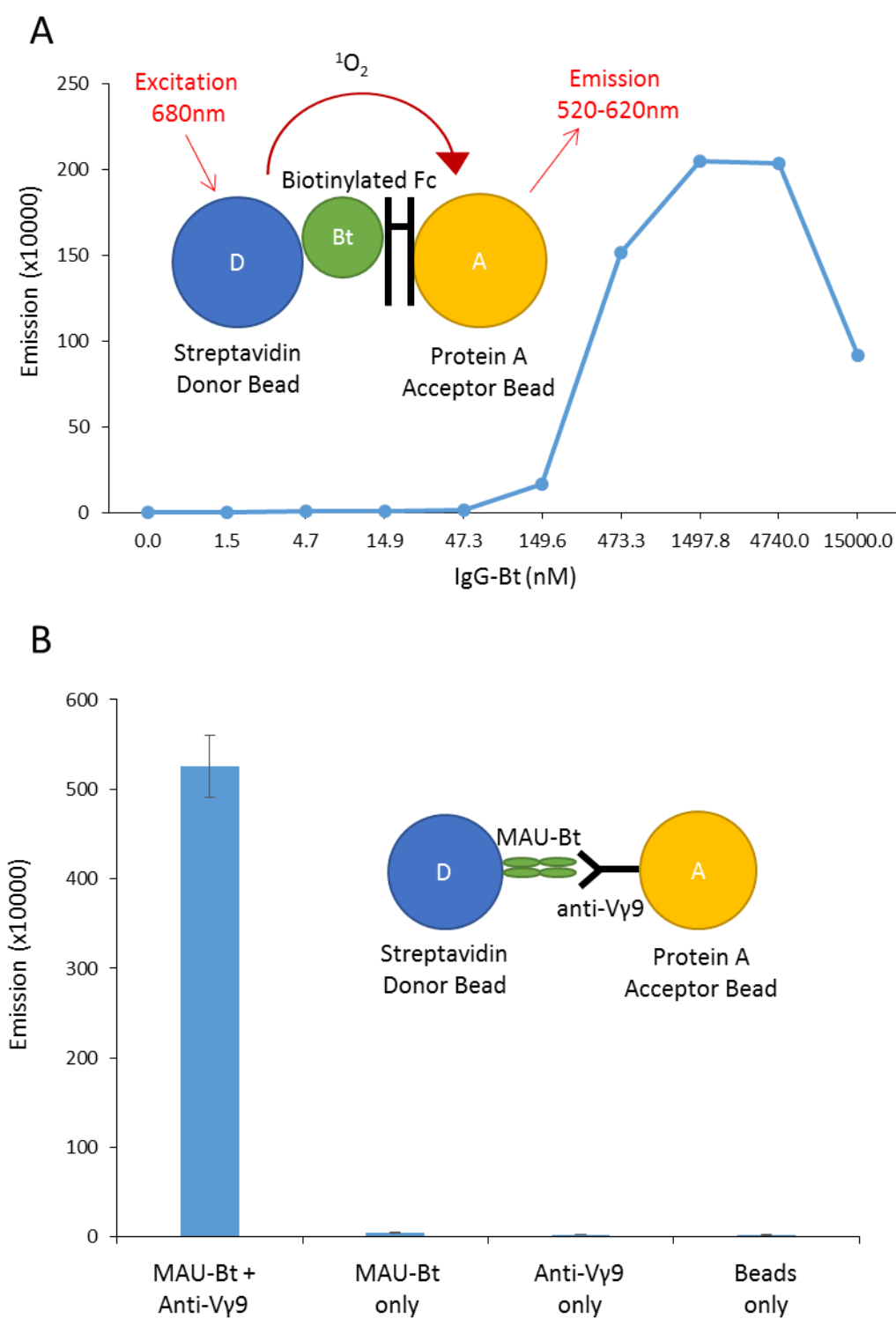


Figure 4.2: Validation of the AlphaScreen methodology

(A) Biotinylated rabbit IgG, which binds both the donor and acceptor beads simultaneously, was used as a control for the AlphaScreen assay (B) MAU-Bt (0.74 μ M) and an anti-Vy9 antibody (0.15 μ M) were incubated with both donor and acceptor beads for 2 hours. Diagrammatic representation of the experiment shown in each figure. ($n=3$, error bars =SD).

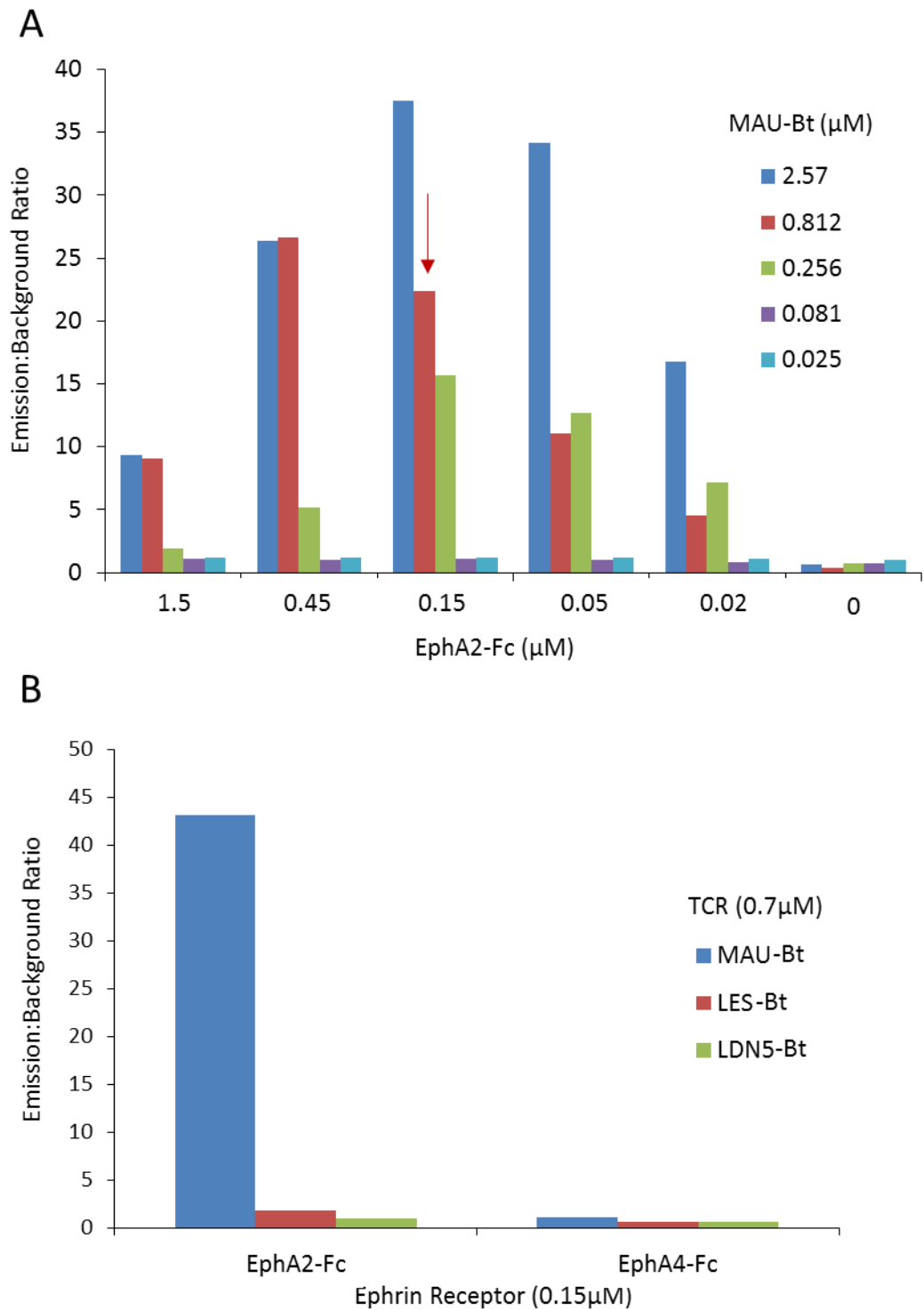


Figure 4.3 : Analysis of the EphA2-Fc/MAU-Bt interaction using AlphaScreen

(A) EphA2-Fc and MAU-Bt were titrated against each other with both the donor and acceptor beads. Optimal concentrations for future experiments is highlighted with a red arrow. (B) Fc-tagged ephrin receptors were incubated with biotinylated TCRs for 2h at RT, demonstrating specific binding between EphA2-Fc and MAU-Bt.

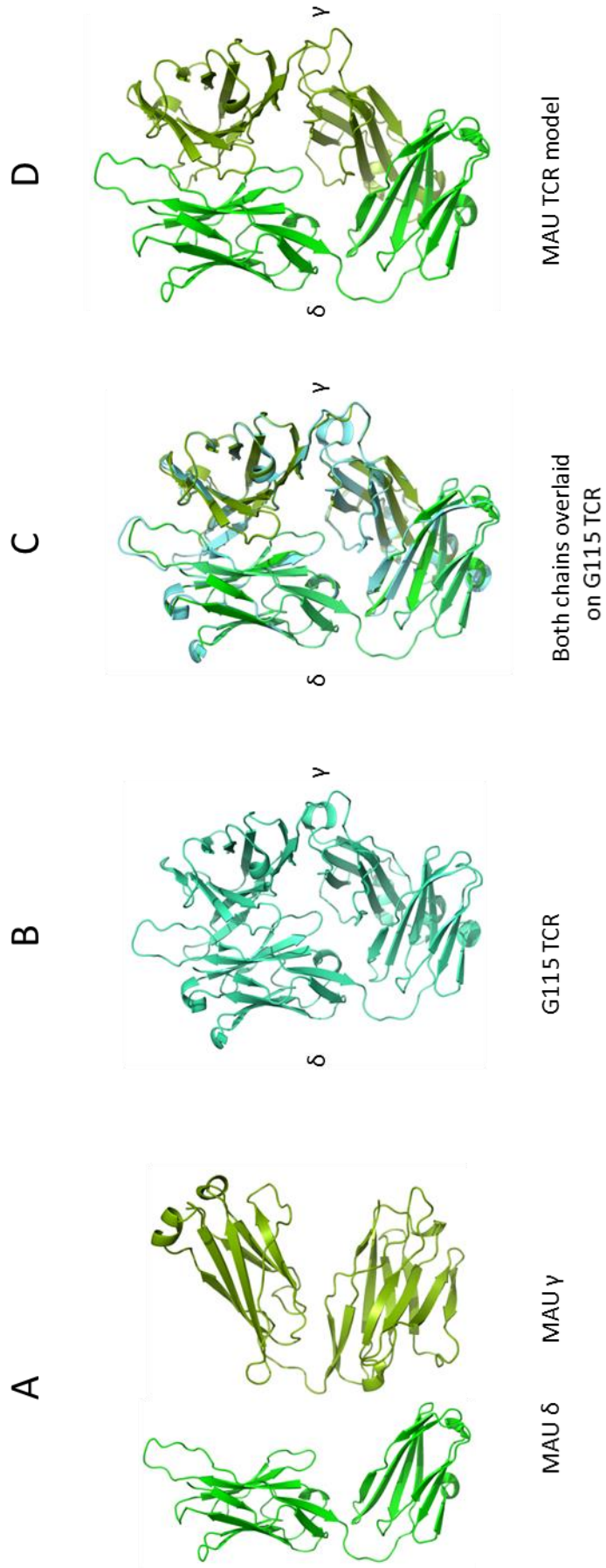


Figure 4.4: Generation of the MAU TCR structural model

(A) Phyre-derived model of the MAU γ and δ chains. (B) Structure of the G115 TCR template used to align the MAU γ and δ chains (PDB: 1HXM) (C) MAU γ and δ chains overlaid on the G115 TCR template (D) Complete MAU TCR model. Structures obtained from the Protein Dank Ban

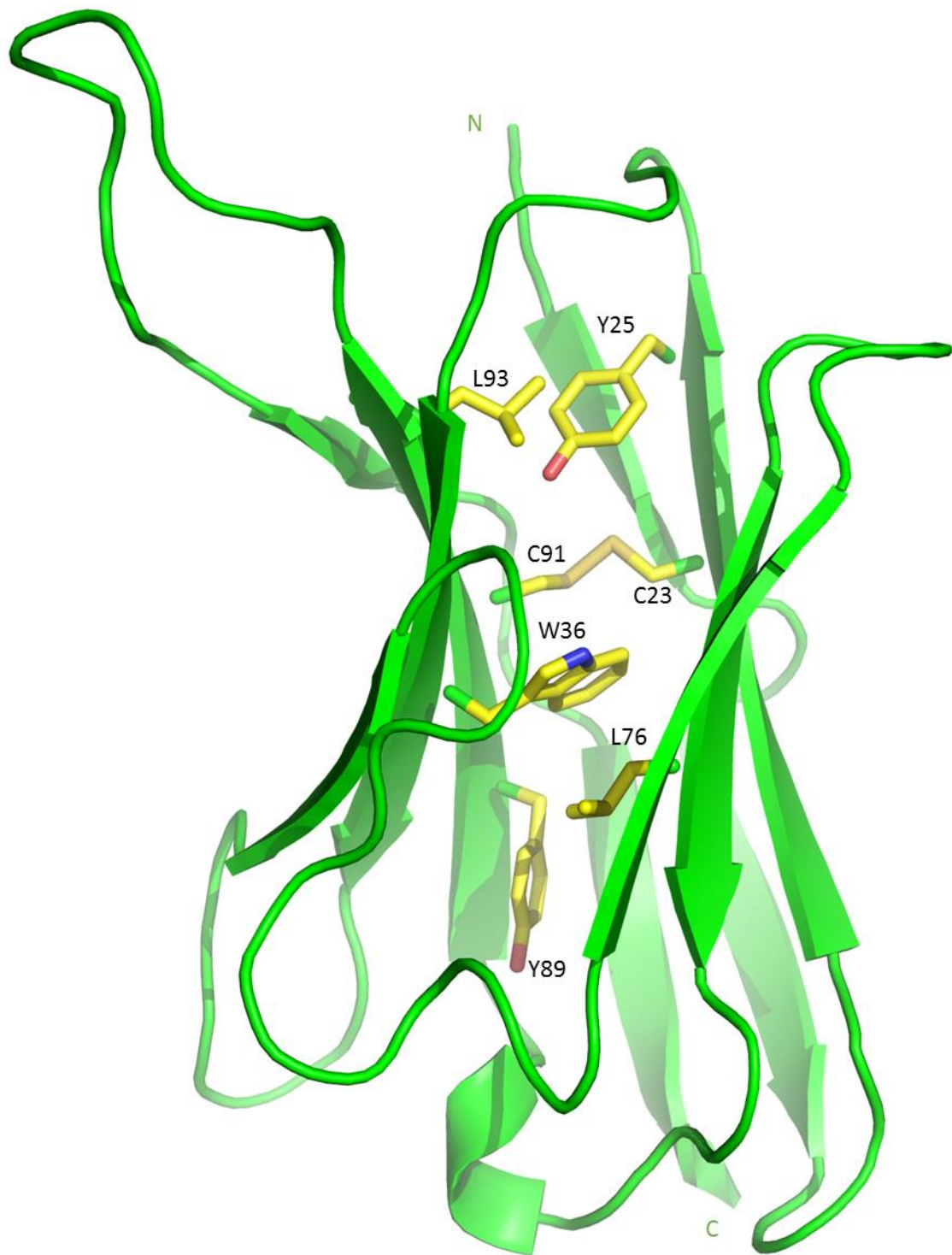


Figure 4.5: Stabilisation of the IgV domain of the Phyre-derived MAU δ chain model

The IgV domain of the MAU δ chain is comprised of 2 characteristic antiparallel β -sheets, stabilised by a disulphide bond formed between C23 and C91, an invariant tryptophan residue (W36), and multiple non-polar interactions mediated by hydrophobic residues, which are represented in stick format.

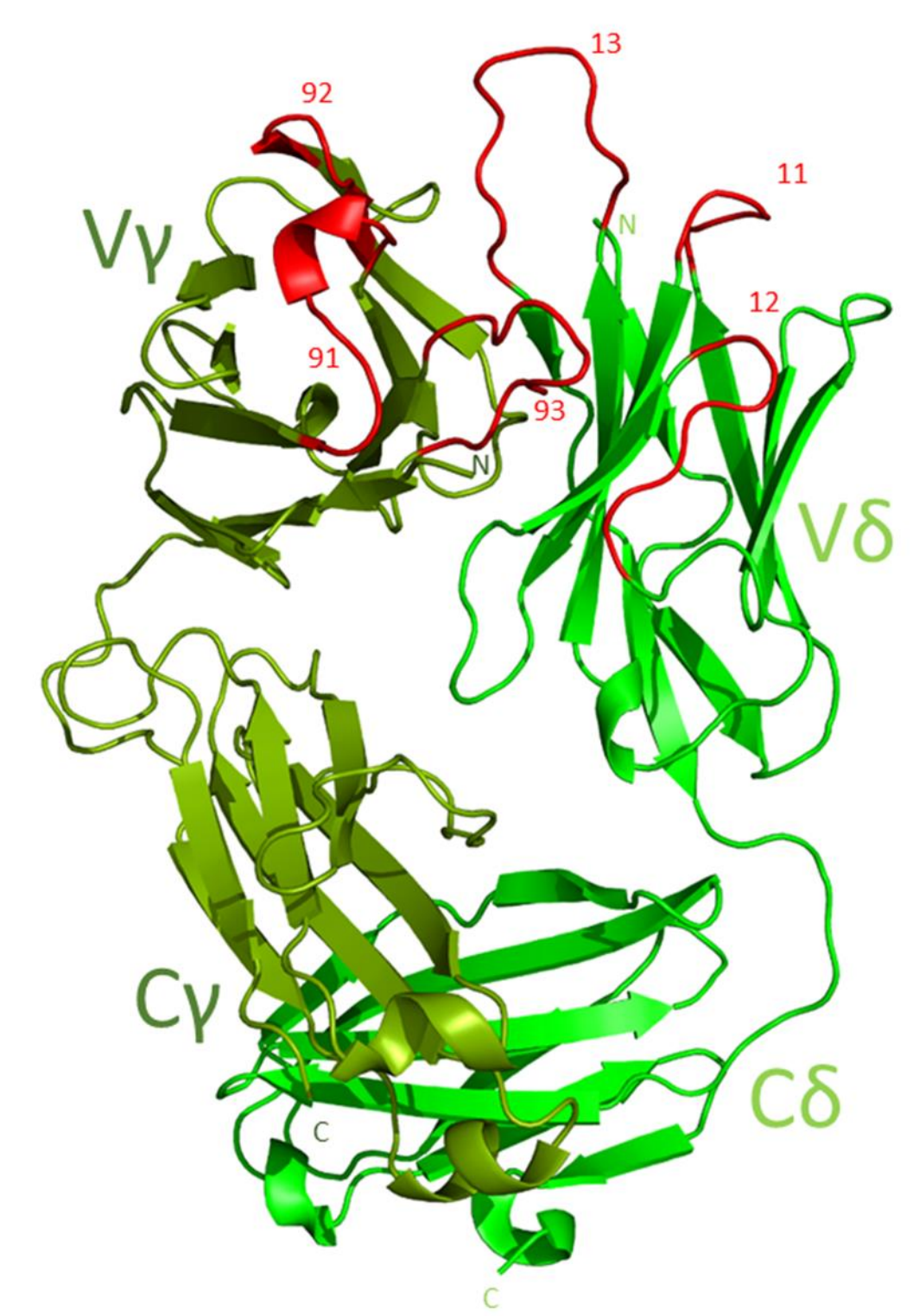


Figure 4.6 : Structural features of the MAU TCR model

Phyre generated model of the MAU $\gamma\delta$ TCR. The CDR loops (red) were identified using IMGT and labelled using a two digit system: first digit = $V\gamma$ chain and second digit = CDR loop. e.g. 91 = $V\gamma$ 9 CDR 1.

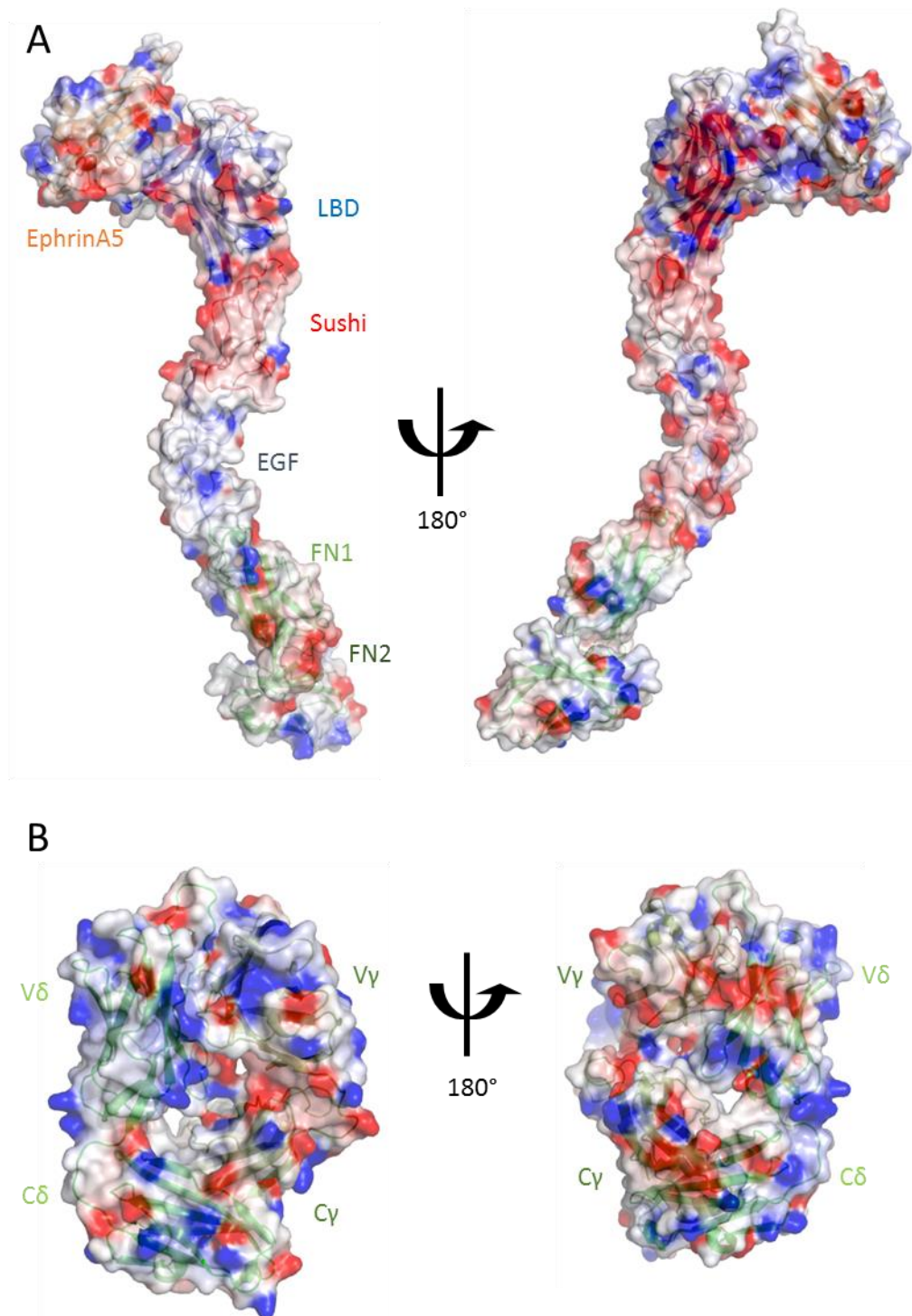


Figure 4.7: Molecular surface electrostatic analysis of EphA2 and MAU TCR

Electrostatic potential maps were calculated using DelPhi for (A) ephrinA5-bound EphA2 (PDB: 2X11) and (B) the Phyre generated MAU TCR model. The analysis revealed no distinct complementary electropositive/electronegative patches on either molecule. The scale ranges from -7 (negative potential, red) to +7 (positive potential, blue) in units of kT/e .

Structure obtained from the Protein Data Bank.

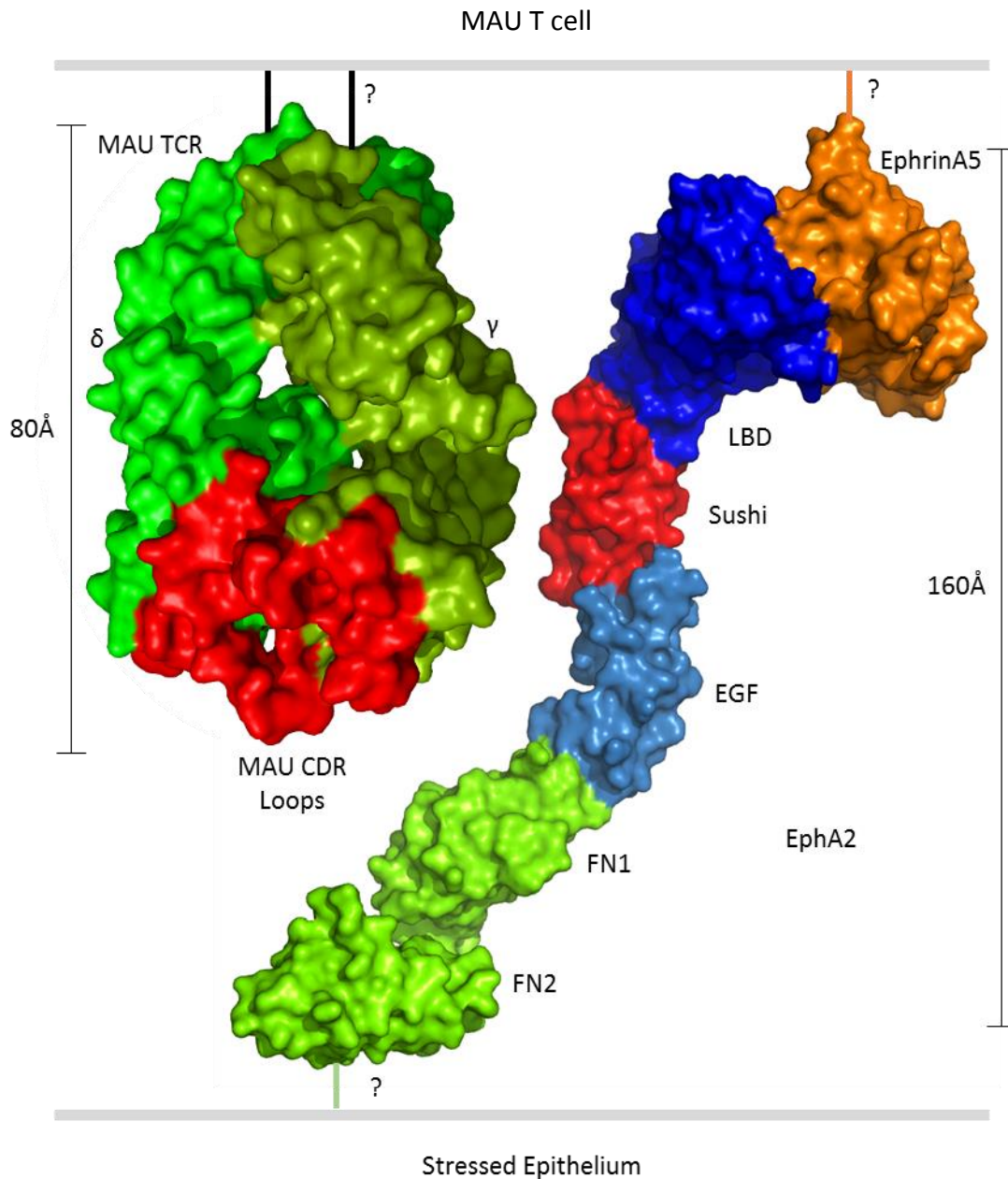


Figure 4.8: Comparison of the size and structure of EphA2 and MAU TCR

Structures of the Phyre generated MAU TCR model and ephrinA5 bound EphA2 (PDB: 2X11) were manually modelled to compare their size and relative orientation of domains. '?' represents the uncertainty with how these molecules are orientated relative to the plasma membrane. MAU CDR loops coloured in red. This model suggests that the MAU TCR is not prevented from binding any region of EphA2.

Structure obtained from the Protein Dank Bank.

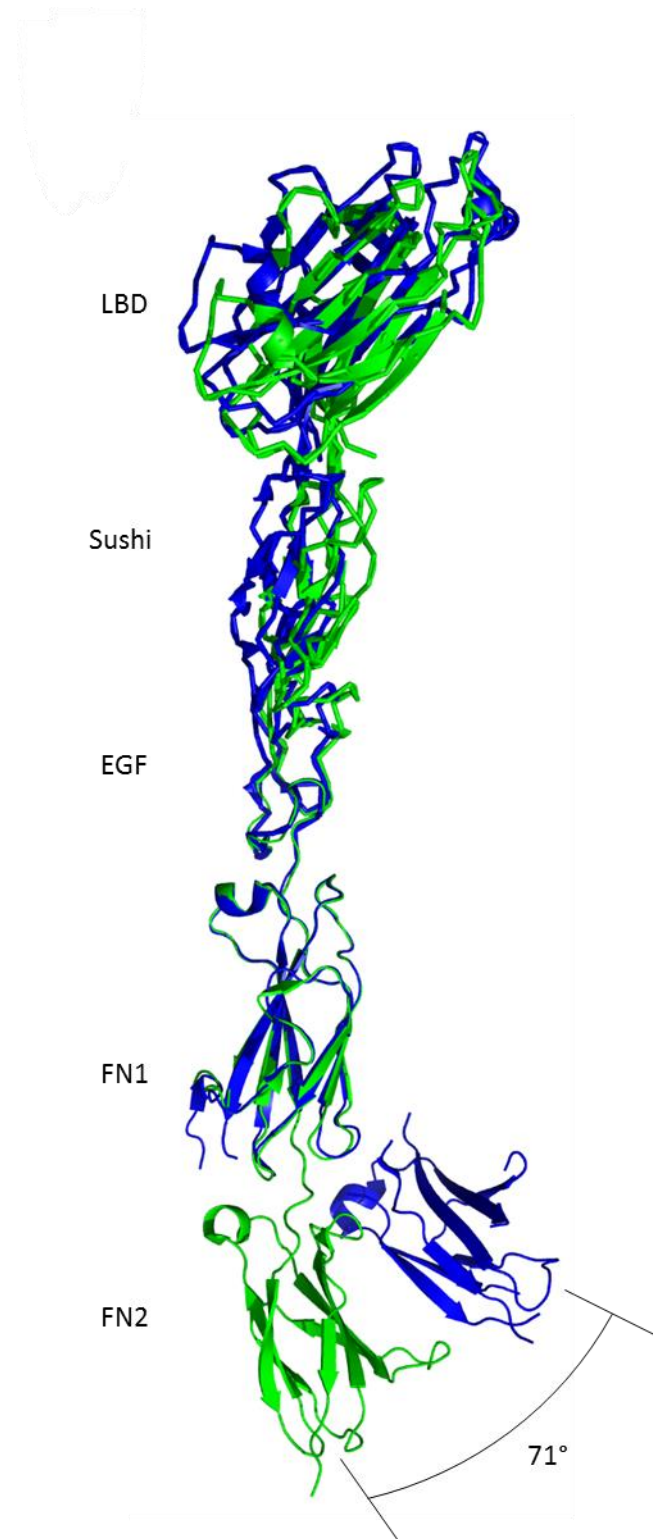


Figure 4.9 : Flexibility between the FN1 and FN2 domains of EphA2

Structural alignment of the EphA2 ectodomain either bound (Blue, PDB: 2X11), and unbound (Green, PDB: 2X10) to ephrinA5. This comparison reveals considerable flexibility of approximately 71° between the FN1 and FN2 domains, which may impact the orientation of EphA2 relative to the cell surface. Structures aligned by FN1 domains.

Structures obtained from the Protein Dank Bank

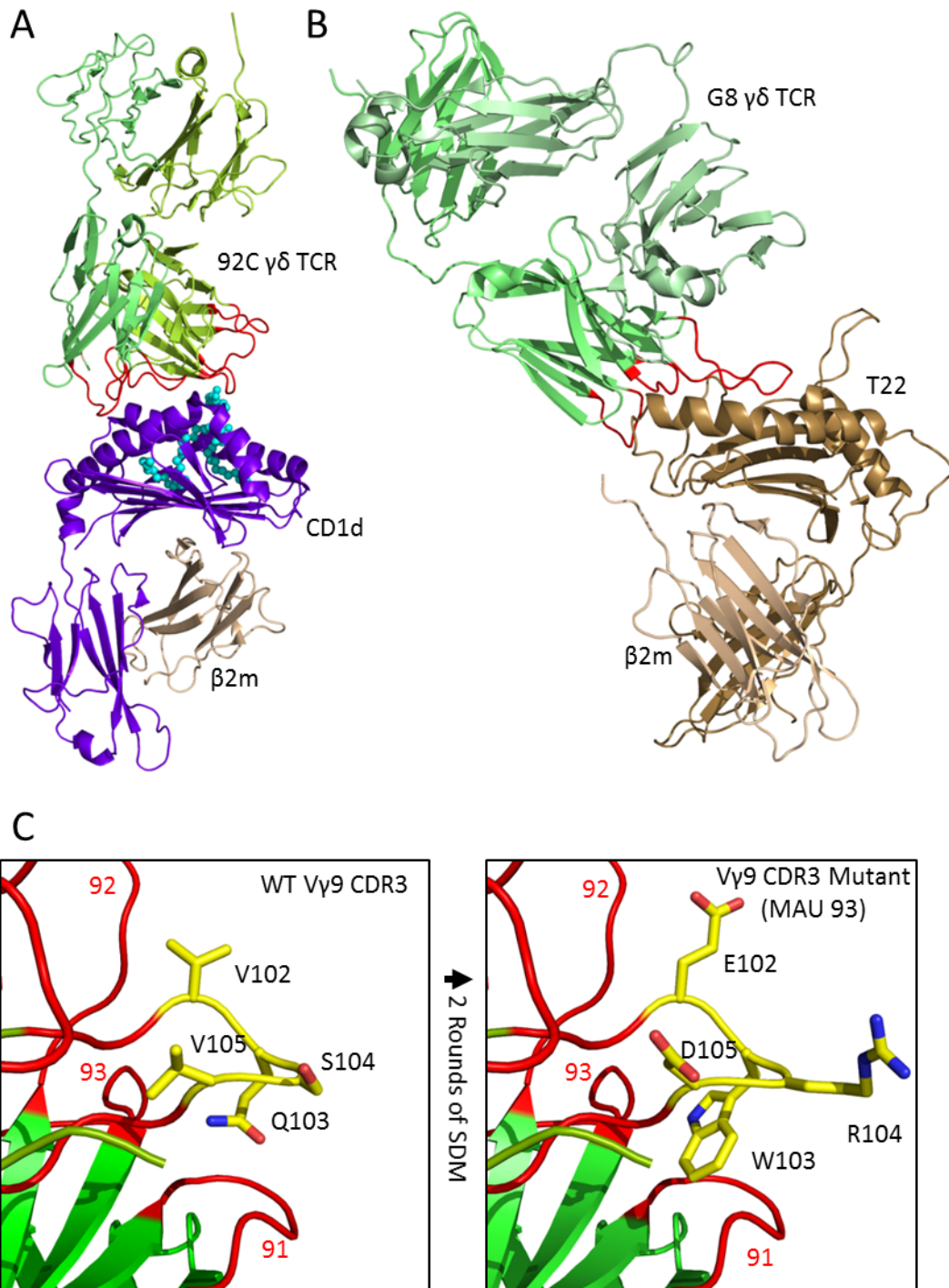


Figure 4.10: The use of CDR loops in $\gamma\delta$ ligand recognition

Crystal complexes of the 92C TCR complexed with lipid bound (blue spheres) CD1d (A, PDB: 4LHU) and G8 TCR complexed with T22 (B, PDB: 1YPZ). Both complexes demonstrate the involvement of various CDR loops (red) in ligand recognition. (C) Model of the mutation strategy of the MAU V γ 9 CDR3 loop. WT residues 102VQSV105 (left) and MAU 93 mutant residues 102EWRD105 (right). CDR loops highlighted in red, two digit CDR labelling system: first digit = V γ chain and second digit = CDR loop. e.g. 93 = V γ 9 CDR 3.

Structures obtained from the Protein Dank Bank.

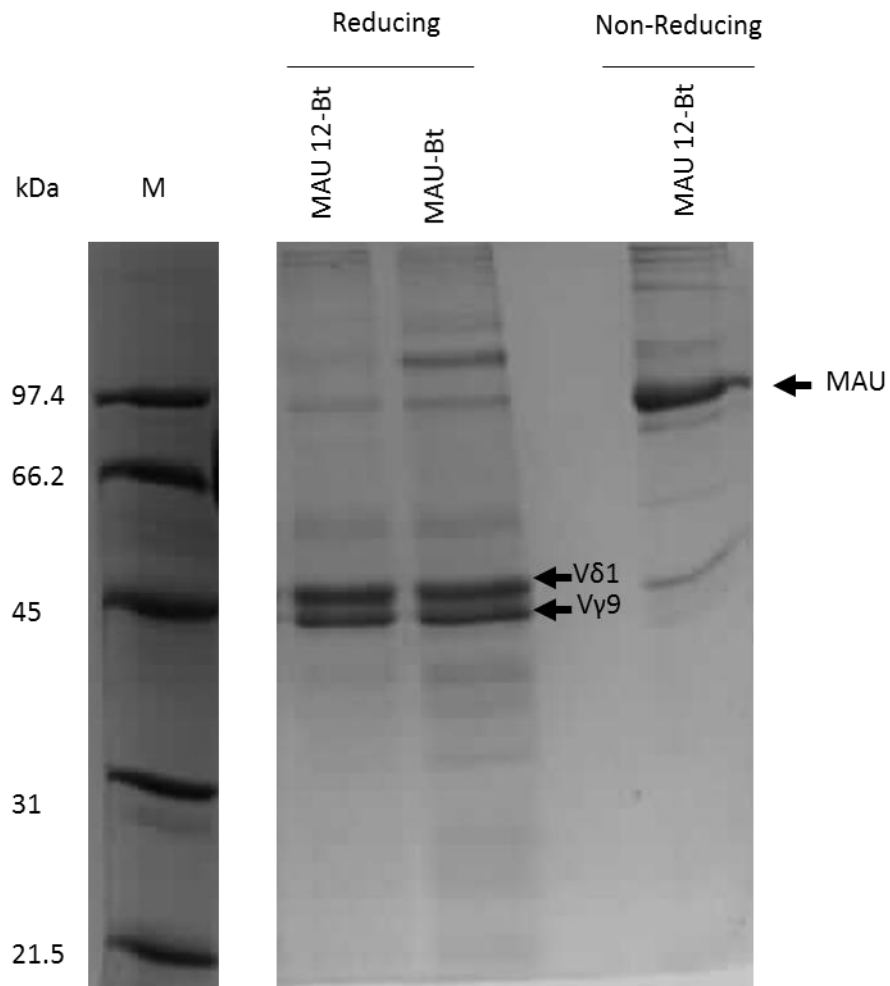


Figure 4.11 : Production of *Drosophila* S2-derived MAU Vδ1 CDR2 mutant (MAU 12)

SDS PAGE analysis (Instant Blue) of the MAU 12 mutant reveals discrete γ and δ chains under reducing conditions, and a single band representing the TCR under non-reducing conditions. The MAU 12 mutant expressed with equivalent yield and purity to the WT control.

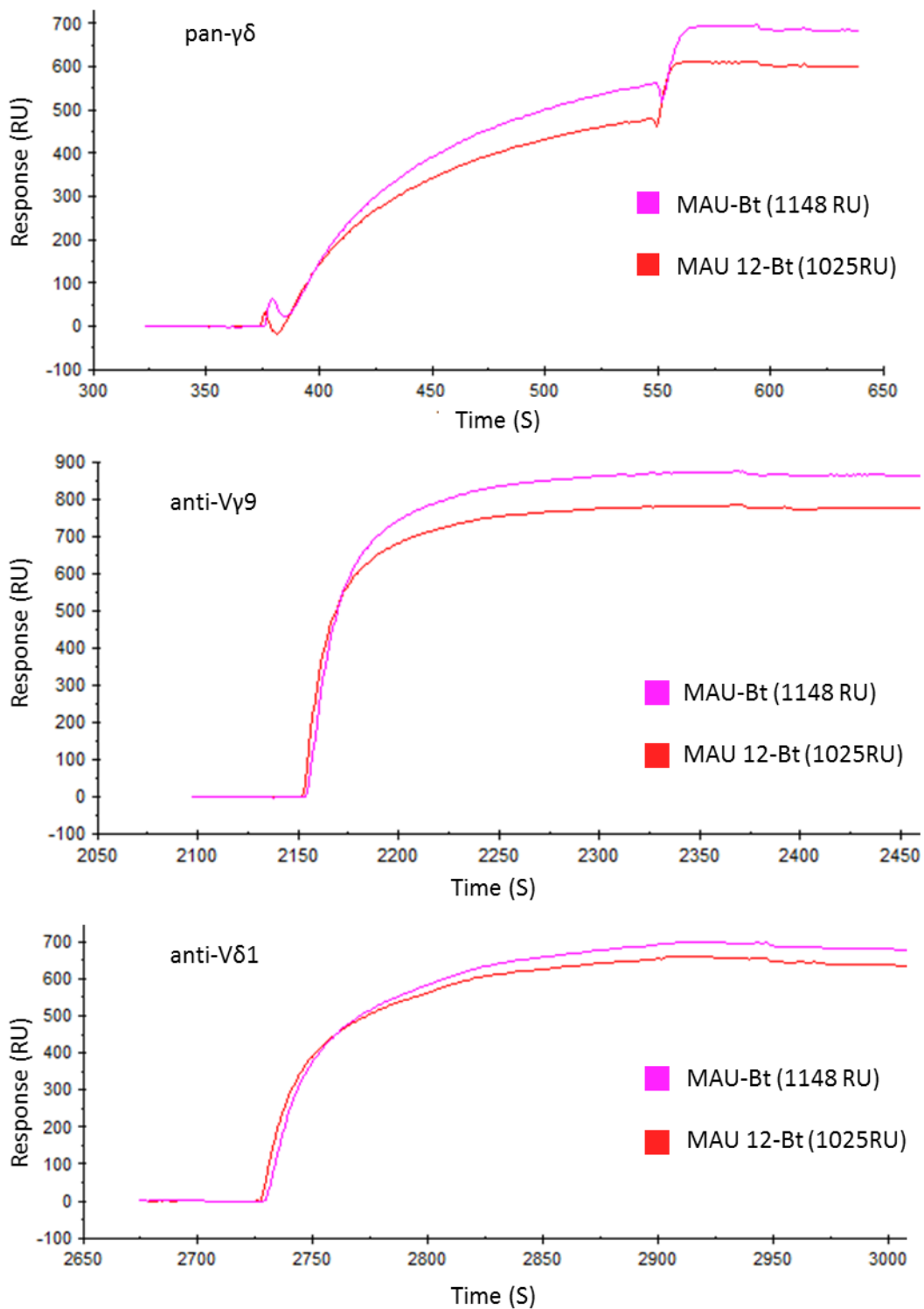


Figure 4.12 : Verification of MAU 12 folding

BIAcore analysis demonstrating binding of pan- $\gamma\delta$, anti-V γ 9 and anti-V δ 1 specific mAbs to the biotinylated MAU V δ 1 CDR2 mutant (MAU 12-Bt). Number in brackets represents amount of TCR immobilised on streptavidin coated CM5 chip.

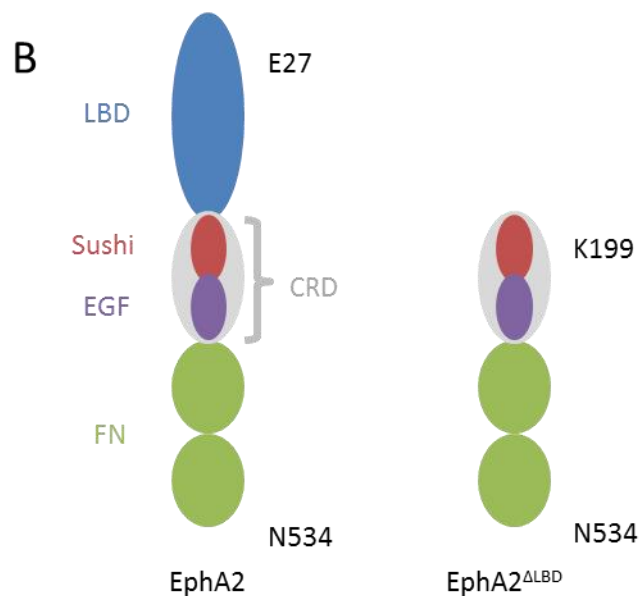
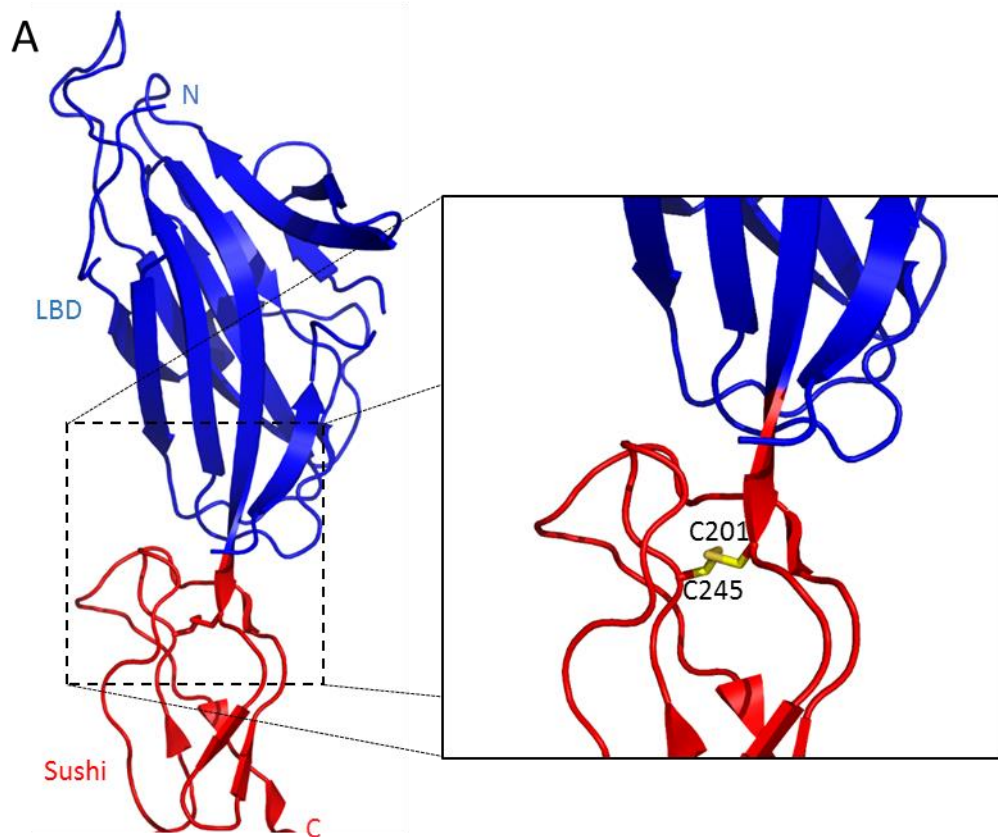


Figure 4.13 : Design of the EphA2^{ΔLBD} construct

(A) Close-up view of the domain boundary between the LBD and Sushi domains of EphA2. C201 was retained in the EphA2^{ΔLBD}-Fc construct as it is involved in forming a disulphide bond with C245, and is therefore important for maintaining the Sushi fold (B) Schematic representation of EphA2^{WT} and EphA2^{ΔLBD} constructs. Residue numbers represent construct boundaries.

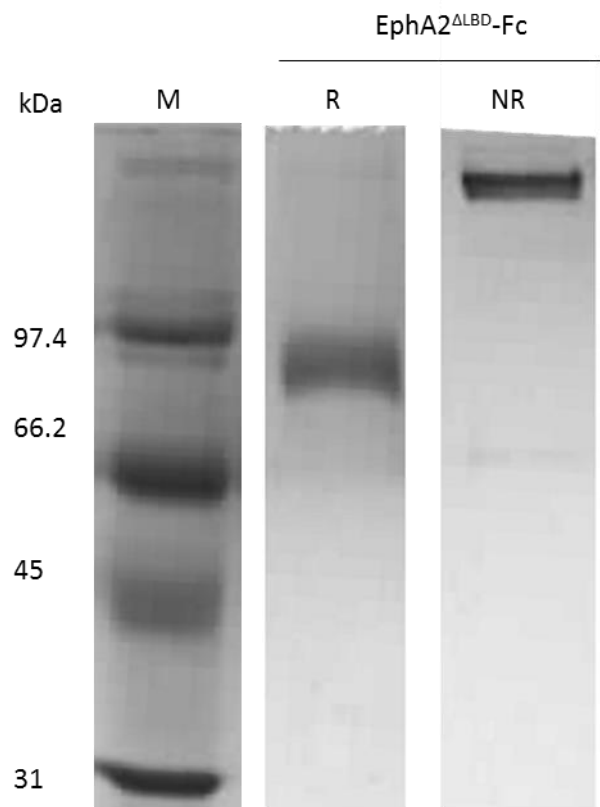


Figure 4.14 : Production of 293T-derived EphA2^{ΔLBD}-Fc

SDS PAGE analysis (Instant Blue) of the Ni-NTA purified EphA2^{ΔLBD}-Fc construct under reducing (R) and non-reducing (NR) conditions. Yield and purity were equivalent to WT EphA2-Fc.

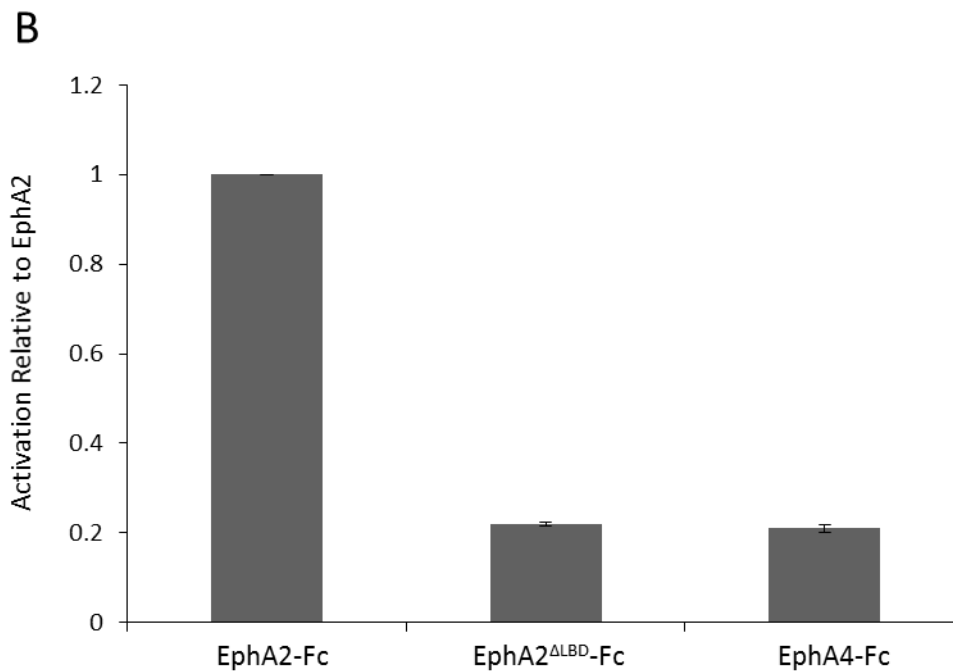
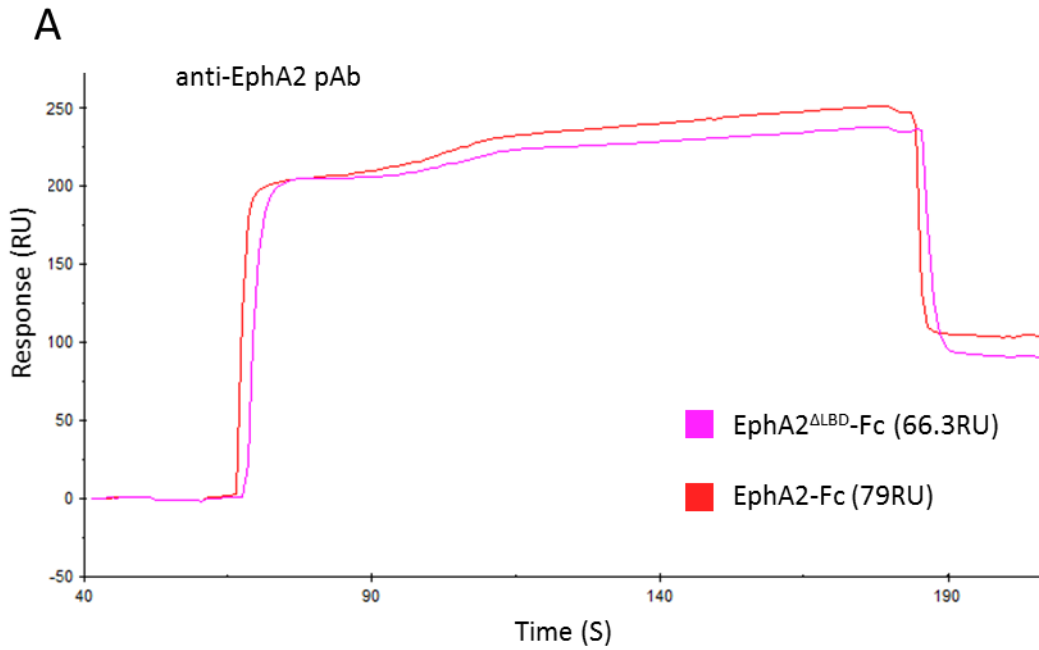


Figure 4.15: Verification and characterisation of EphA2^{ΔLBD}-Fc

(A) BIAcore analysis of anti-EphA2 pAb binding to EphA2^{ΔLBD}-Fc, which was immobilised on a R10Z8E9 coated CM5 chip. Number in brackets represents amount of receptor immobilised on the chip. Binding to a control protein (EphA4-Fc) was not observed (data not shown). (B) Fc-tagged ephrin receptors were bound to a 96-well plate and incubated with JRT MAU cells for 4 hours. Activation was measured by CD69 upregulation. EphA2^{ΔLBD}-Fc failed to activate JRT MAU. ($n=3$, error bars =SD).

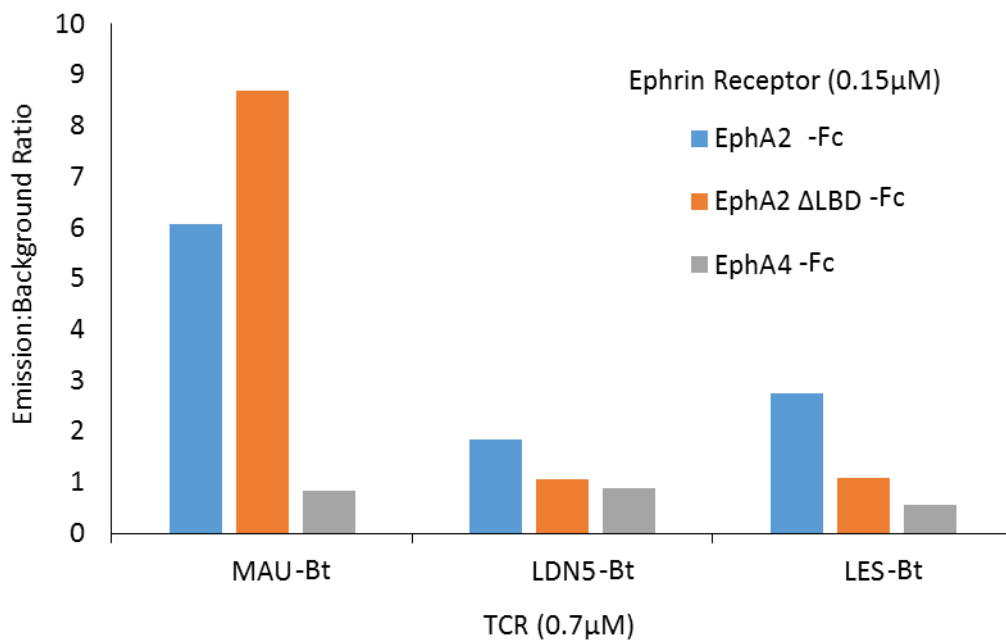


Figure 4.16: Characterising the role of the EphA2 LBD using AlphaScreen

Fc-tagged Ephrin receptors and biotinylated TCRs were incubated with donor and acceptor beads for 2 hours. Specific binding was detected between EphA2^{ΔLBD}-Fc and MAU-Bt. Emission:Background ratios for this experiment were substantially higher than those recorded in Figure 4.3, and the AlphaScreen approach was not used further because of these inconsistent results.

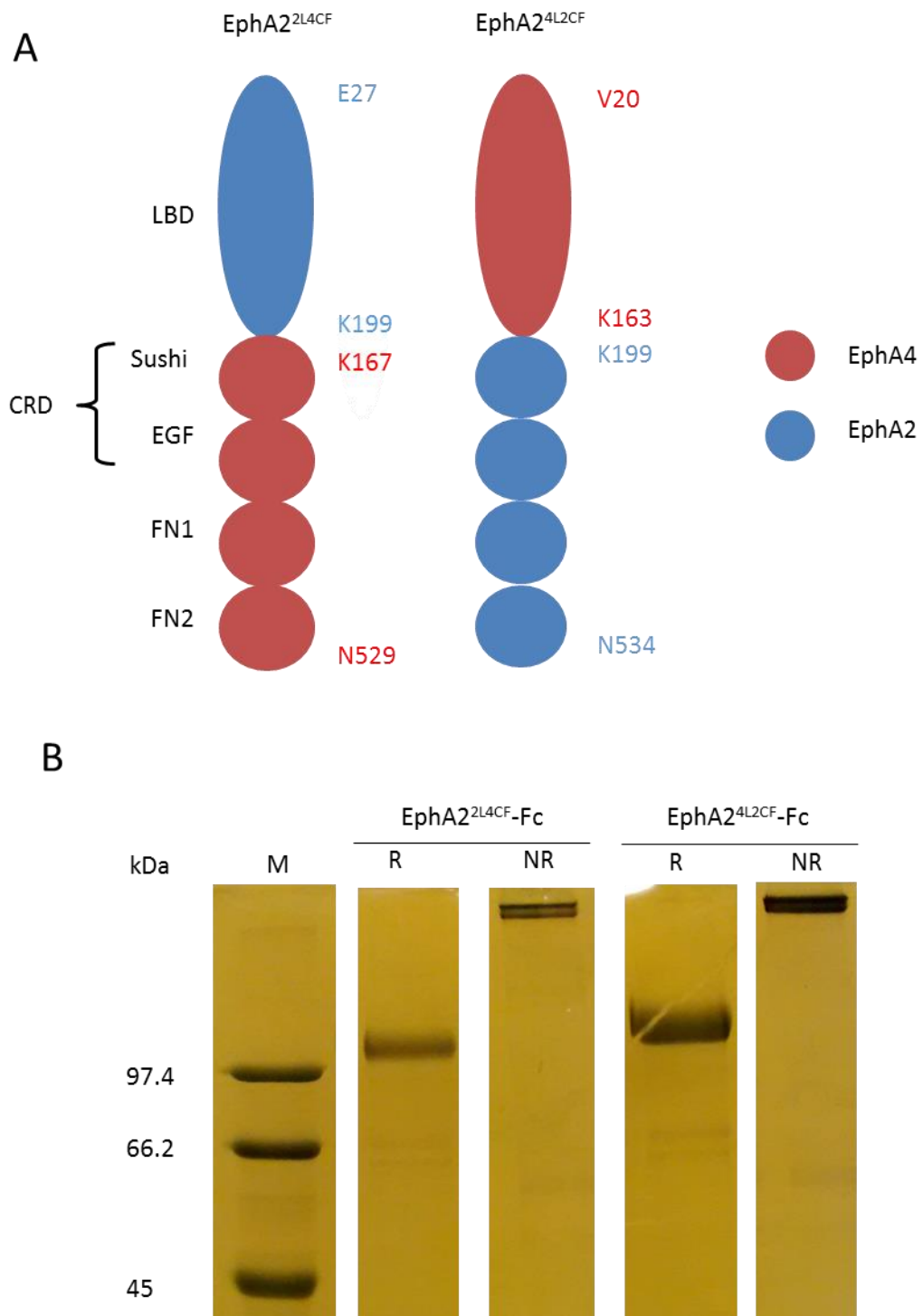


Figure 4.17: Production of EphA2 and EphA4 LBD domain-swap mutants using the 293T expression system

(A) Schematic representation of the EphA2 domain-swap mutants. Residue numbers represent construct boundaries. Domains are coloured based on their source protein; blue = EphA2 and red = EphA4. (B) SDS PAGE analysis (Instant Blue) of Ni-NTA purified LBD swap EphA2-Fc mutants under reducing (R) and non-reducing (NR) conditions. Migration pattern and yields equivalent to the WT EphA2-Fc construct.

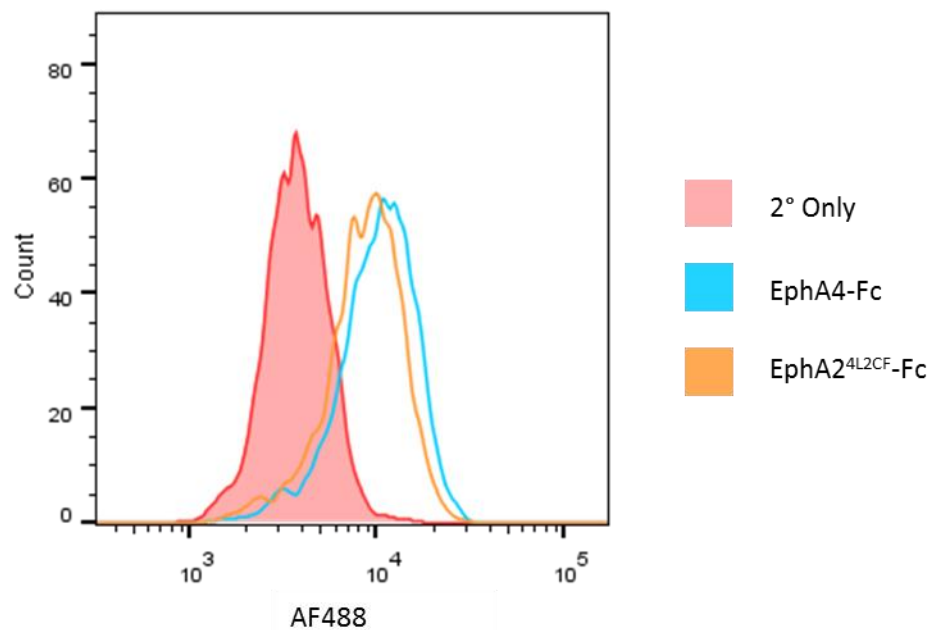
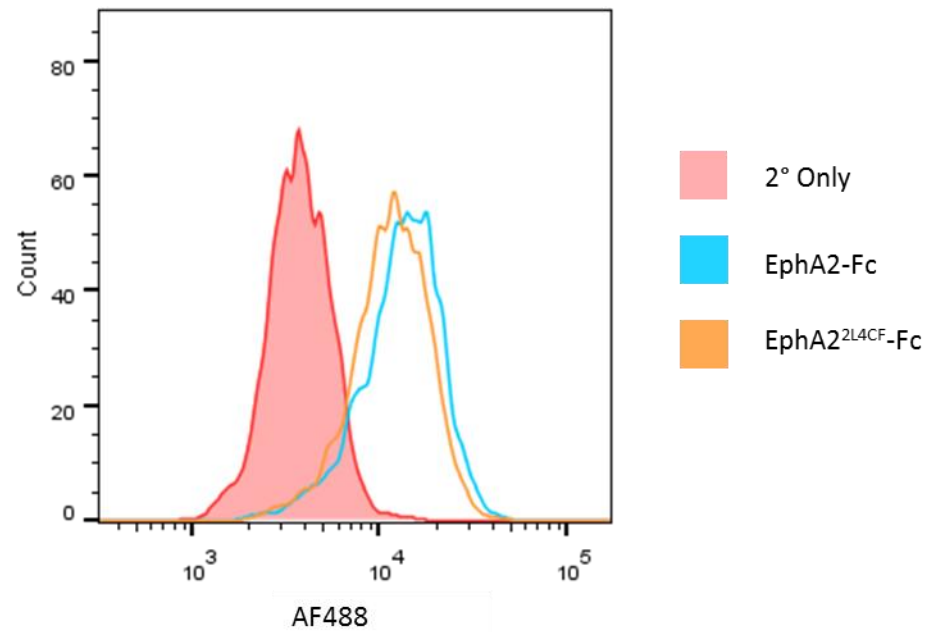


Figure 4.18: Analysis of EphA2 LBD domain-swap mutants binding to ephrins

JRT MAU cells were stained with Fc-tagged ephrin receptors, which were detected using an AF488 conjugated goat anti-human Fc secondary antibody. Equivalent staining was demonstrated between each domain-swap mutant and the WT equivalent. (Representative, $n=3$).

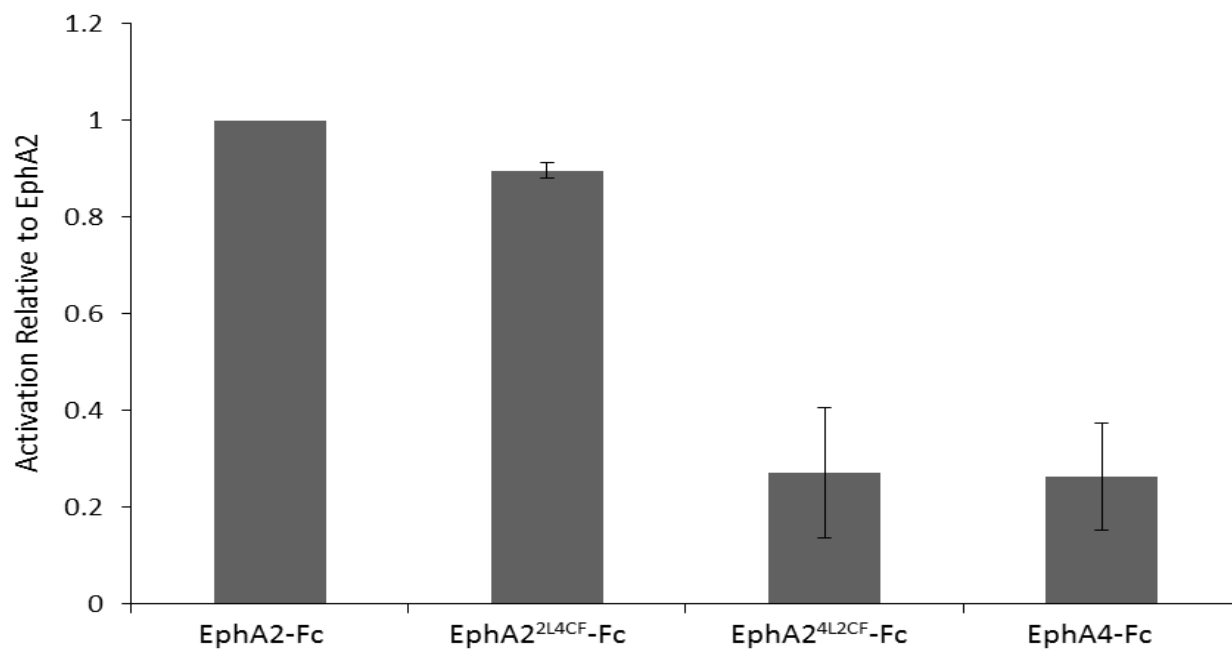


Figure 4.19: JRT MAU activation potential of the EphA2 LBD domain-swap mutants

Fc-tagged ephrin receptors were immobilised on a 96-well plate and incubated with JRT MAU cells for 4 hours. Activation was measured by CD69 upregulation. EphA2^{2L4CF}-Fc activated JRT MAU equivalently to the WT construct, demonstrating that the EphA2 LBD is required for activation ($n=3$, error bars =SD).

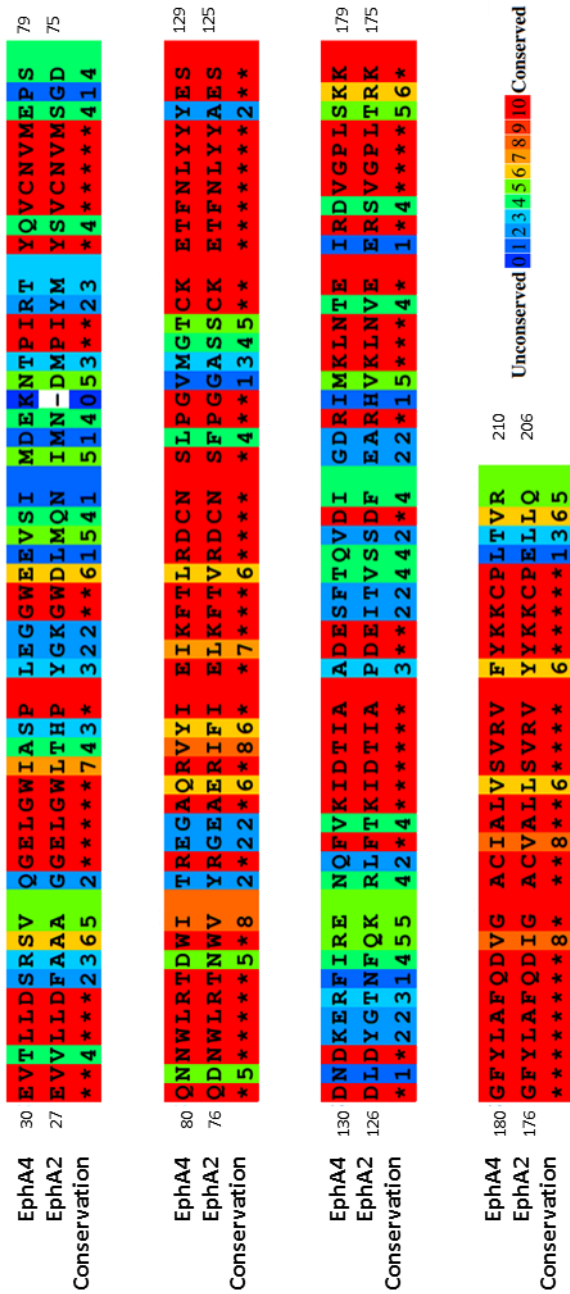


Figure 4.20: Sequence alignments of the EphA2 and EphA4 LBDs

The sequences of EphA2 and EphA4 LBDs were aligned using PRALINE. UniProt accession numbers for EphA2 and EphA4 are P2931 and P5476 respectively. The colour scheme of the alignment is for amino acid conservation, 0= unconserved and 10 = conserved.

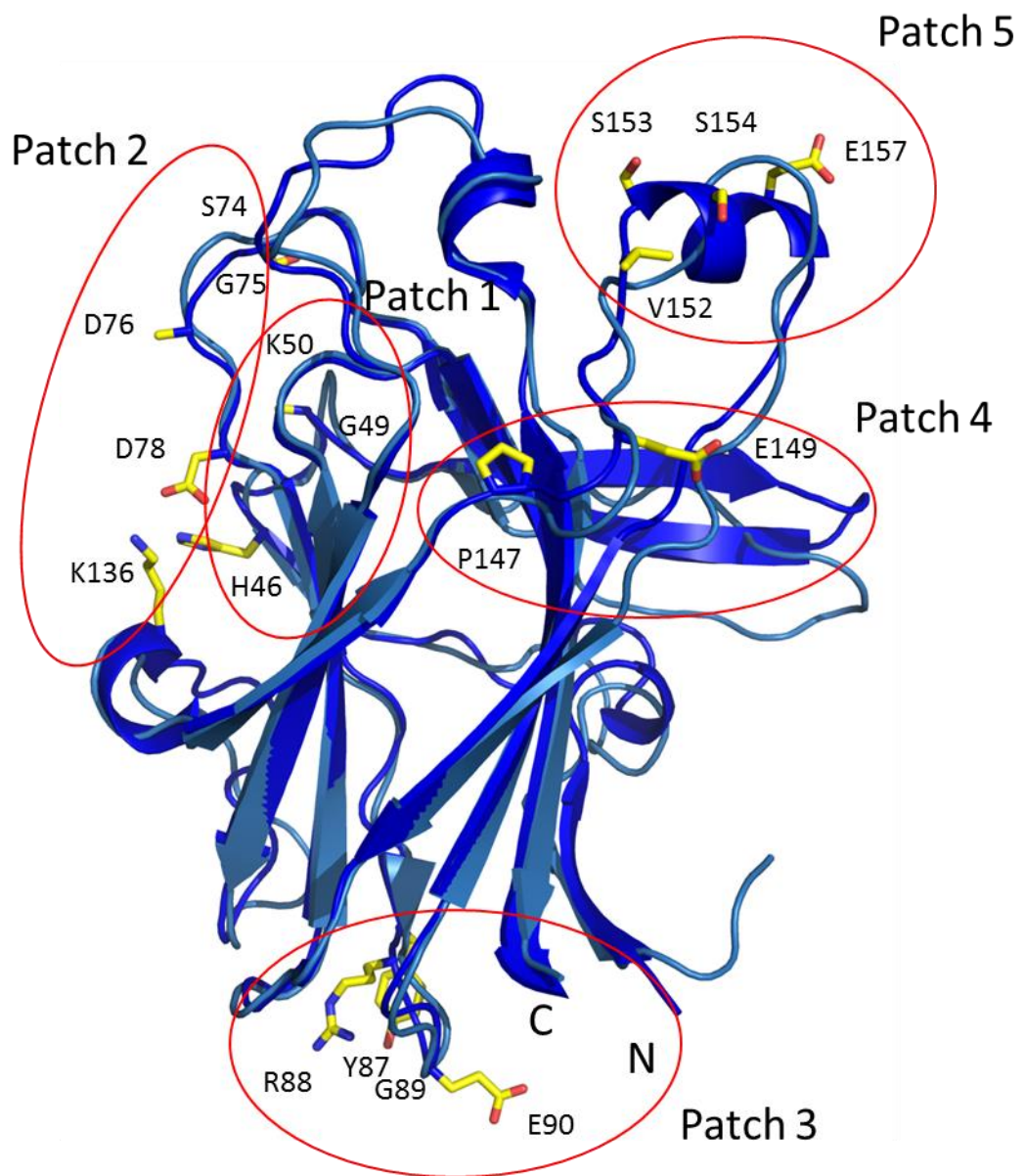


Figure 4.21: Structural comparison of the EphA2 and EphA4 LBDs

Structural overlay of EphA2 (dark blue) and EphA4 (light blue) LBDs. Potential EphA2 residues selected for mutation are highlighted in stick format, and grouped into patches.

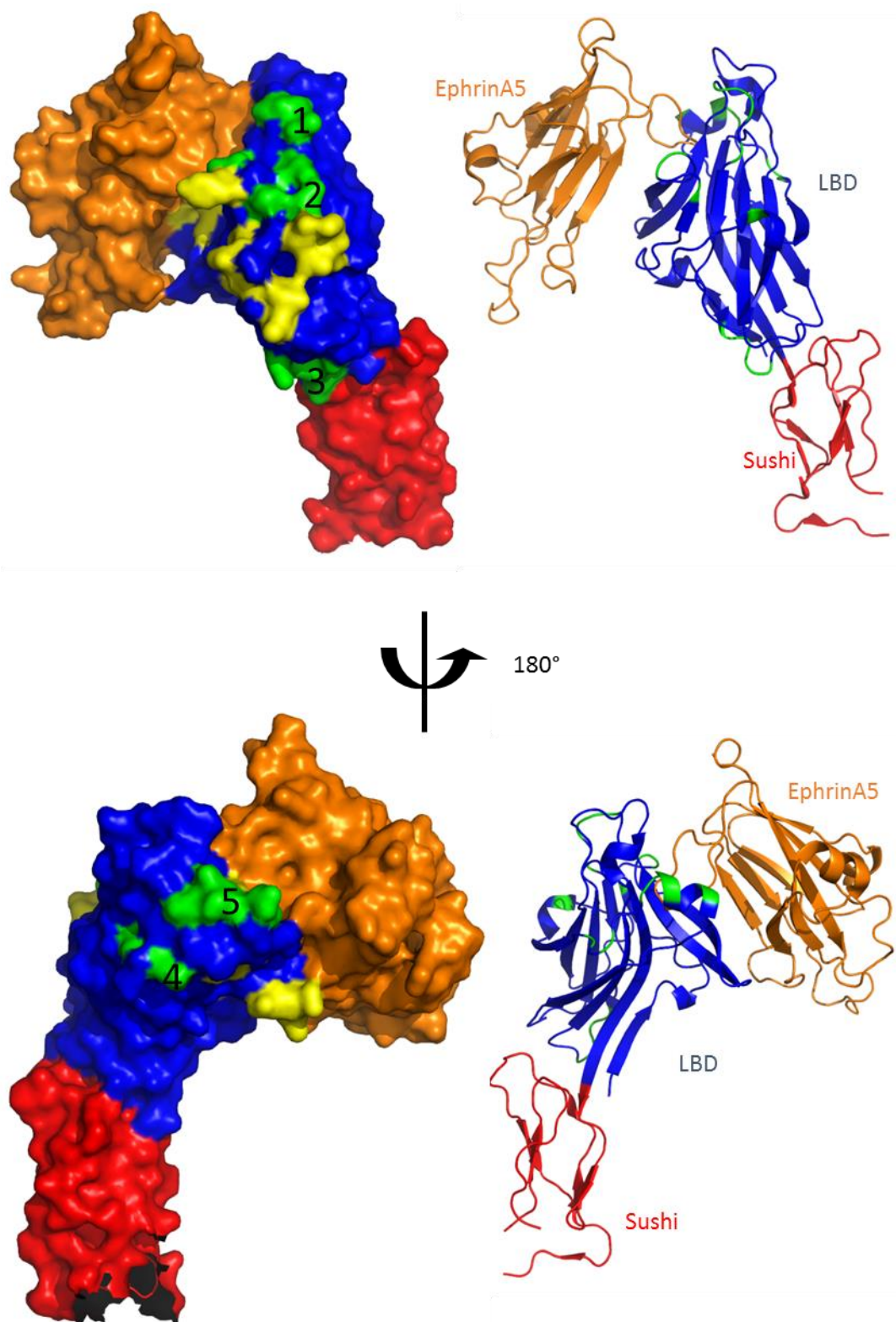


Figure 4.22: Molecular surface representation of the EphA2/ephrinA5 complex

Surface patches to be mutated are highlighted in green, and residues involved in the formation of EphA2 clustering complexes shown in yellow (Structure obtained from the Protein Dank Bank, PDB= 2X11).

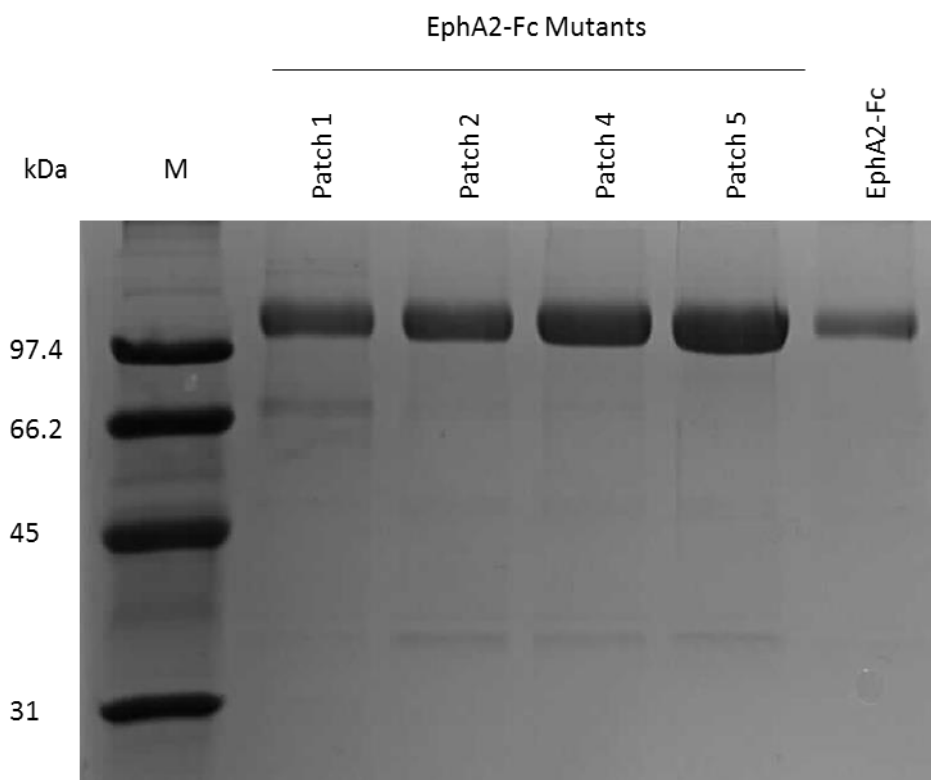


Figure 4.23: Purification of 293T-derived EphA2 patch mutants

Reducing SDS PAGE analysis (Instant Blue) of Ni-NTA purified EphA2 patch mutants, demonstrating equivalent, yield, migration and purity to the WT EphA2-Fc construct.

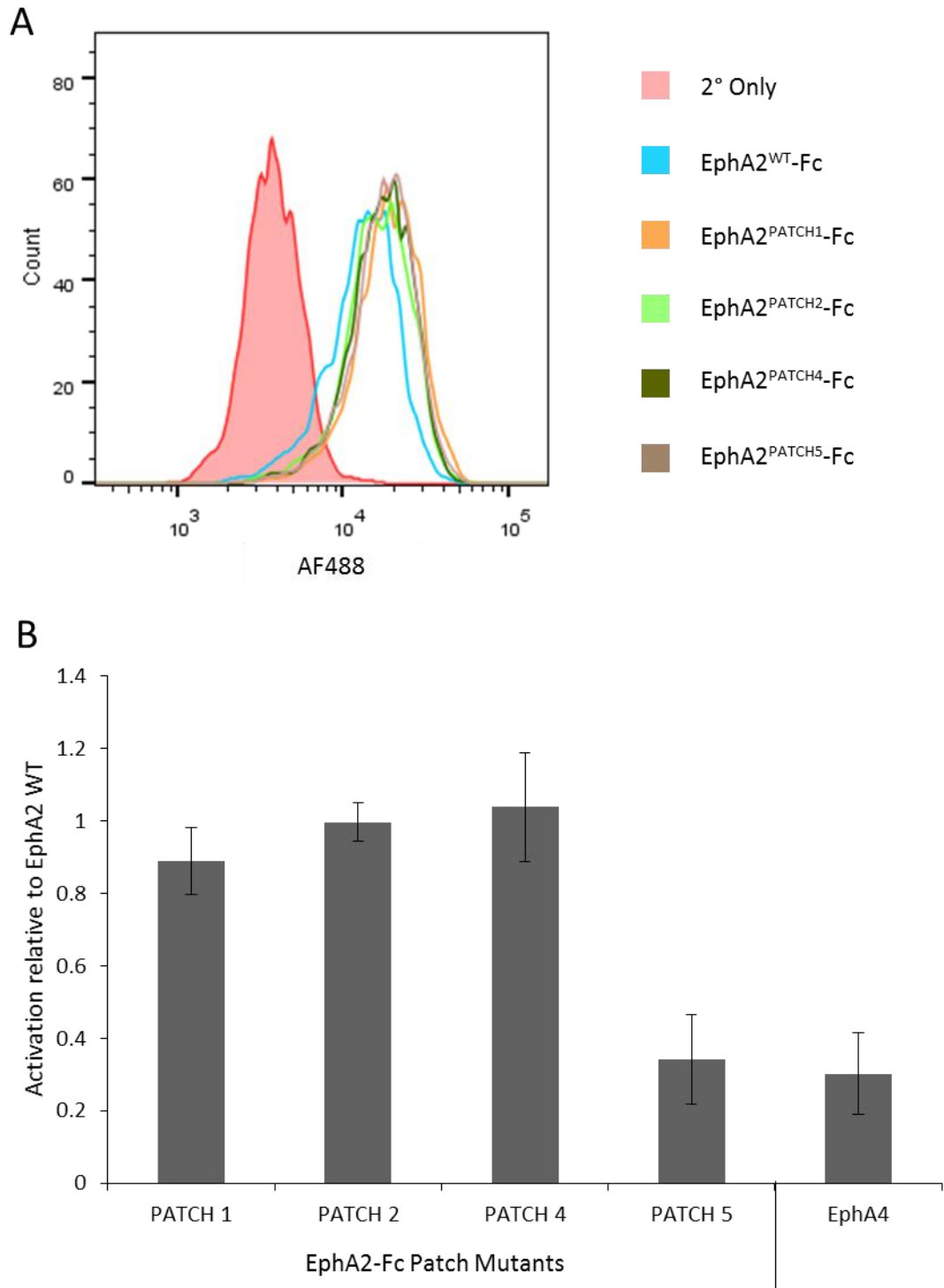


Figure 4.24: Characterisation of EphA2 surface patch mutants

(A) Fc-tagged ephrin receptors were used to stain JRT MAU cells, which were detected using an AF488 conjugated goat anti-human Fc secondary antibody. All patch mutants stain JRT cells equivalently to the ET construct. (B) Fc-tagged ephrin receptors were immobilised on a 96-well plate and incubated with JRT MAU cells for 4 hours. Activation was measured by CD69 upregulation. EphA2^{PATCH5}-Fc failed to activate JRT MAU. ($n=3$, error bars =SD).

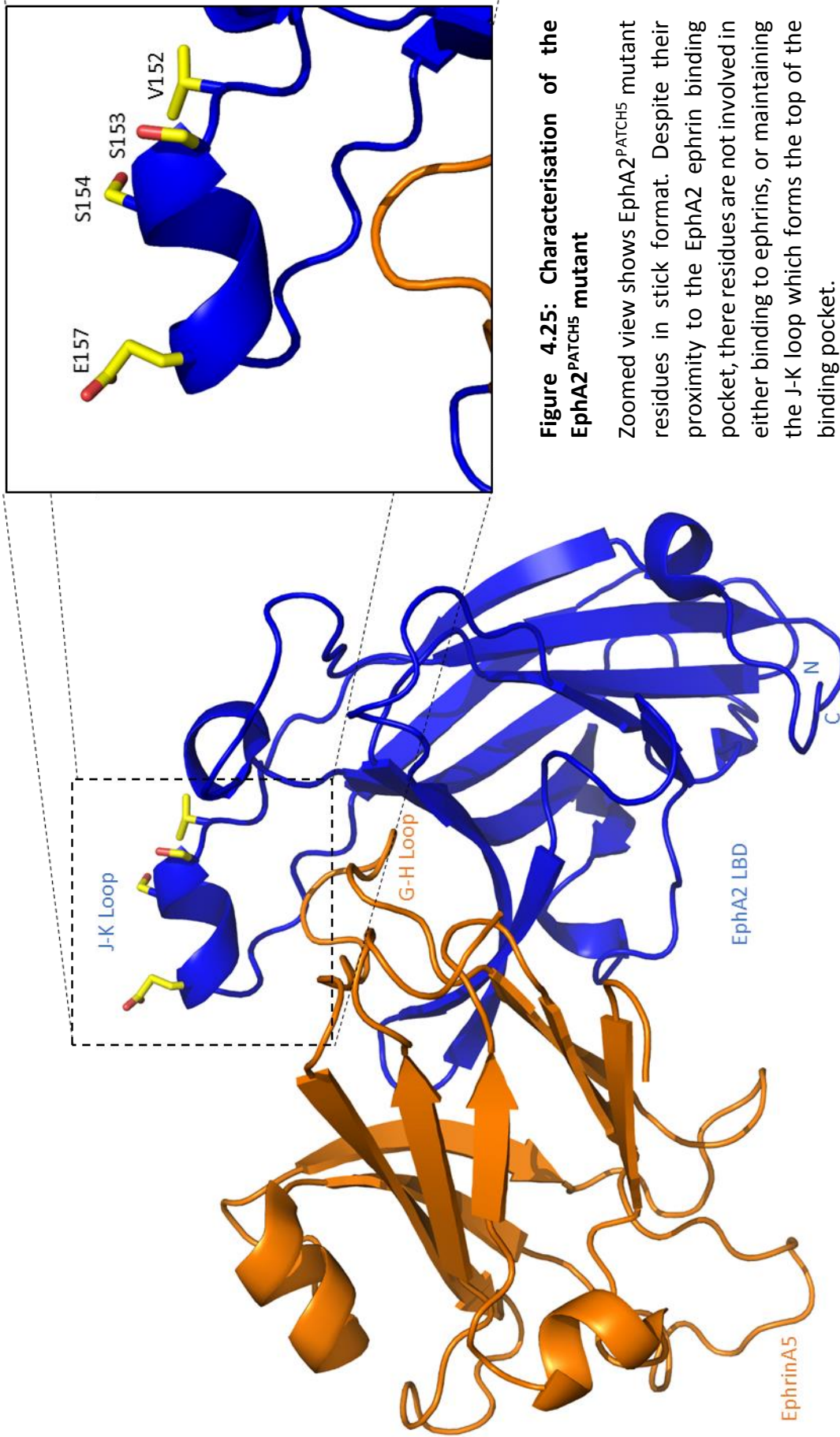


Figure 4.25: Characterisation of the EphA2^{PATCH5} mutant

Zoomed view shows EphA2^{PATCH5} mutant residues in stick format. Despite their proximity to the EphA2 ephrin binding pocket, these residues are not involved in either binding to ephrins, or maintaining the J-K loop which forms the top of the binding pocket.

Analysing the TCR γ Chain Repertoire of $\gamma\delta$ T
Cells in the Liver and Colon

5.1 Introduction

The two preceding chapters have focused on elucidating the molecular basis of the interaction between a $V\delta 1^+$ $\gamma\delta$ T cell, MAU, and an epithelial stress ligand, EphA2. This chapter aims to explore the potential of using sequence-level TCR repertoire analysis to analyse the $\gamma\delta$ T cell compartment in human tissue samples, and to refine these approaches to inform future studies. This approach will also be used to explore the diversity of the $\gamma\delta$ TCR repertoire and to attempt to identify $\gamma\delta$ TCRs of interest, such as MAU, as well as potential public $\gamma\delta$ TCRs in these samples.

The majority of studies characterising $\gamma\delta$ TCRs and their ligands have been focused on T cells generated by cloning¹⁵⁰. While these studies provide insights into the molecular nature of $\gamma\delta$ TCR interactions, it is unclear how representative these examples are of the whole $\gamma\delta$ T cell compartment. Furthermore, as $\gamma\delta$ T cell clones are typically derived from peripheral blood (PB) for these clone-based studies, it is unclear whether these cells are active in PB, or if they can encounter ligand in that environment. For example, the MAU $\gamma\delta$ T cell clone was derived from an expanded $V\delta 2^{\text{negative}}$ $\gamma\delta$ T cell population in PB of a renal transplant patient⁷³. However, as the previous chapters in this study have discussed, the putative ligand for this clone is an epithelial stress ligand, and $V\delta 1^+$ $\gamma\delta$ T cells are thought to predominantly be associated with epithelial surfaces². Furthermore, the MAU clone expressed high levels of integrin $\beta 7$, which is associated with gut localisation⁷³. It is therefore preferable to research such cells in the environment in which they are active and encounter ligand and therefore in this study I will investigate the repertoire in two tissue types, liver and colon, which have been demonstrated to contain large numbers of $V\delta 1^+$ $\gamma\delta$ T cells².

The intestinal mucosa consists of an epithelial layer and underlying connective tissue known as the lamina propria (LP). Colonic lymphocytes are found in both compartments and are characterised depending on their tissue sublocalisation. Intraepithelial lymphocytes (IELs) are present in the intercellular space between the epithelial cells of mucosal linings, and lamina propria lymphocytes (LPLs) are present in the LP¹⁵¹ (Figure 5.1). In mice, the IEL population is largely populated by V γ 7⁺ $\gamma\delta$ T cells¹⁵², which is suggestive of a clonal population, although this has yet to be determined.

Previous studies have suggested that in humans, these IEL and LPL populations are distinct, with individual functional and TCR profiles¹⁵³, although there is evidence that $\gamma\delta$ T cells can migrate from the epithelium into the LP in mice upon microbial challenge¹⁵⁴. This highlights the potential difference between tissue subsets, let alone between blood and tissues, further emphasizing the need to expand on blood-focused $\gamma\delta$ T cell studies by analysing $\gamma\delta$ T cells in tissues.

Repertoire analysis is a powerful tool which has been used extensively to study populations of $\alpha\beta$ T cells in various infections and diseases¹⁵⁵. Despite this, there has been no extensive repertoire analysis of $\gamma\delta$ T cell populations at the TCR sequence-level, and it is unclear whether the human $\gamma\delta$ repertoire will be diverse or of limited diversity as observed in murine epithelial $\gamma\delta$ compartments. Spectratyping analysis has been used to classify populations of $\gamma\delta$ T cells and provide limited information on V region usage, particularly in response to CMV infection⁵⁶. While these studies provide some information on how the size and proportions of $\gamma\delta$ T cell repertoires alter in response to infection, they have failed to provide information on individual TCR usages, which is only possible with sequence-level TCR analysis. Furthermore, repertoire studies have the potential to facilitate more targeted

and unbiased $\gamma\delta$ T cell ligand identification. Critically, such approaches allow for the identification of $\gamma\delta$ T cell populations that are likely to play a physiological role in response to infection, which can then be characterised at a molecular level.

Sequence-level TCR repertoire analysis techniques can broadly be characterised into either DNA-based or RNA-based¹⁵⁵. DNA-based approaches, such as the immunoSEQ platform (Adaptive Biosystems), amplify recombined genomic DNA regions using V and J region specific primers¹¹⁶, and these PCR products are then sequenced. RNA-based approaches, such as the anchored 5'-RACE (rapid amplification of cDNA ends) methodology, generate cDNA from mRNA sequences, from which TCR specific sequences are subsequently sequenced¹¹⁷. For this study the DNA-based immunoSEQ platform was selected, as it is capable of deeper sequence analysis than the RNA methodology available during this study, allowing for the detection of lower abundance sequences¹¹⁷. At the time of this study, immunoSEQ offered only γ chain analysis, and so all sequences discussed in this chapter represent only the γ chain, and therefore no δ chain information is available.

This chapter will explore the feasibility of using DNA-based high throughput, sequence-level TCR repertoire analysis to investigate $\gamma\delta$ T cell repertoires in human tissue samples, and to refine such approaches to shape future experiments. This constitutes a brief analysis of the γ chains of $\gamma\delta$ T cell populations in three human samples, two colon and one liver. Finally, sample preparation and processing techniques to prepare human tissue samples for these analyses will be developed and advanced.

Because of the low number of samples, limited conclusions about these samples can be drawn. However, these studies provide valuable insights into the data, as well as potential

differences which can be exploited to inform more comprehensive hypothesis-driven studies.

5.2 Results

5.2.1 Sample preparation

Refinement of tissue preparation techniques was performed on numerous samples prior to the ones selected for repertoire analysis, and the following section details this process.

Preparation of tissue samples was either carried out mechanically or enzymatically. The liver samples were not to be separated into tissue sub-populations, and so mechanical digestion was used to isolate lymphocytes from the whole tissue. The colon samples were to be separated by tissue compartment, into IEL and LPL populations. Therefore a combination of chemical and enzymatic digestion was used to specifically disrupt the tissue structures containing the required lymphocytes.

The luminal facing epithelial surface of colon tissue was specifically disrupted using a combination of EDTA and DTT to disrupt the cadherin-mediated cell-cell junctions of the epithelium, thus releasing IELs¹⁵⁶. As this approach does not disrupt the basal membrane, LPLs should remain in the tissue. To release the LPLs, collagenase A was used on the EDTA/DTT-treated samples to digest the basal membrane and liberate the LPLs (Figure 5.1).

Several strategies were used to verify the isolation of pure IEL and LPL populations. Firstly, the number of cells released from the tissue after each successive EDTA/DTT treatment was measured. The absolute cell number in the media following washing plateaus after the second 20 minute treatment suggested that 3 to 4 washes of a sample this size results in the complete removal of the IEL population (Figure 5.2A). Secondly, a study has suggested

that the FSC and SSC profiles of IEL and LPL populations in rats are distinct when analysed by flow cytometry¹⁵⁶. This pattern was also observed with these colon samples, as the LPL populations appeared to be larger and more granular than their IEL counterparts, suggesting successful isolation of distinct lymphocyte populations from the colon (Figure 5.2B).

Finally, the tissues were imaged at various stages of the digestion process to visualise the tissue disruption. Four samples were analysed in total, one of the native tissue, one after 2 and 4 EDTA/DTT treatments and one after 4 collagenase washes. These samples were fixed, sectioned and then visualised by hematoxylin and eosin (H&E) staining (Figure 5.3). These images demonstrate incremental disruption of the epithelial cells after EDTA/DTT treatment, compared to the native sample, in line with previous studies¹⁵⁶. It is also apparent that the EDTA/DTT treatment does not disrupt the basal membrane of the tissue, which is fully intact, with the tissue maintaining the original architecture of the crypts (Figure 5.3B, C). However, despite their disrupted morphology, epithelial cells are still present in the crypts after four treatments of EDTA/DTT. Colon tissue treated with collagenase demonstrates considerable disruption of the tissue histology, with no clearly distinct crypt architecture present, and complete disruption of the basal membrane (Figure 5.3D).

Collectively, these data suggest that two discrete populations of lymphocytes are being isolated by this colon sample preparation protocol. The imaging data demonstrate that the basal membrane is not disrupted by the EDTA/DTT treatment, which strongly suggests that the isolated IEL population is devoid of LPLs, which were still in the LP, contained by the basal membrane. However, it is less clear whether IELs are present in the LPL population.

Although EDTA/DTT treatments were applied until no more cells were released, this does not necessarily imply complete disruption of the epithelium, and may represent the limits of the reagents or approach used. Furthermore, the imaging data demonstrate that epithelial cells are still present in the tissue despite 4 treatments with EDTA/DTT, suggesting that IELs may also still be present in the tissue following this treatment, and therefore could be released by the collagenase treatment into the LPL population, which should be considered when analysing the results.

A further tissue processing technique which was refined was the purification of $\gamma\delta$ T cells. Rearrangement of the γ TCR chain is an early recombination event in the development of T cells, concurrent with β and δ chain rearrangement. Therefore, the γ chain is recombined in some $\alpha\beta$ T cells, as well as $\gamma\delta$ T cells¹⁵⁷. The immunoSEQ platform specifically amplifies recombined γ chains, and so if $\alpha\beta$ cells were present in the sample, their γ chains would be sequenced, even though they do not represent surface-expressed $\gamma\delta$ TCRs. To avoid this, two approaches were compared for the removal of $\alpha\beta$ T cells from the single cell suspension from both colon and liver samples. Magnetic beads (Miltenyi) were used to either select cells expressing the $\gamma\delta$ TCR (positive selection, data not shown), or deplete cells expressing an $\alpha\beta$ TCR (negative selection). Negative selection resulted in the highest purity of $\gamma\delta$ T cells in the CD3⁺ lymphocyte population, with up to 99.9% purity (Figure 5.4). Following this refinement, several samples were processed and analysed by immunoSEQ. A summary of these samples used in this analysis is shown in Table 5.1.

5.2.2 Contamination and the presence of PB-associated $\gamma\delta$ chains

Initial analysis of the repertoire sequencing data revealed significant contamination of $\gamma\delta$ TCR γ chains, as well as the presence of typically pAg reactive V γ 9V δ 2 PB-associated V γ 9 sequences.

The γ chain sequence for the MAU $\gamma\delta$ TCR was present in considerable frequencies in all samples and represented up to 90% of sequences (Figure 5.5A). This is likely due to contamination of MAU γ chain DNA used for cloning experiments in the Willcox laboratory. Furthermore, a significant portion of these contaminant sequences matched the mutants generated for MAU TCR mutagenesis studies outlined in Chapter 4. This suggested that these sequences are a result of contamination rather than being genuinely present in the tissues. Therefore, these sequences were disregarded from the subsequent analyses. However, this resulted in potential MAU γ chain sequences legitimately present in the tissue being excluded from the analysis, as it is not possible to differentiate between contamination and sequences present in the original sample.

γ chain sequences associated with the pAg reactive V γ 9V δ 2 PB subset of $\gamma\delta$ T cells were also identified in some of the samples (Figure 5.5B). The V γ 9V δ 2 γ chain typically comprises the V γ 9 V gene segment paired with the JgP*01 joining segment, with the amino acid motif *ELG* in the CDR3 region⁵⁹. Such sequences were highly prevalent in the liver sample, representing 12% of all γ chain sequences. This blood subset signature was also present in both the IEL and LPL populations of the S024141 colon sample. The presence of the PB-associated γ chain in these tissues may be due to the manner in which the samples are washed and processed following resection, and prior to samples being received in our laboratory. Also, the tissue extraction method used to isolate T cells may result in the

presence of PB-associated γ chains in the samples. For example, the liver samples were mechanically digested, and perhaps this is more likely to disrupt blood vessels in the tissue compared to colon samples that were subjected to more specific enzymatic treatments. Moreover, it may also be that there are inherent differences in the vascularisation of the tissue types.

It is unclear whether the PB-associated γ chain sequences are from blood present in the tissue or constitute a component of the tissue resident $\gamma\delta$ TCR repertoire. For these reasons, cells with this signature were excluded from further analysis in this study. However, as will be shown in Chapter 6, γ chains bearing the PB motif can sometimes pair with non V δ 2 δ chains, and so these will not be represented. Finally, sequences which were unproductive, or contained either pseudo-gene or non-functional gene segments according to the IMGT (V γ 1, V γ 6, V γ 7, V γ 10, V γ 11) were also excluded from the analysis¹⁴⁴.

5.2.3 Clonality and shared sequences

Clonality of a repertoire is an important metric, and is currently not well understood for human $\gamma\delta$ T cell repertoires, particularly in tissues. High degrees of clonality are often associated with $\gamma\delta$ T cell populations, particularly in response to CMV infection^{56,158}. While these clonality measurements can provide useful information on the physiological role of $\gamma\delta$ T cells in these conditions, limited studies have been carried out on the individual $\gamma\delta$ TCRs that constitute these populations.

Clonality of the repertoires can be analysed in several ways. Firstly, the abundance of the 10 most prevalent sequences in each sample was plotted, excluding MAU and PB-associated sequences, as previously discussed (Figure 5.6A). This analysis demonstrates that all of the samples have approximately equivalent abundance and diversity of their top

sequences, with the top sequence in each sample representing between 11% and 20% of all sequences. Aside from these most abundant sequences, the remainder of the repertoire appears to be relatively diverse, with the frequency of sequences plateauing after the first 3 top ranking sequences. The clonality metric allows for the quantification of the diversity of sequences in the repertoire analysis, and direct comparison of clonality between samples of the same analysis. The clonality ranges from 0 (diverse, with equal representation of all sequences) to 1 (clonal, only one sequence is present) (Figure 5.6A). This clonality measurement is similar for all 5 samples analysed, ranging between 0.19 and 0.29. This suggested a similar diversity of sequences between all samples. This metric is derived from the normalised Shannon entropy of the TCR γ frequency distribution, which is a measure of the uncertainty in the distribution of the frequencies of the sequences¹⁵⁹. The equation for this calculation is shown below, where n represents the total number of sequences in the sample, and p_i is the fraction of residues of sequence i :

$$\text{Clonality} = 1 - \left(- \sum_{i=1}^n \frac{p_i \log_{10} p_i}{\log_{10} n} \right)$$

Sequence overlap is represented as a proportion of sequences shared between samples (Figure 5.6B). This analysis reveals that the IEL and LPL populations within an individual contain a large number of shared sequences, compared to the equivalent populations between donors. For example, the S024121 IEL and LPL populations share ~90% of their γ chain sequences. This data therefore suggests that in these samples, the IELs and LPLs are not distinct populations, and share a substantial number of γ chain sequences.

To determine whether there was any overlap in these top sequences between samples, the top 10 most abundant sequences from each sample were analysed (Figure 5.7). None of

the top 10 ranking sequences for any sample were present between samples derived from different patients, suggesting highly private, non-overlapping repertoires of γ chains in these tissues. There is a high degree of shared sequences between the IEL and LPL population of each colon sample, again reinforcing that these populations do not appear to have distinct $\gamma\delta$ T cell repertoires.

5.2.4 V region usage

The sequence data collected in this study also allow for the comparison of γ chain V region usage between samples. V region usage for both γ and δ chains is thought to be strongly associated with the localisation and function of $\gamma\delta$ T cells⁸. For example, the pAg reactive PB subset invariably use the V γ 9 and V δ 2 gene segments. Therefore improved understanding of V region usage in tissues may allow for similar characterisation of potentially tissue-associated $\gamma\delta$ T cell subsets.

Similar to the sequence overlap analysis discussed previously in this chapter, this comparison revealed similar V region usage of γ chain sequences between the IEL and LPL populations of the individual colon samples (Figure 5.8A). Between patients however, the V region usage is less conserved. This further supports the observation that the IEL and LPL compartments are not distinct with regards to their γ chain sequences. Due to the small sample sizes, it was not prudent to analyse particular V region usage patterns of the samples, but this has demonstrated the potential importance of such studies in the future.

A further analysis investigated the clonality of sequences with particular V region usage, which is only possible with sequence-level TCR data. All of the samples were combined for this analysis, as when analysed individually, a similar pattern was apparent for all of the samples. This suggests that these patterns may relate to many repertoires and therefore

warrants further investigation (data not shown). This analysis compared the frequency of the V region usage with the proportion of unique sequences which constitute that V region, again omitting MAU and PB-associated sequences (Figure 5.8B). For these samples, ~5% of sequences contained the V γ 9 gene segment, but these chains contained over 30% of the unique nucleotide sequences. This suggests that γ chains containing V γ 9 gene segment are relatively diverse in these samples with regards to their CDR3 region. In contrast, V γ 8 chains account for proportionally much fewer unique nucleotide sequences, suggesting that chains containing this V segment have less diverse CDR3 regions.

5.2.5 Identification of clones of interest

Repertoire studies can also be used to identify previously published clones, or clones currently being investigated in various samples (Table 5.2). This provides information on their relative abundance, information which is not available during the cloning process.

This study revealed the presence of several γ chain sequences from both published clones and TCRs currently being investigated by various groups (Figure 5.9). Most of these sequences are present at low levels and do not constitute the top ranking sequences for each sample. As discussed previously in this chapter, the high prevalence of the MAU γ chain in these samples means it was excluded from this analysis. The LES γ chain was observed in several of the samples, up to 6% in sample S026278I. However, this DNA sequence has also been used in cloning experiments in the Willcox laboratory, and so although not present at exceptionally high levels in all samples like MAU, it cannot be excluded that this also represents contamination. Alternatively, the LES V γ 4 chain is a fairly simple rearrangement, as it does not include many N-nucleotide additions, and so is more likely to be produced by recombination events than chains with more complicated

rearrangements, which may explain its relatively substantial presence in these samples compared to other γ chains¹²³.

Despite the uncertainty with clones being researched by our group due to contamination, this study has demonstrated that this approach is viable for analysing the presence of these clones, and give useful information as to their relative abundance, which may have implications for their physiological functions.

5.3 Discussion

In this chapter I aimed to determine the feasibility of using sequence-level repertoire studies to analyse the $\gamma\delta$ TCR compartment in human tissue samples. Repertoire studies investigating $\alpha\beta$ T cells have greatly increased the understanding of how these cells respond to various viral infections at a population level, and are currently being expanded to include diagnostic applications¹⁵⁵. However, to date there has been limited sequence-level repertoire analysis of human $\gamma\delta$ T cells, and hopefully such studies will increase the understanding of how these cells function. Although the sample number in this study is too low to draw many significant conclusions, these experiments have provided valuable insights into the limitations and possibilities of repertoire studies on $\gamma\delta$ T cells in human tissue samples.

This study revealed significant issues with using DNA-based repertoire sequencing in our laboratory. Primarily, the sequencing methodology is extremely sensitive, and as a result, background contamination from DNA constructs used in the Willcox laboratory were sequenced. Although further steps can be taken to prevent such contamination, such as ensuring procedures are carried out in a PCR clean environment as much as possible, this is logistically difficult when dealing with patient samples. Furthermore, over 50 unique

sequences which matched the MAU γ chain CDR3 region were detected. These sequences all differed in the germline-encoded V gene segment, and therefore are not products of recombination (data not shown). It is likely that these sequences represent intermediate PCR products generated during the MAU TCR mutagenesis study, as the V regions align with the SDM primer complementarity regions. This further demonstrates the sensitivity of the immunoSEQ platform, and the difficulty in processing of samples in a laboratory which routinely handles $\gamma\delta$ TCR DNA. To control for contamination in samples, media controls can be used containing no T cells, which would provide a baseline which can be subtracted from samples to differentiate between contaminant sequences and sequences present in the samples. However, due to the relatively large cost per sample of this technique, this would significantly increase the cost of the study, and work would have to be done to ensure contamination levels in the controls are equivalent to those in the samples. Using an RNA-based repertoire analysis would also mitigate these DNA contamination issues, due to the specific amplification of cDNA constructs generated by the reverse transcription of mRNA¹¹⁷.

Further issues were encountered with the preparation of the colon samples and the generation of pure IEL and LPL populations from colon tissue. The experiments regarding the development of the isolation protocols suggested that distinct populations were generated from the assay, however the sub populations in each colon sample analysed demonstrated considerable sequence overlap and V region usage profiles, which does not align completely with previously published reports¹⁵³. It could be that the IEL and LPL populations in these colon samples are not discrete compartments, and their γ chain repertoires are not specific to each compartment. However, it may also be that the tissue preparation protocol has not successfully produced two pure populations, and are thus

represented as demonstrating substantial overlap. Although the imaging data revealed clear disruption of the epithelial cells after EDTA/DTT treatment, some epithelial cells were still present. Whether these remaining cells still include IELs is unclear, and if these cells are still present in the tissue used for collagenase treatment, then IELs would be expected to be present in the LPL population. What is clear from the imaging data is that the EDTA/DTT treatment does not disrupt the basal membrane, strongly suggesting that the IEL population does not contain any LPLs, and so studies focusing on IEL populations are unlikely to be affected by the presence of LPLs.

To clarify this situation, immunostaining could be used to detect CD3⁺ cells in the fixed samples, and study their localisation over the course of the treatments. This confirmation would allow for more reliable comparison of the IEL and LPL populations, and determine whether they contain distinct repertoires of $\gamma\delta$ T cells, which would provide novel insights into the immunobiology of gut-associated $\gamma\delta$ T cells in humans.

Furthermore, the presence of γ chain sequences commonly associated with the PB-associated V γ 9V δ 2⁺ TCRs emphasizes the importance of large sample sizes and consistency in the handling of these tissue samples. It is unclear whether these sequences are tissue-associated or present as a result of blood in the tissue.

Despite the limitations of this study, several key observations were made, which provide novel insights into the role of $\gamma\delta$ T cells in these tissues. Firstly, analysis of the top 10 ranking sequences in each sample revealed that none of these sequences are shared between patient samples, although there is considerable overlap between the IEL and LPL sub-populations of the colon samples. This suggests that the $\gamma\delta$ T cell compartment in the colon is private, although the sample size is too small to draw definitive conclusions.

Secondly, the γ chain V region usage and clonality analysis provided insights into the V region usage profiles of $\gamma\delta$ T cells, as well as the clonality of γ chains containing particular V regions. The analysis demonstrated that γ chains containing the V γ 9 gene segment have more diverse CDR3 regions than γ chains containing other V regions. Conversely, V γ 8 containing γ chains are less diverse in terms of CDR3 region. These findings could provide novel insights into the immunobiology of V γ 9⁺ and V γ 8⁺ $\gamma\delta$ T cells in these tissues, implying that different γ chains may participate differently in the immune response. Interestingly these findings are consistent among all of the samples analysed, suggesting that this may apply to V γ 9 and V γ 8 chains from various tissues, which warrants further study.

Finally, an omission from repertoire studies using this platform is the δ chain. Although γ chain sequences can provide novel insights into the immunobiology of tissue-associated $\gamma\delta$ T cells, $\gamma\delta$ TCRs function as heterodimeric antigen receptors, therefore information about δ chain sequences as well chain pairing is critical to fully understand these subsets.

Overall, the data presented in this chapter strongly suggest that, despite the inherent difficulties in handling human tissue samples, repertoire analysis of tissue-associated $\gamma\delta$ T cells could provide unique insights into the immunobiology of these cells, and therefore justifies pursuing further controlled, hypothesis-driven studies. Therefore, in the next chapter I specifically address the hypothesis that CMV infection results in clonal expansion of V δ 2^{negative} $\gamma\delta$ T cell populations in the blood.

5.4 Tables

Tissue Type	Sample	Patient Code	Subpopulation
Liver	L3698	L3698	N/A
Colon	S024121I	S024121	IEL
	S024121L		LPL
	S026278I	S026278	IEL
	S026278L		LPL

Table 5.1: Overview of the samples used in the immunoSEQ analysis

Sample column denotes how data sets are referenced through the text. Subpopulation identifies the either the IEL or LPL population of the colon sample.

Clone	V γ	J γ	CDR3	C γ	Ref
LES	4	1*01	CATWDGFYKKLF	1a	¹²³
CHAM	4	1*01	CATWEGYKKLF	1b	¹²³
POS4	8	P1*01	CATWDTTGWFKIF	1b	¹⁰⁹
Wendy	9	P*01	CALWEVTELGKKIKVF	1b	N/A
Clone 26	9	2*01	CALWEGNHYYKKLF	2	N/A

Table 5.2: $\gamma\delta$ clones of interest

CDR3 amino acid sequences of γ chains from $\gamma\delta$ clones either published or currently under investigation in various laboratories.

5.5 Figures

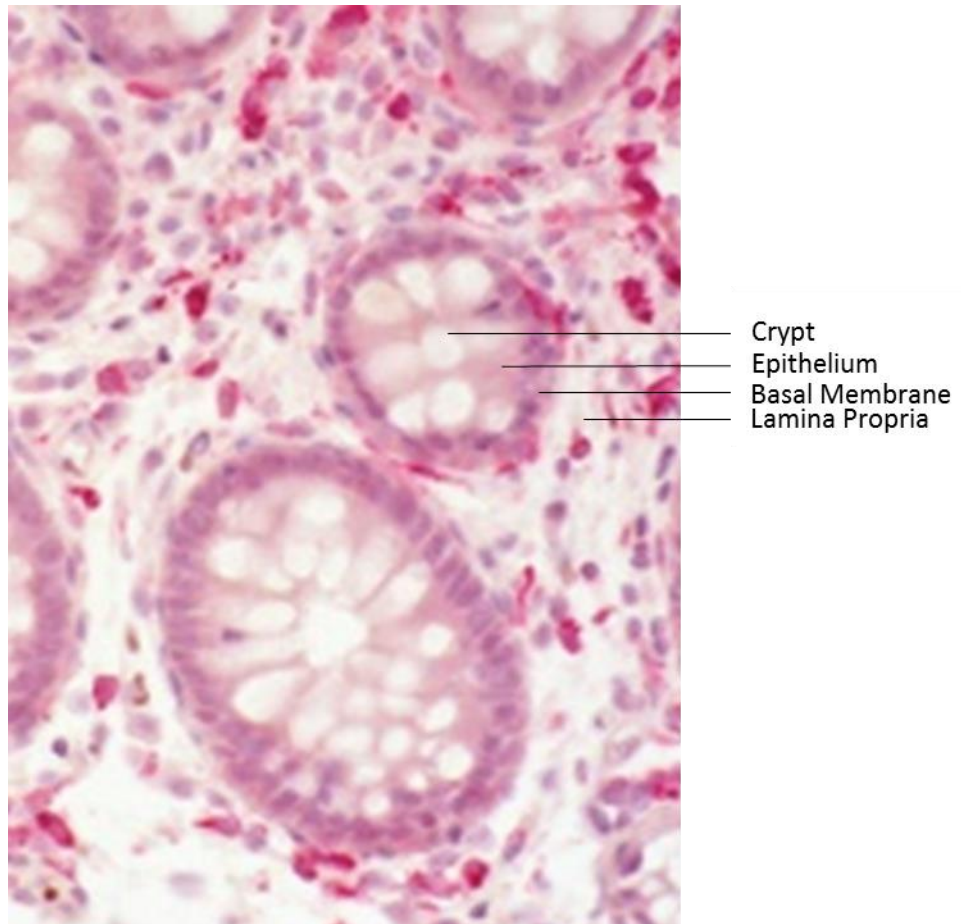


Figure 5.1: Overview of colon histology

Intraepithelial lymphocytes (IELs) are contained within the lumen facing epithelium, which is separated from the lamina propria lymphocyte (LPL) containing lamina propria (LP) by the basal membrane. Top-down view of the luminal surface. H&E Stain, 40X Magnification.

Image modified from¹⁶⁰

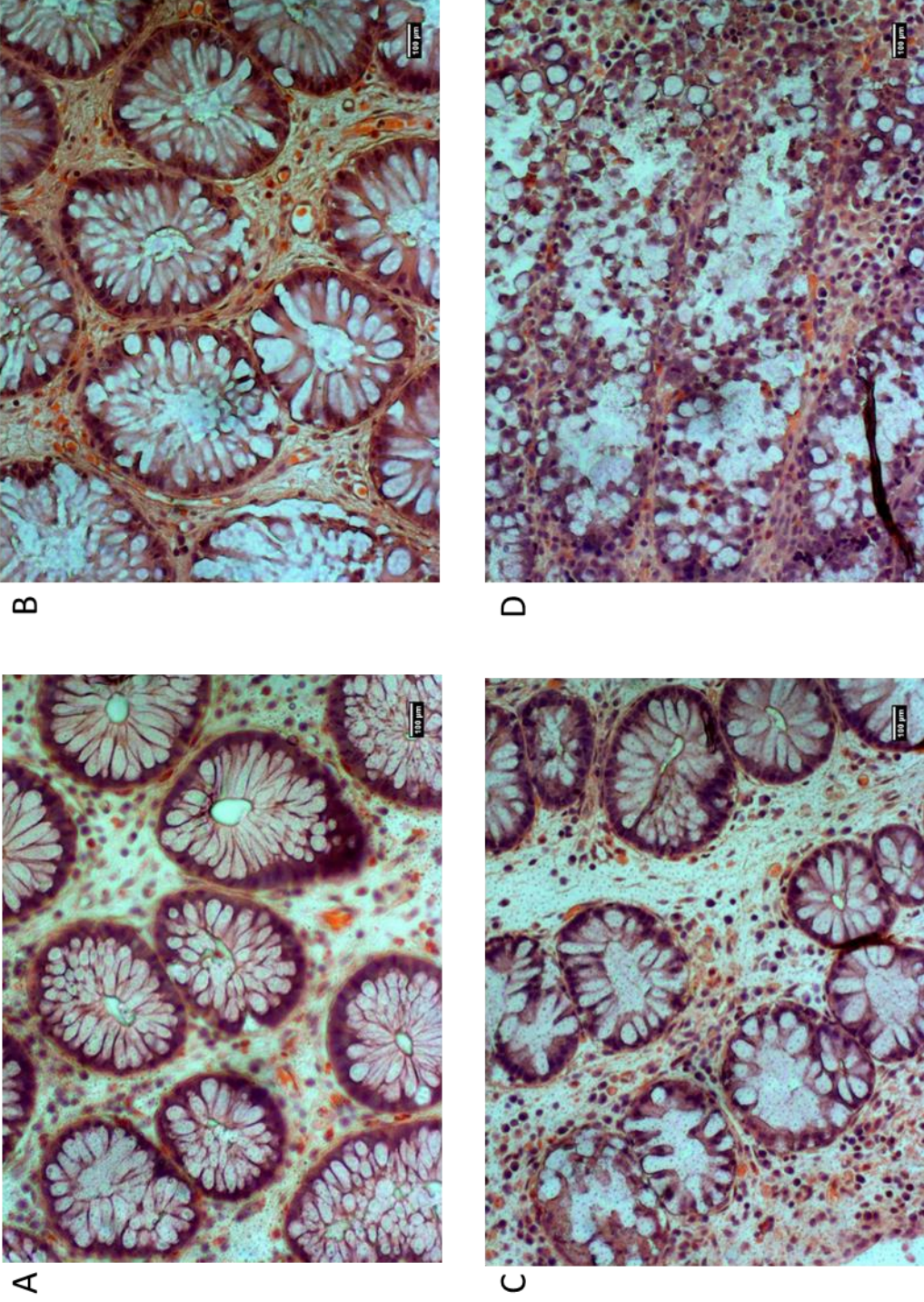


Figure 5.3: Imaging of the colon sample digestion process

Tissues were fixed with formalin, sectioned and visualised using H&E staining (A) Native tissue shows distinct crypt structures separated from the lamina propria by the basal membrane. The epithelial surfaces are disrupted by EDTA/DTT treatment progressively after 2 (B) and 4 (C) treatments. (D) Collagenase treatment disrupts the basal membrane, removing the clearly defined crypts. 20X Magnification, scale bar = 100 μm.

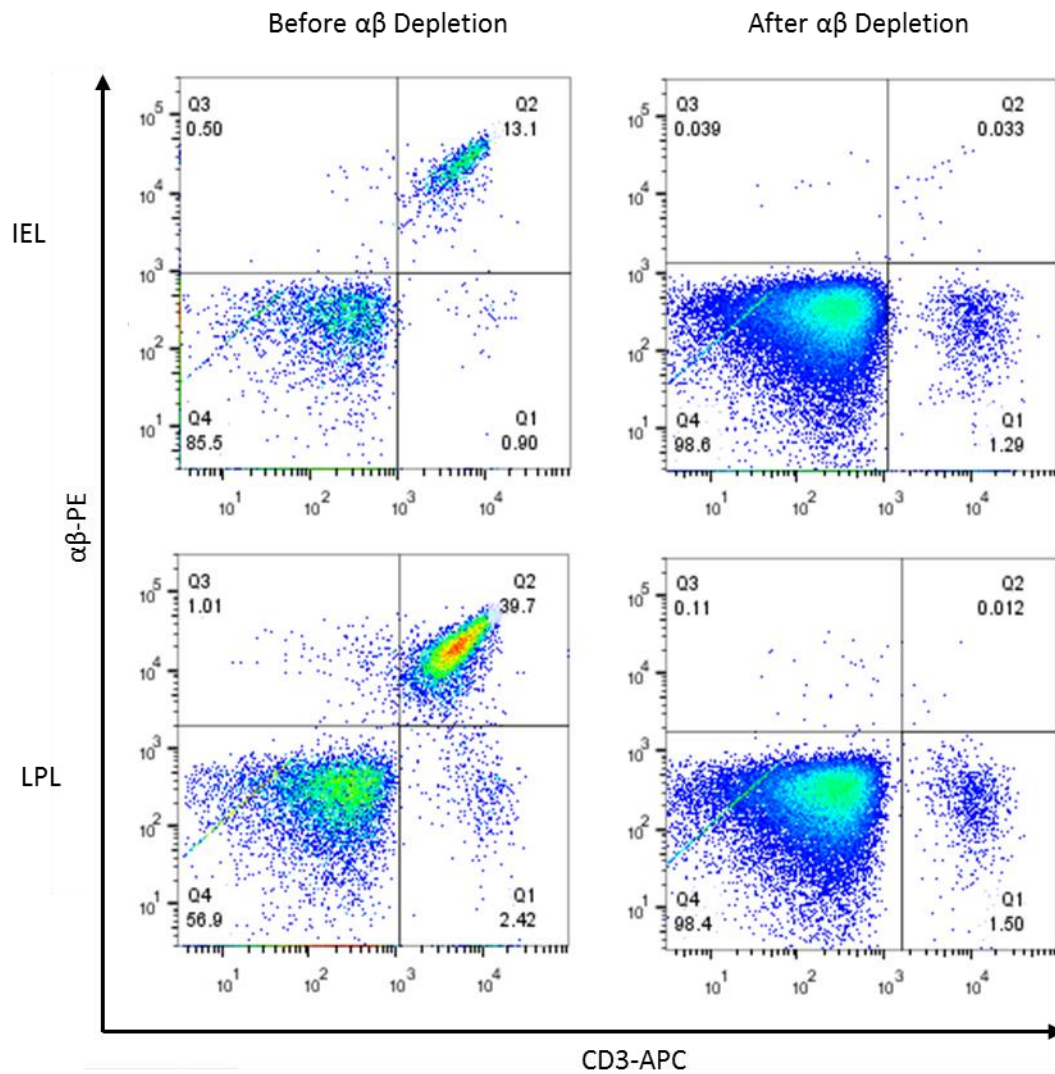


Figure 5.4: Depletion of $\alpha\beta$ T cells from single cell suspensions

$\alpha\beta$ T cells were depleted from the single cell suspensions of liver and colon samples using magnetic bead based separation. An anti $\alpha\beta$ PE-conjugated antibody was used to stain $\alpha\beta$ T cells, and PE-conjugated magnetic beads were used to select stained cells. Representative example from IEL and LPL populations from a colon sample.

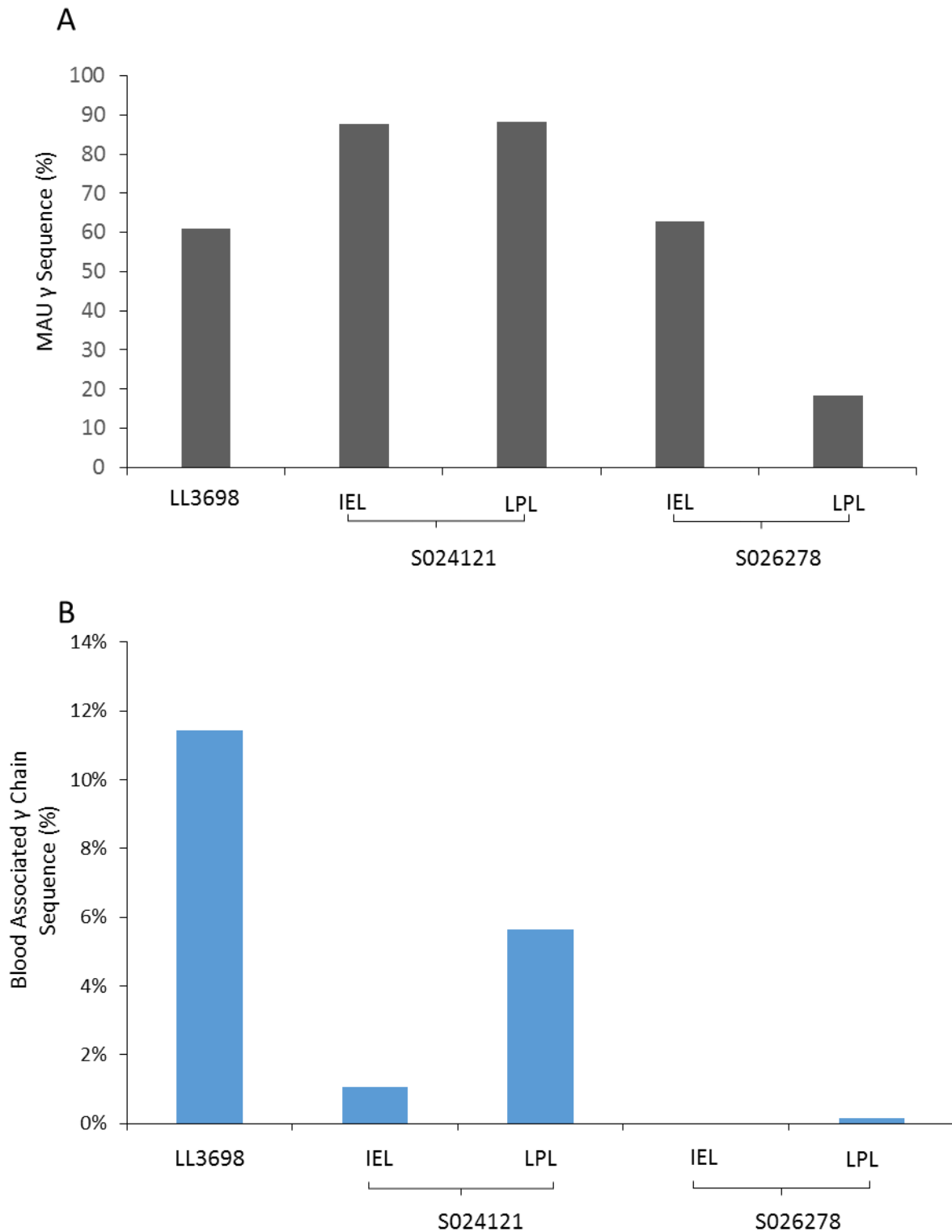


Figure 5.5: Contamination of samples by MAU and the presence of PB-associated γ chains

(A) The MAU γ chain nucleotide sequence was present at high levels in all samples analysed.
 (B) γ chains associated with the pAg reactive PB $\gamma\delta$ T cell subset present in the majority of samples.

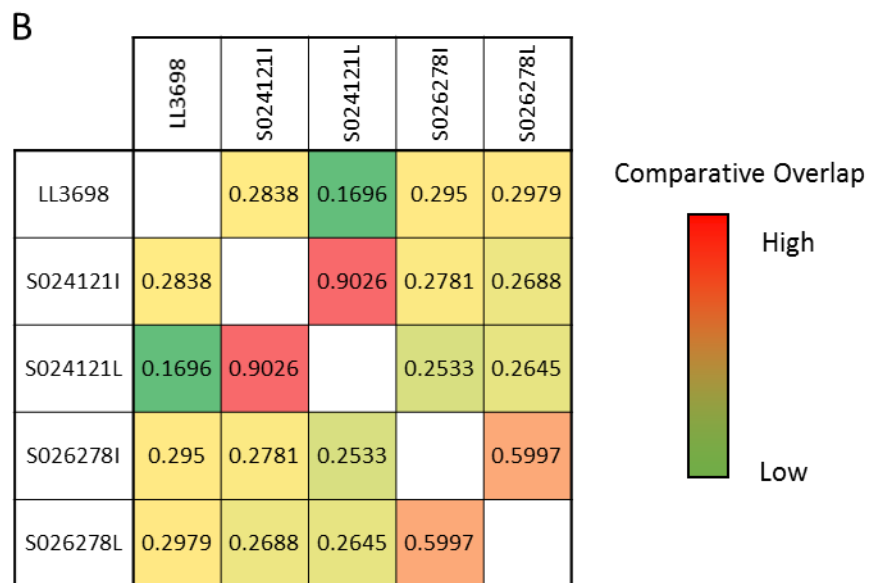
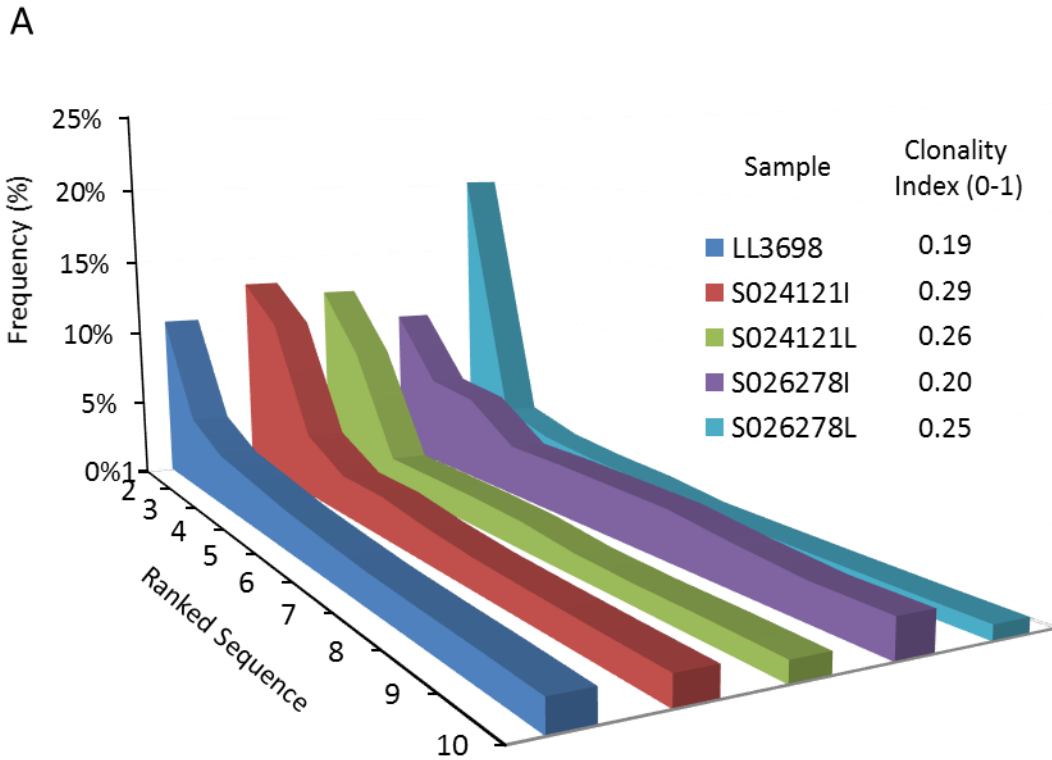


Figure 5.6: Diversity and overlap of γ chain sequences

(A) Frequency of the top 10 ranking γ chain sequences for each sample. Sequence frequency plateaus rapidly after the top 2-3 clones. Clonality was quantified using the clonality index, which was similar for all samples. (Rang 0-1. 0= Diverse, 1=Clonal). (B) Proportion of sequences shared between samples. Relative colour coding ranks overlap from green (low) to red (high).

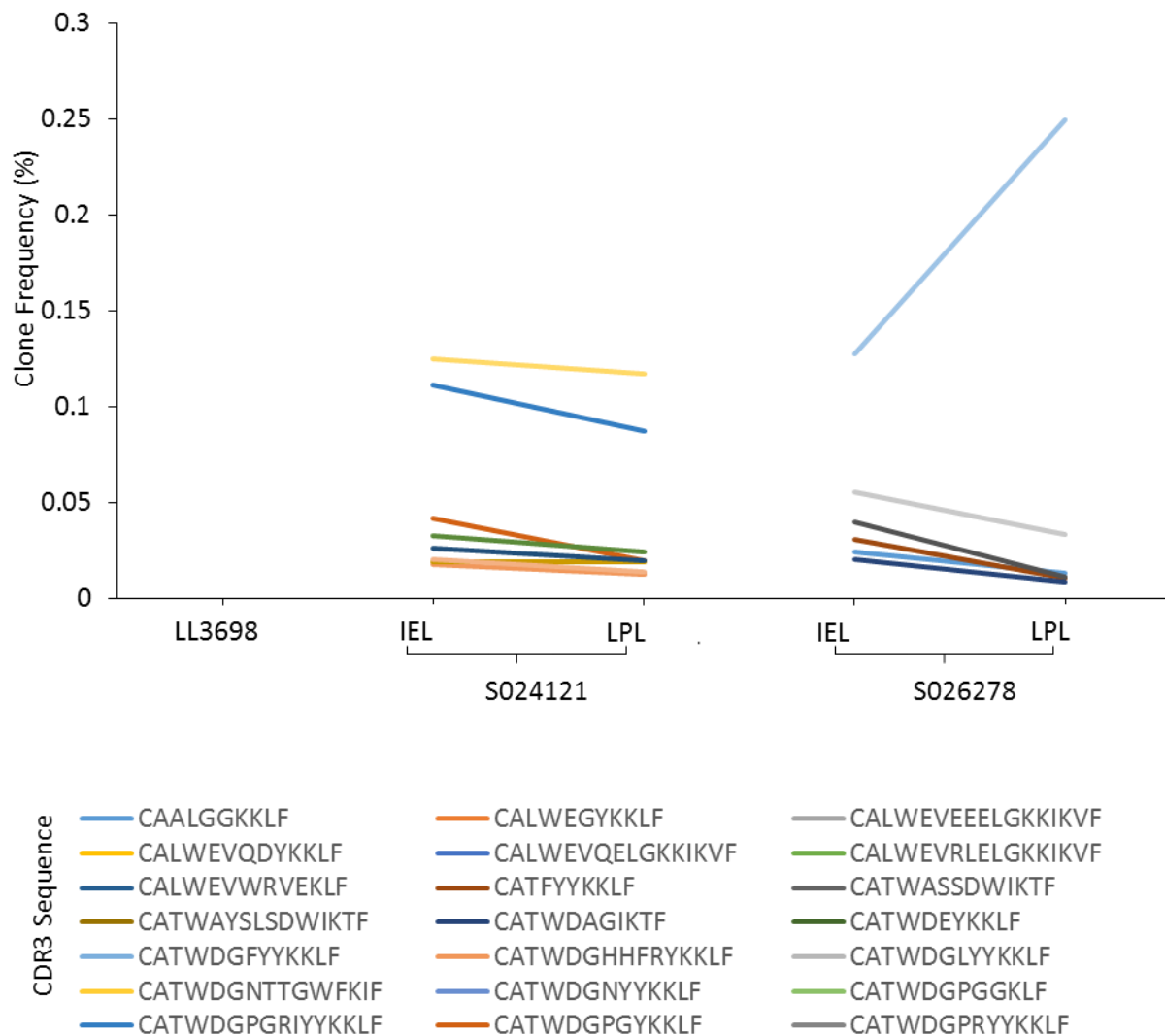


Figure 5.7: Overlap of top ranking sequences

The highest 10 ranking sequences for each sample plotted for all samples. Each of the top 50 sequences only present in samples from the same patient, with shared sequences designated by a coloured line. Sequences not present plotted with no line.

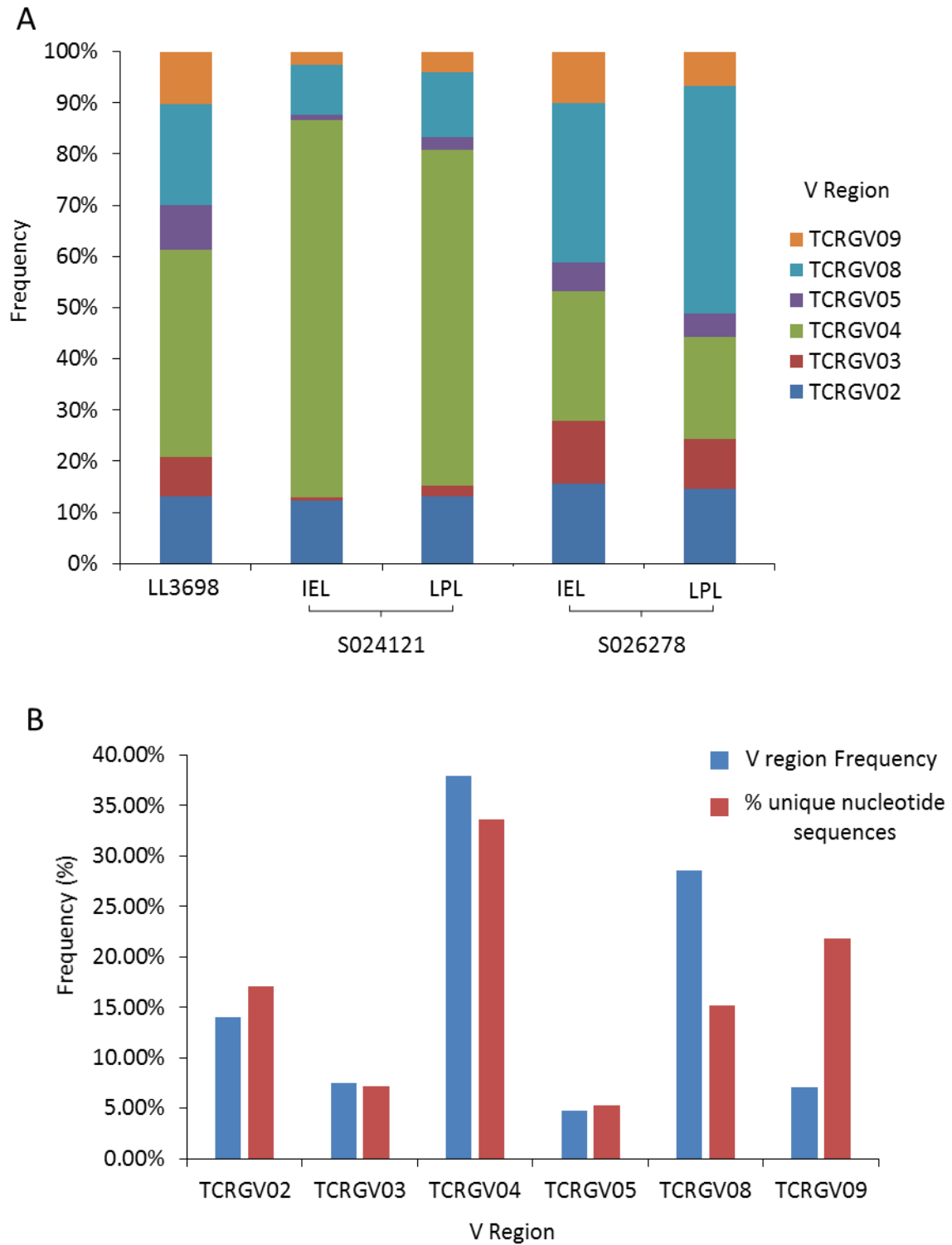


Figure 5.8: γ chain V region usage and clonality

(A) V region usage of γ chain sequences in each sample. (B) Comparison of V region frequency and percentage of unique nucleotide sequences to signify clonality by V region in all samples (pooled). MAU and PB-associated γ chains were excluded from this analysis.

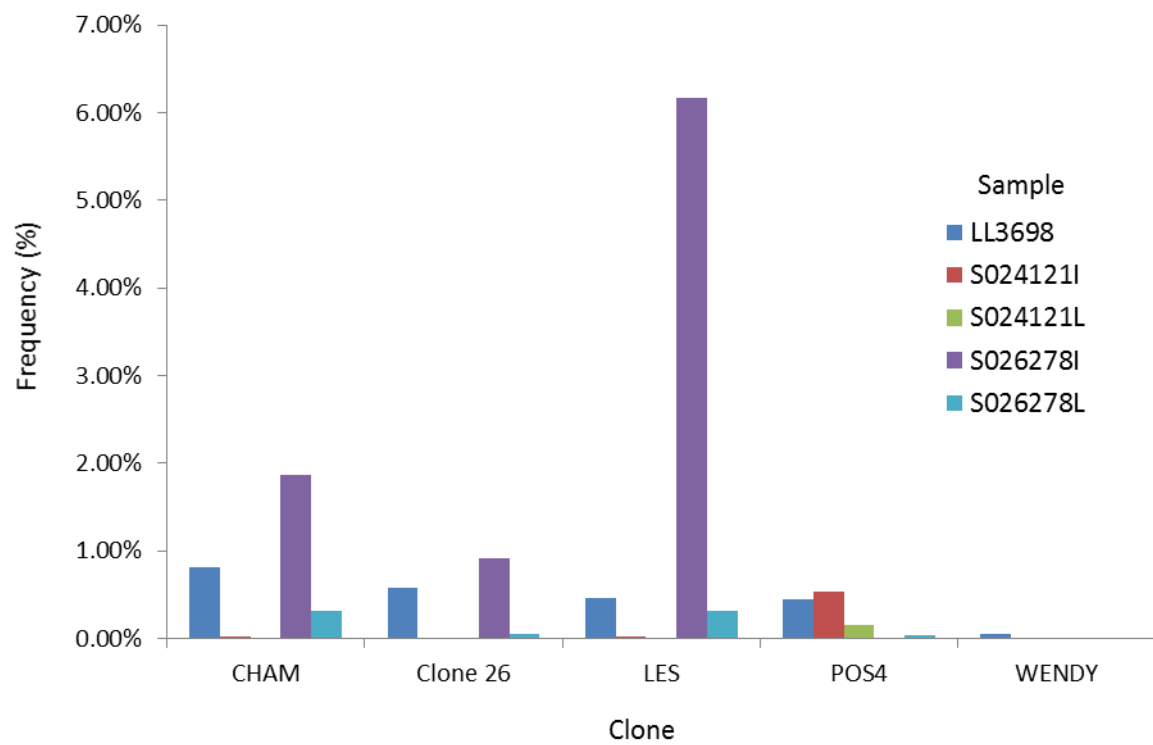


Figure 5.9: Identifying clones of interest in sequencing data

Frequency of γ chains from $\gamma\delta$ clones either published or currently under investigation in various laboratories across all samples. Clone detailed are listed in Table 5.2.

Investigating the Effect of Chronic CMV
Infection on the V δ 1⁺ $\gamma\delta$ T Cell Repertoire in the
Peripheral Blood of Healthy Donors

6.1 Introduction

In Chapter 5, sequence-level repertoire analysis of $\gamma\delta$ TCRs was established as a viable and useful approach for analysing $\gamma\delta$ T cell populations in human tissue samples. In this chapter, these results were expanded by using repertoire analysis to characterise the effect of chronic CMV infection on the $V\delta 1^+$ $\gamma\delta$ T cell repertoire in PB of healthy donors.

CMV is a double-stranded DNA β -herpes virus which chronically infects between 50- 90% of the population⁵². Following acute infection, CMV enters a non-symptomatic latent phase, characterised by a reduction in the production and expression of viral proteins⁵³. Initiation and maintenance of this latent cycle is thought to be largely influenced by chronic immune-suppression of the CMV lytic processes⁵³. Therefore, CMV reactivation often occurs in immunocompromised patients, and can result in severe clinical implications⁵⁴. CMV reactivation can be treated with adoptive transfer of $CD8^+$ $\alpha\beta$ T cells¹⁶¹, further demonstrating the importance of the immune system in maintaining a safe, latent infection.

CMV infection has been directly implicated in the induction of both transient and permanent changes to the immune system. For example, infection often drives the clonal expansion of highly differentiated memory $CD8^+$ $\alpha\beta$ T cells¹⁶², with individual CMV-specific $CD8^+$ T cells occasionally representing up to 10% of the total T cell compartment¹⁶³. These expansions are more pronounced in elderly donors¹⁶⁴, and this process is reflective of immune senescence, which is characterised by an increase in memory responses whilst immune responsiveness to new challenges is decreased¹⁶⁵.

$\gamma\delta$ T cells, particularly the $V\delta 2^{\text{negative}}$ subset, have also been predicted to contribute towards the immune response to CMV, perhaps in a complementary manner to $CD8^+$ $\alpha\beta$ T cells⁴⁶.

One of the immune evasion strategies of CMV is to inhibit the loading of class I MHC molecules with peptide¹⁶⁶, a strategy ineffective at inhibiting $\gamma\delta$ T cells due to their non-MHC-restricted ligand recognition. Therefore $\gamma\delta$ T cells may play a role in controlling virally infected cells which have evaded detection by $\alpha\beta$ T cells. Large expansions of $V\delta 2^{\text{negative}}$ $\gamma\delta$ T cells are often observed in the PB of immunocompromised CMV-seropositive donors⁴⁶ as well as, to some extent, in healthy individuals¹⁵⁸. This strongly suggests that these cells are somehow involved in the immune response to CMV. Indeed, expansions of $\gamma\delta$ T cells in CMV reactivation in immunocompromised transplant patients correlates with resolution of viraemia, suggesting a protective antiviral role for these cells⁵⁵. Finally, several $V\delta 2^{\text{negative}}$ $\gamma\delta$ T cell clones, including MAU and LES, were established from donors possessing such expansions⁷³. Strikingly, the LES clone represented 25% of patient T cells, and the LES $\gamma\delta$ TCR ligand, EPCR, is present on CMV infected cells and critical for CMV-dependent recognition by the LES clone¹²³. However, as these TCRs were isolated by cloning, it is currently unclear how representative these examples are of the whole subset.

Similar to CMV specific $\alpha\beta$ T cells, these expanded $V\delta 2^{\text{negative}}$ populations are highly differentiated¹⁵⁸, and spectratyping studies often characterise these expansions as oligoclonal^{46,56}, suggesting that the expansion is antigen-driven. Such studies provide no information on the particular $\gamma\delta$ TCR chains present in these populations however, and cannot determine diversity of recombined CDR3 regions which, according to the previous structural studies highlighted in Chapters 3 and 4, play a critical role in the recognition of ligands for $\gamma\delta$ TCRs^{50,51}. Furthermore, it is important to determine whether these expanded populations are private or public, with common $\gamma\delta$ TCR chains shared between the donors, as this may have implications for the ligands and ligand recognition strategies for these receptors.

Increased understanding of how $\gamma\delta$ T cells interact with this model virus may expand the potential for advances in existing treatments. For example, immunotherapeutic strategies based on adoptive transfer of CMV-specific CD8⁺ $\alpha\beta$ T cells are currently used in immunocompromised patients undergoing CMV reactivation¹⁶¹, and there is potential for these to be replaced with $\gamma\delta$ T cells, which are not MHC-restricted and therefore can be applied more broadly and overcome MHC down regulation, a common immune evasion mechanism of CMV.

To address these questions, I analysed V δ 2^{negative} $\gamma\delta$ T cell populations from the PB of healthy donors, and analysed the TCR repertoire of 6 donors at the sequence-level, constituting the first analysis of this type. Unlike in the previous chapter which utilised a genomic DNA-based amplification technology, an anchored 5'-RACE RNA approach was used for repertoire analysis of these samples, as this technique allows for the simultaneous analysis of both the γ and δ chains of $\gamma\delta$ T cells in these samples, although it does not provide conclusive information on chain pairings. Furthermore, the DNA contamination issues encountered with the immunoSEQ technology are likely not to effect this study, as sequences generated by the reverse transcription of mRNA are specifically sequenced¹¹⁷.

6.2 Results

6.2.1 Study design and development

When designing studies involving patient samples it is important to consider the wide variation present in many aspects of these samples. The immune system is a highly adaptive and dynamic collection of cells which respond rapidly to a wide range of environmental stimuli, and these stimuli can have large effects on the size and distribution of various

immune cells. Immune senescence results in the abundance of highly differentiated memory T cells, which leaves little proliferative 'space' for the expansion of naïve T cells after encountering antigen, hence reducing the adaptive ability of the immune system¹⁶⁵. This has mainly been described for $\alpha\beta$ T cells in chronic CMV infection, with expansions of highly differentiated effector memory cells¹⁶³.

It is therefore important when considering changes in the immune repertoire due to CMV infection for age to be controlled. Both age and CMV infection have been demonstrated to act independently on the $V\delta 2^{\text{negative}}$ subset of $\gamma\delta$ T cells in the PB of donors¹⁶⁷. The $V\delta 2^{\text{negative}}$ $\gamma\delta$ T cell population was observed to decrease with age, but increase in response to chronic CMV infection. In aging CMV-seropositive donors, the ageing-related decrease in the $V\delta 2^{\text{negative}}$ compartment was counteracted by the effect of CMV, resulting in the maintenance of a relatively stable $V\delta 2^{\text{negative}}$ population. The $V\delta 2^+$ PB population of $\gamma\delta$ T cells was found to be unaffected by both of these factors¹⁶⁷. The most prominent difference in the $V\delta 2^{\text{negative}}$ population is observed in the youngest donor group (median age 23.96 years), who are not also experiencing a decrease in $V\delta 2^{\text{negative}}$ cells due to age. Therefore for this study donors under the age of 30 were selected and analysed, to control for the effect of age on the $V\delta 2^{\text{negative}}$ population.

Sample size is a further consideration when designing comparative experiments using donor blood samples. As previously mentioned, the immune compartment is highly dynamic, and responds rapidly to a range of stimuli. Donors may also have other chronic viral infections such as EBV, which has also been shown to permanently alter the T cell compartment¹⁶⁸. In addition, exercise prior to blood donation has been shown to significantly affect the makeup of the $\gamma\delta$ T cell compartment¹⁶⁹. Ideally, a large sample size

is therefore required to account for these uncontrollable variables, in order to minimise the impact of natural variation on the significance of the results. While this is more readily achievable in more focused studies, such as flow cytometry and spectratyping, repertoire studies are often considerably more expensive and time-consuming, and so large sample sizes are not necessarily always possible.

For this study, 3 CMV-seropositive and 3 CMV-seronegative age-matched donors were selected. CMV-serostatus in these donors was determined by ELISA, which detected CMV antigen-specific antibodies in the plasma of the donors.

6.2.1.1 Immune profiling

Peripheral blood mononuclear cells (PBMCs) were isolated from PB and analysed using flow cytometry. Samples were stained with three antibody panels, each containing different combinations of antibodies and conjugates, to provide a comprehensive analysis of the $\gamma\delta$ T cells in these samples. These panels are detailed in Table 2.3.

Initially it was intended that all $V\delta 2^{\text{negative}}$ $\gamma\delta$ T cells were to be sorted by fluorescence activated cell sorting (FACS) using a combination of pan- $\gamma\delta$ and $V\delta 2$ antibodies that has been used previously^{56,167}. Upon closer inspection of the staining data, it appeared that the $V\delta 2$ -FITC and pan- $\gamma\delta$ -PE antibodies cannot be used in combination, as in some donors the number of $V\delta 2^+$ $\gamma\delta$ T cells identified was substantially lower than in the panel in which the $V\delta 2$ -PE antibody was used without a pan- $\gamma\delta$ antibody (Figure 6.1). This suggested that in some donors, the epitopes for the two antibodies were similar or overlapped, resulting in competition to occupy the epitope and hence a decrease in the number of $V\delta 2^+$ cells reported, therefore suggesting the presence of $V\delta 2^+$ cells in the $V\delta 2^{\text{negative}}$ population. For this reason it was decided to instead sort on the $V\delta 1^+$, $CD3^+$ T cell population, an antibody

combination which has not demonstrated such issues previously in our group. While this strategy omits both the V δ 3 and V δ 5 chains, the majority of V δ 2^{negative} $\gamma\delta$ T cells in most donors is comprised of V δ 1⁺ cells, when analysed with the 'Phenotyping' panel (Table 2.3 and data not shown). Furthermore this approach would also provide limited chain pairing information, as all γ chains sequenced would be paired with a V δ 1 chain, although specific chain pairings would not necessarily be known. An example of the phenotypic analysis is shown in Figure 6.2.

The V δ 1⁺ population was not found to be expanded in the CMV-seropositive donors when analysed by flow cytometry (Figure 6.3A). Also, no expansions of V γ 9V δ 1⁺ populations were observed in this cohort (Figure 6.3B).

6.2.2 Analysis of sequencing data

V δ 1⁺ $\gamma\delta$ T cells were isolated by FACS, and the anchored 5'-RACE TCR sequencing protocol (Detailed in section 2.6.2) was conducted by our collaborator Professor David Price at the University of Cardiff. cDNA products amplified by C γ /C δ specific and anchor-complementary primers were cloned in to *E. coli*, and 96 transformed colonies were selected for sequencing. The sequence results for the 6 samples are included as Appendix 6.2.

Initial analysis of the data demonstrated that all but two δ chains contained the V δ 1 gene segment, with the two exceptions containing the V δ 2 and V δ 5 gene segments. These sequences may have arisen from cells in which the V δ 2 or V δ 5 were successfully recombined on one chromosome, but due to the relative low stringency of allelic exclusion mechanisms in the development of $\gamma\delta$ T cells¹⁷⁰, expressed a V δ 1⁺ TCR originating from the

sister chromosome. Despite these non-V δ 1 chains, these findings validate the sorting technique and confirm that largely V δ 1⁺ chains were analysed.

In two donors, some of the V γ 9 sequences had hallmarks of V γ 9 chains of the pAg reactive V γ 9V δ 2 population, namely the JgP*01 J region and an *ELG* motif in the CDR3 region (Figure 6.4)⁵⁹. If these V γ 9V δ 2-associated V γ 9 chains predominantly pair with V δ 2, one possible explanation for the presence of these cells is that the V δ 2 chain failed to recombine. It could also be that these motifs are not unique to pAg reactive V γ 9V δ 2 TCRs, and form functional TCRs with non-V δ 2 δ chains. Such γ chains were also observed in liver and colon samples in the previous chapter, and were discounted as blood contamination of the samples. However, this observation suggests that these chains could constitute genuine non-V δ 2 chain pairings, and perhaps should not be discounted in future studies. However, the antigen specificity of these cells is unknown, and so further investigation as to whether they can confer pAg reactivity is warranted, although it is thought that the V δ 2 chain is required for reactivity⁵⁹.

6.2.3 MAU and other clones of interest were not represented in these samples

The V γ 9 chain was the most common γ chain in all of the samples, suggesting that the V γ 9V δ 1 pairing is common in these donors (Figures 6.6A), which is interesting as V γ 9V δ 1 pairings have not previously been described to a great extent. Despite the abundance of V γ 9V δ 1 receptors however, none of the V γ 9⁺ or V δ 1⁺ CDR3 sequences matched the MAU TCR amino acid sequence exactly. However, exact requirements for EphA2 reactivity by $\gamma\delta$ T cells have not yet been fully determined, so although the CDR3 sequences do not match exactly some sequences may still satisfy the reactivity criteria, and so should ideally be

tested for EphA2 reactivity. Identification of further EphA2 reactive $\gamma\delta$ TCRs would greatly enhance understanding of the recognition modality of MAU and EphA2.

In addition to MAU, the γ or δ chain sequences of other clones of interest, either in published studies or currently under investigation in our laboratory, were not identified in these samples (Table 5.2). The anchored 5'-RACE RNA-based clonotyping approach used in this chapter represents a limited sample of the overall $\gamma\delta$ T cell repertoire, and provides approximately 100 sequences per sample. This therefore means that the most abundant sequences are more likely to be sequenced. The absence of particular clones of interest from these samples therefore does not necessarily imply that they are absent in PB of these donors, as conceivably they may be present at levels low enough to be excluded from this representative sample. As this procedure provides sequences derived from RNA, cells which are actively proliferating will also be more highly represented by this approach by virtue of an increase in intracellular RNA during the mitotic stage of the cell cycle¹⁷¹. This therefore implies that active cells are more likely to be represented, and therefore such clones may alternatively conceivably be present in the donors but not necessarily actively involved in immune responses to persistent viral infection.

6.2.4 V δ 1⁺ TCR repertoires are highly private

Murine $\gamma\delta$ T cells, and to an extent certain human populations, have been proposed to recognise a limited range of ligands¹⁵⁰. If similar criteria apply to V δ 1⁺ $\gamma\delta$ T cells in humans, it might be expected that there would be a high degree of overlap in the $\gamma\delta$ TCR sequences between donors.

Between all 6 donors, only two amino acid sequences were found to be shared between individuals, both of which were δ chains (Appendix 6.2). Although these sequences were

present at low frequencies, the samples containing the shared sequences were processed on separate days, substantially reducing the possibility that these represent contamination between the samples. Furthermore, no conserved γ chains were observed between these donors, and so the conserved δ chains do not necessarily constitute conserved TCR heterodimers.

Interestingly, in a CMV-seropositive donor KM, two γ chain mosaics were observed (Appendix 6.2). These sequences possessed different $V\gamma$ gene elements (hence distinct CDR1 and CDR2 regions) yet have identical CDR3 regions, and the presence of these mosaics suggests an antigen-driven expansion of these cells based on their suspected role in $\alpha\beta$ TCR mediated responses, but their significance in $\gamma\delta$ T cells has not yet been explored¹⁷².

6.2.5 $V\delta 1^+$ populations are polyclonal

The sequencing data were also used to determine if there are any differences in the $V\delta 1^+$ $\gamma\delta$ T cell repertoire of CMV-seropositive and CMV-seronegative donors. Given the large spread of the data collected by inherently variable human donors, the number of samples collected in this study is not sufficient to draw robust conclusions from specific comparisons, but it can be used to provide novel and important insights into the effect of CMV infection on the size and diversity of the $V\delta 1^+$ $\gamma\delta$ T cell population, as well as highlight potentially significant γ or δ chains.

Analysis of the top 30 sequences for either the CMV-seropositive and CMV-seronegative donors reveals a similar distribution of the top ranking γ and δ chains (Figure 6.5). For both the γ and δ chains, the CMV-seronegative donors appear to have a more restricted $V\delta 1^+$ $\gamma\delta$ T cell population, particularly with the highest ranked clone for each chain, however the

sample size is insufficient to definitively conclude this. This property of the samples can also be expressed numerically using the clonality metric, which is derived from the Shannon entropy of the frequency distribution of individual sequences (Figure 6.5C)¹⁵⁹. The clonality ranges from 0 (diverse, with equal representation of all sequences) to 1 (clonal, only one sequence is present). The equation for this calculation is shown below, where n represents the total number of sequences in the sample, and p_i is the fraction of residues of sequence i :

$$\text{Clonality} = 1 - \left(- \sum_{i=1}^n \frac{p_i \log_{10} p_i}{\log_{10} n} \right)$$

When both the γ and δ chains are collectively analysed in this way, the clonality of the $V\delta 1^+$ populations of CMV-seronegative donors is 0.17, higher than the CMV-seropositive value of 0.09. Therefore, this numerical analysis also suggests that for these donors, the CMV-seronegative donors have a more restricted $V\delta 1^+$ population than their CMV-seronegative counterparts.

Previous studies suggest that chronic CMV infection results in a clonal expansion of $V\delta 2^{\text{negative}} \gamma\delta$ T cells (which in many donors consists mainly of $V\delta 1^+$ $\gamma\delta$ T cells), and the data presented so far does not align with these reports (Figure 6.5). These previous studies largely determine clonality using spectratyping analysis, which measures CDR3 length distribution between samples, and the size of this distribution is then inferred as clonality, assuming that populations with a large number of cells with similar CDR3 lengths are comprised of identical cells. However, when comparable analyses are performed using this current repertoire data, no comparable differences were detected, despite the variances in clonality observed (data not shown). Given that previous spectratyping studies that have

noted significant differences in clonality of V δ 2^{negative} subset from CMV-seropositive and CMV-seronegative individuals have been based on large sample sizes, it is likely that the limited number of samples in our current study is the reason I was not able to draw equivalent, statistically-significant conclusions. In one such spectratyping study, the sample size was 186 donors, and demonstrated substantial overlap in relative V δ 2^{negative} population sizes¹⁵⁸, highlighting that smaller sample sizes are unlikely to significantly demonstrate this difference.

6.2.6 V region usage of γ chain sequences

Another analysis that can be uniquely performed using TCR sequence-level repertoire data is an unbiased analysis of γ chain usage. Such approaches are not possible using flow cytometry, which relies on the availability and compatibility of antibodies for all γ chains, and as shown in this chapter, $\gamma\delta$ TCR-specific antibodies are sometimes incompatible in certain combinations. As with the clonality measurements, the spread of data is large for V γ chain usage, with a large amount of variation between donors. Therefore although specific conclusions cannot be drawn regarding the γ chain usage of receptors in these samples, this analysis can provide novel information of V γ chain distributions in the V δ 1⁺ $\gamma\delta$ T cell compartment.

Analysis of the V γ region usage of the sequences revealed that the V γ 9 chain is heavily represented across all samples, suggesting that the V γ 9V δ 1 pairing is common amongst all donors (Figure 6.6A). Interestingly, the V γ 5 chain is exclusively present in the CMV-seropositive donors. The V γ 5 chain is present in all 3 of the CMV-seropositive donors (Figure 6.6B), and is therefore not due to a-typical V γ 5 usage in one donor. It may be that TCRs bearing the V γ 5 chain play a role in the control of chronic CMV infection, and so is

expanded in CMV-seropositive donors. This has not previously been noted, perhaps due to the lack of a V γ 5 specific antibody, and therefore this clearly warrants validation in a larger cohort, and further investigation of V γ 5V δ 1⁺ T cells in terms of function and ligand recognition.

Another advantage of sequence-level TCR repertoire analysis is that it also allows for determination of the diversity of chains bearing particular V regions. This analysis is achieved by comparing the proportion of sequences using a particular V region to the number of unique sequences which constitute chains with that V region (Figure 6.7). Therefore, V regions with a large percentage of the total unique nucleotide sequences compared to their V region usage can be considered more diverse than V regions with a comparatively small number of unique sequences. These data are particularly interesting as the spread of data seems relatively small compared to other measurements in this chapter, suggesting that these patterns may be representative of a large number of donors. In the CMV-seronegative donors, although the V γ 9 chain is the most highly represented, it is comprised of only 30% of the unique sequences for all of the donors, suggesting that γ chains bearing this V region element are relatively restricted compared to the other chains. Conversely, V γ 8⁺ chains are comprised of relatively more unique sequences which suggests that these chains are much more diverse than V γ 9 chains. This is the opposite of the finding in Chapter 5, which established V γ 9 chains as being highly diverse in colon and liver samples and V γ 8 chains being less diverse (Figure 5.8). This disparity may represent the small sample number in both studies, but if this finding is reproducible, it signifies the importance of differentiating studies of $\gamma\delta$ T cells between tissue and blood samples.

The V γ 5 sequences present in the CMV-seropositive donors appear to be equally as diverse as sequences containing other V gene segments (Figure 6.7B), suggesting that although cells bearing V γ 5⁺ chain are likely expanded in CMV-seropositive donors, the expansion does not appear to be clonal. This comparison also appears to demonstrate an increase in the diversity of V γ 9 chains and a decrease in the clonality of V γ 8 chains in CMV-seropositive donors compared to their CMV-seronegative counterparts. Again, although the sample sizes are too small to draw definitive conclusions from these data, it does strongly suggest that chronic CMV infection may have an impact on the clonality of γ chains with particular V γ regions, which may be an indication that particular chains play a more important role in the immune response to CMV than other V γ chains.

6.3 Discussion

The primary aim of this chapter was to determine how CMV infection affects the V δ 1⁺ $\gamma\delta$ T cell repertoire, and to detect any public γ or δ TCR chains in the PB of either CMV-seronegative or CMV-seropositive healthy donors. No shared γ chains were detected between the donors, although two conserved δ chains were observed. Although the sample size is too small to draw statistically robust conclusions, it does provide several insights into the nature of the V δ 1⁺ repertoire in CMV-seropositive and CMV-seronegative donors, and also provides a basis for generating hypotheses as to how these receptors may be interacting with their ligands. Overall, the data presented in this chapter suggests that the V δ 1⁺ $\gamma\delta$ T cell repertoire in both CMV-seropositive and CMV-seronegative healthy donors is predominantly private, with little CDR3 overlap between donors.

Unfortunately the study had to be limited to the V δ 1⁺ population, due to issues encountered with the FACS-based sorting of V δ 2^{negative} populations. These issues

demonstrate the limitations of using antibodies to analyse $\gamma\delta$ TCR chain usages of populations, as these studies rely on having a panel of compatible antibodies which do not compete for epitopes on a single receptor. Furthermore, antibodies for all γ and δ chains are not yet available. In this study, antibody combinations which have previously been used in published studies were found to give unreliable results and do not always accurately represent the chain usage of $\gamma\delta$ TCR populations. This highlights a significant advantage of unbiased repertoire analyses which are not affected by these biases, and give a more accurate representation of all chains.

Previous studies have shown slight increase in the frequency of $V\delta 2^{\text{negative}}$ $\gamma\delta$ T cells in CMV-seropositive healthy donors¹⁵⁸, and spectratyping studies have suggested that these cells are more restricted than the non-expanded, CMV negative populations⁵⁶. The results obtained in this chapter do not align with these previous studies, as $V\delta 1^+$ populations were not found to be larger in CMV-seropositive donors, and no significant difference in clonality of TCR sequences was observed. Although in a study by Pitard *et al.*, the average age of donors was 40 years, and so maybe these differences were exaggerated by the effect of age on the $V\delta 2^{\text{negative}}$ population.

The sample size of this study is small compared to previous samples, and given the large spread of data observed in the previous studies^{56,158}, it is not surprising that such differences are not apparent with a smaller sample size. The large sample sizes required to identify such differences are not viable for repertoire studies, due to the relatively high cost per sample. One potential approach would be to limit the study to donors who display expanded $V\delta 1^+$ populations by flow cytometry, to determine if these expanded populations differ to the non-expanded ones discussed in this chapter. It may be that increases in

clonality are associated with the expanded populations, which does not occur in all CMV-seropositive donors. However, the V γ 5 sequences exclusively found in the CMV-seropositive donors do not appear to be clonally expanded, further demonstrating that the V δ 2^{negative} populations may not be homologous with regards to the immune response to CMV.

With these sample size limitations in mind, assuming the data accurately represents the repertoires of these respective donor groups, it does have some interesting implications for how these $\gamma\delta$ T cells may interact with their targets. The diverse, unique CDR3 regions of both γ and δ chains suggest the recognition of wide range of antigens by these cells, when viewed in the context of $\alpha\beta$ T cells⁷². In $\alpha\beta$ T cells, ligand recognition is facilitated by all three CDR regions, CDR1 and CDR2 interact mainly with the two α -helices of the MHC peptide-binding platform, and CDR3 specifically recognised the bound peptide⁷². Therefore, in ligand recognition by $\alpha\beta$ TCRs, specific CDR3 sequences enable TCRs to recognise a specific peptide, although there is substantial degeneracy in this recognition, as multiple different clonotypes can recognise the same peptide-MHC combination.

Recognition of ligands by $\gamma\delta$ T cells is not mediated by class I and class II MHC molecules, and antigen presentation machinery is unlikely to be involved, as the majority of the ligands characterised so far for the V δ 2^{negative} subset are whole protein antigens. Indeed, even though recognition of CD1d by $\gamma\delta$ T cells is often reported to be lipid dependent, it cannot be excluded that it is being recognised as a whole protein antigen, due to the observation of V δ 1⁺ $\gamma\delta$ T cells which can recognise CD1d independently of lipid⁵⁰, and the differences in TCR binding footprint of different reactive T cells³³.

Given such fundamental differences between ligand recognition strategies between $\alpha\beta$ and $\gamma\delta$ T cells, it is unlikely that the roles of the CDR loops would be conserved. For example, EPCR is an MHC-like molecule, and even with related $\alpha 1/\alpha 2$ platforms forming a lipid binding pocket, is recognised by a $\gamma\delta$ clone LES at a distal site¹²³. Also, T22 is an MHC-like molecule recognised by the murine $\gamma\delta$ TCR G8 in a mechanism distinct from $\alpha\beta$ TCR/MHC interactions³¹. These studies suggest that the recognition modalities of $\alpha\beta$ and $\gamma\delta$ TCRs are substantially distinct, and therefore it is not necessarily accurate to assume that distinctive γ or δ CDR3 sequences denote the recognition of a unique ligand.

This is further supported by the distinct tissue distribution of $\gamma\delta$ T cells by their V region. This is particularly well documented in mice, but is also partly characterised in humans. In mice, the $V\gamma 5V\delta 1$ DETC subset is uniquely found in the skin, although no peripheral ligand has yet been identified. In humans the best defined subset is the $V\gamma 9V\delta 2$ blood subset, which recognises non-peptidic pAgs via BTN3A1. This conservation of V regions has several possibilities as to how it affects antigen recognition. It may be that the V regions facilitate migration and maintain residence in the required tissues, or that these V regions (i.e. non-CDR3 regions) are directly involved in the recognition of ligands which are present at these anatomical sites. There is also evidence to suggest that V regions are responsible for $\gamma\delta$ T cell selection in the murine thymus, and contribute towards the upregulation of transcriptional signatures promoting homing receptors, as has been demonstrated for the $V\gamma 5V\delta 1$ DETC subset¹⁷³.

If this latter suggestion is the case, it is unclear which parts of the V region are involved in antigen recognition. In the $\gamma\delta$ TCR and complexes characterised so far, CDR1 and CDR2 are exposed, flexible loops, making them viable candidates for ligand recognition, and are

inherent components of the V region, and so is consistent with involvement of particular V regions in ligand recognition at different tissues. It could also be that non CDR framework regions play a key role in ligand recognition, although these regions are more closely conserved between V regions.

These insights into the molecular nature of ligand recognition of the V δ 1⁺ $\gamma\delta$ T cell subset demonstrate a previously unexplored use of the repertoire data, but studying the composition of these cells can help to direct more focused clone based experiments such as those described in earlier chapters using physiological information, instead of the more clone-dependent approaches used here. In order to investigate this area further, it is important to characterise a range of $\gamma\delta$ TCR interactions to establish such patterns, such as the significance of CDR3. Repertoire studies such as this complement such ligand recognition studies by directing focus to areas of biological interest, allowing further hypothesis-driven molecular studies.

In terms of future experiments building on the results comparing the repertoires of CMV-seropositive and CMV-seronegative donors, they would be greatly improved by an increased sample size, in order to increase the chance of identifying public clones. What these results do show is that in order to identify differences between the two cohorts, increasing the sample size is not necessarily going to yield statistically significant results, and to do so, statistical power calculations would be advisable.

The spread of data is large, and in order to reach significant conclusions the number of samples would have to be very large, which is not very efficient and arguably a waste of the depth of such a technique. The results discussed in this chapter clearly suggest a difference in the use of the V γ 5 chain between CMV-seropositive and CMV-seronegative donors. To

expand on these findings, a real-time RT-PCR (qRT-PCR) experiment could be designed in which V γ 5-specific primers are used to detect the presence of the V γ 5 sequence in V δ 1⁺ $\gamma\delta$ T cells in a larger cohort of donors at much higher throughput.

Another obvious extension to the study is to more accurately categorise infection status. This study defined the cohorts as either CMV-seropositive or CMV-seronegative depending on the presence of CMV-antigen specific antibodies in serum. Previous studies have shown an expansion with acute infection and so a repertoire study on such samples would likely yield interesting results⁵⁵. Furthermore, recent data suggest that, in acute CMV infection the V δ 2^{negative} $\gamma\delta$ T cell repertoire highly focused in chronic myeloid leukaemia (CML) patients, significantly more so than in patients with chronic CMV infection (D. Lewis, unpublished). The ultimate study would be a longitudinal one, whereby a cohort is monitored over a period of a few years, and repertoire analyses performed before and after infection on donors that contract CMV during the study.

This study has compared the use of two approaches to $\gamma\delta$ TCR repertoire analysis, DNA-based immunoSEQ and RNA-based anchored 5'-RACE. immunoSEQ used high throughput sequencing and provides a relatively deep view of the repertoire¹¹⁶, whereas the RNA-based anchored 5'-RACE approach is much lower throughput and yields around 100 sequences for each sample¹¹⁷. It would be useful to determine how representative the anchored 5'-RACE-acquired sequences are of the entire repertoire. To achieve this, identical samples could be processed by both techniques and compared. This would also give an indication of how much of an effect activation and proliferation status has on the sequences gained by the RNA approach.

Finally, neither of these approaches offers paired chain sequences. Large expansions can be tentatively paired by matched chains with similar abundances, but this is not useful for the lower frequency sequences. $\gamma\delta$ TCRs exist as heterodimer pairs, and so information on only one of the chain pairs is unlikely to convey all of the characteristics of the complete receptor. Low-throughput, single-cell PCR approaches are available to analyse both the γ and δ chains of single $\gamma\delta$ TCRs¹⁷⁴. Such an analysis would be able to expand upon the observation that that only conserved δ chains were identified in this study, whereas no γ chains were conserved. If it is assumed that these chains are conserved because they recognise the same antigen it could be that the majority of antigen recognition is facilitated by one chain, with the other either redundant or changeable, in order to add fine sensitivity to antigen recognition, or conceivably affect the kinetics of the response. However, the extent of $\gamma\delta$ TCR redundancy in recognition of specific ligands is unclear. This is also supported by data for the V γ 9V δ 1 clone MAU, where our collaborators have preliminary evidence suggesting that the gamma chain can be swapped with other chains and some activity towards EphA2 is maintained, whereas the V δ 1 chain appears to be critical to recognition.

6.4 Figures

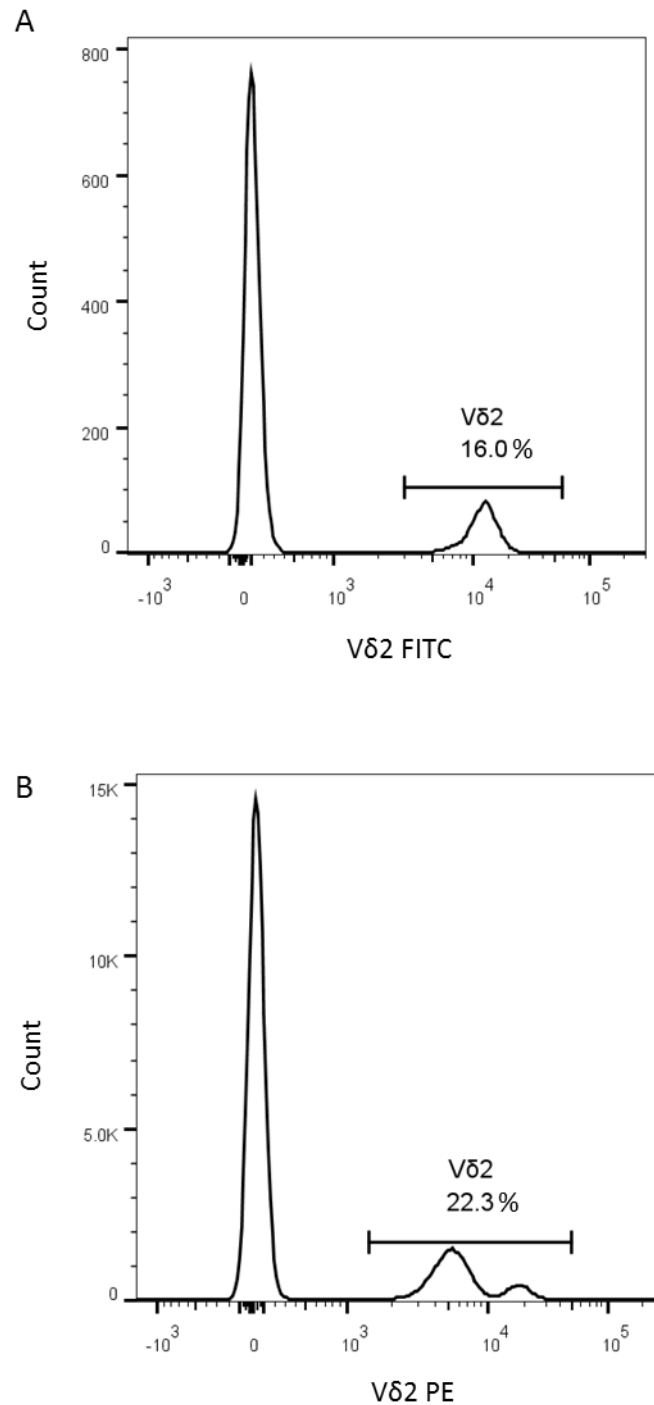


Figure 6.1: Development of $\gamma\delta$ T cell sorting strategy

PBMCs from the same KKHD sample were stained with CD3-APC. PBMCs in (A) were also stained with pan- $\gamma\delta$ -PE and Vδ2-FITC antibodies and PBMCs in (B) were instead stained with a Vδ2-PE antibody. Histograms are gated on the Vδ2⁺ populations. The Vδ2 populations differ between the antibody panels used in panels A and B, and the Vδ2-FITC antibody used in conjunction with the pan- $\gamma\delta$ -PE antibody stained fewer cells than the Vδ2-PE antibody alone.

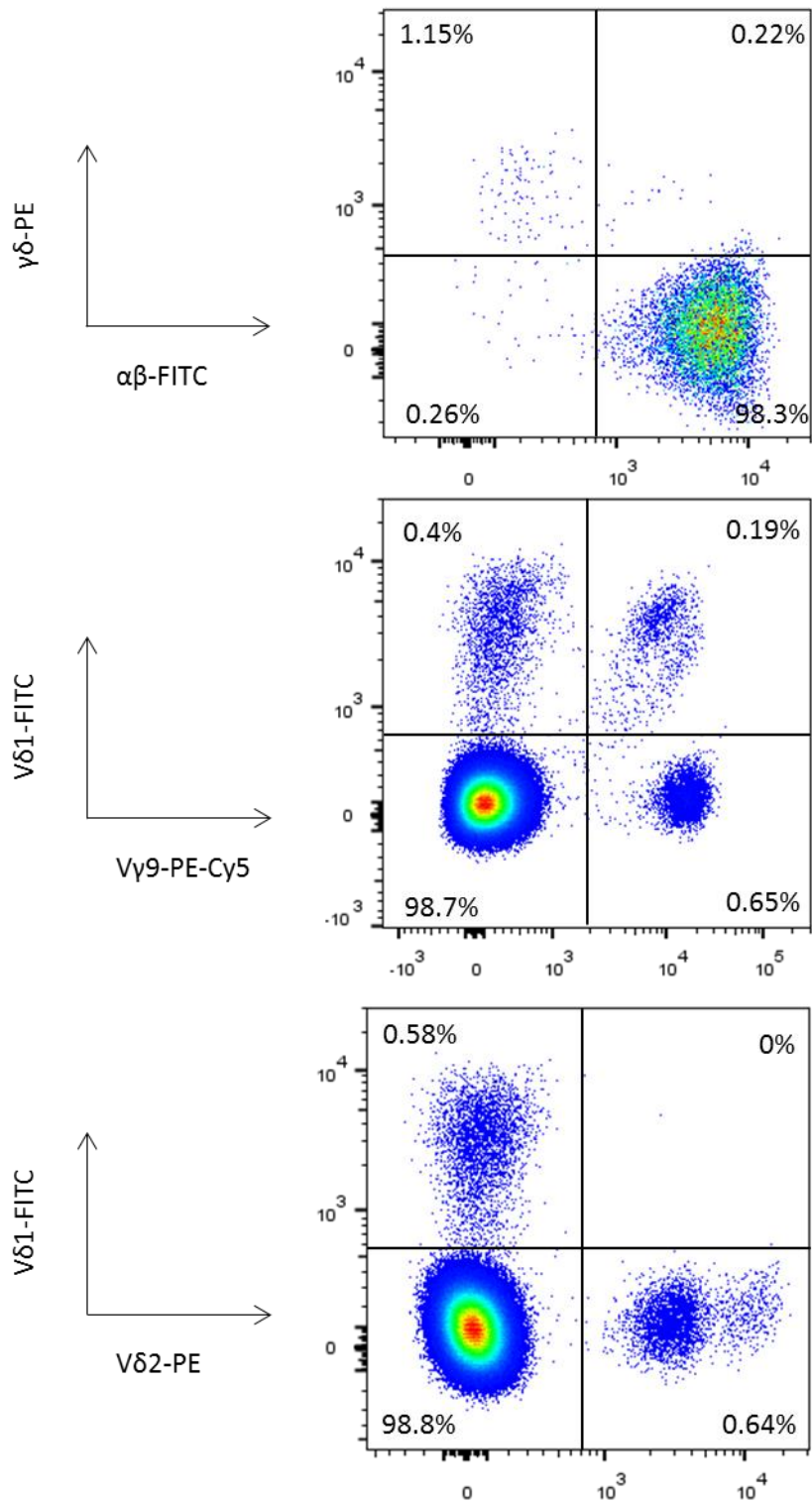


Figure 6.2: Representative phenotyping of $\gamma\delta$ T cells

PBMCs from the AWHD donor were stained with CD3-APC and various $\gamma\delta$ phenotyping antibodies. Gating strategy shown in Appendix 6.1.

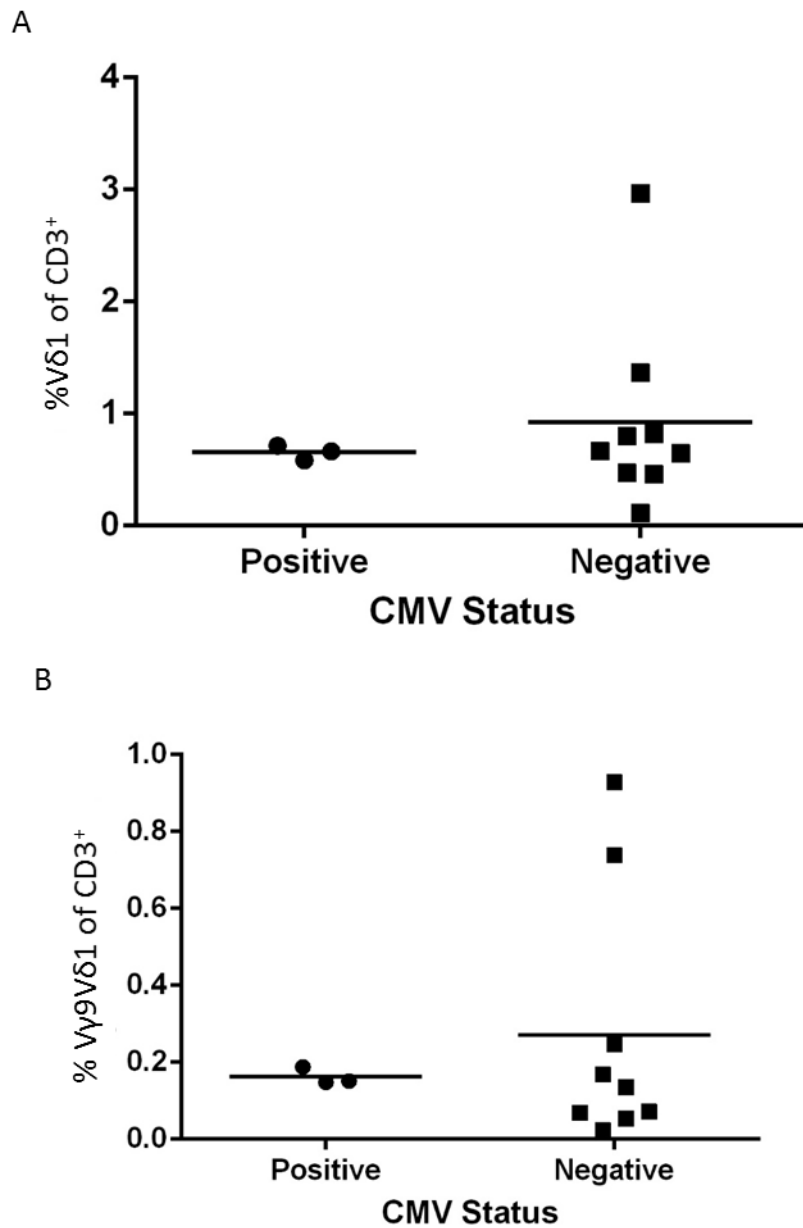


Figure 6.3: The effect of CMV infection on $\gamma\delta$ T cell populations

All donors (including those not sequenced) were grouped into CMV-seropositive or seronegative cohorts using an IgG ELISA and populations were gated on CD3. Demonstration of the effect of CMV-serostatus on (A) V δ 1 cells and (B) V γ 9V δ 1 cells.

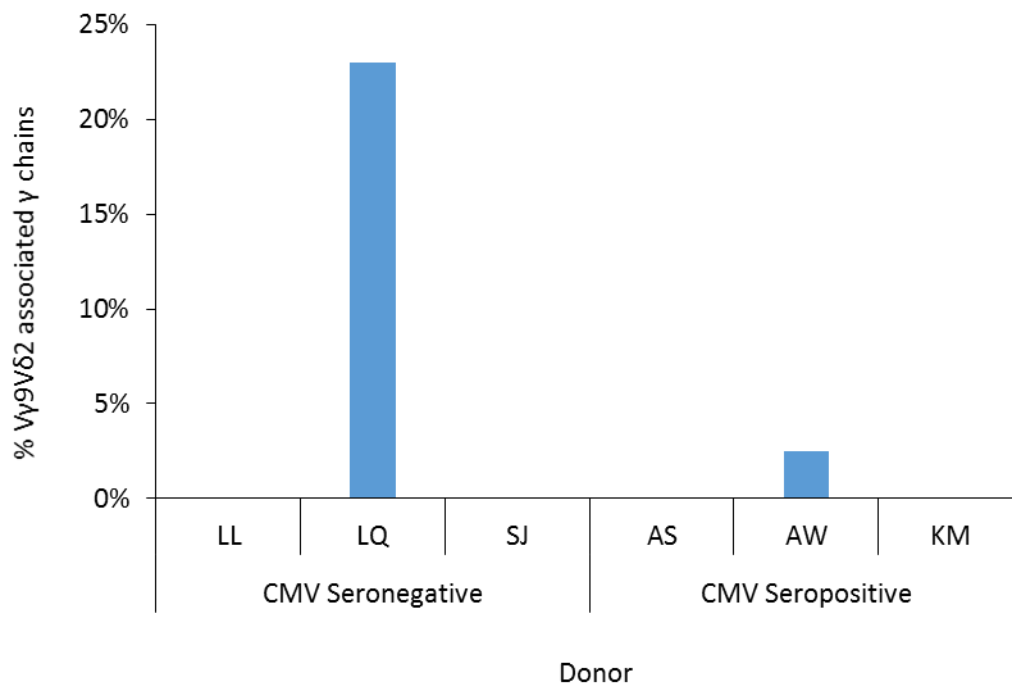


Figure 6.4: Vy9Vδ2-associated γ chain sequences

Proportion of γ chains with characteristics of pAg reactive Vy9Vδ2-associated γ chains. These chains are characterised by the Vy9 gene segment joined with the JgP*01 joining segment, with the short *ELG* amino acid motif in the CDR3 region.

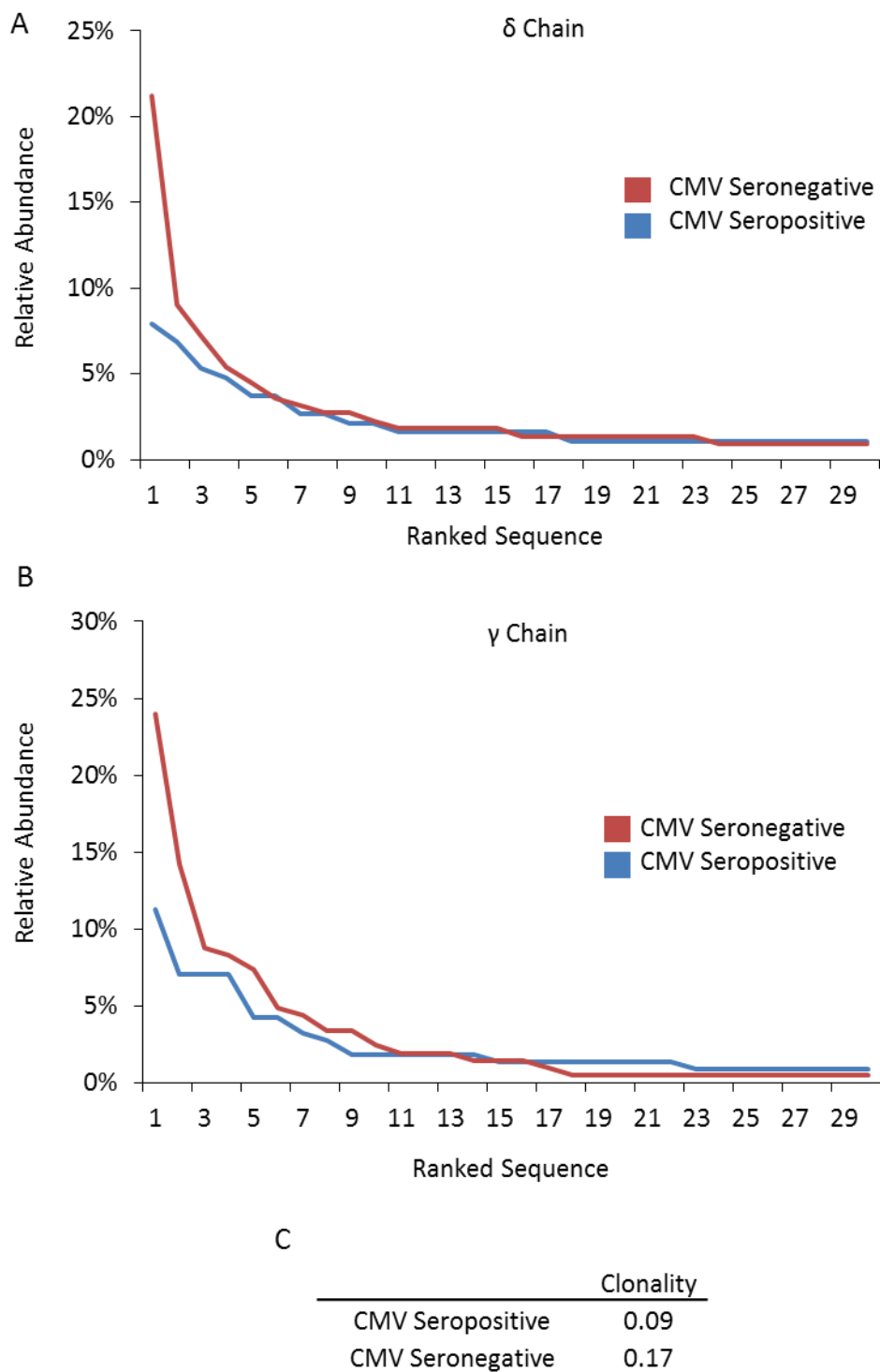


Figure 6.5: Clonality of the top 30 γ and δ chains

The relative abundance 30 most abundant δ (A) and γ (B) chains for the CMV-seropositive and CMV-seronegative donors were compared. (C) Clonality measurement of both γ and δ chains for CMV-seropositive and CMV-seronegative donors. 0 = Diverse and 1 = clonal.

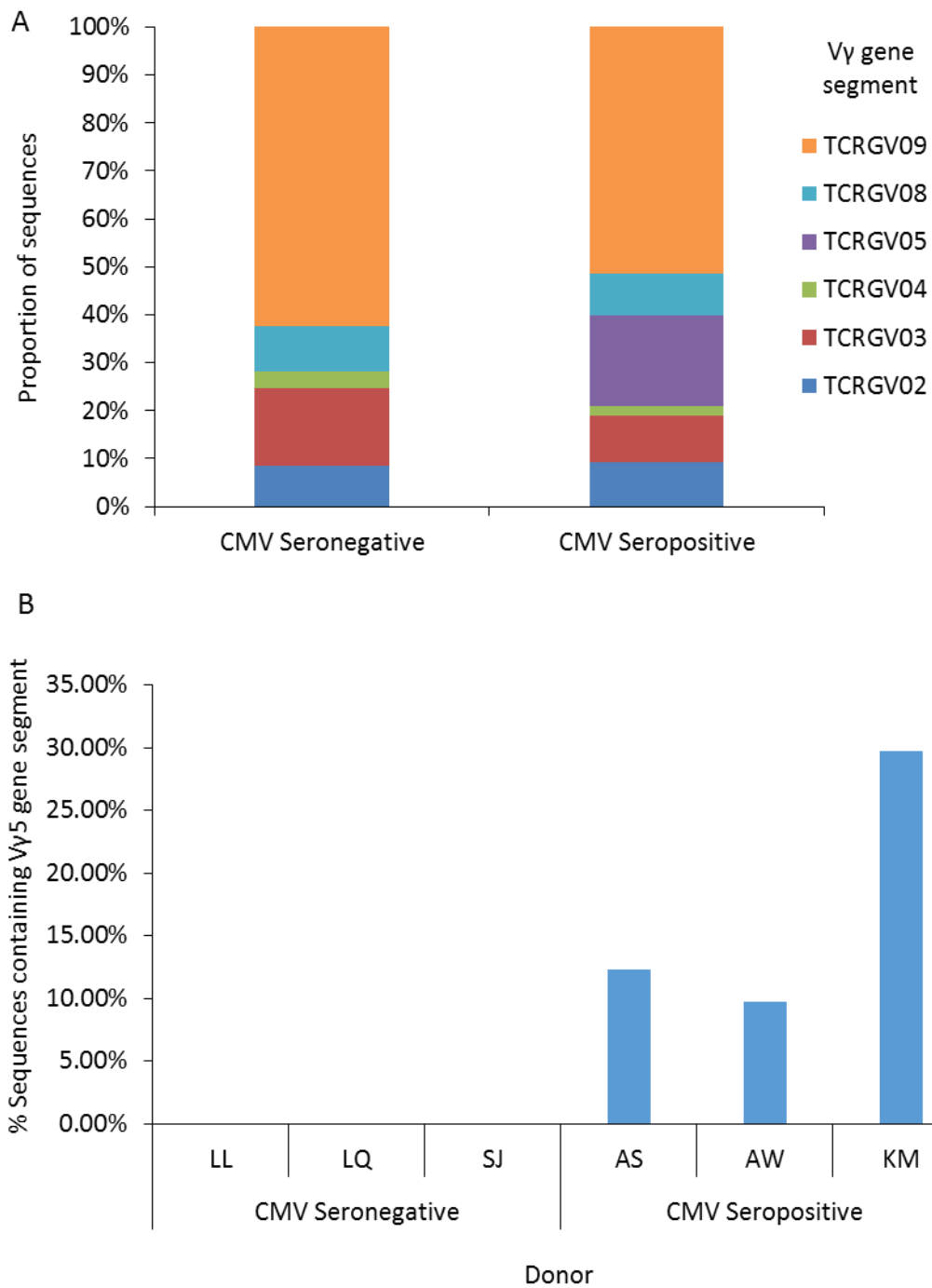


Figure 6.6: Usage of γ chain gene segments by CMV-serostatus

(A) γ chain usage by CMV-serostatus for all donors analysed. (B) Percentage of γ chain sequences containing V γ 5 gene segment for individual donors.

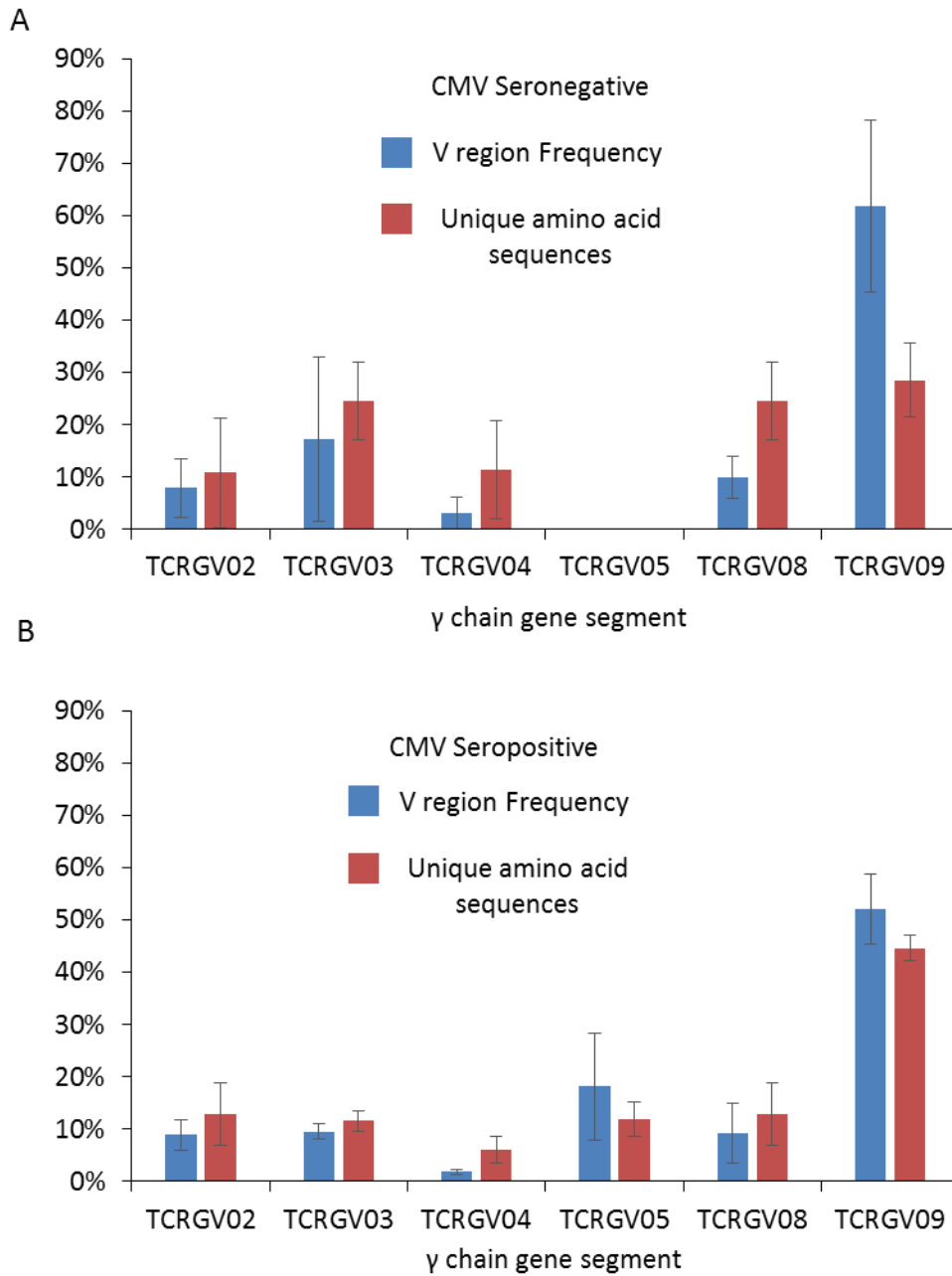


Figure 6.7: Clonality of specific γ chains

The relative proportion of sequences containing γ chain gene segments compared to the number of unique amino acid sequences which constitute those chains for (A) CMV-seronegative and (B) CMV-seropositive donors. Populations which demonstrate a large number of unique sequences relative to the proportion of sequences bearing that chain are considered more diverse than populations with a low number of unique sequences relative to the proportion of sequences bearing that chain.

Overall Discussion

7.1 Introduction

In this thesis I aimed to explore the role of V δ 1⁺ $\gamma\delta$ T cells in lymphoid stress surveillance. This involved the determination of the molecular basis for recognition of an epithelial stress ligand, EphA2, by a V δ 1⁺ $\gamma\delta$ T cell, MAU. This resulted in the proposal of a tripartite recognition complex, with a requirement for ephrin binding by EphA2. Additionally, I identified a 355Å² patch on the LBD of EphA2, which potentially constitutes the MAU TCR binding site.

I also explored the potential of using various sequence-level TCR repertoire analysis techniques to analyse $\gamma\delta$ T cell populations in human tissue and blood samples. This study was concluded by investigating the effects of CMV infection on the V δ 1⁺ $\gamma\delta$ T cell compartment in PB of healthy donors. Collectively, these studies have contributed to the understanding of how v δ 1⁺ $\gamma\delta$ T cells function in stress surveillance.

7.2 Ligand recognition by $\gamma\delta$ T cells

Despite their increasing implication in immune responses to a range of conditions, and continued exploration for therapeutic use³⁴, $\gamma\delta$ T cells are still poorly understood, both in terms of our knowledge of the ligands they recognise and the molecular nature of TCR/ligand interactions.

There have recently been significant advances in the understanding of how pAg-reactive V γ 9V δ 2⁺ $\gamma\delta$ T cells interact with infected and stressed cells, as butyrophilin family member BTN3A1 has been shown to be essential for the recognition of cells with increased levels of intracellular pAgs by these V γ 9V δ 2⁺ $\gamma\delta$ T cells¹⁷⁵. However, even within this well-characterised subset the exact molecular requirements of this interaction are still unclear.

Despite significant advances in this area⁶⁹, direct binding has yet to be convincingly demonstrated between a V γ 9V δ 2 TCR and BTN3A1 by BIAcore, even though these two components have been found to be essential for the detection of stressed cells by V γ 9V δ 2⁺ $\gamma\delta$ T cells.

7.2.1 Ligand recognition by V δ 2^{negative} $\gamma\delta$ T cells

Ligand recognition by V δ 2^{negative} $\gamma\delta$ T cells is less clearly understood than for V γ 9V δ 2⁺ $\gamma\delta$ T cells, and unlike for V γ 9V δ 2⁺ $\gamma\delta$ T cells, there is currently no discrete subset of ligand or recognition strategy for these cells, suggesting that ligand recognition by this subset is much less conserved.

In Chapter 3 I characterised the molecular requirements for the recognition of EphA2 by MAU $\gamma\delta$ T cells. Despite the weight of evidence suggesting that this interaction is mediated by the MAU TCR, such as being able to confer reactivity to EphA2 by transducing JRT3.5 cells with MAU TCR genes, I was unable to detect direct binding between recombinant versions of EphA2 and MAU TCR proteins by BIAcore. This result is perhaps similar to the difficulty in the detection of binding between V γ 9V δ 2 TCRs and BTN3A1, mentioned above, and suggests that either the molecular requirements for these interactions have not been met in *in vitro* experimental systems, or that the interactions exhibit an affinity beyond the sensitivity of techniques such as BIAcore. The strength of the accompanying evidence for the involvement of BTN3A1 in the recognition of pAgs by V γ 9V δ 2⁺ $\gamma\delta$ T cells reinforces the conclusion that, although direct binding cannot be detected by BIAcore between EphA2 and MAU TCR, it likely still represents a physiologically relevant interaction.

Collectively, these observations suggest that ligand recognition by some $\gamma\delta$ TCRs may not always be easily modelled with a simple binary receptor-ligand interaction, and the involvement of other molecules, co-receptors or clustering requires further investigation.

7.2.1.1 Recognition of non-MHC-like ligands by $V\delta 2^{\text{negative}}$ $\gamma\delta$ T cells

The majority of ligands proposed to date for $V\delta 2^{\text{negative}}$ $\gamma\delta$ T cells, such as EPCR¹²³ and CD1d³³, are MHC-like molecules. However, there is currently insufficient evidence to conclusively suggest that $V\delta 2^{\text{negative}}$ $\gamma\delta$ T cells exclusively recognise MHC-like molecules. Therefore non-MHC-like ligands, such as EphA2, are still viable candidates as ligands for $V\delta 2^{\text{negative}}$ $\gamma\delta$ T cells, and future research should not be restricted to the identification of MHC-like ligands.

This view is consistent with the observation that some $V\delta 2^{\text{negative}}$ $\gamma\delta$ TCRs interact with MHC-like ligands in a manner unlike conventional $\alpha\beta$ TCR/MHC interactions. One such example is the $V\delta 2^{\text{negative}}$ $\gamma\delta$ TCR LES, which has been shown to interact with the MHC-like molecule EPCR. TCR specificity was determined to be mediated by residues located on the underside of the lipid binding platform¹²³, which suggests that the LES TCR does not form any contacts with the lipid binding platform. Furthermore, TCR binding was shown to be dependent on all 6 CDR loops of the LES TCR (C. Willcox, unpublished), suggesting an antibody-like method of recognition of a 3D epitope, as opposed to the CDR1 and CDR2 mediated recognition of the lipid binding platform demonstrated by $\alpha\beta$ T cells⁷².

Another example of this is the variation in recognition mode of the same MHC-like molecule, CD1d, by different $V\delta 1^+$ $\gamma\delta$ TCRs^{50,51}. The two structures demonstrated strikingly distinct TCR binding modes to the CD1d lipid binding platform, which does not align with conserved recognition of an individual ligand. Furthermore, in these studies CD1d

tetramers occasionally stained <1% of V δ 1⁺ $\gamma\delta$ T cells, strongly suggesting that CD1d recognition is restricted to a small subset of V δ 1⁺ $\gamma\delta$ T cells.

This apparent over-representation of MHC-like molecules as ligands for V δ 2^{negative} $\gamma\delta$ T cells in published studies could be explained by the familiarity with MHC-like molecules in structural immunology research. Such familiarity can greatly expedite research involving these molecules, particularly in X-ray crystallographic studies, which use previously resolved structures as a template for model building. Therefore structures and complexes involving less well-characterised molecules may take longer to elucidate, and therefore would not be reported as readily. Furthermore, the cloning process by which the majority of $\gamma\delta$ TCRs used for ligand identification studies were isolated could conceivably introduce biases to expand cells reactive towards particular types of molecules, depending on the expansion protocol used.

These issues highlight the importance for advancing unbiased ligand identification studies, to gain a better understanding of the molecules V δ 2^{negative} $\gamma\delta$ T cells are interacting with *in vivo*. Such an approach would be greatly facilitated by sequence-level TCR repertoire analyses, such as the technologies utilised in Chapters 5 and 6 of this thesis. These approaches allow for the identification of $\gamma\delta$ T cell populations which demonstrate characteristics of being physiologically important, such as bearing TCRs which are shared between donors, or that are clonally expanded during infection, tumourigenesis, or even during therapeutic expansion protocols. This would then allow for the unbiased focusing of ligand determination attempts on these receptors, using molecular approaches such as those employed in Chapters 3 and 4.

7.2.2 The role of the $\gamma\delta$ TCR and additional molecules in ligand recognition

To date, the role of co-receptors in $\gamma\delta$ T cells is largely undetermined. This study highlights the potential importance of additional molecules for antigen recognition by these cells. The results from Chapter 3 suggest that that, despite being essential for the interaction, the MAU $\gamma\delta$ TCR may not be the main determining factor for recognition of EphA2, with specificity being partly determined by A-ephrins. It may be that the ephrins on the surface of the T cell are serving as the conventional ligand recognition molecule, and the MAU TCR is recruited to the signalling complex to provide co-stimulatory-like functions.

In Chapter 4 I identified a potential TCR binding site on the LBD of EphA2. It was not possible to definitively prove this region was the MAU TCR binding site, as it may represent a region which mediates contacts to additional, as yet unidentified, molecules on the surface of MAU T cells that are critical for activation by EphA2. Viable candidates for these molecules are the TM signalling molecules which facilitate reverse signalling by the GPI linked A-ephrins¹³⁶. Therefore it may be that the MAU TCR is not directly interacting with EphA2, but interacts with these signalling molecules, which would explain the difficulty in obtaining BIAcore data establishing a direct interaction between EphA2 and MAU TCR. Such molecules could potentially be identified by conducting co-IP experiments to isolate molecules involved in the signalling complex, with subsequent identification of them by mass spectrometry.

To date, only one signalling partner has been identified for A-ephrins, P75(NTR), which is involved in neuronal development and positioning¹³⁹. However, it is unknown whether this molecule is also involved in facilitating A-ephrin reverse signalling in T cells. Therefore the

identification of other A-ephrin-associated signalling molecules may contribute towards other fields where A-ephrin reverse signalling is important, not solely in immune function.

These findings raise important questions regarding the role of the $\gamma\delta$ TCR in these $\gamma\delta$ T cell populations, and suggest that it is unlikely to act solely as an antigen receptor in some cases. This emphasises the difficulty of studying these receptors in isolation, and the current dependence on direct binding studies to validate ligands is one such challenge.

7.2.3 The significance of the $\gamma\delta$ TCR CDR loops

The significance of the $\gamma\delta$ TCR CDR loops has yet to be established for ligand binding by $\gamma\delta$ T cells. Their role is unlikely to be conserved between all receptors, since several studies have suggested the requirement of different CDR loops, on different TCR chains, for ligand recognition¹⁵⁰. Indeed, even different models of the same ligand with different TCRs demonstrate different CDR loop involvement^{50,51}. Understanding of CDR loop involvement for $\gamma\delta$ TCRs has implications for many areas of $\gamma\delta$ T cell immunobiology, such as development and trafficking, not just the molecular nature of their interactions with ligands.

$\alpha\beta$ T cells typically use the less variable CDR1 and CDR2 loops to form interactions with the helices of the antigen binding pocket and use the more variable CDR3 to differentiate between presented peptides⁷². Antibodies however typically utilise all of the CDR loops to recognise three-dimensional epitopes of whole protein antigens¹⁷⁶. Therefore, determining which of these approaches utilised by $\gamma\delta$ T cells may provide insights into how they recognise ligands and interact with their target molecules.

Unfortunately, I was unable to establish the importance of the CDR loops of the MAU TCR in the interaction with EphA2 in this study, due to the lack of a reliable direct binding assay.

However, this remains an important question, and the MAU CDR mutant constructs that I created in Chapter 4 could be used for the transduction of JRT cells in future studies, to assess the impact of the CDR mutations on EphA2 reactivity.

7.2.4 Classification of V δ 2^{negative} $\gamma\delta$ T cell subpopulations

A further aspect which is still unclear regarding V δ 2^{negative} $\gamma\delta$ T cells is the heterogeneity of this population, pertaining to the ligands they recognise and their ligand recognition strategies. There is currently insufficient evidence to establish whether the population can be further sub-categorised into populations with conserved ligands or recognition modalities.

In Chapter 3 of this thesis I established that recognition of EphA2 by MAU T cells requires the presence of GPI-linked A-ephrins on the T cell surface to form a tripartite recognition complex with EphA2 and the MAU TCR. This potentially represents a novel recognition modality which has not been described previously for $\gamma\delta$ TCRs. It is important to establish whether this recognition strategy is employed by other, as yet unidentified, $\gamma\delta$ T cells or represents a completely unique utilisation of non-immune receptor/ligand interaction by immune cells to detect stress. Therefore, full characterisation of this interaction will assist in research to determine whether this mode of recognition can be extended to other receptors. Furthermore, it could potentially act as a template to expedite discovery of similar ligands, equivalently to how to knowledge of MHC-like molecules may be facilitating the identification of MHC-like ligands for V δ 2^{negative} $\gamma\delta$ T cells.

This study has also highlighted the importance of antigenic context in immune receptor studies. According to the model generated in Chapter 3, MAU is specifically recognising mislocalised EphA2, i.e. EphA2 that is not bound to ligand or localised at cell-cell junctions.

This therefore demonstrates that it is important to exercise caution when interpreting data from analyses such as microarray studies, as they only provide information on whether proteins are likely either upregulated or downregulated under certain conditions. For ligand identification however, this does not necessarily indicate their viability as an antigen, therefore it is important to consider antigen context, such as localisation or whether it is able to bind ligand, when considering candidate $\gamma\delta$ TCR ligands emerging from such studies.

7.3 Using TCR repertoire analysis to analyse $\gamma\delta$ T cell populations

The use of repertoire studies to analyse populations of $\gamma\delta$ T cells in human blood and tissue samples was addressed in Chapters 5 and 6. The study detailed in Chapter 6 constitutes, to my knowledge, the first sequence-level analysis of $\gamma\delta$ TCRs in response to CMV infection. These studies drew novel conclusions about the use of these technologies to examine $\gamma\delta$ T cell populations, and will greatly inform future experiments in this field.

TCR repertoire studies can be conducted using either DNA-based or RNA-based approaches. In this study I utilised both technologies to analyse $\gamma\delta$ T cell subsets in either tissue or blood samples, and the advantages and limitations of each approach were appraised. This evaluation could prove to be highly beneficial when selecting which technology to use in future studies, depending on the research objectives.

The repertoire study analysing colon and liver samples described in Chapter 5 was performed using the DNA-based sequencing platform by immunoSEQ. This approach yields a very large number of sequences and can detect much lower abundance sequences than the anchored 5'-RACE RNA methodology available for my studies at the time. This technology is extremely sensitive to DNA contamination however, which became a significant issue as our group routinely works with the DNA of various $\gamma\delta$ TCRs. In future

studies great care would need to be taken to ensure all stages of the sample preparation were undertaken in PCR-clean conditions, to minimise such issues.

The RNA-based anchored 5'-RACE technology as utilised in Chapter 6 yields much fewer sequences than the DNA approach, but there was no evidence of sequence contamination using this technology. What remains undetermined is how representative this subset of sequences is of the entire repertoire. Therefore it would be desirable to perform both the DNA- and RNA- based techniques on the same sample, to assess how much of the repertoire the this RNA-based approach covers, and also determine if there are any further differences between the sequences obtained by either approach. This would also prove useful to determine the impact of variation in mRNA levels, for example due to expansion of activated $\gamma\delta$ T cells, on results from RNA-based approaches compared to the sequencing of genomic DNA by immunoSEQ.

A further issue encountered with the repertoire studies was that that experiments with human samples need to be large to account for the substantial amount of variation inherent between samples. However, given the scope and relative expense of repertoire studies, the use of larger sample sizes to reach statistical significance is not always possible. These issues can be countered by expanding these studies to include more donors, but considering the spread of data observed in this study, careful calculation of ideal sample sizes using power-calculations is required¹⁷⁷.

Alternatively, these studies could be complemented by more focused, smaller scale approaches with have a lower cost-per-sample. An example of such an approach would be the use of qRT-PCR to analyse the presence of recombined V γ 5 chains in V δ 1⁺ $\gamma\delta$ T cells in PB. This could be used to determine the significance of the results discussed in Chapter 6

that V γ 5 chains were exclusively found in the V δ 1⁺ $\gamma\delta$ T cell populations in the PB CMV-seropositive donors, by analysing a much larger cohort of donors.

If the observation that V γ 5 chains are either exclusive or more abundant in the V δ 1⁺ $\gamma\delta$ T cell populations in CMV-seropositive donors is determined to be significant after expanding the study, this finding could provide novel insights into the molecular nature of how these $\gamma\delta$ T cells interact with CMV-associated antigens. The observation that responses may be V region specific suggests a role for CDR loops 1 and 2 in the response of $\gamma\delta$ T cells to CMV, and perhaps they play a central role in antigen recognition.

7.3.1 Combining repertoire and ligand identification studies

Sequence-level TCR repertoire studies provide a unique platform from which to investigate ligand recognition by $\gamma\delta$ T cells, and if combined with detailed molecular studies such as those performed in Chapters 3 and 4, could point the way towards novel insights into ligand recognition strategies of not only individual receptors, but also whole $\gamma\delta$ T cell populations.

Both of the repertoire studies discussed in Chapters 5 and 6 of this thesis suggest very diverse CDR3 regions of $\gamma\delta$ TCRs in both blood and tissues samples. This can be interpreted in several ways, and so molecular studies need to be expanded to better understand the significance of the CDR3 loop in $\gamma\delta$ T cell immunobiology. One possibility is that each individual CDR3 region is specific for an individual ligand, with an unknown contribution by the CDR 1 and 2 loops. Alternatively, it could also be that there is a large amount of tolerance of variation in the CDR3 sequence for recognition of individual ligands. This is similar to the V γ 9 chain of the pAg reactive V γ 9V δ 2⁺ $\gamma\delta$ T cell subset, whose criteria for pAg reactivity has been shown to require a specific J region and a three amino acid motif in the

CDR3 loop⁵⁹, therefore although other chains may not match each other perfectly, they are still reactive for the same antigen.

Ultimately, the significance of the CDR3 loops cannot be known unless molecular studies into ligand recognition by $\gamma\delta$ T cells are progressed, and a more complete understanding of the roles of the individual CDR loops is determined for other $\gamma\delta$ TCRs. However, if such advances can be made, the combination of repertoire and molecular approaches may provide a powerful perspective on the activity and ligand recognition capabilities of these cells.

7.3.2 Expanding $\gamma\delta$ TCR repertoire studies

There is scope to extend the repertoire study from Chapter 6 to viruses other than CMV, such as viruses with more wide-spread clinical significance, where the understanding how $\gamma\delta$ T cells are involved in the immune response to these viruses may influence clinical intervention.

Finally, expansion of the repertoire studies would benefit from single cell PCR approaches. These technologies amplify both the γ and δ chains from single cells, which is the only approach to obtain definitive chain pair information. This information is important because $\gamma\delta$ TCRs function as heterodimers, and so it is likely that both the γ and δ chains contribute to antigen recognition. If the link between $V\gamma5V\delta1^+$ $\gamma\delta$ T cell populations and CMV-positivity were firmly established in additional repertoire studies, then single cell PCR approaches would be crucial in highlighting paired $V\gamma5$ and $V\delta1$ TCR sequences that could be used for subsequent ligand identification and molecular studies.

Appendices

Patch	Eph Receptor														Mutant	Notes	
	#	A2	A4	B2	A1	A3	A5	A6	A7	A8	A10	B1	B3	B4			B6
1	46	H	S	H	D	Y	F	Y	S	Y	L	N	H	F	Y	S	Large polar to small polar
	49	G	E	S	K	H	N	N	H	N	S	S	V	G	E	E	Small flexible to large polar residue
	50	K	G	G	D	G	G	G	G	G	G	G	D	G	G	G	G promotes flexibility (G49 also). Large charged to small non-charged.
2	74	S	E	.	G	D	E	E	E	S	E	.	.	R	G	E	Small polar to large charged.
	75	G	P	E	R	H	Q	P	P	P	E	E	A	A	P	P	G/P suggests structural change due to flexibility/P bend
	76	D	S	S	D	S	N	N	N	N	N	S	G	G	G	G	Flexible. Different conformation in EphA2 and EphA4
	78	D	N	N	D	N	N	N	N	N	D	N	N	A	D	A	Forms ion pairs with K136 - conformational change
4	136	K	E	E	R	E	E	P	E	E	G	E	E	E	L	E	Forms ion pairs with D78 (E in EphA4, shorter, therefore fold change)
	147	P	A	A	A	A	A	A	A	A	A	A	P	A	A	A	Potential conformational change - causes changes in E149, facing outwards.
	149	E	E	E	Q	E	E	E	E	E	E	E	E	H	E	A	Same residue but different conformation likely due to P147 (E = large and negatively charged)
5	152	V	T	S	T	T	T	T	T	T	T	S	S	R	P	T	Solvent exposed non-polar residue in EphA2 (polar in EphA4)
	153	S	Q	Q	I	Q	E	Q	Q	G	Q	Q	R	K	S	Q	Small polar to large, polar
	154	S	V	V	R	M	L	M	G	A	G	V	L	R	S	M	Small polar in EphA2 to small and non-polar in EphA4
	157	E	G	G	A	C	G	G	G	G	G	G	G	A	S	G	Large and negatively charged to small, non-polar and flexible

Appendix 4.3: EphA2 surface patch mutagenesis strategy

Mutagenesis strategy for the EphA2 patch mutants, with residue characteristics and mutational justifications. Residue numbers correspond to EphA2.

Patch 1	WT	A C A	C A C	C C G	T A T	G G C	A A A	G G G
	Mutant	T H	P Y	G	K	G	G	G
Patch 2	WT	A T G	T C T	G G C	G A C	C A G	G A C	A A C
	Mutant	M S	D Q	D	D	Q	D	N
Patch 4	WT	G C G	C C C	G A T	G A G	A T C		
	Mutant	A P	D E	I				
Patch 5	WT	A C C	G T C	A G C	A G C	G A C	T T C	G A G
	Mutant	T V	S S	S D	F E			

WT	A T G	G A G	C C G	G G T	C A G	G C A	A A C
Mutant	M E	P Q	G	Q	A	N	

WT	G C G	C C C	G A T	G A G	A T C
Mutant	A P	D E	I		

WT	A C C	G T C	A G C	A G C	G A C	T T C	G A G
Mutant	T V	S S	S D	F E			

WT	A T G	G A G	C C G	G G T	C A G	G C A	A A C
Mutant	M E	P Q	G	Q	A	N	

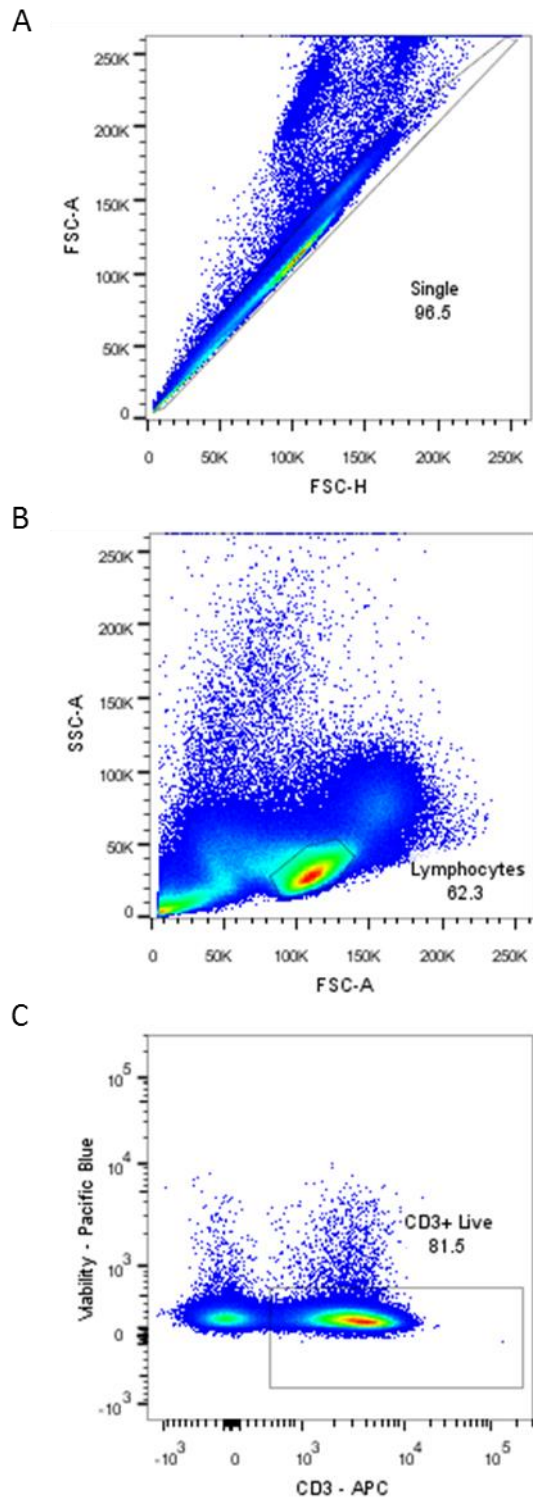
WT	C A G	A A G	C G C
Mutant	Q K	R	

WT	C A G	G A A	C G C
Mutant	Q E	R	

...136NT ...

Appendix 4.4: EphA2 surface patch mutant construct design

Codon changes used for the generation of gBlocks for the EphA2 surface patch mutants.



Appendix 6.1: HD PB Gating Strategy

Gating strategy for the selection of A) Single cells, B) Lymphocytes and C) CD3 positive/Viability stain negative cells from mononuclear cells isolated from donors peripheral blood for flow cytometry analysis

Appendix 6.2: CMV Sequencing Data

CMV Sequencing data from RNA-based anchored 5'-RACE analysis of healthy donor peripheral blood. CDR3 column represents amino acid translation of nucleotide sequences. Highlighted rows of the same colour denote shared sequences between multiple samples.

Mosaic sequences with identical CDR3 regions but different V γ segments are coloured and labelled.

KM HD – CMV-Seropositive

TRDV	CDR3	TRDJ	Freq (%)	Count
1	CALGDLLGDT PVLHNTDKLI F	1	17.0	15
1	CALGEPKPSYWGTYTDKLI F	1	14.8	13
1	CALGENI LAFLRGDI TYTDKLI F	1	11.4	10
1	CALGELL YVGI LVTDKLI F	1	10.2	9
1	CALGAVPTPLYVGI RVI YTDKLI F	1	8.0	7
1	CALGDPLPLL PFRLLI TGDHTDKLI F	1	2.3	2
1	CALGDLVGDT PVLHNTDKLI F	1	2.3	2
1	CALGELMEGLGVGVTDKLI F	1	2.3	2
1	CALGEDSSTFPRGGI DDKLI F	1	2.3	2
1	CALGEGCSFPEVPTDKLI F	1	2.3	2
1	CALGELVGGI REDTDKLI F	1	2.3	2
1	CALGDLYPYDF GTDKLI F	1	2.3	2
1	CALGELL VGI MESELI F	1	2.3	2
1	CALGKPRGASYVGKYVGMGVYTDKLI F	1	1.1	1
1	CALGEI QGPLEAGVKDTDKLI F	1	1.1	1
1	CALGELLSTLFRGLGDTDKLI F	1	1.1	1
1	CALGELPLLTWVVGDDTDKLI F	1	1.1	1
1	CALGELHSGAHVGI RVTDKLI F	1	1.1	1
1	CALGEVGPDYVGDTHTDKLI F	1	1.1	1
1	CALGDLEGDTPGI HNTDKLI F	1	1.1	1
1	CALGLPSYVPRGVRATDKLI F	1	1.1	1
1	CALGDTDGHVWLPHYTDKLI F	1	1.1	1
1	CAVGEVGHAVGI RGVTDKLI F	1	1.1	1
1	CALGATPGHAGRYTDKLI F	1	1.1	1
1	CALGDHHLVGI TRADKLI F	1	1.1	1
1	CALGDPI LGDI VDKLI F	1	1.1	1
1	CALGEPCCGLDTAQLFF	1	1.1	1
1	CALGDSI LGDI VDKLI F	1	1.1	1
1	CALGAMRLSGDRGLI F	1	1.1	1
2	CACDEVLGDTDKLI F	1	1.1	1
1	CALQLADKLI F	1	1.1	1
			100	88

TRGV	CDR3	TRGJ	Freq (%)	Count
9	CALWEVHLTGWFKI F	P1	17.9	15
5	CATWFLVGKLF	1	17.9	15
5	CATVDRRAYKLF	1	9.5	8
3	CATVDRRNYKLF	1	9.5	8
9	CALWEVRKGNYYKLF	1	4.8	4
2	CATWDGHFYKLF	1	4.8	4
9	CALWVGKLF	1	3.6	3
9	CALWEVRYKLF	1 or 2	3.6	3
10	CAAWDFTTGWFKI F	P1	2.4	2
9	CALWEVHLTGWFKVF	P1	2.4	2
10	CAAAGATWFKI F	P1	2.4	2
10	CAASGSTWFKI F	P1	2.4	2
9	CALSDTTGWFKI F	P1	2.4	2
9	CALVELHGVKLF	1	2.4	2
5	CATVDRPGKLF	1	2.4	2
4	CATVDGL LGDYKLF	1	1.2	1
9	CALWEVRYKLF	1	1.2	1
2	CATWDGGYKLF	1	1.2	1
2	CATVDRRAYKLF	1	1.2	1
2	CATVDRRNYKLF	1	1.2	1
10	CAAMGTWFKI F	P1	1.2	1
9	CALVDPDHKLF	1	1.2	1
3	CATWDGRYKLF	1	1.2	1
8	CATWENI YKLF	2 or 1	1.2	1
4	CATVALEKLF	1	1.2	1
			100	84

msai c
msai c

msai c
msai c

AS HD – CMV-Seropositive

TRDV	CDR3	TRDJ	Freq (%)	Count
1	CALGEHTRRAQVADKLI F	1	12.96	7
1	CALGERLLYWGRGKLI F	1	9.26	5
1	CALGGPRPLYTDKLI F	1	9.26	5
1	CALGTLAQPSYSRYVGTNTDKLI F	1	5.56	3
1	CALGELPLPSGGSTYTDKLI F	1	5.56	3
1	CALGEPGGTPRTYTDKLI F	1	5.56	3
1	CALQPPYALPVTDKLI F	1	5.56	3
1	CALGEPGGYKLI F	1	5.56	3
1	CALGERTGDTKGI RAVGKYTDKLI F	1	3.70	2
1	CALGGPSLHHPVNVGVADKLI F	1	3.70	2
1	CALGELPYPVWSPSDTKLI F	1	3.70	2
TRAV29/ DV5	CAARALYYRYCRALDKLI F	1	3.70	2
1	CALGELELLGFPTDKLI F	1	3.70	2
1	CALGESAFDPKLI F	1	3.70	2
1	CALGENI PRVVDWGGYTDKLI F	1	1.85	1
1	CALGEGGAFLLGDTGTDKLI F	1	1.85	1
1	CALGEPSPYGSAGTYTDKLI F	1	1.85	1
1	CALGERSSFGGTLYTDKLI F	1	1.85	1
1	CALGKGFLLLGNTDKLI F	1	1.85	1
1	CALGETFRLLGGPNTDKLI F	1	1.85	1
1	CALGERRPVGPYTDKLI F	1	1.85	1
1	CALGEHPSLGELTDKLI F	1	1.85	1
1	CALGVTRDGGYTDKLI F	1	1.85	1
1	CALGEQTRSPYTDKLI F	1	1.85	1
			100	54

TRGV	CDR3	TRGJ	Freq (%)	Count
9	CALWHPYKLF	1	26.32	15
9	CALWGLVTTGWFKI F	P1	12.28	7
5	CATWDRRGKLF	1	7.02	4
8	CATWDRRGSDW KTF	P2	5.26	3
2	CATWDHTTGWFKI F	P1	5.26	3
3	CATWDI KLF	1 or 2	5.26	3
9	CALWEVRGTGWFKI F	P1	3.51	2
9	CALWEVLMNYYKLF	1	3.51	2
9	CALWEVI MNYYKLF	1	3.51	2
9	CALWEGYKLF	1	3.51	2
8	CATWSLGGKLF	1	3.51	2
5	CATWGGYKLF	1	3.51	2
8	CATWDGRKLF	1 or 2	3.51	2
9	CALWEVI SGSLGKKI KVF	P	1.75	1
8	CATWDDYTTGWFKI F	P1	1.75	1
4	CATWDGVLYYKLF	1	1.75	1
3	CATWDGGYKLF	1	1.75	1
9	CALWGGYKLF	1	1.75	1
5	CATWDRLNYYKLF	1	1.75	1
9	CALWGDYKLF	2	1.75	1
3	CATWDRQYKLF	1	1.75	1
			100	57

AW HD – CMV-Seropositive

δ Chain

TRDV	CDR3	TRDJ	Freq (%)	Count
1	CALGELRVNPPGGYDTDKLI F	1	8.51	4
1	CALGELLGSTGGGYTDKLI F	1	8.51	4
1	CALGERTSFLVGI RPDPHLYTDKLI F	1	6.38	3
1	CALGERGLLRRVGI DDKLI F	1	6.38	3
1	CALGEPQVEI RVDVGI VRWVDGYTDKLI F	1	4.26	2
1	CALGVLRHPTTSYWESTPTSYPDKLI F	1	4.26	2
1	CALGDPKRSYRTGDTGTDKLI F	1	4.26	2
1	CALGEDTTNRAVGI RWTDKLI F	1	4.26	2
1	CALGQPMGDTYTLPTGKLI F	1	4.26	2
1	CALGEWAFLSRTTFTDKLI F	1	4.26	2
1	CALGELYGVPLRGYTDKLI F	1	4.26	2
1	CALGERI LPSGGAVDKLI F	1	4.26	2
1	CALGERTSFLVGI RPDPHLHTDKLI F	1	2.13	1
1	CALGEFNL LRVYVGI KDKRVTDKLI F	1	2.13	1
1	CALGELRAFLVWQSRGI RPTDKLI F	1	2.13	1
1	CALGELEWGLPYWGRQGGTDKLI F	1	2.13	1
1	CALGENLGPTWGLHPYTDKLI F	1	2.13	1
1	CALGELFYVLHVLGDPYTDKLI F	1	2.13	1
1	CALGELSRFRHWGI PLYTDKLI F	1	2.13	1
1	CALGDCKVTQGDTPPYTDKLI F	1	2.13	1
1	CALGEPLNPWGTGGYATDKLI F	1	2.13	1
1	CALGELPYQYWGRGNTDKLI F	1	2.13	1
1	CALGELPVPYFGTYTDKLI F	1	2.13	1
1	CALGPPLGTGGYPLARDKLI F	1	2.13	1
1	CALGEYYRTGGHRYTDKLI F	1	2.13	1
1	CALGELSQATRYRGI YKLI F	1	2.13	1
1	CALGEHQFMVGHSYTDKLI F	1	2.13	1
1	CALGEPSPSLLGAEVGKLI F	1	2.13	1
1	CALGDLTLPTRGYAKLI F	1	2.13	1
			100	47

γ Chain

TRGV	CDR3	TRGJ	Freq (%)	Count
9	CALVERGLGKKI KVF	P	33.33	24
2	CATVDGQYKCLF	1 or 2	8.33	6
8	CATVDQGYKCLF	1	5.56	4
3	CATVDSPPYKCLF	1	5.56	4
5	CATVDRNKCLF	1 or 2	5.56	4
9	CALVEAFYKCLF	1	4.17	3
8	CATVDNRRYKCLF	1	4.17	3
5	CATVDGNKCLF	1 or 2	4.17	3
9	CALVDLGGELGKKI KVF	P	2.78	2
9	CALVEAFRYKCLF	1	2.78	2
9	CALVDLGGELEKKI KVF	P	1.39	1
9	CALVGLGGELGKKI KVF	P	1.39	1
9	CALGERGLGKKI KVF	P	1.39	1
9	CALVEVRLGYKCLF	1	1.39	1
8	CATVDNPSNYYKCLF	2	1.39	1
4	CATVEGKWNYYKCLF	1	1.39	1
3	CATVDRTTYKCLF	1	1.39	1
2	CATVDRHLYKCLF	1	1.39	1
9	CALVGGLGWFKI F	P1	1.39	1
9	CALVEVQYKCLF	1 or 2	1.39	1
9	CALVEKYKCLF	1 or 2	1.39	1
9	CALVEGYKCLF	1 or 2	1.39	1
2	CATVAGLYI KCLF	1	1.39	1
2	CATVDGLYSKCLF	1	1.39	1
3	CATVDMFYKCLF	1	1.39	1
9	CALFQKYKCLF	1	1.39	1
8	CATVDFYKCLF	1 or 2	1.39	1
			100	72

LL HD – CMV-Seronegative

	TRGV	CDR3	TRDJ	Freq (%)	Count
δ Chain	1	CALGLPAFLYTGFADKLI F	1	57.3	47
	1	CALGSPLPI TTLWTGGTDKLI F	1	24.4	20
	1	CALGEHPKSFRSTGGFTDKLI F	1	4.9	4
	1	CALGSGFPVLGDWLI GKLI F	1	3.7	3
	1	CALGVLEAFLSGGDPSETDKLI F	1	2.4	2
	1	CALGELLGLLDCPLLI NTDKLI F	1	2.4	2
	1	CALGTFLLPNTGGLYTDKLI F	1	2.4	2
	1	CALGPGFPVLGDWLI GKLI F	1	1.2	1
	1	CALGERPQGANTDKLI F	1	1.2	1
				100	82

	TRGV	CDR3	TRGJ	Freq (%)	Count
γ Chain	9	CALWEVYYKRLF	1 or 2	60.5	49
	2	CATWDGPHYKRLF	1	12.3	10
	3	CATWDRLEKLF	1 or 2	6.2	5
	4	CATWDSNYYKRLF	2	4.9	4
	8	CATWGMNYYKRLF	2	3.7	3
	9	CALWEAYYKRLF	1	3.7	3
	8	CAAWGMNYYKRLF	2	1.2	1
	3	CATWDRSNYYKRLF	2	1.2	1
	4	CAAWDSNYYKRLF	2	1.2	1
	9	CALWEVPGYKRLF	1	1.2	1
	9	CALWEVVRGKRLF	1	1.2	1
	4	CATWDPNYYKRLF	2	1.2	1
	9	CTLWEVYYKRLF	1 or 2	1.2	1
			100	81	

LQ HD – CMV-Seronegative

	TRDV	CDR3	TRDJ	Freq (%)	Count
δ Chain	1	CALGEPGGFELI F	1	18.75	12
	1	CALGEPFLRTKYTDKLI F	1	15.63	10
	1	CALGVARGTRGYTDKLI F	1	10.94	7
	1	CALGEVSLGASYSTGGYPGTDKLI F	1	6.25	4
	1	CALGDPLPLLPFRLI TGDHTDKLI F	1	6.25	4
	1	CALGELLGGGYGYTDKLI F	1	4.69	3
	1	CALGDPLPTGGYGDKLI F	1	4.69	3
	1	CALGEPRVGI RGTDKLI F	1	4.69	3
	1	CALGDTSLRADKLI F	1	4.69	3
	1	CALGEPEPPRGVWGSLYTDKLI F	1	3.13	2
	1	CALSHLLVYWGSETDKLI F	1	3.13	2
	1	CALGHLGAYAGAGGDKLI F	1	3.13	2
	1	CALGEVSLGASYTTGGYPGTDKLI F	1	1.56	1
	1	CALGTLSTRSFGGGVYTDKLI F	1	1.56	1
	1	CALGAPSSYKWWGI RVGKLI F	1	1.56	1
	1	CALGERI FLPVGI LDPDKLI F	1	1.56	1
	1	CALSHGVVYWGSETDKLI F	1	1.56	1
	1	CALGEVI LGRGNPTYTDKLI F	1	1.56	1
	1	CALGAFRALVGI REFDKLI F	1	1.56	1
	1	CALGELHKFSEKLI F	1	1.56	1
1	CALGEGSPCDKLI F	1	1.56	1	
				100	64

	TRGV	CDR3	TRGJ	Freq (%)	Count	
γ Chain	9	CALWEKROELGKKI KVF	P	46.77	29	
	9	CALWEVQTGVFKI F	P1	29.03	18	
	8	CATWANTGVFKI F	P1	11.29	7	
	3	CATWDRQELGKKI KVF	P	1.61	1	
	10	CAAWDYKVVGYKKLF	1	1.61	1	
	3	CATWDSLLEYKKLF	1	1.61	1	
	3	CATWDSLVIYKKLF	1	1.61	1	
	10	CAALI PVYKKLF	1	1.61	1	
	8	CATWEGI YHKKLF	1	1.61	1	
	8	CATWEGI YYKKLF	1	1.61	1	
	4	CATRNLQYKKLF	1	1.61	1	
					100	62

SJ HD – CMV-Seronegative

δ Chain	TRDV	CDR3	TRDJ	Fr eq (%)	Count
		1	CALGAQPRRSPTNTRPDGLI F	1	21.05
	1	CALGELSRARVGYFLMGDKLI F	1	10.53	8
	1	CALGEI PFPPLVGLV/GTDKLI F	1	7.89	6
	1	CALEKDSVRV/GTDKLI F	1	7.89	6
	1	CALGSRLPPYTDKLI F	1	6.58	5
	1	CALGECVMGV/NTDKLI F	1	5.26	4
	1	CALGAHMGV/HSREKLI F	1	5.26	4
	1	CALGGLNMGW/WDKLI F	1	3.95	3
	1	CALGDDLPI GATDKLI F	1	3.95	3
	1	CALGATYTDKLI F	1	3.95	3
	1	CALGEQ/RLPSSVGPV/RTDKLI F	1	2.63	2
	1	CALG/TVFRRRGEYTDKLI F	1	2.63	2
	1	CALGATFPGPLFTDKLI F	1	2.63	2
	1	CALGEVLGDKYTDKLI F	1	2.63	2
	1	CALGEVSGGYTDKLI F	1	2.63	2
	1	CALGEVLGTRVPTGTGGYI SGYTDKLI F	1	1.32	1
	1	CALGERHFI PRLWV/GFNTDKLI F	1	1.32	1
	1	CALGELSRARVGYFV/MGDKLI F	1	1.32	1
	1	CALGELLPSYAGGHYTDKLI F	1	1.32	1
	1	CALG/TVFRRRREYTDKLI F	1	1.32	1
	1	CALGECVMGV/STDKLI F	1	1.32	1
	1	CALGDDLPI GGTDKLI F	1	1.32	1
	1	CALGPRSLGDHKLI F	1	1.32	1
				100	76

γ Chain	TRGV	CDR3	TRGJ	Fr eq (%)	Count
		3	CATWDRPPYYKFLF	1	27.87
	9	CALWEGNYYKFLF	1	24.59	15
	9	CALWEEVEKFLF	2	14.75	9
	3	CATWDRPGYKFLF	1	11.48	7
	8	CATWDSRTNYYKFLF	2	6.56	4
	2	CATWDGPAYKFLF	1	6.56	4
	2	CATWDRNYYKFLF	2	4.92	3
	8	CATWDGRYYKFLF	1	3.28	2
				100	61

References

1. Medzhitov R, Janeway C, Jr. Innate immune recognition: mechanisms and pathways. *Immunol Rev.* 2000; 173: 89-97
2. Hayday AC. $\gamma\delta$ Cells: A Right Time and a Right Place for a Conserved Third Way of Protection. *Annu Rev Immunol.* 2000; 18: 975-1026
3. Hedrick SM, Cohen DI, Nielsen EA, Davis MM. Isolation of cDNA clones encoding T cell-specific membrane-associated proteins. *Nature.* 1984; 308(5955): 149-53
4. Hein WR, Dudler L. Divergent evolution of T cell repertoires: extensive diversity and developmentally regulated expression of the sheep $\gamma\delta$ T cell receptor. *EMBO J.* 1993; 12(2): 715-24
5. Vantourout P, Hayday A. Six-of-the-best: unique contributions of gammadelta T cells to immunology. *Nat Rev Immunol.* 2013; 13(2): 88-100
6. Caux C, Zitvogel L. Recent successes of cancer immunotherapy: a new dimension in personalized medicine? *Target Oncol.* 2012; 7(1): 1-2
7. Banchereau J, Steinman RM. Dendritic cells and the control of immunity. *Nature.* 1998; 392(6673): 245-52
8. Hayday AC. $\gamma\delta$ T cells and the lymphoid stress-surveillance response. *Immunity.* 2009; 31(2): 184-96
9. Poltorak A, He X, Smirnova I, Liu MY, Van Huffel C, Du X, et al. Defective LPS signaling in C3H/HeJ and C57BL/10ScCr mice: mutations in Tlr4 gene. *Science.* 1998; 282(5396): 2085-8
10. Rock KL, Kono H. The inflammatory response to cell death. *Annu Rev Pathol.* 2008; 3: 99-126
11. Janeway CA, Jr., Jones B, Hayday A. Specificity and function of T cells bearing $\gamma\delta$ receptors. *Immunol Today.* 1988; 9(3): 73-6
12. Bauer S, Groh V, Wu J, Steinle A, Phillips JH, Lanier LL, et al. Activation of NK cells and T cells by NKG2D, a receptor for stress-inducible MICA. *Science.* 1999; 285(5428): 727-9
13. Shires J, Theodoridis E, Hayday AC. Biological insights into TCRgammadelta+ and TCRalpha+ intraepithelial lymphocytes provided by serial analysis of gene expression (SAGE). *Immunity.* 2001; 15(3): 419-34
14. Bergstresser PR, Cruz PD, Jr., Takashima A. Dendritic epidermal T cells: lessons from mice for humans. *J Invest Dermatol.* 1993; 100(1): 80S-83S
15. Wang L, Kamath A, Das H, Li L, Bukowski JF. Antibacterial effect of human $V\gamma 2V\delta 2$ T cells in vivo. *J Clin Invest.* 2001; 108(9): 1349-57
16. Brandes M, Willimann K, Lang AB, Nam KH, Jin C, Brenner MB, et al. Flexible migration program regulates $\gamma\delta$ T cell involvement in humoral immunity. *Blood.* 2003; 102(10): 3693-701
17. Brandes M, Willimann K, Moser B. Professional antigen-presentation function by human gammadelta T Cells. *Science.* 2005; 309(5732): 264-8

18. Himoudi N, Morgenstern DA, Yan M, Vernay B, Saraiva L, Wu Y, et al. Human gammadelta T lymphocytes are licensed for professional antigen presentation by interaction with opsonized target cells. *J Immunol.* 2012; 188(4): 1708-16
19. Strid J, Sobolev O, Zafirova B, Polic B, Hayday A. The intraepithelial T cell response to NKG2D-ligands links lymphoid stress surveillance to atopy. *Science.* 2011; 334(6060): 1293-7
20. Bonneville M, O'Brien RL, Born WK. $\gamma\delta$ T cell effector functions: a blend of innate programming and acquired plasticity. *Nat Rev Immunol.* 2010; 10(7): 467-78
21. Heilig JS, Tonegawa S. Diversity of murine γ genes and expression in fetal and adult T lymphocytes. *Nature.* 1986; 322(6082): 836-40
22. Lefranc MP, Rabbitts TH. A nomenclature to fit the organization of the human T-cell receptor γ and δ genes. *Res Immunol.* 1990; 141(7): 615-8
23. Strid J, Tigelaar RE, Hayday AC. Skin immune surveillance by T cells - a new order? *Semin Immunol.* 2009; 21: 110-20
24. Barbee SD, Woodward MJ, Turchinovich G, Mention JJ, Lewis JM, Boyden LM, et al. Skint-1 is a highly specific, unique selecting component for epidermal T cells. *Proc Natl Acad Sci U S A.* 2011; 108(8): 3330-5
25. Jameson J, Ugarte K, Chen N, Yachi P, Fuchs E, Boismenu R, et al. A role for skin $\gamma\delta$ T cells in wound repair. *Science.* 2002; 296(5568): 747-9
26. Girardi M, Oppenheim DE, Steele CR, Lewis JM, Glusac E, Filler R, et al. Regulation of cutaneous malignancy by gammadelta T cells. *Science.* 2001; 294(5542): 605-9
27. Shiohara T, Moriya N, Hayakawa J, Itohara S, Ishikawa H. Resistance to cutaneous graft-vs.-host disease is not induced in T cell receptor δ gene-mutant mice. *J Exp Med.* 1996; 183(4): 1483-9
28. Chodaczek G, Papanna V, Zal MA, Zal T. Body-barrier surveillance by epidermal $\gamma\delta$ TCRs. *Nat Immunol.* 2012; 13(3): 272-82
29. Komori HK, Witherden DA, Kelly R, Sendaydiego K, Jameson JM, Teyton L, et al. Cutting edge: dendritic epidermal $\gamma\delta$ T cell ligands are rapidly and locally expressed by keratinocytes following cutaneous wounding. *J Immunol.* 2012; 188(7): 2972-6
30. Aydintug MK, Roark CL, Chain JL, Born WK, O'Brien RL. Macrophages express multiple ligands for $\gamma\delta$ TCRs. *Mol Immunol.* 2008; 45(11): 3253-63
31. Adams EJ, Chien YH, Garcia KC. Structure of a $\gamma\delta$ T cell receptor in complex with the nonclassical MHC T22. *Science.* 2005; 308(5719): 227-31
32. Mestas J, Hughes CC. Of mice and not men: differences between mouse and human immunology. *J Immunol.* 2004; 172(5): 2731-8
33. Luoma AM, Castro CD, Adams EJ. gammadelta T cell surveillance via CD1 molecules. *Trends Immunol.* 2014; 35(12): 613-621
34. Hannani D, Ma Y, Yamazaki T, Dechanet-Merville J, Kroemer G, Zitvogel L. Harnessing $\gamma\delta$ T cells in anticancer immunotherapy. *Trends Immunol.* 2012; 33(5): 199-206

35. Tanaka Y, Morita CT, Tanaka Y, Nieves E, Brenner MB, Bloom BR. Natural and synthetic non-peptide antigens recognized by human $\gamma\delta$ T cells. *Nature*. 1995; 375(6527): 155-158
36. Gober H-J, Kistowska M, Angman L, Jenö P, Mori L, De Libero G. Human T Cell Receptor $\gamma\delta$ Cells Recognize Endogenous Mevalonate Metabolites in Tumor Cells. *J Exp Med*. 2003; 197(2): 163-168
37. Goldstein JL, Brown MS. Regulation of the mevalonate pathway. *Nature*. 1990; 343(6257): 425-30
38. Puan KJ, Jin C, Wang H, Sarikonda G, Raker AM, Lee HK, et al. Preferential recognition of a microbial metabolite by human V γ 9V δ 2 T cells. *Int Immunol*. 2007; 19(5): 657-73
39. Fisch P, Malkovsky M, Kovats S, Sturm E, Braakman E, Klein BS, et al. Recognition by human V γ 9/V δ 2 T cells of a GroEL homolog on Daudi Burkitt's lymphoma cells. *Science*. 1990; 250(4985): 1269-73
40. De Libero G, Casorati G, Giachino C, Carbonara C, Migone N, Matzinger P, et al. Selection by two powerful antigens may account for the presence of the major population of human peripheral gamma/delta T cells. *J Exp Med*. 1991; 173(6): 1311-22
41. Scotet E, Martinez LO, Grant E, Barbaras R, Jenö P, Guiraud M, et al. Tumor recognition following V γ 9V δ 2 T cell receptor interactions with a surface F1-ATPase-related structure and apolipoprotein A-I. *Immunity*. 2005; 22(1): 71-80
42. Rajasekar R, Sim GK, Augustin A. Self heat shock and $\gamma\delta$ T cell reactivity. *Proc Natl Acad Sci U S A*. 1990; 87(5): 1767-71
43. Sciammas R, Johnson RM, Sperling AI, Brady W, Linsley PS, Spear PG, et al. Unique antigen recognition by a herpesvirus-specific TCR $\gamma\delta$ cell. *J Immunol*. 1994; 152(11): 5392-7
44. Dai Y, Chen H, Mo C, Cui L, He W. Ectopically expressed human tumor biomarker MutS homologue 2 is a novel endogenous ligand that is recognized by human gammadelta T cells to induce innate anti-tumor/virus immunity. *J Biol Chem*. 2012; 287(20): 16812-9
45. Fisch P, Meuer E, Pende D, Rothenfusser S, Viale O, Kock S, et al. Control of B cell lymphoma recognition via natural killer inhibitory receptors implies a role for human V γ 9/V δ 2 T cells in tumor immunity. *Eur J Immunol*. 1997; 27(12): 3368-79
46. Dechanet J, Merville P, Lim A, Retiere C, Pitard V, Lafarge X, et al. Implication of gammadelta T cells in the human immune response to cytomegalovirus. *J Clin Invest*. 1999; 103(10): 1437-49
47. Cohen NR, Garg S, Brenner MB. Antigen Presentation by CD1 Lipids, T Cells, and NKT Cells in Microbial Immunity. *Adv Immunol*. 2009; 102: 1-94
48. Takahara M, Kang K, Liu L, Yoshida Y, McCormick TS, Cooper KD. iC3b arrests monocytic cell differentiation into CD1c-expressing dendritic cell precursors: a mechanism for transiently decreased dendritic cells in vivo after human skin injury by ultraviolet B. *J Invest Dermatol*. 2003; 120(5): 802-9
49. Spada FM, Grant EP, Peters PJ, Sugita M, Melian A, Leslie DS, et al. Self-recognition of CD1 by $\gamma\delta$ T cells: implications for innate immunity. *J Exp Med*. 2000; 191(6): 937-48

50. Luoma AM, Castro CD, Mayassi T, Bembinster LA, Bai L, Picard D, et al. Crystal structure of Vdelta1 T cell receptor in complex with CD1d-sulfatide shows MHC-like recognition of a self-lipid by human gammadelta T cells. *Immunity*. 2013; 39(6): 1032-42
51. Uldrich AP, Le Nours J, Pellicci DG, Gherardin NA, McPherson KG, Lim RT, et al. CD1d-lipid antigen recognition by the gammadelta TCR. *Nat Immunol*. 2013; 14(11): 1137-45
52. Harari A, Zimmerli SC, Pantaleo G. Cytomegalovirus (CMV)-specific cellular immune responses. *Hum Immunol*. 2004; 65(5): 500-6
53. Moss P, Khan N. CD8(+) T-cell immunity to cytomegalovirus. *Hum Immunol*. 2004; 65(5): 456-64
54. Frantzeskaki FG, Karampi ES, Kottaridi C, Alepaki M, Routsis C, Tzanela M, et al. Cytomegalovirus reactivation in a general, nonimmunosuppressed intensive care unit population: Incidence, risk factors, associations with organ dysfunction, and inflammatory biomarkers. *J Crit Care*. 2014:
55. Lafarge X, Merville P, Cazin MC, Berge F, Potaux L, Moreau JF, et al. Cytomegalovirus infection in transplant recipients resolves when circulating gammadelta T lymphocytes expand, suggesting a protective antiviral role. *J Infect Dis*. 2001; 184(5): 533-41
56. Knight A, Madrigal AJ, Grace S, Sivakumaran J, Kottaridis P, Mackinnon S, et al. The role of Vdelta2-negative gammadelta T cells during cytomegalovirus reactivation in recipients of allogeneic stem cell transplantation. *Blood*. 2010; 116(12): 2164-72
57. Sperling AI, Cron RQ, Decker DC, Stern DA, Bluestone JA. Peripheral T cell receptor $\gamma\delta$ variable gene repertoire maps to the T cell receptor loci and is influenced by positive selection. *J Immunol*. 1992; 149(10): 3200-7
58. Allison TJ, Winter CC, Fournie JJ, Bonneville M, Garboczi DN. Structure of a human $\gamma\delta$ T cell antigen receptor. *Nature*. 2001; 411(6839): 820-4
59. Wang H, Fang Z, Morita CT. Vgamma2Vdelta2 T Cell Receptor recognition of prenyl pyrophosphates is dependent on all CDRs. *J Immunol*. 2010; 184(11): 6209-22
60. Wencker M, Turchinovich G, Di Marco Barros R, Deban L, Jandke A, Cope A, et al. Innate-like T cells straddle innate and adaptive immunity by altering antigen-receptor responsiveness. *Nat Immunol*. 2014; 15(1): 80-7
61. Fergusson JR, Smith KE, Fleming VM, Rajoriya N, Newell EW, Simmons R, et al. CD161 defines a transcriptional and functional phenotype across distinct human T cell lineages. *Cell Rep*. 2014; 9(3): 1075-88
62. Testi R, D'Ambrosio D, De Maria R, Santoni A. The CD69 receptor: a multipurpose cell-surface trigger for hematopoietic cells. *Immunol Today*. 1994; 15(10): 479-83
63. Morita CT, Beckman EM, Bukowski JF, Tanaka Y, Band H, Bloom BR, et al. Direct presentation of nonpeptide prenyl pyrophosphate antigens to human gamma delta T cells. *Immunity*. 1995; 3(4): 495-507
64. Wei H, Huang D, Lai X, Chen M, Zhong W, Wang R, et al. Definition of APC presentation of phosphoantigen (E)-4-hydroxy-3-methyl-but-2-enyl pyrophosphate to Vgamma2Vdelta 2 TCR. *J Immunol*. 2008; 181(7): 4798-806

65. Wang H, Lee HK, Bukowski JF, Li H, Mariuzza RA, Chen ZW, et al. Conservation of nonpeptide antigen recognition by rhesus monkey V gamma 2V delta 2 T cells. *J Immunol.* 2003; 170(7): 3696-706
66. Harly C, Guillaume Y, Nedellec S, Peigne CM, Monkkonen H, Monkkonen J, et al. Key implication of CD277/butyrophilin-3 (BTN3A) in cellular stress sensing by a major human gammadelta T-cell subset. *Blood.* 2012; 120(11): 2269-79
67. Compte E, Pontarotti P, Collette Y, Lopez M, Olive D. Frontline: Characterization of BT3 molecules belonging to the B7 family expressed on immune cells. *Eur J Immunol.* 2004; 34(8): 2089-99
68. Vavassori S, Kumar A, Wan GS, Ramanjaneyulu GS, Cavallari M, El Daker S, et al. Butyrophilin 3A1 binds phosphorylated antigens and stimulates human gammadelta T cells. *Nat Immunol.* 2013; 14(9): 908-16
69. Sandstrom A, Peigne CM, Leger A, Crooks JE, Konczak F, Gesnel MC, et al. The intracellular B30.2 domain of butyrophilin 3A1 binds phosphoantigens to mediate activation of human Vgamma9Vdelta2 T cells. *Immunity.* 2014; 40(4): 490-500
70. Shin S, El-Diwany R, Schaffert S, Adams EJ, Garcia KC, Pereira P, et al. Antigen recognition determinants of $\gamma\delta$ T cell receptors. *Science.* 2005; 308(5719): 252-5
71. Bai L, Picard D, Anderson B, Chaudhary V, Luoma A, Jabri B, et al. The majority of CD1d-sulfatide-specific T cells in human blood use a semiinvariant Vdelta1 TCR. *Eur J Immunol.* 2012; 42(9): 2505-10
72. Sundberg EJ, Deng L, Mariuzza RA. TCR recognition of peptide/MHC class II complexes and superantigens. *Semin Immunol.* 2007; 19(4): 262-71
73. Halary F, Pitard V, Dlubek D, Krzysiek R, de la Salle H, Merville P, et al. Shared reactivity of V δ 2 $\gamma\delta$ T cells against cytomegalovirus-infected cells and tumor intestinal epithelial cells. *J Exp Med.* 2005; 201(10): 1567-78
74. Dietrich J, Menne C, Lauritsen JP, von Essen M, Rasmussen AB, Odum N, et al. Ligand-induced TCR down-regulation is not dependent on constitutive TCR cycling. *J Immunol.* 2002; 168(11): 5434-40
75. Wykosky J, Debinski W. The EphA2 receptor and ephrinA1 ligand in solid tumors: function and therapeutic targeting. *Mol Cancer Res.* 2008; 6(12): 1795-806
76. Hirai H, Maru Y, Hagiwara K, Nishida J, Takaku F. A novel putative tyrosine kinase receptor encoded by the eph gene. *Science.* 1987; 238(4834): 1717-20
77. Flanagan JG, Vanderhaeghen P. The ephrins and Eph receptors in neural development. *Annu Rev Neurosci.* 1998; 21: 309-45
78. Pasquale EB. Eph receptors and ephrins in cancer: bidirectional signalling and beyond. *Nature reviews Cancer.* 2010; 10: 165-80
79. Pasquale EB. Eph-ephrin promiscuity is now crystal clear. *Nat Neurosci.* 2004; 7(5): 417-8
80. Seiradake E, Harlos K, Sutton G, Aricescu AR, Jones EY. An extracellular steric seeding mechanism for Eph-ephrin signaling platform assembly. *Nat Struct Mol Biol.* 2010; 17(4): 398-402

81. Singla N, Goldgur Y, Xu K, Paavilainen S, Nikolov DB, Himanen JP. Crystal structure of the ligand-binding domain of the promiscuous EphA4 receptor reveals two distinct conformations. *Biochem Biophys Res Commun.* 2010; 399(4): 555-9
82. Himanen JP, Goldgur Y, Miao H, Myshkin E, Guo H, Buck M, et al. Ligand recognition by A-class Eph receptors: crystal structures of the EphA2 ligand-binding domain and the EphA2/ephrin-A1 complex. *EMBO Rep.* 2009; 10(7): 722-8
83. Hafner C, Schmitz G, Meyer S, Bataille F, Hau P, Langmann T, et al. Differential gene expression of Eph receptors and ephrins in benign human tissues and cancers. *Clin Chem.* 2004; 50(3): 490-9
84. Lindberg RA, Hunter T. cDNA cloning and characterization of eck, an epithelial cell receptor protein-tyrosine kinase in the eph/elk family of protein kinases. *Mol Cell Biol.* 1990; 10(12): 6316-24
85. Walker-Daniels J, Hess AR, Hendrix MJ, Kinch MS. Differential regulation of EphA2 in normal and malignant cells. *Am J Pathol.* 2003; 162(4): 1037-42
86. Coffman KT, Hu M, Carles-Kinch K, Tice D, Donacki N, Munyon K, et al. Differential EphA2 Epitope Display on Normal versus Malignant Cells. *Cancer Res.* 2003; 63: 7907-7912
87. Liu YN, Lee WW, Wang CY, Chao TH, Chen Y, Chen JH. Regulatory mechanisms controlling human E-cadherin gene expression. *Oncogene.* 2005; 24(56): 8277-90
88. Surawska H, Ma PC, Salgia R. The role of ephrins and Eph receptors in cancer. *Cytokine & growth factor reviews.* 2004; 15: 419-33
89. Sulman EP, Tang XX, Allen C, Biegel JA, Pleasure DE, Brodeur GM, et al. ECK, a human EPH-related gene, maps to 1p36.1, a common region of alteration in human cancers. *Genomics.* 1997; 40(2): 371-4
90. Winter J, Roepcke S, Krause S, Muller EC, Otto A, Vingron M, et al. Comparative 3'UTR analysis allows identification of regulatory clusters that drive Eph/ephrin expression in cancer cell lines. *PLoS One.* 2008; 3(7): e2780
91. Dohn M, Jiang J, Chen X. Receptor tyrosine kinase EphA2 is regulated by p53-family proteins and induces apoptosis. *Oncogene.* 2001; 20(45): 6503-15
92. Wykosky J, Gibo DM, Stanton C, Debinski W. Interleukin-13 receptor alpha 2, EphA2, and Fos-related antigen 1 as molecular denominators of high-grade astrocytomas and specific targets for combinatorial therapy. *Clin Cancer Res.* 2008; 14(1): 199-208
93. Thaker PH, Deavers M, Celestino J, Thornton A, Fletcher MS, Landen CN, et al. EphA2 expression is associated with aggressive features in ovarian carcinoma. *Clin Cancer Res.* 2004; 10(15): 5145-50
94. Zeng G, Hu Z, Kinch MS, Pan CX, Flockhart DA, Kao C, et al. High-level expression of EphA2 receptor tyrosine kinase in prostatic intraepithelial neoplasia. *Am J Pathol.* 2003; 163(6): 2271-6
95. Zantek ND, Azimi M, Fedor-Chaiken M, Wang B, Brackenbury R, Kinch MS. E-cadherin regulates the function of the EphA2 receptor tyrosine kinase. *Cell Growth Differ.* 1999; 10(9): 629-38

96. Zelinski DP, Zantek ND, Stewart JC, Irizarry AR, Kinch MS. EphA2 overexpression causes tumorigenesis of mammary epithelial cells. *Cancer Res.* 2001; 61(5): 2301-6
97. Macrae M, Neve RM, Rodriguez-Viciano P, Haqq C, Yeh J, Chen C, et al. A conditional feedback loop regulates Ras activity through EphA2. *Cancer Cell.* 2005; 8(2): 111-8
98. Wykosky J, Gibo DM, Debinski W. A novel, potent, and specific ephrinA1-based cytotoxin against EphA2 receptor expressing tumor cells. *Mol Cancer Ther.* 2007; 6(12 Pt 1): 3208-18
99. Carles-Kinch K, Kilpatrick KE, Stewart JC, Kinch MS. Antibody targeting of the EphA2 tyrosine kinase inhibits malignant cell behavior. *Cancer Res.* 2002; 62(10): 2840-7
100. Tanaka Y. Human $\gamma\delta$ T cells and tumor immunotherapy. *J Clin Exp Hematop.* 2006; 46(1): 11-23
101. Bubeník. Tumour MHC class I downregulation and immunotherapy (Review). *Oncology Reports.* 2003; 10(6): 2005-2008
102. Meraviglia S, Eberl M, Vermijlen D, Todaro M, Buccheri S, Cicero G, et al. In vivo manipulation of V γ 9V δ 2 T cells with zoledronate and low-dose interleukin-2 for immunotherapy of advanced breast cancer patients. *Clin Exp Immunol.* 2010; 161(2): 290-7
103. Dieli F, Vermijlen D, Fulfaro F, Caccamo N, Meraviglia S, Cicero G, et al. Targeting human $\{\gamma\delta\}$ T cells with zoledronate and interleukin-2 for immunotherapy of hormone-refractory prostate cancer. *Cancer Res.* 2007; 67(15): 7450-7
104. Wilhelm M, Kunzmann V, Eckstein S, Reimer P, Weissinger F, Ruediger T, et al. $\gamma\delta$ T cells for immune therapy of patients with lymphoid malignancies. *Blood.* 2003; 102(1): 200-6
105. Matsuda S, Kudoh S, Katayama S. Enhanced formation of azoxymethane-induced colorectal adenocarcinoma in $\gamma\delta$ T lymphocyte-deficient mice. *Jpn J Cancer Res.* 2001; 92(8): 880-5
106. Ma Y, Aymeric L, Locher C, Mattarollo SR, Delahaye NF, Pereira P, et al. Contribution of IL-17-producing $\gamma\delta$ T cells to the efficacy of anticancer chemotherapy. *J Exp Med.* 2011; 208(3): 491-503
107. von Lilienfeld-Toal M, Nattermann J, Feldmann G, Sievers E, Frank S, Strehl J, et al. Activated $\gamma\delta$ T cells express the natural cytotoxicity receptor natural killer p 44 and show cytotoxic activity against myeloma cells. *Clin Exp Immunol.* 2006; 144(3): 528-33
108. Kunzmann V, Bauer E, Feurle J, Weissinger F, Tony HP, Wilhelm M. Stimulation of $\gamma\delta$ T cells by aminobisphosphonates and induction of antiplasma cell activity in multiple myeloma. *Blood.* 2000; 96(2): 384-92
109. Vermijlen D, Brouwer M, Donner C, Liesnard C, Tackoen M, Van Rysselberge M, et al. Human cytomegalovirus elicits fetal $\gamma\delta$ T cell responses in utero. *J Exp Med.* 2010; 207(4): 807-21
110. Couzi L, Levaillant Y, Jamai A, Pitard V, Lassalle R, Martin K, et al. Cytomegalovirus-induced $\gamma\delta$ T cells associate with reduced cancer risk after kidney transplantation. *J Am Soc Nephrol.* 2010; 21(1): 181-8

111. Emsley P, Lohkamp B, Scott WG, Cowtan K. Features and development of Coot. *Acta Crystallographica Section D*. 2010; 66(4): 486-501
112. Kelley LA, Sternberg MJ. Protein structure prediction on the Web: a case study using the Phyre server. *Nat Protoc*. 2009; 4(3): 363-71
113. Sarkar S, Witham S, Zhang J, Zhenirovskyy M, Rocchia W, Alexov E. DelPhi Web Server: A comprehensive online suite for electrostatic calculations of biological macromolecules and their complexes. *Commun Comput Phys*. 2013; 13(1): 269-284
114. Bawono P, Heringa J. PRALINE: a versatile multiple sequence alignment toolkit. *Methods Mol Biol*. 2014; 1079: 245-62
115. Aricescu AR, Lu W, Jones EY. A time- and cost-efficient system for high-level protein production in mammalian cells. *Acta Crystallogr D Biol Crystallogr*. 2006; 62(Pt 10): 1243-50
116. Robins HS, Campregher PV, Srivastava SK, Wachter A, Turtle CJ, Kahsai O, et al. Comprehensive assessment of T-cell receptor beta-chain diversity in alphabeta T cells. *Blood*. 2009; 114(19): 4099-107
117. Quigley MF, Almeida JR, Price DA, Douek DC. Unbiased molecular analysis of T cell receptor expression using template-switch anchored RT-PCR. *Curr Protoc Immunol*. 2011; Chapter 10: Unit10 33
118. Life Technologies Inc. Vector Maps [cited 2014 11]. Available from: <https://www.lifetechnologies.com/search/support/supportSearchAction.action?query=&supportSearchArea=Vector+Maps&newSearch=true&refineSearch=true>.
119. Cheli R, Cornaggia M, Testino G, De Iaco F. Gastric metaplasia in normal (inflammation-free) duodenal mucosa. *J Clin Gastroenterol*. 1994; 18(3): 240-1
120. Cheli R, Nicolo G, Bovero E, Salvi S, Testino G, De Iaco F. Epidemiology and etiology of "autonomous" nonspecific duodenitis. *J Clin Gastroenterol*. 1994; 18(3): 200-5
121. D'Ambrosio D, Cantrell DA, Frati L, Santoni A, Testi R. Involvement of p21ras activation in T cell CD69 expression. *Eur J Immunol*. 1994; 24(3): 616-20
122. Chow KK, Naik S, Kakarla S, Brawley VS, Shaffer DR, Yi Z, et al. T cells redirected to EphA2 for the immunotherapy of glioblastoma. *Mol Ther*. 2013; 21(3): 629-37
123. Willcox CR, Pitard V, Netzer S, Couzi L, Salim M, Silberzahn T, et al. Cytomegalovirus and tumor stress surveillance by binding of a human gammadelta T cell antigen receptor to endothelial protein C receptor. *Nat Immunol*. 2012; 13(9): 872-9
124. Abraham RT, Weiss A. Jurkat T cells and development of the T-cell receptor signalling paradigm. *Nat Rev Immunol*. 2004; 4(4): 301-8
125. Risueno MC, Testillano PS. Cytochemistry and immunocytochemistry of nucleolar chromatin in plants. *Micron*. 1994; 25(4): 331-60
126. Biondi A, Rovelli A, Cantu-Rajoldi A, Fenu S, Basso G, Luciano A, et al. Acute promyelocytic leukemia in children: experience of the Italian Pediatric Hematology and Oncology Group (AIEOP). *Leukemia*. 1994; 8 Suppl 2: S66-70
127. Testino G. Serum pepsinogen A and pepsin secretion in duodenal ulcer: *Helicobacter pylori* influence. *Acta Gastroenterol Latinoam*. 1994; 24(3): 149-52

128. UniProt C. Activities at the Universal Protein Resource (UniProt). *Nucleic Acids Res.* 2014; 42(Database issue): D191-8
129. Stubenrauch K, Wessels U, Lenz H. Evaluation of an immunoassay for human-specific quantitation of therapeutic antibodies in serum samples from non-human primates. *J Pharm Biomed Anal.* 2009; 49(4): 1003-8
130. Lorenzini L, De Martino A, Testi W, Sorbellini F, Bisozzi L, Terzuoli L, et al. Radioimmunoassay of folic acid and its correlation with age. *Adv Exp Med Biol.* 1994; 370: 791-3
131. Davis MM, Boniface JJ, Reich Z, Lyons D, Hampl J, Arden B, et al. Ligand recognition by alpha beta T cell receptors. *Annu Rev Immunol.* 1998; 16: 523-44
132. Willcox BE, Gao GF, Wyer JR, O'Callaghan CA, Boulter JM, Jones EY, et al. Production of soluble alphabeta T-cell receptor heterodimers suitable for biophysical analysis of ligand binding. *Protein Sci.* 1999; 8(11): 2418-23
133. Beckett D, Kovaleva E, Schatz PJ. A minimal peptide substrate in biotin holoenzyme synthetase-catalyzed biotinylation. *Protein Sci.* 1999; 8(4): 921-9
134. Krummel MF, Sjaastad MD, Wulfing C, Davis MM. Differential clustering of CD4 and CD3zeta during T cell recognition. *Science.* 2000; 289(5483): 1349-52
135. Holen HL, Shadidi M, Narvhus K, Kjøsnes O, Tierens A, Aasheim H-C. Signaling through ephrin-A ligand leads to activation of Src-family kinases, Akt phosphorylation, and inhibition of antigen receptor-induced apoptosis. *Journal of leukocyte biology.* 2008; 84: 1183-91
136. Holen HL, Shadidi M, Narvhus K, Kjosnes O, Tierens A, Aasheim HC. Signaling through ephrin-A ligand leads to activation of Src-family kinases, Akt phosphorylation, and inhibition of antigen receptor-induced apoptosis. *J Leukoc Biol.* 2008; 84(4): 1183-91
137. Salmond RJ, Filby A, Qureshi I, Caserta S, Zamoyska R. T-cell receptor proximal signaling via the Src-family kinases, Lck and Fyn, influences T-cell activation, differentiation, and tolerance. *Immunol Rev.* 2009; 228(1): 9-22
138. Artyomov MN, Lis M, Devadas S, Davis MM, Chakraborty AK. CD4 and CD8 binding to MHC molecules primarily acts to enhance Lck delivery. *Proc Natl Acad Sci U S A.* 2010; 107(39): 16916-21
139. Lim YS, McLaughlin T, Sung TC, Santiago A, Lee KF, O'Leary DD. p75(NTR) mediates ephrin-A reverse signaling required for axon repulsion and mapping. *Neuron.* 2008; 59(5): 746-58
140. Yin Y, Wang XX, Mariuzza RA. Crystal structure of a complete ternary complex of T-cell receptor, peptide-MHC, and CD4. *Proc Natl Acad Sci U S A.* 2012; 109(14): 5405-10
141. Xu B, Pizarro JC, Holmes MA, McBeth C, Groh V, Spies T, et al. Crystal structure of a $\gamma\delta$ T cell receptor specific for the human MHC class I homolog MICA. *Proc Natl Acad Sci U S A.* 2011; 108(6): 2414-9
142. Boyd AW, Bartlett PF, Lackmann M. Therapeutic targeting of EPH receptors and their ligands. *Nat Rev Drug Discov.* 2014; 13(1): 39-62

143. Bork P, Holm L, Sander C. The immunoglobulin fold. Structural classification, sequence patterns and common core. *J Mol Biol.* 1994; 242(4): 309-20
144. Brochet X, Lefranc MP, Giudicelli V. IMGT/V-QUEST: the highly customized and integrated system for IG and TR standardized V-J and V-D-J sequence analysis. *Nucleic Acids Res.* 2008; 36(Web Server issue): W503-8
145. Himanen JP, Yermekbayeva L, Janes PW, Walker JR, Xu K, Atapattu L, et al. Architecture of Eph receptor clusters. *Proc Natl Acad Sci U S A.* 2010; 107(24): 10860-5
146. Seiradake E, Schaupp A, del Toro Ruiz D, Kaufmann R, Mitakidis N, Harlos K, et al. Structurally encoded intraclass differences in EphA clusters drive distinct cell responses. *Nat Struct Mol Biol.* 2013; 20(8): 958-64
147. Goujon M, McWilliam H, Li W, Valentin F, Squizzato S, Paern J, et al. A new bioinformatics analysis tools framework at EMBL-EBI. *Nucleic Acids Res.* 2010; 38(Web Server issue): W695-9
148. Davy A, Gale NW, Murray EW, Klinghoffer RA, Soriano P, Feuerstein C, et al. Compartmentalized signaling by GPI-anchored ephrin-A5 requires the Fyn tyrosine kinase to regulate cellular adhesion. *Genes & Development.* 1999; 13: 3125-3135
149. Pelicci PG, Subar M, Weiss A, Dalla-Favera R, Littman DR. Molecular diversity of the human T-gamma constant region genes. *Science.* 1987; 237(4818): 1051-5
150. Chien YH, Konigshofer Y. Antigen recognition by gammadelta T cells. *Immunol Rev.* 2007; 215: 46-58
151. Chiba M, Bartnik W, ReMine SG, Thayer WR, Shorter RG. Human colonic intraepithelial and lamina propria lymphocytes: cytotoxicity in vitro and the potential effects of the isolation method on their functional properties. *Gut.* 1981; 22(3): 177-86
152. Dalton JE, Cruickshank SM, Egan CE, Mears R, Newton DJ, Andrew EM, et al. Intraepithelial gammadelta+ lymphocytes maintain the integrity of intestinal epithelial tight junctions in response to infection. *Gastroenterology.* 2006; 131(3): 818-29
153. Holtmeier W, Kabelitz D. gammadelta T cells link innate and adaptive immune responses. *Chem Immunol Allergy.* 2005; 86: 151-83
154. Edelblum KL, Shen L, Weber CR, Marchiando AM, Clay BS, Wang Y, et al. Dynamic migration of gammadelta intraepithelial lymphocytes requires occludin. *Proc Natl Acad Sci U S A.* 2012; 109(18): 7097-102
155. Dziubianau M, Hecht J, Kuchenbecker L, Sattler A, Stervbo U, Rodelsperger C, et al. TCR repertoire analysis by next generation sequencing allows complex differential diagnosis of T cell-related pathology. *Am J Transplant.* 2013; 13(11): 2842-54
156. Lee JS, Oka K, Obara M, Nishimukai M, Yoo YC, Yamada K, et al. Improved isolation methods for mucosal leukocytes from small and large intestines in rats. *Biosci Biotechnol Biochem.* 2009; 73(8): 1732-40
157. Sherwood AM, Desmarais C, Livingston RJ, Andriesen J, Haussler M, Carlson CS, et al. Deep sequencing of the human TCRgamma and TCRbeta repertoires suggests that TCRbeta rearranges after alphabeta and gammadelta T cell commitment. *Sci Transl Med.* 2011; 3(90): 90ra61

158. Pitard V, Roumanes D, Lafarge X, Couzi L, Garrigue I, Lafon ME, et al. Long-term expansion of effector/memory Vdelta2-gammadelta T cells is a specific blood signature of CMV infection. *Blood*. 2008; 112(4): 1317-24
159. Shannon CE. The mathematical theory of communication. 1963. *MD Comput*. 1997; 14(4): 306-17
160. Mehandru S. The Gastrointestinal Tract in HIV-1 Infection: Questions, Answers, and More Questions! *The PRN Notebook*. 2007; 12: 1-10
161. Walter EA, Greenberg PD, Gilbert MJ, Finch RJ, Watanabe KS, Thomas ED, et al. Reconstitution of cellular immunity against cytomegalovirus in recipients of allogeneic bone marrow by transfer of T-cell clones from the donor. *N Engl J Med*. 1995; 333(16): 1038-44
162. Gillespie GM, Wills MR, Appay V, O'Callaghan C, Murphy M, Smith N, et al. Functional heterogeneity and high frequencies of cytomegalovirus-specific CD8(+) T lymphocytes in healthy seropositive donors. *J Virol*. 2000; 74(17): 8140-50
163. Khan N, Shariff N, Cobbold M, Bruton R, Ainsworth JA, Sinclair AJ, et al. Cytomegalovirus seropositivity drives the CD8 T cell repertoire toward greater clonality in healthy elderly individuals. *J Immunol*. 2002; 169(4): 1984-92
164. Looney RJ, Falsey A, Campbell D, Torres A, Kolassa J, Brower C, et al. Role of cytomegalovirus in the T cell changes seen in elderly individuals. *Clin Immunol*. 1999; 90(2): 213-9
165. Hodes RJ. Aging and the immune system. *Immunol Rev*. 1997; 160: 5-8
166. Halenius A, Hauka S, Dolken L, Stindt J, Reinhard H, Wiek C, et al. Human cytomegalovirus disrupts the major histocompatibility complex class I peptide-loading complex and inhibits tapasin gene transcription. *J Virol*. 2011; 85(7): 3473-85
167. Roux A, Mourin G, Larsen M, Fastenackels S, Urrutia A, Gorochov G, et al. Differential impact of age and cytomegalovirus infection on the gammadelta T cell compartment. *J Immunol*. 2013; 191(3): 1300-6
168. Hislop AD, Annels NE, Gudgeon NH, Leese AM, Rickinson AB. Epitope-specific evolution of human CD8(+) T cell responses from primary to persistent phases of Epstein-Barr virus infection. *J Exp Med*. 2002; 195(7): 893-905
169. Anane LH, Edwards KM, Burns VE, Drayson MT, Riddell NE, van Zanten JJ, et al. Mobilization of gammadelta T lymphocytes in response to psychological stress, exercise, and beta-agonist infusion. *Brain Behav Immun*. 2009; 23(6): 823-9
170. von Boehmer H, Aifantis I, Azogui O, Feinberg J, Saint-Ruf C, Zober C, et al. Crucial function of the pre-T-cell receptor (TCR) in TCR beta selection, TCR beta allelic exclusion and alpha beta versus gamma delta lineage commitment. *Immunol Rev*. 1998; 165: 111-9
171. Bolotin DA, Mamedov IZ, Britanova OV, Zvyagin IV, Shagin D, Ustyugova SV, et al. Next generation sequencing for TCR repertoire profiling: platform-specific features and correction algorithms. *Eur J Immunol*. 2012; 42(11): 3073-83
172. Miles JJ, Elhassen D, Borg NA, Silins SL, Tynan FE, Burrows JM, et al. CTL recognition of a bulged viral peptide involves biased TCR selection. *J Immunol*. 2005; 175(6): 3826-34

173. Turchinovich G, Hayday AC. Skint-1 identifies a common molecular mechanism for the development of interferon-gamma-secreting versus interleukin-17-secreting gammadelta T cells. *Immunity*. 2011; 35(1): 59-68
174. Dash P, McClaren JL, Oguin TH, 3rd, Rothwell W, Todd B, Morris MY, et al. Paired analysis of TCRalpha and TCRbeta chains at the single-cell level in mice. *J Clin Invest*. 2011; 121(1): 288-95
175. Wang H, Henry O, Distefano MD, Wang YC, Raikonen J, Monkkonen J, et al. Butyrophilin 3A1 plays an essential role in prenyl pyrophosphate stimulation of human Vgamma2Vdelta2 T cells. *J Immunol*. 2013; 191(3): 1029-42
176. Smith AM, Benjamin DC, Hozic N, Derewenda U, Smith WA, Thomas WR, et al. The molecular basis of antigenic cross-reactivity between the group 2 mite allergens. *J Allergy Clin Immunol*. 2001; 107(6): 977-84
177. Venturi V, Kedzierska K, Turner SJ, Doherty PC, Davenport MP. Methods for comparing the diversity of samples of the T cell receptor repertoire. *J Immunol Methods*. 2007; 321(1-2): 182-95